Exploring the germinal centre and peripheral roles of CD21

Emily Taylor

PhD

University of York
Biology

August 2019

1. Abstract:

Secondary lymphoid organs (SLOs), including lymph nodes, tonsils and Peyer's patches, contain highly organised microenvironments in which adaptive and innate immune cells interact with stromal fibroblasts. It is within these organs that germinal centres (GCs) form; structures that function to permit the development of high affinity antigen-specific humoral immune responses. Follicular dendritic cells (FDCs) and B cells are the cells primarily responsible for driving formation and function of the GC.

B cells scan FDC stromal cell networks for antigen complement complexes bound to the CD21 receptor through the complement component C3dg. CD21 is expressed on both cell types, permitting transfer of antigen complexes from B cells to FDCs where it is retained and presented permitting antigen-specific B cell activation and initiating a cyclical cycle of selection and expansion leading to high affinity antibody selection. Human FDCs are reported to express a long isoform of the CD21 receptor (CD21L), whereas B cells express a short isoform (CD21S). In this thesis I utilised a flow cytometry-based assay to investigate the different potential mechanism of CD21 isoform function in B cells and FDCs; revealing that FDC express a significantly higher number of CD21 molecules on their cell surface and provide evidence that this may be a mechanism of antigen transfer between the two cells types.

CD21 and the complement pathway, including C3 and its derivatives, have been implicated in autoimmune diseases, including Rheumatoid Arthritis (RA). Soluble CD21 (sCD21) concentration is consistently decreased within the serum of RA patients compared with age-matched healthy control samples. Here I show that lower sCD21 concentrations correlate with increased disease phenotype. Additionally, I show that sCD21 can block C3dg complex binding to peripheral B cells and consequently prevent co-activation through the CD19/CD21 complex on the surface of B cells. Together these results suggest a role for sCD21 in suppressing human immune responses.

Author's Declaration:

I declare that this thesis is a presentation of original work and I am the sole author. This work has not previously been presented for an award at this, or any other, University. All sources are acknowledged as References.

2. Acknowledgements:

The last 4 years haven't been particularly easy, in fact at points they were hell; and like most PhD students there were many times in which I almost threw in the towel completely. But now as I come to the end of writing my thesis, I can't help but smile and think, I did this! I wrote a book! But really, it wouldn't have been possible without my amazing support network around me, who believed in me even when I didn't, so first and foremost I dedicate my thesis to them.

To Mum, who's been there through thick and thin, listened to me moan and virtually dried my tears countless times from back home, I can't put into words how grateful I am to have a mother and best friend like you. To Dan, who phoned every day in the darkest of days and gave endless hugs whenever we were together, thanks for sticking with my craziness, I can't wait for the next chapter in our very own book. To Grandad, who always knew I could do it, I know you are still watching over me. To all my friends and family, I don't know where I would be without you all.

I would also like to thank my supervisors. Firstly, Chris and Laura at GSK for making me feel welcome in my final year and who both dedicated so much time and effort into bringing this thesis to life. Thank you for your continued support. Thanks to Mark and Ian, for teaching me that science is not easy. And thanks to Paul and Dimitris for their support as thesis advisors. Because of you all, I have grown over the last 4 years into a better scientist.

Thanks to the lab crew in the CII. Version 1 of the Q crew, Hayley, Megan, Katrina, Liz, I missed you guys after you had finished your projects and know I used your achievements as inspiration to finish my own PhD. I hope to see you all very soon! To those that came after, version 2 of the Q crew. Katie, Hilary and Connor, thanks for all the fun times in the lab, and special thanks to Katie (she knows why!).

Finally, I'd like to thank all the support staff in the Technology Facility at the University of York, especially Karen and Graham, whom spend endless hours sorting cells with me and helping me learn the art of flow cytometry.

I'm not afraid to admit that blood, sweat and a lot of tears went into this thesis (and yes, I did cry while writing this acknowledgement!), but I come out of the other side a stronger person, because if I can make it through the last 4 years, I can make it through anything, all with a little help from my friends (and family!).

3. TABLE OF CONTENTS

4. LIST OF FIGURES

5. LIST OF TABLES

6. ABBREVIATIONS

AIM	Apoptosis inhibitor of macrophages
APCs	Antigen presenting cells
Anti-CCP	Anti-cyclic citrullinated peptide
BAFF	B cell activating factor
BRC	B cell receptor
CD21L	CD21 long
CD21S	CD21 short
CD40L	CD40 ligand
CVID	Common variable immune deficiency
CII	Collagen type II
EBV	Epstein-Barr Virus
FDC	Follicular Dendritic cell
FRC	Follicular Reticular cell
GC	Germinal centre
GPI	Glycosylphosphatidylinositol
HEK	HEK293T cells
HEV	High endothelial venules
IBD	Inflammatory bowel disease
ICAM1	Intracellular adhesion molecule 1
IHC	Immunohistochemistry
INFα	Interferon alpha
KLH	Keyhole limpet hemocyanin
LPS	Lipopolysaccharide
LT	Lymphotoxin
LTβR	Lymphotoxin β receptor
Mfge8	Milk Fat Globule-EGF Factor 8 protein
MFI	Mean fluorescent intensity
MRC	Marginal reticular cell
MZ	Marginal zone
PALS	Periarteriolar lymphoid sheath
RA	Rheumatoid Arthritis
rc-CD21	Recombinant CD21
RhF	Rheumatoid factor
RT	Room temperature
sCD21	Soluble CD21

SCS	Subcapsular sinus
SCR	Short consensus repeat
SLE	Systemic lupus erythematosus
SLO	Secondary lymphoid organ
SS	Sjogren’s syndrome
S1P	Sphingosine-1-phosphate
TBMs	Tingible body macrophage
TGFβ	Transforming growth factor beta
TLR2	Toll-like receptor 2
TLR4	Toll-like receptor 4
TLR7	Toll-like receptor 7
TLT	Tertiary lympoid tissue
TNF	Tumour necrosis factor
TNFR1	Tumour necrosis factor receptor 1
TSH	Thyroid stimulating hormone
VCAM1	Vascular cell adhesion protein 1
wt	Wildtype

7. Introduction

Development of high affinity adaptive immune responses take place within the highly organised and specialised secondary lymphoid organs (SLOs) including spleen, Peyer's patches and lymph nodes (LN). These lymph and blood filtration organs provide the microenvironment to both drive robust adaptive immune responses including antibody-mediated (humoral) and cellular mediated immune responses producing cytokines and for cytotoxic lymphocytes to help clear and prevent infection as well as accelerating tissue repair. It is the unique structure and function of these lymphoid tissues that coordinate the dynamics and efficiency of immune responses and control the cellular chorography required to drive antigen specific immune responses. Deficiencies in key cell types and proteins required for normal formation, structure and function of lymphoid tissues leads to formation of chronic inflammatory disease, T cell mediated immunity and humoral deficiency, highlighting the critical importance of secondary lymphoid organs in normal health and homeostasis of the immune system.

7.1 Secondary lymphoid organs

Formation of primary B cell follicles occurs independently of antigen; their main components are recirculating B cells that are recruited and retained within a network of follicular dendritic cells (FDCs) (Howard et al., 1972). Follicles develop in humans during the second trimester of foetal life, and FDCs become apparent within a few days of the formation of B cell clusters (Timens et al., 1987). In mice, SLOs development occurs between embryonic days 13.5 and 18.5, with B cell follicles forming within 72hr during post-natal development with B cells initially forming a donut like structure (Randall et al., 2008).

Secondary follicles contain lymphoid cells that are not actively involved in antigen-driven processes. However, once these cells become activated, an enhanced adaptive immune response can occur. This can occur as a result of three different mechanisms and, in certain circumstances, these may coexist. These are; the formation of germinal centres to select for

high affinity B cells, the proliferation of memory B blasts within the follicles and follicular proliferation in response to T cell-independent antigens which is independent of germinal centre reaction and involves low affinity IgM responses. The focus of this thesis will be on the germinal centre reaction and the cells within this structure.

Within the SLO, there are three main stromal cell populations; follicular dendritic cells (FDCs), fibroblast reticular cells (FRCs) and marginal reticular cells (MRCs). FRCs contribute to the structure and function of the T-cell zone and MRCs are important for the function and structure of the marginal zone (MZ) (den Haan et al., 2012). FDCs are important for maintenance of B cell follicle structure, antigen presentation to B cells and homeostasis of naïve T cells through the production of survival factors. These cells and processes are discussed in more detail below.

The structure of the lymph node is essential to its proper function. Within the lymph node there are three separate regions named the cortex, the paracortex, and the medulla, all encompassed in the subcapsular sinus. The outer most layer, the cortex, contains B cells, macrophages and follicular cells, arranged into primary follicles. The cortex is the area in which B cell follicles are found and in which germinal centre development occurs. The paracortex is the second most outer layer, containing T cells, dendritic cells and fibroblast reticular cells (FRCs). FRCs support prolonged interactions between the T cells and dendritic cells within this compartment and form a conduit network permitting small antigens to enter into the paracortex and cortical structures of the LN. The medulla is the inner layer of the lymph node and is made from lymphatic tissue named medullary cords. These tissues are separated by spaces filled with lymph drained from the medullary sinuses. The vascular network of the LN consists of high endothelial venules (HEV), through which T and B cells enter the organ from the blood. The lymphatic vessels of the lymph node are lined by lymphatic endothelial cells (LECs) (Burrell et al., 2011).

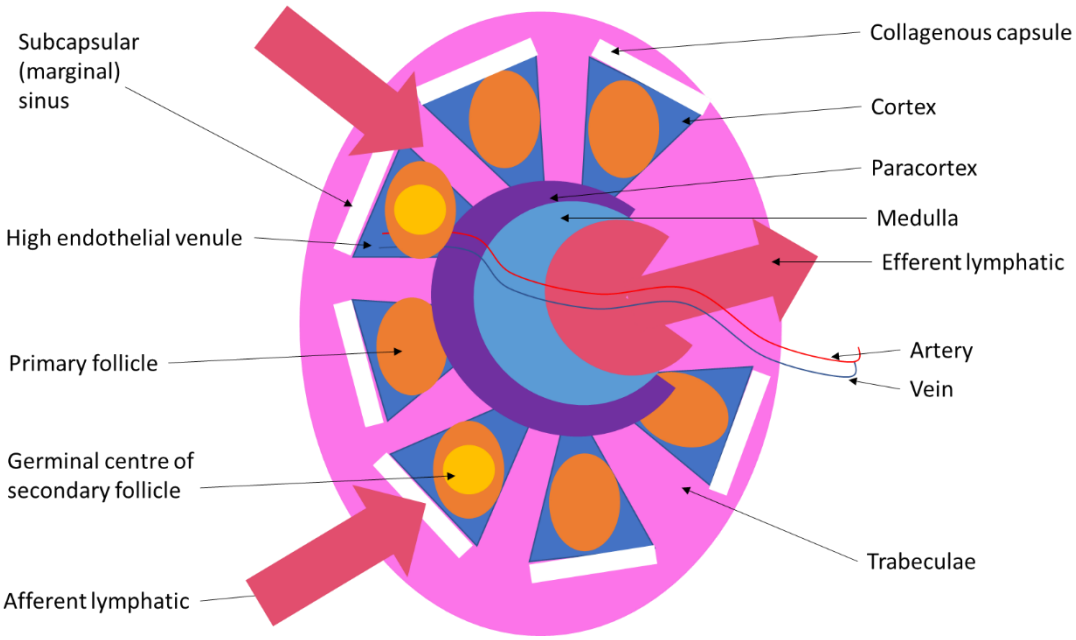

Figure 7. 1: Structure of the human Lymph node

Lymph node structure is essential to its function. The cortex contains B cell follicles and the paracortex contains B cells, dendritic cells and Fibroblast reticular cells. The medulla is the inner layer of the lymph node and is made from lymphatic tissue name medullary cords. The vascular network of the LN consists of high endothelial venules, as well as other lympathic vessels, supplying the organ with nutrients and allowing the movement of cell types in and out of the organ. (Figure adapted from https://www.open.edu/openlearn/ocw/mod/oucontent/view.php?id=65373&extra=thumbnailfigure_idp794560)

7.1.2 The structure of the spleen

The spleen is surrounded by a capsule that extends many projections into the interior to form a compartmentalised structure. The spleen has two compartments, the red and the white pulp, and a marginal zone that separates the compartments. A network of sinusoids, populated by macrophages and red blood cells, makes up the red pulp compartments and the white pulp forms a periarteriolar lymphoid sheath (PALS) populated by T cells. In this structure, the B cell follicles form next to the PALS. Interestingly, separation of splenic red and white pulp occurs before birth in a Lymphotoxin-αβ-independent (LT) manner (Vondenhoff et al., 2008). LT is not detected on B cells until 4 days after birth, therefore prenatal development of the white pulp of the spleen occurs in the absence of LT. Postnatal development, however, involves an influx of T cells and depends on LTαβ expression by B cells (Vondenhoff et al., 2008). The outer boundary of the white pulp is defined by the marginal sinus and its associated with a layer of FRC and MOMA-1 staining metallophilic macrophages (Burrell et al., 2011).

7.1.3 The role of Lymphotoxin in Secondary Lymphoid Organ development

Lymphotoxin-β is a member of the TNF family that forms a heteromeric complex with Lymphotoxin-α on the cell surface (Browning et al., 1993). It can exist in two forms, a secreted homotrimer, LTα3, or a membrane bound heterotrimer, LTα1β2. The membrane bound complex is expressed on the surface of activated T and B cells and has a key role in B cell follicle formation.

This molecule, along with other molecules of the same family, has been implemented in the induction of lymphoid organ development and has been shown to induce expression of adhesion molecules VCAM1, ICAM1, E-selectin and MAdCAM1 by murine endothelial cells (Cuff et al., 1998); a potential mechanism leading to LT-dependent organ development. Mice deficient in LT have abnormal development of lymphoid organs; animals were shown to have

no morphologically detectable lymph nodes or Peyer's patches, although development of the thymus appeared to be normal in this study (De Togni et al., 1994). Histology revealed that normal segregation of B and T cells failed to develop within the spleen of these mice. Studies have also shown $LT^{-/-}$ mice develop lymph nodes upon treatment with agonist anti-LTβR antibody; induction of signalling through the LT receptor mediated lymph node genesis (Rennert et al., 1998). In contrast, normal mice treated with anti-LTβ lacked lymph nodes, further confirming the essential role for LT in SLO development.

7.1.4 Embryonic SLO formation

The stromal cells within the SLOs develop as part of a network. During prenatal development, retinoic acid induces lymphoid tissue organiser cells to produce CXCL13, attracting lymphoid tissue inducer cells (LTi cells) to the sites where lymph nodes are to form (van de Pavert et al., 2009). However, this process is not required for SLO development as mice deficient for CXCL13 or its receptor CXCR5 have normal lymph node development. Signalling induced by LT on LTβR expressed on LTi cells, induces the expression of adhesion molecules, along with various chemokines, promoting the clustering of haematopoietic cells, leading to the expansion and differentiation of the stromal network (Figure 7.2).

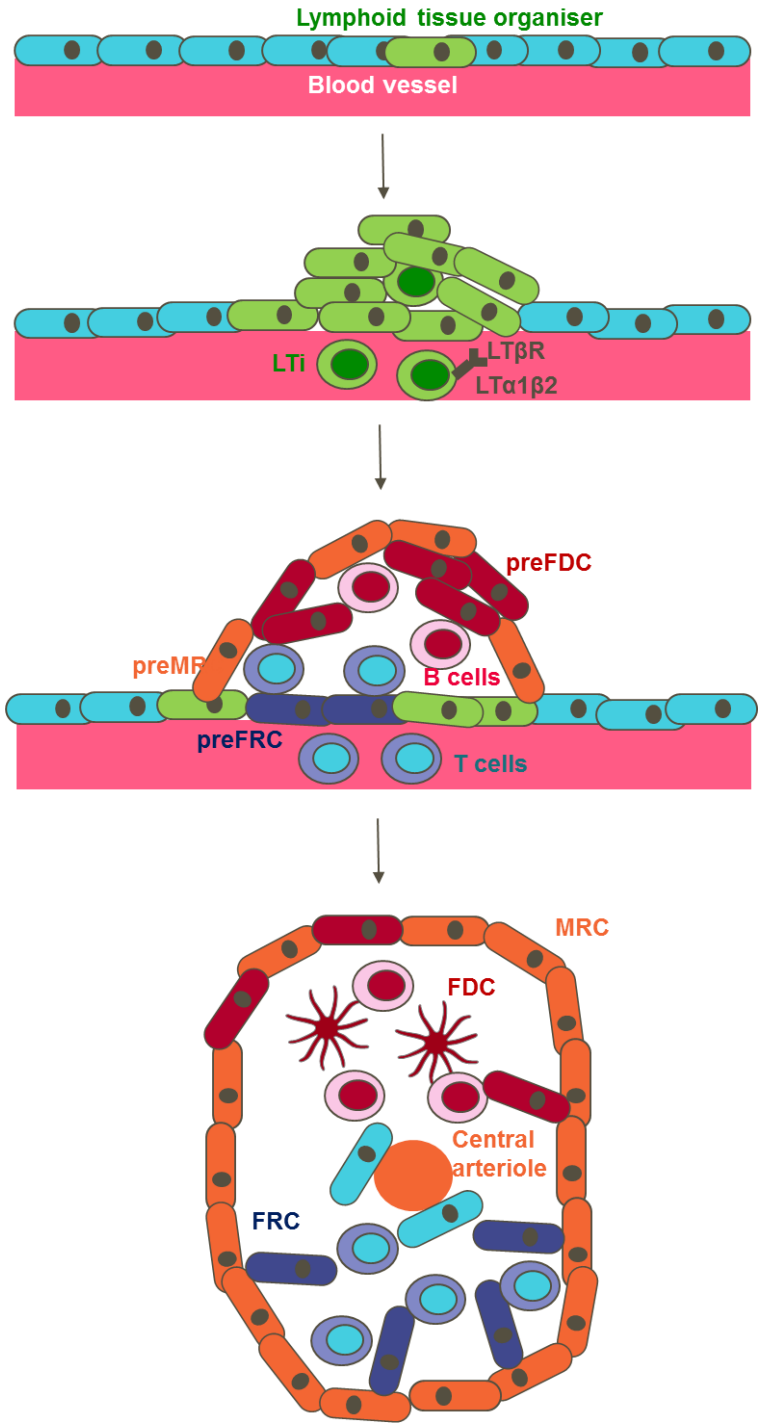

Figure 7. 2: Secondary lymphoid organ and FDC development

(Figure adapted from Kranich et al. 2016) Lymphoid tissue organiser cells line blood vessels at places where future lymphoid tissues develop. Lymphoid tissue inducer cells (Lti) express membrane bound LTαβ and trigger expansion of organiser cells, along with the upregulation of CXCL13. Recruitment of T and B cells providing more LT leads to the induction of MRC, FDC and FRC precursors.

CXCL13 expression by stroma (FDCs and MRCs) induces the homing of B lymphocytes to the B cell follicles. CXCL13 acts as a B cell chemoattractant through the CXCR5 receptors expressed on the B cell surface. Transfer experiments showed that B cells derived from the bone marrow migrate to the follicles due the expression of this receptor (Parrott et al., 1971). CXCR5 is not expressed on pre-B cells but is upregulated in development of immature B cells in parallel with other B cell maturation markers such as IgD and CD21 (Forster et al., 1994); this upregulation leads to acquisition of these cells to the B cell follicles (Cyster et al., 1997). *In vitro* studies have demonstrated that the level of CXCL13 present in an area directly affects CXCR5 expression on B cells (Cyster et al., 1999). The data from this study suggested that the CXCL13 gradient within the follicle was steep and was the first investigation to suggest that the protein was associated with the membrane processes of the follicular stromal cells. Recently our data (under review, 2019) shows that the gradient of CXCL13 is mediated by an ectoenzyme CathepsinB which cleaves the heparin binding domain off CXCL13 to induce a soluble gradient (Cosgrove et al., under review, 2019). Further studies have shown that CXCR5-deficient mice have disorganised germinal centres, the same observation was made within CXCL13$^{-/-}$ mice; these results confirm that CXCL13 is required for recruitment and retention of B cells in an organised structure within the secondary lymphoid organs (Voigt et al., 2000). As with SLO development, LT and Tumour necrosis factor (TNF) are also required for B cell follicle development; CXCL13 is reduced 20-fold in mice deficient in LT and 3-4-fold in TNF-deficient mice (Ngo et al., 1999), due to the role of these molecules in FDC development and activation, highlighted by the absence of FDCs within this model. Therefore, defective formation of B cell follicles in mice deficient in LT or TNF can be, in part, attributed to the reduced expression of CXCL13 (Cyster et al., 2000). In addition to mediating chemoattraction of B cells to the follicle, CXCL13 also induces upregulation of LT by B cells; resulting in increased CXCL13 expression due to increased FDC activation by the greater concentration of LT available (Ansel et al., 2000). These observations were made by using gene-targeted mice, deficient for CXCL13 or CXCR5. Wild-type B cell transfer to CXCR5$^{-/-}$ mice showed that LT upregulation only occurs

once the cells are within the follicular areas where CXCL13 is present and not in non-lymphoid organs; showing that B cells upregulate LT as they migrate to B cell follicles in response to CXCL13. In further support of these findings, it has been shown that ectopic expression of BLC induces B cell-dependent and LT-dependent lymphoid neogenesis (Mebius et al., 1997), expression of ectopic CXCL13 in the pancreas likewise lead to neo-lymphoid tissue genesis (Luther et al., 2000). These data conclude that establishment of a positive feedback loop between CXCL13 and LT expression is important in B cell follicle development and homeostasis but it is unclear if these processes are simply regulated by positioning or as a result of CXCR5 GPCR signalling independent of its role in cellular motility.

7.1.5 FDC development

While FDCs are essential for the maintenance of B cells within the germinal centre, B cells have an essential role in FDC development and maintenance by providing TNF and lymphotoxin (LT), showing a mutual dependence of the two cell types within SLOs. LT has also been shown to have roles in the development of the SLOs, discussed above. Both TNF and lymphotoxin (LT) are essential for the key steps in the differentiation and induction of FDC function (Rogni et al., 1994). Pre-FDC development requires LTβR but not TNFR1 signalling and FDC maturation strictly requires B cells expressing LTαβ (Krautler et al., 2013). Further to these observations, the disruption of the LT pathway in adult mice leads to defects in FDC and GC development, whereas disruption of the TNF pathway does not. Disruption of this pathway affects mice during gestation; confirming that both the TNF and LT pathways must be functional to allow for mature splenic FDC networks to form (Mackay et al., 1997). Studies have also shown that lymphoid organs lacking B cells, TNF or LT are devoid of FDCs (Allen et al., 2008), highlighting the essential functions of these factors in FDC development. Mice deficient in TNF and LT were also shown to lack polarised B cell follicles in the spleen and experiments within the same study revealed that treatment of wildtype (wt.) mice with agonists against LT receptor leads to decreased CXCL13

expression (Ngo et al., 1999). Together these data show that LT and TNF have a role upstream of CXCL13 expression in the process of follicle formation; this role is known to be in FDC development which then produce CXCL13, subsequently allowing polarisation of B cells within the follicle. Adoptive transfer of functional $CD19^+$ B cells in CD19-deficient mice rescued GC formation and FDC activation, further confirming that FDC activation required the CD19-dependent upregulation of LT on activated B cells (Myers et al., 2013). In addition to the initial generation of FDCs, sustained LT signalling has been shown as essential for maintenance of FDCs in a differentiated and functional state (Mackay et al., 1997). Transcriptome analysis highlighted down-regulation of key functional genes in FDCs upon treatment with anti-LTβR treatment (Huber et al., 2005). For example, clusterin is down-regulated upon LTβR signalling suppression, suggesting this protein has a role as an FDC-derived trophic factor for GC B cells.

Compiling all that is known about FDC development, a three-stage development for FDCs has been suggested; LTβR signalling induces the development of FDC precursors in the marginal zone, TLR4 signalling induces the development of FDCs in the splenic B cell zone and TNFR1 signalling elicits the clustering of FDCs accompanied by lymphoid follicle formation (Milicevic et al., 2011). In addition to the initial generation of FDCs, sustained LT signalling has been shown as essential for maintenance of FDCs in a differentiated and functional state (Mackay et al., 1997). LT has also been shown to cause the upregulation of FDC derived CXCL13, highlighting its importance for FDC and GC biology (Aguzzi et al., 2014). FDC activation has also been shown to increase with immune-complex engagement of FcγRIB on the FDC cell surface (Shikh et al., 2006); therefore, as immune-complexes are delivered to the GC, FDCs can become more activated, ready to influence the GC response in a greater manner (Figure 7.3).

Interestingly, FDCs can also be generated *de novo* in nonlymphoid organs during chronic inflammatory conditions resulting from autoimmune inflammation and follicular lymphoma resulting from a combination of inflammatory signals and the persistent presence of antigen

can elicit tissue reorganisation into tertiary lymphoid tissues (TLT's) containing GCs and fully differentiated FDCs (Aloisi et al., 2006). As TLT's can arise almost anywhere in the body, the FDC precursor must possess considerable motility or be ubiquitously present in all tissues. In a murine model of chronic inflammation, transgenic overexpression of LT lead to the formation of TLT's in kidneys, which contain fully matured FDCs (Mackay et al., 1997). Upon treatment with anti-LTβR, mature FDCs were removed and the kidney was transplanted into recipient mice. FDCs reformed within these mice, exclusively derived from cells of the transplanted donor mouse. These results further suggested that FDC precursor cells are tissue-intrinsic. Consistent with these results, it was recently shown using a mouse model of TLT formation in the salivary gland that FDCs arise from mesenchymal progenitors in an IL4 and TNF dependent process (Nayar et al., 2019).

FDCs were originally, mistakenly, assumed to be a subset of conventional dendritic cells due to their location within lymphoid organs and their dendritic like appearance, however FDCs are stromal fibroblasts, unlike conventional dendritic cells, which are hematopoietic in origin. The origin of FDCs was controversial for some time; gene expression by FDCs was compared with that of follicular stromal cells from the spleen of SCID mice, revealing 90% of genes are expressed in these cells from the SCID mice (Wilke et al., 2010) suggesting that FDCs develop from the residual network of reticular cells and only minor modification in gene expression is sufficient for differentiation of precursor cells into mature FDCs. Recent data using fate mapping in mice confirmed the origin of FDCs to be mesenchymal, arising from the clonal expansion and differentiation of MRCs (Jarjour et al., 2014). This conclusion is further supported by data from Melzi et al., 2016, in which it is shown that MRCs, FDCs and sinus lining cells can be infected by BTV (an endotheliotropic virus), suggesting a common endothelial progenitor for these cell types, as replication of the virus was not identified in the stromal cells of the T cell zone (Melzi et al., 2016). FDCs, FRCs and MRCs also share the expression of cell surface markers, LTβR, TNFR1, VCAM1 and ICAM1, further indicating they are closely related (Cyster et al., 2000). Studies using reporter genes

have shown that these cells all develop from embryonic splenopancreatic mesenchymal cells of the NK2x2.5^{+}Islet^{+} lineage (Castagnaro et al., 2013). Transplantation of these mesenchymal cells into mice led to the generation of all lymphoid stromal subsets (FDCs, FRCs and MRCs) and *de novo* lymphoid tissues. Thus, with the help of specific sets of hematopoietic cells, these cells types can differentially develop from a common precursor cell. Although cells have been shown to develop from a common precursor, a recent study has confirmed that cells are distinct in their gene expression after differentiation. Single-cell RNA sequencing performed on isolated mouse pLN CD45^{-} CD31^{-} cells revealed nine conserved stromal cell clusters when unsupervised clustering was performed on samples (Rodda et al., 2018).

7.1.6 FDCs as the antigen presenters for B cells

FDCs have a key role in priming high affinity B cell responses through presenting unprocessed antigen to B cells during the germinal centre (GC) reaction. Naïve B cells are recruited to germinal centres within the first week following administration of antigen and recruitment is complete by the time mature germinal centres have developed (Gray et al., 1986). The germinal centre reaction initiates through rapid B cell scanning of the FDC network leading to antigen specific B cells interacting with cognate antigen complexed with the C3dg complement component bound to CD21 on FDCs (Figure 7.3).

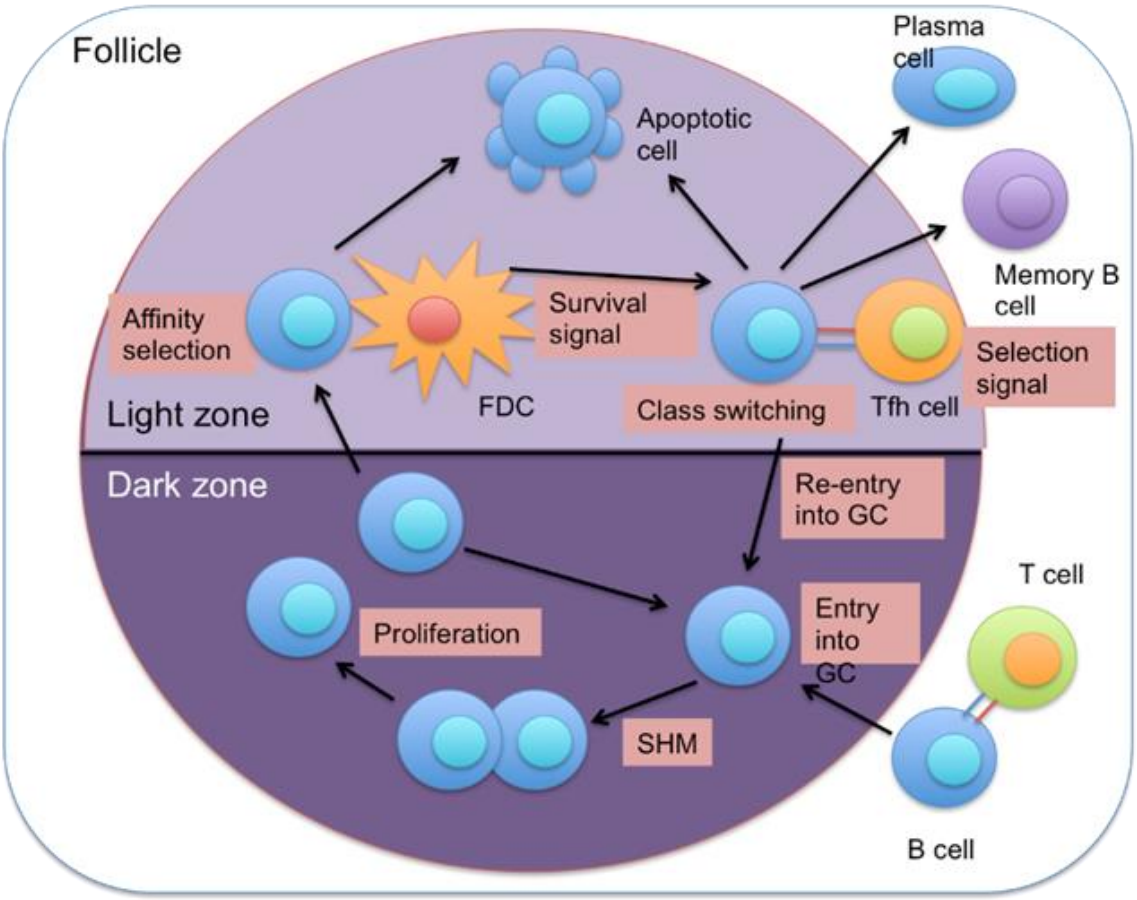

Figure 7. 3: The germinal centre reaction

B cells that carry antigen require T cell help, in order to receive this they must first process this antigen into a form that can be presented on an MHC class II molecule, which is then recognised by the T cell receptor. The germinal centre is split into the light and dark zone. B cells enter the dark zone from the follicle after receiving T cell help. B cells undergo somatic hypermutation (SHM) of their B cell receptor and proliferation. A CXCL13 gradient then causes the B cells to migrate to the light zone and encounter antigen presented on FDC CD21 membrane receptors. High affinity interactions between BCR and antigen lead to class switching, plasma cell and memory cell production. Interactions of low affinity lead to B cell apoptosis of the B cell. B cell class switching occurs with the help of T follicular helper cells (Tfh cell) which make IL21 and promote class switching from IgM antibodies to IgA and IgE, therefore creating a more specific secondary immune response.

Cognate B cells with antigen bound by their BCR migrate to the T-B cell boarder of the GC where they can be co-stimulated by T cells through CD40-CD40 ligand (CD40L) signalling. B cells present processed antigen on MHCII molecules to T cells, recognised by the α/β T cell receptor. Processing of antigen by the B cell occurs through the internalisation of the antigen bound BCR using clathrin-dependent, BCR-mediated endocytosis (Natkanski et al., 2013). MHCII α and β associate with I chain trimers to form nonamers (Blum et al., 2013). These complexes are transported to mature endosomes where the I chain is sequentially proteolysed to yield the residual I chain fragment, CLIP. The antigen is processed by various proteases in order to form a peptide that is able to bind to the ligand binding site in the MHCII molecule within late endosomes upon displacement of the CLIP protein. The interaction between internalised BCR/antigen with intracellular MHCII has been observed using pulldowns and biotin-labelled antigen (Barroso et al., 2015). Surprisingly, a rare (10%) conformation of MHCII is the predominant conformer found in complex with the BRC/antigen; this form of MHCII has been shown to be highly effective for T cell activation (Busman-Sahay et al., 2011). Therefore, it is thought that this conformation may contribute to the efficiency of BCR-meditated antigen presentation. The MHCII/peptide complex is then transported to the cell surface, but this process has not been delineated in mechanistic detail at present (Adler et al., 2017). T cells are then activated by the antigen presenting B cell through two signals; the ligating signal through the TCR, provided by the MHCII/peptide complex, and a costimulatory signal, in the form of CD28 ligation by B7 molecules expressed on the B cell surface (Healy et al., 1998). These signals result in the increased production of IL21, IL10 and IFNγ, which subsequently, along with CD40-CD40L interactions, activate the B cells (Margry et al., 2013). CD40 has been show to mediate CXCR4 upregulation on B cells (Moir et al., 1999); therefore allowing fully activated B cells to migrate into the dark zone of the GC supported the CXCL12 chemokine gradient created by fibroblast within this site.

Direct evidence of somatic hypermutation and proliferation of B cells within the light zone was obtained by the microdissection of germinal centre cells from sections of mice spleen undergoing responses to antigen-protein conjugates (Jacob et al., 1991). The cycles of proliferation and hypermutation drive class switching and affinity maturation through cyclical migration into the light zone to compete for C3dg-immune complexes on FDCs. B cells with high affinity receptor (BCR) are selected for antigen specificity, those with the highest specificity are activated under antigen limiting conditions and are the cells that receive help from T follicular helper cells. These T cells induce the iterative process of proliferation and selection of cells, allowing the process of affinity maturation to proceed over days and weeks, resulting in dozens of generations of GC B cells (Crotty et al., 2011). T follicular helper cells provide stimulatory signals to GC B cells via multiple pathways, including CD40L, IL4, IL21, PD-1 and BAFF. B cell division, somatic hypermutation of immunoglobulin genes and engagement of T follicular helper cells are directly proportional to the amount of antigen captures and presented on MHCII (Gitlin et al., 2014). Cells then both continue cycling and re-enter the dark zone to undergo further proliferation or exit the GC either as specialised antibody secreting plasma cells or long-term memory B cells (Heester et al. 2014). It is this cyclical process allows the selection of high-affinity antibody producing cells. Any cells with a low affinity BCR receives death signals from the FDC, resulting in apoptosis. There is a high death rate among the B cells within germinal centres due to this selection by FDCs. Analysis revealed that half of the cells undergoing apoptosis are located in the basal light zone, 25% in the dark zone and 25% in the basal light zone (Hardie et al., 1993).

Germinal centre B cells have unique phenotypes, expressing high levels of CD38 and low or absent levels of CD44 and CD39 (Ling et al., 1987). The level of surface Ig expressed by these cells is lower than that expressed by follicular mantle or marginal zone cells (Liu et al., 1991). Dark zone B cells are characterised by increased expression of CXCR4 protein and mRNA, along with upregulation of cell cycle and somatic hypermutation machinery. Light zone B cells however, were shown to upregulate CD86 mRNA (CD28 ligand) and protein

and display increased transcription of gene programs essential for antigen presentation (Victoria et al., 2010). Cell cycle regulator c-Myc was shown to be transiently expressed in subsets of GC B cells in the light zone (Calado et al., 2012). This transient expression was suggested to initiate downstream regulators, such as AP4, to mediate multiple rounds of division and somatic hypermutation in the dark zone. High expression of transcription factor, FOXO1 in B cells found in the dark zone, appears to control formation, organisation and gene expression; likely working in concert with Bcl6, a regulator of GC B cell function (Nurieva et al., 2009). Additionally, the expression of FOXO1 in the light zone suggests an initiation program for dark zone entry established during cognate selection.

High affinity antibody reactions occur due to class-switching of IgM antibodies to IgG, IgA and IgE antibodies in a cytokine dependent process. The majority of IgG and IgA production in bone marrow is derived from B cells activated in the spleen and peripheral lymph nodes, while a high proportion of the IgA-secreting plasma cells of the lamina propria of the gut surfaces are activated in Peyer's patches, or mesenteric lymph nodes (Hall et al., 1977). As the life-span of plasma cells in the bone marrow of rats is around 1 month (Ho et al., 1986), there must be continued plasma cell production throughout antibody responses that last many months.

7.1.7 Germinal centres develop within SLO's

Antigen and inflammatory signals (adjuvant, pathogen products, damaged/modified self-proteins, e.g. collagen fragments) can drive formation of Germinal Centres (GCs) within the B cell follicle. The function of this unique microenvironment is to stimulate high affinity antibody responses. This process can occur in both secondary and tertiary immune structures including; lymph nodes, spleen, Peyer's patches, isolated lymphoid follicles and tertiary lymphoid tissues. Studies using mice immunised with (4-hydroxy-3-nitrophenyl)acetyl revealed the formation of two anatomically and phenotypically distinct zones within GCs in direct response to antigen (Jacob et al., 1991). These zones are termed the light and dark zone, due the density of B cells found within each section; this was originally observed using

histological sections of SLO tissue, in which B cells were described to reside in two compartments (MacLennan et al., 1994). The zones are characterised by the presence of CXCL13 expressing FDCs in the light zone and CXCL12 expressing stromal fibroblasts in the dark zone (Wang et al., 2011). Immunohistological staining of human tonsil follicles indicates that further subdivisions can be made within germinal centres on the basis of molecules expressed by their constituent cells. B cells in the dark zone are characterised by their expression of the cell cycle-associated nuclear antigen Ki67 (Gerdes et al., 1983). Whereas, the light zone contains FDCs; identified by their dendritic processes and expression of CD21 and I-CAM1. (Hardie et al., 1993). The outer zone, located immediately next to the follicular mantle, contains the greatest concentration of T cells in secondary follicles, as well as some B cells and plasmacytes (Hardie et al., 1993). As the B cells that give rise to GC structures are initially activated outside the follicle by follicular helper T cells in T cells zones, the close proximity of T cells in the follicular mantle is highly important in this process.

Upon challenge with adjuvant-antigen complexes, antigen-specific B cell activation initiates rapidly (min to a few hours) (Liu et al., 1991). Naive B cells do not respond to antigen localised on FDCs but are activated outside follicles by T cells and subsequently migrate to B follicles and form germinal centres (Jacob et al., 1992). Congenital deficiency of CD40 ligand (Van der Eertwegh et al., 1993) and blocking antibodies against CD40 ligand (Kortheuer et al., 1993) are associated with an absence of germinal centres. These findings are consistent with a requirement for continued T cell presence to maintain germinal centres.

It was first demonstrated that germinal centre development is oligoclonal using irradiated chimeric mice (Kroese et al., 1987), which was further confirmed in human (Kuppers et al., 1993) by the analysis of the Ig v-region structure in GC B cells. 72hr after antigen encounter, between 10^4 and $1.5x10^4$ antigen-specific B cells are found in the FDC network of each of the follicles within immunised rats (Liu et al., 1991). Thymidine-uptake studies found the cell cycle time for GC B cells to be 6-7hrs (Zhang et al., 1988). When the light-zone FDC

network becomes filled with B cells, the chemokine gradients generated induce B lymphocyte migration to one pole of the network to form the dark zone of the germinal centre. The chemokine responsible for this was thought to be solely CXCL12, produced by marginal reticular cells, however more recently, CCL21, produced by FRCs, has been shown to induce larger and more organised infiltrates (Luther et al., 2019); demonstrated through the comparison of CCL19 transgenic mice and mice expressing CCL21. This study demonstrated that CCL19 and CCL21 induce invasive infiltrates containing predominantly B cells and dendritic cells, whereas CXCL12 recruits mainly B cells, dendritic cells and plasma cells. Additionally, CCL21 and CCL19 were shown to induce LT expression on naïve CD4 T cells whereas CXCL12 failed to do so.

Thus the physical organisation of the GC is reflective of and intimately tied to its spatiotemporal function (Figure 7.4).

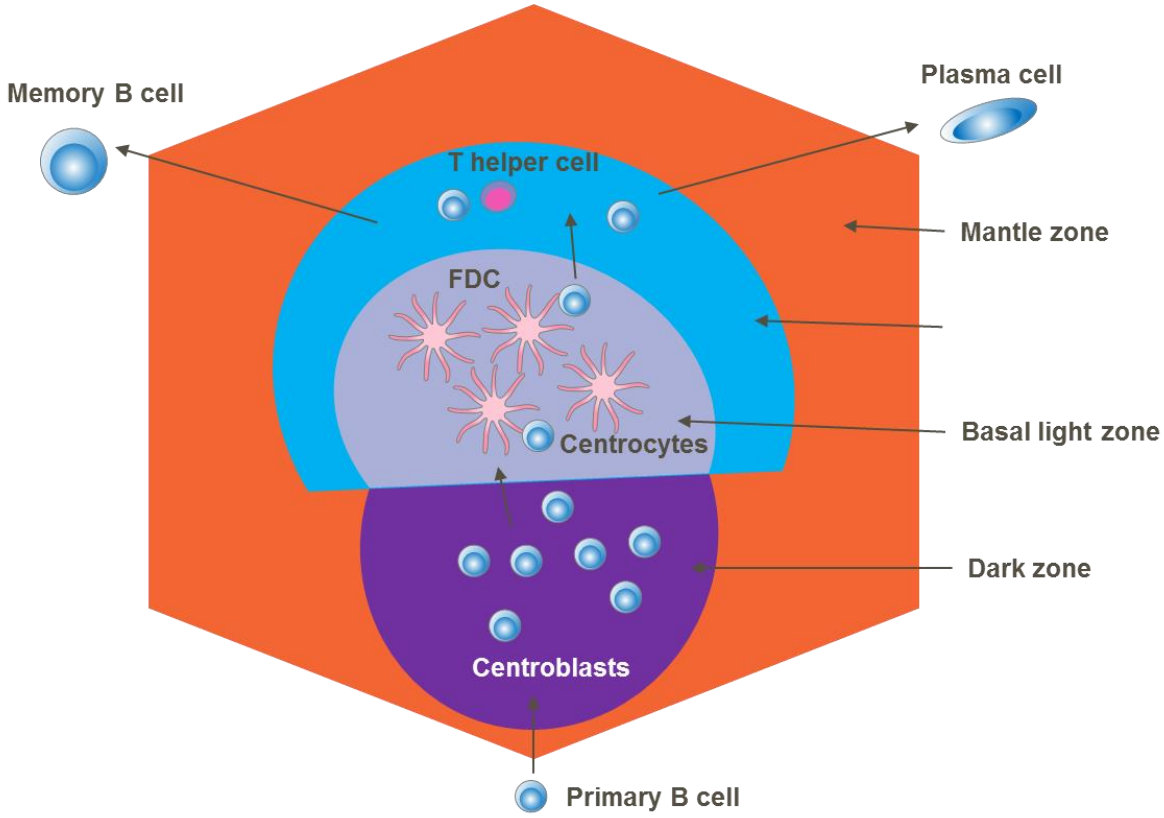

Figure 7. 4: The germinal centre structure

Adapted from https://doi.org/10.1007/3-540-27806-0_607. Germinal centres are found within B cell follicles. They are made of the dark zone and the light zone. Expansion and mutation of B cells occurs in the dark zone. In the basal light zone, FDCs reside and helper T cells are found in the apical light zone. The light and dark zones are surrounded by the mantle zone.

7.2 FDCs

FDCs were originally identified because of their ability to trap immune complexed antigen in B cell follicles and their unique dendritic morphology (Aguzzi et al., 2014). Initial experiments, using bone marrow chimeras (Humphrey et al., 1984), indicated that FDCs are a stromal, radioresistant cell whose main function is the presentation of C3dg-complexed antigen to B cells via the CD21 receptor, to recruit and retain B cells to the GC through CXCL13 expression and induce B cell survival or apoptosis of autoreactive B cell clones (Figure 7.5).

One common observation in early studies was, even though these cells were phagocytic and endocytosed antigen they encountered, some remained presented extracellularly on the surface of cells (Miller et al., 1964). Later electron-microscopy studies revealed that antigen was associated with the dendritic processes of these cells and that FDCs formed web-like structures (Nossal et al., 1968). In 1978, a study further revealed that FDCs have unique cellular structures, including large, irregular nuclei, containing little heterochromatin, and only few organelles. FDCs only have small cell bodies, while their cytoplasm extends into many filiform dendrites, forming an extensive net-like structure within secondary follicles. It was in this report that these cells were officially termed FDCs, after many published studies using alternative names, due to their long cytoplasmic processes (Chen et al., 1978).

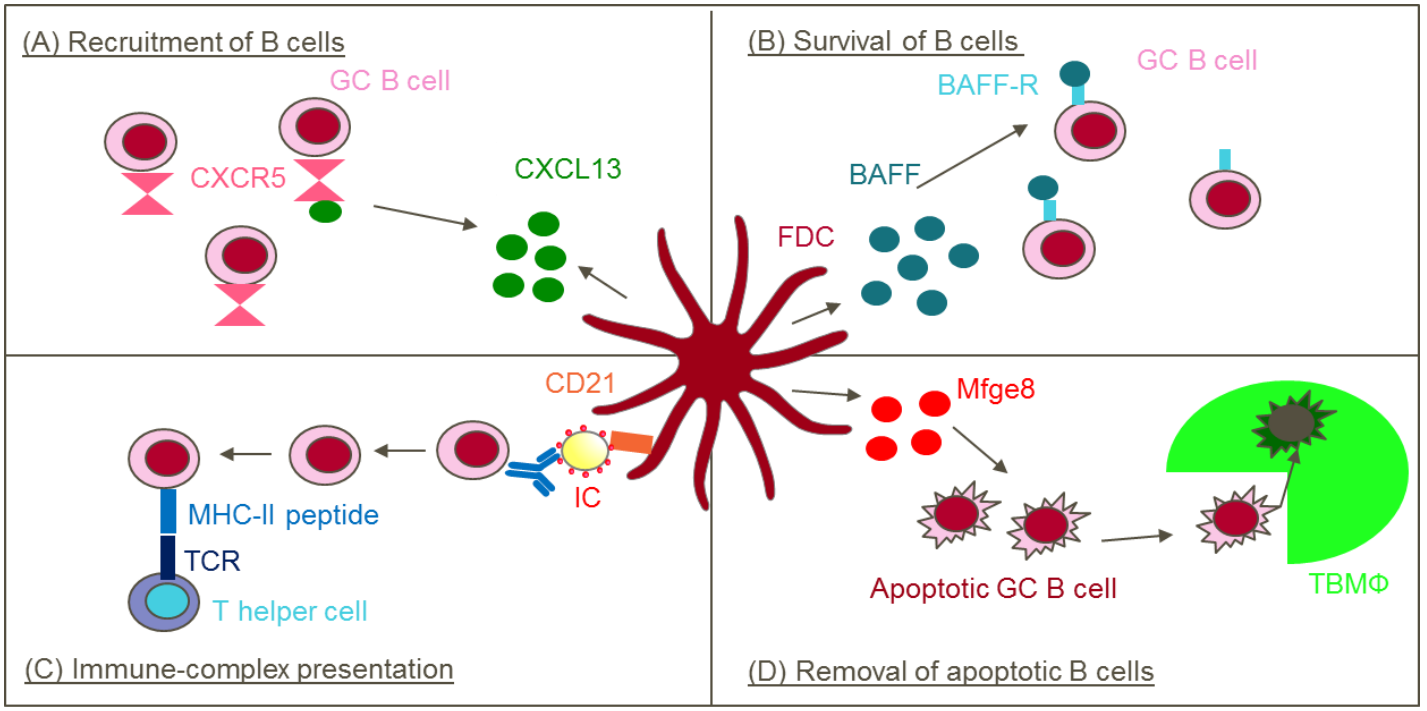

Figure 7. 5: The function of FDCs

(A) FDCs express CXCL13 which binds to CXCR5 expressed on B cells and causes migration of cells to FDCs. (B) FDCs express BAFF, which binds to BARR receptors on GC B cells and enhances B cell survival. (C) Immune complexes (IC) are presented on the CD21 on the membrane of the FDC. Specific BCRs on GC B cells bind to this complex and, with T cell help, produce antigen-specific antibodies. (D) FDCs secrete the protein Mfge8 leading to macrophage recruitment and subsequent engulfment of apoptotic B cells.

7.2.1 The function and phenotype of FDCs

Antigen presentation

An essential role of FDCs is the recruitment of B cells to the light zone of the GC to encounter antigen-complexes presented on the cell surface of FDCs upon CD21 receptors which ultimately lead to high-affinity antibody responses; therefore, immune-complex trapping is the cardinal function of FDCs. Complement containing immune complexes can often be formed very early in responses to pathogen due to the alternative or lectin pathway of complement activation. These complexes are transported and deposited on FDCs within GC light zones (Heesters et al., 2013). FDCs are described as “dynamic antigen libraries” and have the ability to retain this antigen for extended time periods. This presentation of antigen is essential to GC maintenance, robust B cell somatic hypermutation and the promotion of long-term immune memory (Mandel et al., 1980). GC B cells interact with the antigen on the surface of FDCs in order to receive survival signals and undergo affinity maturation. Antigen-complexed to C3dg are presented and retained on CD21 receptors, highly expressed by FDCs (Liu et al., 1997). FDCs preserve antigen by trapping immune complexes in recycling endosomal compartments, thereby protecting the antigen from degradation, and periodically cycle the antigen-bound CD21 receptors to the cell surface (Heesters et al., 2013). CD21 was shown to be essential for humoral immune function by many studies, including those that demonstrated blocking CD21 on murine B cells, using a blocking antibody, reduces antibody responses (Qin et al., 1998), as this interaction between antigen on FDCs and B cells can no longer occur. The importance of CD21 expression was further confirmed in studies which expressed human CD21 in $CD21^{-/-}$ mice increases the IgG1 titres in these mice, therefore restoring the GC immune response (Marchbank et al., 2000). The observation of decreased immune responses is due to the inability of FDCs to retain antigen when CD21 is not present (Fischer et al., 1998), therefore indicating this function of FDCs is of the upmost importance.

B cell migration and GC organisation

FDCs also have a role in maintenance of the unique microarchitecture of the GC. Within two days of FDC ablation, primary follicles lose their homogeneity and become disorganised; this study also showed that the removal of FDCs in mice abrogates the GC response and B cells do not undergo class switch recombination or make antigen-specific antibodies (Wang et al., 2011). Therefore, confirming that FDCs are essential for the GC response and maintenance of the GC structure.

The expression of adhesion molecules ICAM1 and VCAM1 have been shown as unessential to maintain naïve follicular B cells within the follicle. Disrupting the interaction of these molecules with their cognate receptors, αLβ2 and α4β1, respectively, using blocking antibodies does not affect the localisation of B cells within the follicles (Lo et al., 2003). Thus, it is not this mechanism that makes FDCs essential for the organisation of the GC structure. However, mice deficient in stromal CD21/CD35 have reduced T-dependent antibody responses, particularly with low doses of antigen (Roozendaal et al., 2007). And as discussed above, expression of human CD21 in $CD21^{-/-}$ mice restores humoral immune function, increasing IgG1 titres in $hCD21^{+}$ mice, and was shown to interact with mCD19 on the mouse B cells to form the CD19/CD21 complex (Marchbank et al., 2000). This suggests that CD21 is an important receptor expressed by FDCs responsible for humoral immune responses, although there is no evidence that expression of this receptor has a role in GC organisation.

CXCL13 has been shown to be expressed in FDC-enriched cell preparations (Tjin et al., 2005), cultured FDC cell lines (Toellner et al., 1995) and FDCs present within inflammation-induced ectopic lymphoid follicles (Shi et al., 2001). CXCL13 is the chemokine, expressed by FDCs, responsible for the migration of B cells to the light zone of the GC and therefore it can be presumed that depletion of FDCs from the GC results in disorganisation of the microarchitecture due to the loss of CXCL13 expression. CXCL13 signals to B cells through the receptor CXCR5 on their cell surface and, among other responses, causes an increase

in LT production (Aguzzi et al., 2010). It is known that a direct result of LT on FDCs is upregulation of CXCL13 production (Aguzzi et al., 2014); therefore, a feedback loop is created between the two cells. CXCL13 has been detected in concentrations as high as 1 ng/mg of total spleen and lymph node tissue, indicating that local concentrations are likely to be highly chemotactically active (Luther et al., 2002). S1PR2, a receptor for chemokine sphingosine 1 phosphate (S1P), is upregulated on GC B cells due to the mandatory expression of the receptor for entering the GC (Green et al., 2012). S1P has been shown to inhibit the attracting effect of CXCL13 on GC B cells and FDCs produce low amounts of this molecule compared to other fibroblasts in surrounding tissues. This suggests the S1PR2 signalling on GC B cells is necessary to actively exclude them from SIP^{+} areas outside the GC; allowing access to CXCL13 producing GC FDCs (Green et al., 2012). Other signalling molecules including oxysterol 7a25-dihydroxycholestrol which binds to the GPCR EBI2 (GPR183) and S-Geranylgeranyl-L-glutathione (GGG) that binds to P2RY8 GPCR guide the localisation of B cell in the follicle (Pereira et al., 2009, Lu et al., 2019). Interestingly the enzyme gamma-glutamyltransferase-5 (GGT5) is highly expressed by FDCs generating a gradient of GGG that costrains B cells to the follicle (Lu et al., 2019).

Toll-like receptor expression

FDCs express Toll like receptors (TLRs), which are known to trigger and shape the adaptive immune response to pathogens and stress. FDCs express TLR4 which responds to lipopolysaccharide (LPS) from Gram-negative bacteria. Expression of TLR4 is upregulated during GC responses, suggesting that FDCs can influence the adaptive immune responses through detection of innate immunity ligands (Shikh et al., 2007). Deletion of TLR4 expression in the stromal compartment results in reduction of GC size and affinity maturation is diminished (Garin et al., 2010). In addition to this observation, deletion of downstream signalling molecule myeloid differentiation primary response protein 88 (Myd88), abolishing TLR4 signalling, or by depleting vitamin A, results in smaller GCs, fewer FDCs and a reduced level of IgA antibodies, showing class switch recombination is recurring less

frequently and the GC response is reduced. The effects of LPS on FDC activation were shown to be TNFR1 independent (Milicevic et al., 2011). Bone marrow chimeric mice that lack TLR4 expression on stromal cells, were shown to have lower levels of SHM and high-affinity antibody production than wt. mice, further suggesting the expression and signalling pathways of TLR4 in FDCs is crucial for robust antibody responses (Garin et al., 2010). Although there is likely a complex interplay between TLR4 expressing innate immune cells that produce inflammatory cytokines and chemokines and the stromal fibroblast populations.

Additionally, stimulation of FDC expressing TLR2 and TLR4 induced increased expression of TGFβ and BAFF, leading to IgA class switching in B cells (Suzuki et al., 2010). This study also suggested that TLR signalling may regulate FDC function due to the increase of chemokine and adhesion molecule expression upon stimulation with TLR ligands. Mice immunised with nanoparticles containing antigen and ligand for TLR4 and TLR7 caused sustained GCs that persisted for more than 1.5 years (Kasturi et al., 2011). The presence of these ligands enhanced B cell affinity maturation, suggesting that, as FDC expression of TLRs is crucial for GC B cell SHM, therefore TLR ligands may cause increased B cell responses by directly affecting FDC function.

Interestingly, FDC activation by TLR ligands may have the capacity to promote autoreactive B cell responses (Das et al., 2016). Exposure of FDCs to self-antigen lead to the expression of INFα and TLR7 activation. FDCs were shown to have the ability to cycle and present self-antigen after internalisation through CD21 and further activate TLR7. The IFNα expressed by these cells was shown to promote autoreactive B cell survival, therefore this mechanism of FDC activation could enhance autoimmune reactions.

Prevention of autoimmunity and induction of apoptosis in GC B cells

Random gene rearrangements and point mutations as part of the mutagenesis process in the GC reaction by B cells can result in these cells becoming self-reactive. FDCs prevent

autoimmunity by regulating the clearance of apoptotic GC B cells, of which there are large numbers as a result of the evolutionary selection process, as the vast majority of B cells within the GC do not achieve high antigen affinity. FDCs control GC B cell survival and show highly specialised macrophages, TBMs, which cells to phagocytose, thereby ensuring that apoptotic bodies are properly disposed of (Kranich et al., 2008). The protein responsible for induction of engulfment of apoptotic germinal centre B cells by TBMs is the secreted phosphatidylserine-binding protein milk fat globule epidermal growth factor 8 (Mfge8). Splenic Mfge8, in a study using bone marrow chimera transfer between wild-type and Mfge8$^{-/-}$ mice, was shown to be derived from FDCs. TBMs acquire Mfge8 if they are situated in the proximity of Mfge8-expressing FDCs or in the lymph nodes that drain exogenous Mfge8. Mfge8$^{-/-}$ mice are seen to have impaired engulfment of GC B cell corpses by TBMs and suffer from autoimmunity, confirming that expression of this protein by FDCs is essential to facilitate the removal of apoptotic and self-reactive B cells which could lead to disease.

A mouse model, in which the animals were engineered to conditionally express a membrane-bound self-antigen on FDCs, was used to show that self-antigen displayed on FDCs can mediate the elimination of self-reactive B cells at the transitional stage within SLOs (Yau et al., 2013). This study suggests that long term retention of self-antigen on FDCs may be an important function of these cells even under circumstances where the exposure to self-antigen is transient. Results from other studies complement these observations. It was shown that FDCs had the ability to retain autoantigen-containing immune complexes in a study that observed self-reactive IgG-expressing memory B cells and plasma cells generation was a by-product of random V gene diversification in the germinal centre (Scheid et al., 2011). Additionally, studies in human and mice have shown that complement deficiencies are associated with lupus-like symptoms; these symptoms were attributed to defects in immune complex removal as well as direct effect on B cell selection, therefore allowing the survival of autoreactive B cells (Carroll et al., 2000). Finally, studies show that loss of FcγRIIB, an important negative regulator of B cell activation, results

in loss of B cell tolerance (Tiller et al., 2010). Conclusions as to whether FcγRIIB-mediated retention of self-antigens by FDCs contributes to the maintenance of B cell tolerance have not been determined (Sharp et al., 2012).

Although FDCs play a role in preventing autoimmunity by promoting ingestion of dying B cells, presentation of autoimmune complexes by FDCs can also contribute to autoimmune disorders when appropriate regulation of these interactions fail to occur. This presentation can also sometimes lead to subsequent FDC-mediated recruitment of self-reactive follicular helper T cells which in turn lead to the selection of autoreactive B cells. Diseases in which FDCs have been implicated in diseases such as Rheumatoid Arthritis (RA) and SLE (Vinusea et al., 2009). Using an RA mouse model, it was shown that mice develop high levels of anti-glycosylphosphatidylinositol (GPI) autoantibodies targeting GPI-anchored surface proteins. Drugs, such as decoy receptors for TNF and LT, ameliorate RA in mice and humans by interfering with FDC integrity. Natural IgM is present in the serum in the absence of an antigenic stimulus and has been shown to have low levels of self-reactivity (Coutinho et al., 1995). In RA, natural IgM binds to nuclear protein released from dying cells, resulting in immune complex (IC) deposition on FDCs and presentation to and selection of autoreactive GC B cells (Fu et al., 2011). There are also increased levels of IgM antibodies in obesity associated inflammation (Arai et al., 2013). The study revealed that IgM loaded with antigen formed a large immune complex, containing various elements, including apoptosis inhibitor of macrophage (AIM); it was shown that these complexes were responsible for the increased autoantibody production in mice fed a high-fat diet. As AIM was contained within the immune complexes, renal excretion of this protein was prevented, increasing blood AIM levels. While associated with AIM, IgM binding to the Fcα/μ receptor on FDCs was inhibited, preventing internalisation of IgM molecules through this receptor. Increased IgM levels in the blood supported IgM-dependent autoantigen presentation to B cells, which in turn stimulated IgG autoantibody production. In contrast, within $AIM^{-/-}$ mice, these responses were abrogated (Arai et al., 2013). These data suggest a model in which

increased IgM and AIM within these mice leads to the generation of isotype-switched pathogenic autoantibodies.

Expression of other factors affecting the GC response

FDCs have also been shown to provide a variety of factors with putative roles in the GC reaction. Human tonsil FDCs have been shown to express ligands for Notch, DII1 and Jg1, and *in vitro* experiments that block Notch signalling using gamma-secretase in FDC cell lines resulted in reduced GC B cell survival, therefore the expression of these proteins are thought to function to protect GC B cells from apoptosis (Yoon et al., 2009). Further supporting this observation is the cooperation between Notch and BAFF produced by FDCs known to support GC B cell growth; this was shown through blockage of both molecules simultaneously resulting in further decrease in B cell survival compared to blockage of the protein's individually (Yoon et al., 2009). Additionally, Wnt5a expression by FDCs in culture has been shown to increase GC B cell survival by inducing Wnt/Ca^{2+}-dependent activation of NFAT, NFκB, and BCL6 (Kim et al., 2012).

Using an *in-silico* subtraction approach, the transcriptome of murine FDCs was analysed, identified transcripts for well-established FDC markers, such as CXCL13, Mfge8 and MadCAM1, as well as molecules such as, Serpina1, Cochlin, Perostin, the prion protein and Enpp2, which has not previously been associated with FDCs (Wilke et al., 2010). The function of many of these proteins on the GC reaction have not been investigated in detail, however a recent study on the extracellular matrix protein, cochlin, revealed a role in modulating innate immune responses (Py et al., 2013). This protein was shown the be specifically expressed by FDCs and selectively localised in the extracellular network of conduits in the spleen and lymph nodes. Upon inflammation, cochlin is cleaved and released into the blood stream where it acts on the production of cytokines, recruitment of innate immune effectors, and bacterial clearance. *Choch*$^{-/-}$ mice had defects in cytokine production, recruitment of immune effector cells and bacterial clearance, leading to reduced survival in models of lung infection with *Pseudomonas aeruginosa* and *Staphylococcus aureus*. As the

deficient mouse model show no defects in germinal centre formation, immunoglobulin responses or antibody affinity maturation, this protein is not thought to be involved in the FDC function of activation of B cells. These data suggest FDCs use this protein affect the innate immune response, but studies into the importance of this protein in these cells have not been undertaken at present.

An additional important role for FDCs is the provision of survival signals and cytokines to enhance the GC reaction. FDCs are a source of BAFF (Suzuki et al., 2010), a B cell survival factor required for B cell homeostasis, and therefore may impact the survival of GC B cells through this mechanism. Studied undertaken in mice deficient in BAFF or its receptor initially develop GC responses, but these are not sustained (Vora et al., 2003). Additionally, high-affinity antibody responses within these mice were attenuated, but analysis of the V region gene indicated that somatic hypermutation is still able to occur. Together these data provide evidence that BAFF is required for the maintenance, but not the initiation, of the GC reaction. Targeting of BAFF by Belimumab (GSK) has shown clinical success in the treatment of SLE.

FDCs are also a source of the pro-inflammatory cytokine IL6; mice deficient in this cytokine have a reduction in the size of their GCs (Kopf et al., 1998). These mice also exhibit defective upregulation of C3, this reduction in complement-mediated signalling is thought to be associated with the altered GC phenotype. Another study confirmed that IL6 produced by immune complex-active FDCs promotes GC reactions, IgG responses and somatic hypermutation (Wu et al., 2009). They showed that activating FDCs with immune complexes increases the production of IL6 and that antibodies against IL6, inhibited specific antibody production *in vitro*.

7.3 B cells

Mature B cells can be divided into two lineages named B1 and B2 (Browning et al., 2006). B1 cells are long-lived, emerging early in development, are self-renewing and produce polyreactive IgM's that are considered essential for defence against encapsulated bacteria, also known as natural antibodies. In contrast, B2 cells, found within the B cell follicle, have the capacity to generate hypermutated class switched antibodies. B2 cells are routed into a mature follicular B cell or marginal zone B cell program. Follicular B cells traffic through SLOs and are involved in the adaptive humoral response. Through the GC reaction B cells undergo rapid proliferation and can differentiate into either plasmablasts that differentiate into plasma cells or memory B cells. Plasma cells derived from this mechanism express a unique signature of chemokine receptors and decrease expression of receptors for CXCL13, CCL21 and CCL19, allowing their migration from the GC to the medullary zone and then to the bone marrow, where they typically reside for 6-12 months in mice (Kunkel et al., 2003). Marginal zone B cells reside in the marginal zone of organs allowing them to sample the blood stream for pathogens.

B cell activation requires interactions between antigen-primed B cells and follicular helper T cells via a CD40 ligand (CD40L) and secretion of the cytokine IL4 (Purwada et al., 2015). CD40 signal alone can induce activated B cells to differentiate down the memory pathway but not into germinal centre cells; for this additional cytokine signalling is required (Rickert et al., 2005). IL21 has been shown to upregulate BCL6 in B cells, which is a crucial factor for germinal centre formation and maintenance. FDC presentation of antigen by CD21 is known to be important for B cell activation as IgG titres are declined in CD21 deficient mice (Carroll et al., 2012).

Activation of B cells is controlled by a number of regulatory molecules, including the surface immunoglobulin receptor complex. This complex is formed of a surface IgM molecule (BCR), CD19, CD21, CD81 and CD228 (Leu-13). CD19 and CD21 non-covalently associate in this multimolecular signal transduction complex to enhance B cell activation by lowering the

threshold for this mechanism to occur (Matsumoto et al., 1991). CD19 is a 95 kDa Ig superfamily glycoprotein expressed from the early stages of B cell development until plasma cell differentiation; its expression is restricted to B cells and FDCs (Tedder et al., 1994). Studies using CD19 monoclonal antibodies *in vitro* first suggested a role for this receptor in activation of B cells, as blockage of signalling resulted in a decreased activation of these cells (Bradbury et al., 1992). As CD21 is expressed much later in development than CD19 and CD81, it is thought that signalling via this complex is developmentally regulated (Tedder et al., 1994). As CD21 has the ability to bind C3dg, binding of immune-complexes by this complex results in delivery of co-stimulatory signals to B cells, lowering the activation threshold. This will be discussed in further detail throughout the thesis.

7.3.2 B cell function

The main and most well-known function of B cells is their role in humoral immunity. In addition to this essential role, B cells also mediate many other functions important for immune homeostasis. B cells are required of the initiation of T cell immune responses. This was first discovered using administration of anti-IgM antiserum to deplete mice of B cells at birth (Ron et al., 1981). Animals were subsequently primed *in vivo* by antigen and *in vitro* analysis of their draining lymph node revealed that their T cell proliferative responses were severely impaired. Most recent studies in which B cells were depleted using CD20 depleting antibodies in normal adult mice, confirmed these early studies revealing that B cells are essential for optimal CD4 T cell activation during immune responses to low-dose foreign antigens (Bouaziz et al., 2007). Within these mice, plasma cells still remain, as this cell subset is $CD20^-$. Additionally, *in vivo* dendritic cell ablation revealed both B cells and dendritic cells are needed for optimal antigen-specific CD4 T cell priming.

B cell deficient mice have many abnormalities within the immune system, including a decrease in T cell number and diversity, defects within the spleen DC and T cell compartments and the absence of FDC networks (LeBien et al., 2008). These observations reveal a critical role in the development of the immune system but also show B cells are

important for its maintenance. B cells have been shown to release immunomodulatory cytokines which have been shown to influence antigen-presenting cell function, regulate wound healing and influence tumour immunity (LeBien et al., 2008). A subset of TNF-1 and IL10 expressing B cells have been described and are termed regulatory B cells (Mizoguchi et al., 2006). These cells were shown to regulate T cell-mediated inflammatory responses. In IBD, regulatory B cells have been shown to suppress inflammation by directly dampening proinflammatory responses such as IL1 and TNFα production by macrophages (Mizoguchi et al., 2000).

7.4 Autoimmune disease

In healthy individuals, the immune system is a complex set of mechanisms with the role of protecting hosts from infectious pathogens; however, this system can become dysregulated. Deficiencies in immune components can eliminate the system's ability to respond to pathogenic threat. Alternatively, the failure of the immune system to distinguish self from nonself antigen, leading to a breach in tolerance, ultimately leads to the manifestation of autoimmune disease.

Autoimmunity and its mechanisms that lead to clinical disease were first recognised around 50 years after the work by Macfarlane Burnett and his hypothesis of the "forbidden clone" that won the Nobel Prize in 1960. This hypothesis initially proposed that autoimmunity develops due to activation of clones of cells that can react against the body by a viral infection or some metabolic change. These clones were thought to attack the tissues of the body resulting in the presentation of disease. Since then, studies have confirmed this hypothesis and contemporary theories now suggest that the development of an autoimmune disease requires a genetic predisposition and environmental factors that trigger the pathways leading to tissue destruction (Wang et al., 2015). It is now thought that 3-5% of the

population are affected by autoimmune disease, with autoimmune thyroid disease and type I diabetes being the most common reported conditions (Jacobson et al., 1997).

Autoreactive cells prevail when immune tolerance is lost. Central tolerance in the thymus and bone marrow plays a key role in shaping immune system homeostasis. In healthy individuals, lymphocytes with potential self-reactivity are negatively selected and deleted in the thymic medulla. Upon exciting the thymus, mature T cells are selected again, in a process named peripheral tolerance; during this process most self-reactive T cells are deleted or rendered anergic. Immature B cells are usually deleted by a process named clonal deletion or clonal anergy if they express surface IgM that recognises self-surface proteins. Mature B cells also undergo peripheral tolerance, but autoreactive B cells are known to escape deletion by the process of receptor editing.

It is possible for cells with self-reactive properties to be missed by this tolerance system as many cells are made on a daily basis. However, in otherwise healthy individuals this does not necessarily lead to disease. Autoantibodies are often observed in healthy individuals, such as antinuclear antibodies and rheumatoid factor and these are thought to help detection and degradation of self-antigens (Panda et al., 2015). When immune tolerance is broken, and autoantibodies and self-reactive lymphocytes become involved in inflammation, autoimmunity develops.

7.4.2 Autoreactive B cells

B cells can contribute to autoimmune diseases in a number of ways. These include; secretion of autoantibodies, presentation of autoantigen, secretion of inflammatory cytokines, modulation of antigen processing and presentation and generation of ectopic GCs.

Autoantibodies are detected in many autoimmune diseases and in some diseases these antibodies themselves can have a pathogenic effect. Somatic hypermutation is one mechanism in which autoreactive antibodies can be produced. Autoantibodies are found in

patients with Rheumatoid Arthritis (RA); these antibodies typically target rheumatoid factor, type II collagen (CII) and citrullinated proteins and are found in the synovial fluid and serum of ~70% of patients with early RA (Cook et al., 1994). Rheumatoid factors (RhF) are autoantibodies specific for the Fc portion of IgG, 30% of healthy individuals have detectable levels of these antibodies within their serum, however, because they are low affinity and low titre, these antibodies do not cause any significant pathology (Kyburz et al., 1999). In disease, it is thought that RhFs form complexes with antigen to promote release of inflammatory factors, leading to increased disease pathology (Sakaguchi et al., 2003). CII-specific autoantibodies were shown to have a pathogenic role in a study using an animal model termed collagen-induced arthritis (Holmdahl et al., 1986). Native collagens consist of three polypeptide chains linked in triple helices, type II collagen is composed of three α1-type II chains (Trentham et al., 1978). Mice were immunised with CII antigen and developed CII-specific antibodies which lead to the triggering of arthritic symptoms; interestingly some antibodies against auto-antigens were shown to be more pathogenic than others. Passive transfer of these antibodies (Stuart et al., 1982), antibodies from RA patients (Wooley et al., 1984) or monoclonal antibodies specific to CII (Nandakumar et al., 2003) also caused healthy mice to develop arthritic symptoms to varying levels dependent on CII-specificity, isotype and Fc receptor dependency, further supporting their pathogenic role in disease. High doses of mAb are needed to provoke arthritic responses, concentrations as high as 9 mg of mAb were needed to induce moderate arthritis in mice (Nandakumar et al., 2003); as anti-CII epitopes are likely located in a repetitive structure on the surface of cartilage, it is possible that multimeric complexes form on joint surfaces, favouring arthritogenicity and also explaining why high doses of antibody are needed to elicit this response. Antigens of type I and III collagen however are not arthritogenic, even at high doses (Trentham et al., 1978). Indeed, CII-specific antibodies are thought to mediate immune complex formation in the joint resulting in complement activation and recruitment of inflammatory cells. Once cells are recruited to the joint and have been activated, proinflammatory cytokines will be produced, further activating the immune response. These cytokines will recruit synovial macrophages

and infiltrating mononuclear cells, leading to the eventual release of tissue-degrading enzymes that cause cartilage damage and worsen disease (Firestein et al., 2003). Passive transfer of anti-DNA antibodies into healthy mice induced features of SLE, showing that these autoantibodies also contribute to the pathogenesis of this disease (Tsao et al., 1992).

Within diseases such as systemic lupus erythematosus, rheumatoid arthritis and Sjogren's syndrome, the deposition of immune complexes composed of autoantigens bound by autoantibodies is a prominent feature that contributes to disease pathology (Hampe 2012). These complexes trigger inflammation through activation of complement and Fc-receptor-dependent effector functions, such as antibody-dependent-cell-mediated cytotoxicity (Martin et al., 2004). Experimental models have shown that activation of complement by these immune complexes and have also been observed in the kidneys of patients with SLE and lupus nephritis (Quigg et al., 2004).

Autoreactive B cells can act to stimulate or inhibit receptor functions through the action of autoantibody production. This was illustrated in a study focusing on autoantibodies targeting the thyroid stimulating hormone (TSH) receptor (Ando et al., 2005). TSH receptor autoantibodies are found in Graves' disease and have been shown to stimulate the receptor function. This leads to the release of thyroid hormones and development of hyperthyroidism. In contrast, other autoantibodies against the TSH receptor found in autoimmune hypothyroidism block the binding of TSH to the receptor, thereby inhibiting the receptors function (Michalek et al., 2009).

Autoantibodies also facilitate the uptake of self-antigen by antigen presenting cells (APCs). Monocytes and dendritic cells have been shown to use the Fc receptors expressed on the cell surface to take up antigen complexed with autoantibodies (Takai et al., 2005). Normal T cell tolerance is broken by presentation of these autoantigens to T cells by the APCs. This mechanism was confirmed in studies using autoantibodies to thyroid peroxidase antigens, in which these antibodies enhanced the uptake of antigens by APCs and consequently,

activated thyroid peroxidase-specific T cells (Nielsen et al., 2001). This response can be blocked by using blocking antibodies against FcγRs (Nielsen et al., 2009).

In contrast to these functions, autoantibodies have also been reported to have protective functions and natural autoantibodies are often found in healthy individuals (Shoenfeld et al., 2005). These antibodies are usually polyreactive and react with both self and non-self-antigens. The natural autoantibodies present in mice are secreted by the B1 subset of B cells and are often of the IgM isotype (Baumgarth et al., 2005). One role for the nonspecific and low-affinity binding action of these natural autoantibodies may be to prevent autoreactive clones from reacting vigorously with self-antigens; it is thought that binding of natural autoantibody may mask the epitopes of pathogenic autoantibodies (Shonefeld et al., 2005). Higher levels of IgM are associated with apoptotic cell clearance and lower disease activity in patients with SLE (Gronwall et al., 2012). Pathogenic IgG autoantibodies are symmetrically glycosylated, whereas it was found that 10-20% of the total IgG molecules in sera are asymmetrically glycosylated (Mathov et al., 1995). The asymmetric glycosylation of these autoantibodies fail to trigger immune effector mechanisms or form insoluble complexes with antigens; therefore, these molecules are self-specific but have no deleterious effect in normal individuals and act as autoprotective antibodies. Competition for self-antigen between these antibodies and the pathogenic symmetrically glycosylated autoantibodies resulted in protection from severe immune responses in rats, confirming their protective role (Margni et al., 1998). Rheumatoid factor (RhF) autoantibodies are found in many autoimmune diseases. There is controversy over whether the presence of RhF antibodies exerts protection or induces disease. The presence of these autoantibodies in SLE patients was directly related with disease prevalence (Turner-Stokes et al., 1989), however many other studies have demonstrated a protective role against the development of lupus nephritis for example (Shonefeld et al., 2005). In another study RhF antibodies were shown to have the ability to block attachment of C3b, which is capable of reacting with

glomeruli receptors, indicating that these antibodies may have a role in inhibiting binding of immune complexes (Bolton et al., 1982).

B cells also act as antigen-presenting cells in autoimmune diseases such as rheumatoid arthritis (O'Neill et al., 2005) and type 1 diabetes (Wong et al., 2004). Using nonobese diabetic (NOD) mice engineered to express a transgene encoding a mutant heavy chain immunoglobulin allowing presentation on the cell surface but prevents secretion of antibodies, the importance of antigen presentation in type 1 diabetes, in the absence of antibody production, thought to be unimportant in this disease, was investigated (Wong et al., 2004). Compared with transgene-negative B cell deficient mice, there was increased insulitis and incidence of diabetes in transgenic mice; implicating an antigen presenting function of B cells in disease development; however, disease level is not restored to that of wildtype NOD mice. Due to presentation of antigen through antigen-specific BCRs, rather than internalisation of antigen in other APCs, B cells are able to present antigen present at low concentrations; this mechanism is 1,000-10,000-fold more efficient than pinocytosis and is thought to be the mechanism allowing autoantigens to be presented (Lanzavechia et al., 1987).

The production of proinflammatory cytokines by activated B cells, such as IL6, IFNγ and IL4, further increase the inflammatory response by modulating the migration of dendritic cells, activating macrophages and providing feedback stimulatory signals for further B cell activation (Hampe 2012).

Additionally, autoreactive B cells are able to aid in the *do novo* generation of ectopic GCs within inflamed tissues (Martin et al., 2006). These structures have been described in numerous autoimmune diseases such as RA, SLE and Graves' disease. It is thought that ectopic GCs are not a unique disease-specific occurrence but a consequence of chronic inflammation. Inflammation is maintained within these structures due to residing plasma cells secreting autoantibodies (Manzo et al., 2005).

Autoreactive B cells may occur due to loss of tolerance which could be faulted by genetic mutations at tolerance checkpoints. The Sle1 locus located on the telomeric chromosome 1 has been linked to SLE in several mouse models and human patients (Wakeland et al., 2001). Functional analyses carried out in B6.Sle1 congenic mice carrying Sle1 on a non-autoimmune B6 background, revealed this locus induces a loss of tolerance to nuclear antigens in B cells and activation of $CD4^+$ T cells (Mohan et al., 1999). Further studies using a mouse model carrying the lupus susceptibility locus, it was shown that faulty negative selection at the immature B cell stage leads to spontaneous development of severe lupus nephritis in these animals through the action of anti-histone autoreactive T cells (Chen et al., 2005). Over-expression of CD19 in mice was shown to lead to increased levels of serum antibodies, resulting in increased B cell activation (Engel et al., 1995). As surface CD19 lowers the threshold for B cell activation, these results show that increased B cell signalling by overexpression of signalling molecules is another factor that can lead to autoimmunity. Interestingly, loss of CD19 reversed the phenotypes observed when the receptor is overexpressed (Zhou et al., 1994). Additionally, mouse studies highlighted that, lack of FcγRIIB expression on B cells leads to autoimmunity (Boross et al., 2011), which was also reflected in humans when the finding that patients with lupus express lower levels of this receptor due to a polymorphism in their FcγRIIB promoter (Blank et al., 2005).

B cell activation factor (BAFF) overexpression in transgenic mice was shown to cause an expansion of peripheral B cells (Manca et al., 1991). These animals had increased autoantibody levels and developed a lupus-like disease. In addition to this observation, increased levels of BAFF have been observed in the serum of patients with RA (Rochas et al., 2009), SLE (Pers et al., 2005) and Sjorgren's syndrome (Youinou et al., 2012). By measuring the levels of circulating BAFF and sCD23, an indication of B cell activation, it was shown that there was no correlation between BAFF concentration and B cell activation in patients with SLE or RA; however high levels of BAFF were associated with the presence of autoantibodies, ds-DNA antibodies in SLE and rheumatoid factors in RA (Pers et al., 2005).

An Ig/HEL-double transgenic mouse model further demonstrated the importance of BAFF in autoreactive B cell survival and function (Lesley et al., 2004). These autoreactive cells were shown to have an increased dependence on BAFF for survival; the increased BAFF concentration received by these cells lead to increased levels of NFκB, p52 and prosurvival kinase Pim2. The greater dependence of these autoantigen binding B cells on BAFF cause them to be poor competitors relative to non-autoantigen binding B cells. When placed in a diverse B cell compartment, these cells undergo apoptosis as BAFF receptor engagement and signalling is reduced. In elevated BAFF levels all autoantigen-engaged cells to be rescued from rapid competitive elimination; therefore, individuals that produce high BAFF levels may be more susceptible to the survival of autoantigen binding B cells (Lesley et al., 2004). Furthermore, as deficiencies in apoptosis have been shown to lead to the development of lupus-like diseases, BAFF might also play an anti-apoptotic role in B cell tolerance loss (Pers et al., 2005).

7.5 Complement and its role in autoimmune disease

The complement system is composed of a network of over 30 tightly regulated proteins, either present as soluble proteins in the blood or membrane-associated proteins, that play an important role in host defence and inflammation. Activation of the complement pathway leads to opsonisation of pathogens, resulting in a number of mechanisms resulting in an immune response, the most common of these being removal of opsonised pathogens by phagocytes, attracted by the formation of anaphylatoxins C3a and C5a, and cell lysis (Sarma et al., 2012). Inappropriate activation of this pathway, as well as complement deficiencies, lead to many autoimmune diseases such as SLE and asthma. The complement system was first thought to be involved only in the innate immune response, but more recently increasing evidence has shown an important role for these proteins in adaptive immunity, specifically helping the elimination of pathogens by T and B cells and in maintaining immunologic memory preventing pathogenic re-invasion (Dunkelberger et al., 2010).

7.5.2 The complement pathway

Complement activation occurs through three individual pathways, which converge at C3, the most abundant complement protein found in the blood (Sarma et al., 2012). These pathways are named; the alternative, classical and lectin pathways, and all result in the formation of the membrane attack complex. The alternative pathway is triggered by carbohydrates, lipids and proteins found on non-self surfaces and the lectin pathway is activated by mannose binding lectin or Ficolin binding to their ligands on the surfaces of yeast, bacteria, parasites and viruses (Qu et al., 2009). The classical pathway is initiated by immune complex binding to pathogens or non-self-antigens. Immune complexes are formed from IgG or IgM molecules binding to said antigen. It is this pathway that is the focus of this thesis.

The classical pathway begins with the C1 complex, formed of C1q, C1r and C1s, which binds to the Fc portion of the IgG or IgM molecule on the immune complex. Binding is specifically through C1q to the exposed Fc portion of the antibody, which subsequently activates C1s and C1r. C1s is a protease than cleaves C4 and C2 to form the C3 convertase of the classical pathway, C4bC2a. Each pathway has its own complex that is able to cleave C3 to release C3a and C3b. C3b acts as an opsin, thereby helping to amplify complement activation by amplifying its own cleavage, in addition to aiding with phagocytosis in the continuation of the pathway. Other C3b molecules complex with C3 convertases to form a C5 convertase. This complex is composed of C3bBbC3b and C4bC2aC3b. C5 convertases cleave C5 into C5a and C5b. When C5b binds to C6 and C7, the membrane attack complex is initiated. C8 and multiple C9 molecules bind the C5bC6C7 complex to enable the MAC complex to insert itself into cell membranes and form a pore, allowing cell lysis to occur as the final result (Sarma et al., 2012) (Figure 7.6).

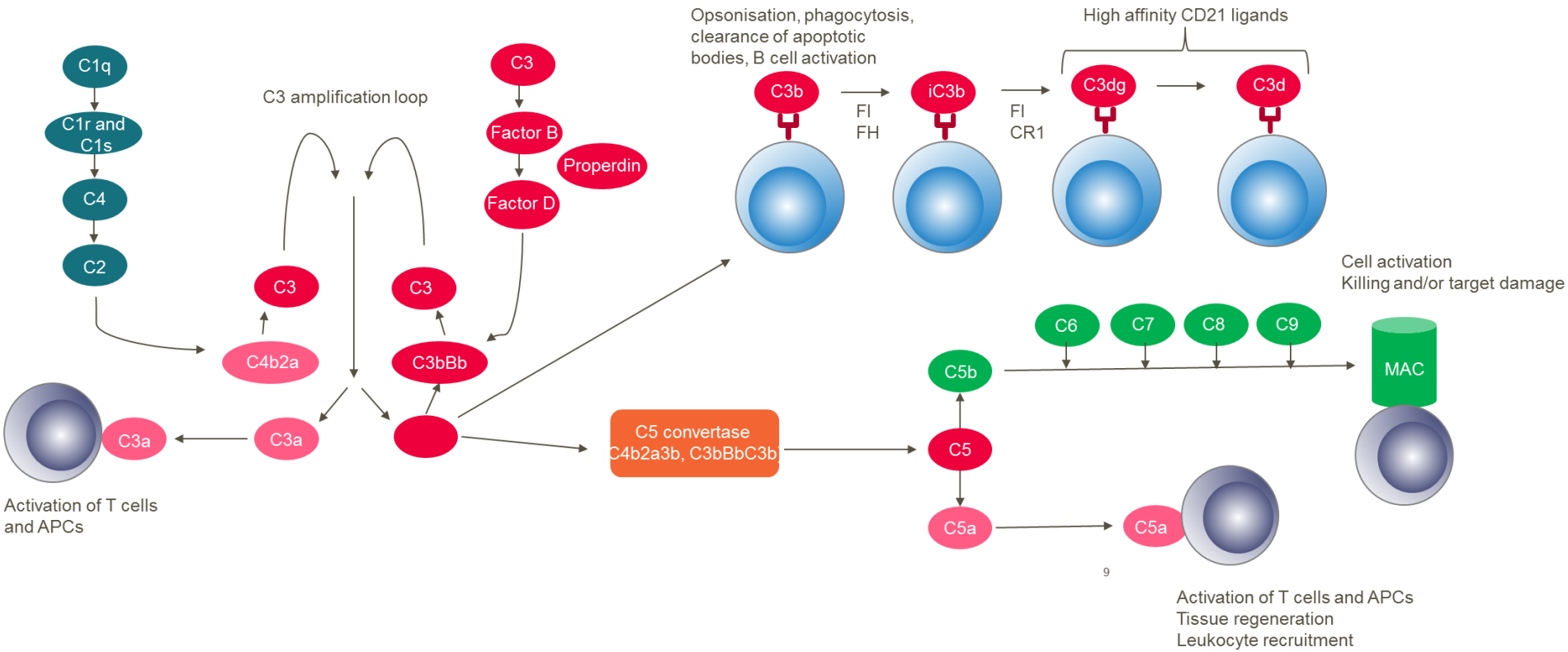

Figure 7. 6: The classical complement pathway

The C1q complex binds to the Fc portion of the IgG or IgM molecule on an immune complex, which activated C1s and C1r. C1s cleaves C4 and C2 to form the C3 convertase. C3 is cleaved and releases C3a and C3b. C3b acts as an opsin, amplifying complement activation by cleaving additional C3. Other C3b molecules complex with C3 convertases to form the C5 convertase. This leads to the cleavage of C5 into C5a and C5b. The membane attack complex is formed when C5b binds to C6 and C7. C8 and multiple C9 molecules allow the complex to insert itself into cell membrane. C3b can also be further modified in order to bind to CD21 expressed on B cells, which lowers the threshold for activation of these cells.

7.5.3 The function of C3 and C3 derivatives

C3 contains an internal thioester bond that undergoes spontaneous hydrolysis, increasing its susceptibility to cleavage to form C3b (Platt et al., 2017). The C3b derivative of C3 has an exposed carbonyl group which can form bonds with neighbouring nucleophiles; depending on the surfaces bound by C3b determines whether it will form a catalytic complex and continue the complement cascade, or whether cleavage occurs to form a catalytically inactive fragment C3d. C3b binds to the surface of antigen and interacts with CD35 and is converted to iC3b by fluid phase factor I and H. Further editing by factor I, using CD35 as a cofactor, results in cleavage to form C3dg (Topanta et al., 2006). C3d is the final derivative of this pathway, cleaved from C3dg. C3d does not further activate complement but results in C3d/g-tagged antigen that has the capacity to bind to CD21 expression on FDCs and B cells (Carroll et al., 2012), although C3dg binds with a higher affinity.

C3d and C3dg opsonised immune complexes, composed of antigen and IgM or IgG molecules, allow recognition of the antigen by FDCs and B cells through the interaction of C3dg and CD21. Binding of these derivatives of C3 to CD21 enhances antibody responses by reducing the threshold for B cell activation, due to simultaneous ligation of CD21 and surface Ig by opsonised immune complexes (Dempsey et al., 1996) and allows retention and internalisation of antigens by FDCs (Heesters et al., 2013). However, C3d has also been shown to enhance antibody titres in the absence of CD21, indicating that this protein can also enhance the immune response through CD21-independent mechanisms. In a study where CD21 knockout mice were immunised with streptavidin conjugated to C3dg or HIV-1 Env gp120-C3dg proteins, mice were shown to have increased titres of antigen specific antibodies compared to mice immunised with antigen alone (Haas et al., 2004). A couple of mechanisms for CD21-independent responses have been proposed including; a prolonged half-life of the antigen by opsonisation with C3dg or there could be a secondary receptor for C3dg that elicits this response. Indeed, C3dg has been reported to bind to many other proteins found in physiology (Karen et al., 2004).

C3dg opsonised antigen-complexes were shown to enhance recognition and specific antibody synthesis by antigen-specific B cells, even though the complexes can be taken up by both antigen-specific and non-specific B cells (Thornton et al., 1996). Primary protein keyhole limpet hemocyanin (KLH) was opsonised with C3dg to form immune complexes. These complexes were able to bind to the CD21 expressed on KLH-non-specific B cells, leading to antigen processing and presentation on MHCII molecules to KLH-specific helper T cells. It is these cells that then go fourth and activate the KLH-specific B cells. The opsonised immune-complexes were also shown to induce expression of CD80 co-stimulatory molecule on B cells by simultaneous CD21 ligation with C3dg and FcγRII stimulation by IgG. Ligation to either of these receptors resulted in the activation of a secondary co-stimulatory molecule, LFA-1 (CD11a, CD18).

It was hypothesised that C3dg could be used as a natural adjuvant to enhance the secondary humoral immune response. One study investigated the adjuvant effect of C3dg by immunising mice with an antigen of the influenza virus conjugated to three tandem copies of C3d (Ross et al., 2000). Antigen complexed with C3d induced a similar antibody titre to that in mice immunised with antigen alone. However, antibody avidity maturation was enhanced in those mice immunised with C3dg-immune complexes, which correlated with a more rapid appearance of protective immunity and complete protection from live virus challenge. These mice also had antibodies able to protect them from heterologous virus challenge, whereas mice immunised with antigen only, did not. In another study, self-antigen collagen type II was opsonised with C3d and injected into a mouse model for collagen-induced arthritis (Del Nagro et al., 2005). Mice were also inoculated with complete Freund's adjuvant (CFA), which is needed in many several animal models because it causes local inflammation and enhances antigen uptake. Mice that received opsonised antigen developed rheumatoid arthritis even in the absence of CFA, whereas mice that received CII alone did not develop RA, unless they heterologously received CFA. These results showed that C3d bypasses the need for a broad immunostimulatory effect elicited by a classical adjuvant.

As well as its possible role in disease, C3d may also have the potential to enhance immune responses by acting as an adjuvant in vaccines. DNA vaccines have been designed using C3d as the adjuvant leading to increased antibody titres against HIV-1 Env gp120 (Bower et al., 2006). Also fusion of hepatitis B antigen to C3d enhanced the antigen-specific antibody response in mice (Wang et al., 2004). Another study showed that free C3d inside tumour cells, or associated with irradiated tumour cells, accelerates anti-tumour T cell responses, allowing the prevention, and in some cases the reversal, of tumour growth (Platt et al., 2017). These effects on tumour immunity were shown to be B cell-independent; instead C3d was seen to increase tumour infiltrating $CD8^+$ T cells, by depleting Tregs and by preventing the expression of programmed cell death protein 1. These results suggest a potential role for free C3d in immune surveillance.

7.5.4 The role of complement in autoimmune disease

Although the complement system is important in the elimination of pathogens and mounting enhanced immune responses, dysregulation of this system has been shown to be involved in the pathogenesis of several autoimmune diseases such as SLE, Sjogren's Syndrome, systemic sclerosis and rheumatoid arthritis (RA) (Chen et al., 2010). As the mechanisms of this system as delicately balanced, when dysregulation occurs, the complement system has the ability to cause damage, mediating tissue inflammation (Ballanti et al., 2013). Additionally, complement deficiencies have been associated with an increased risk in autoimmune disease development.

Most heterozygotic complement-deficiencies are clinically normal; however homozygotic complement-deficient individuals develop clinical diseases (Ballanti et al., 2013). As complement deficiencies are usually caused by null alleles, from which functional protein is not produced, most heterozygotes produce half the normal plasma level of specific complement protein (Pettigrew et al., 2009). Exceptions to this observation are X-linked

recessive properdin deficiency, deficiency of C1 inhibitor which is autosomal dominant and mannose-binding lectin and factor I deficiencies which are autosomal co-dominant (Winkelstein et al., 2003). Deficiencies in complement components lead to presentation of; recurrent bacterial infections, HAE, rheumatic disorders, leukocyte adhesion deficiency, and haemolytic uremic syndrome (Pettigrew et al., 2009). Specifically, complement deficiencies within the mannose-binding lectin pathway lead to increased bacterial infections and more frequent *Neisseria* infections occurs as a result of deficiencies within the alternative pathway. Deficiencies in components of the classical pathway have been shown to lead to increased susceptibility to encapsulated bacterial infections and are implicated in SLE (Pettigrew et al., 2009). 30% of patients with SLE are deficient in C2 and nearly 80% of patients are deficient in either C3 or C4 (Etzioni et al., 2003). C3 deficiency in these patients presents as recurrent pyogenic infections and membranoproliferative glomerulonephritis rashes (Walport et al., 2001).

Interestingly, C3 or factor B deficiency within the collagen-induced arthritis (CIA) mouse model resulted in protection against disease development upon immunisation with CII (Hietala et al., 2002). These mice displayed a decrease in their CII-specific IgG antibody response compared to wild-type mice; suggesting that C3 and factor B have a role in the development of disease phenotype. Repeat administration of antigen triggered arthritis in all mice, including those with complement deficiencies. Interestingly, arthritic score within these mice was lower than that in wild-type. This study implicates both the classical and alternative pathway in the development of CIA. Within humans, plasma levels of C3 within patients with active RA is significantly higher than in controls (Di Muzio et al., 2011); increased C3 levels represented a negative prognostic factor for anti-TNF therapy. It is of note that synthesis of C3 has also been shown to occur in chronically inflamed tissues, such as the rheumatoid joint. Cells responsible for the production of this protein include, lining cells, fibroblasts, mononuclear phagocytes and endothelial cells (Whaley et al., 1992). Additionally, evidence that complement system activation occurs in the synovial fluid is abundant. Decreased levels

of complement components within the synovial fluid of patients are observed, but increased levels of cleavage products, C3a, C3c, C5a etc., are found within these compartments suggesting high levels of complement activation (Jose et al., 1990). Mechanisms leading to increased activation of the complement pathway in RA patients could include, an increased level of circulating immune-complexes, including rheumatoid factors which have the ability to activate the classical complement pathway (Zubler et al., 1976). Increased levels of anti-cyclic citrullinated peptide/protein antibodies are also found in RA patients; these may activate complement via both the classical and the alternative pathways (Trouw et al., 2009).

The report discussed above in which C3d conjugated CII was injected into a mouse model for collagen-induced arthritis (Del Nagro et al., 2005), was the first to demonstrate that C3d can induce pathogenic autoantibodies and suggest that this molecule could be involved in the development of other B cell-dependent autoimmune diseases.

Patients with systemic sclerosis (SSc) also have been shown to have lower C3 levels and this protein is now used as a candidate parameter for inclusion in the American College of Rheumatology classical criteria for SSc (Arthritis Rheum, 1980). Sjogren's syndrome (SS) is an autoimmune disorder of the exocrine glands and is associated with lymphocytic infiltrates of the affected glands. Low levels of C3 has also been observed in patients with SS, however it is the decreased C4 levels, and thus C3dg levels, that show the closest statistical association with mortality and lymphoproliferation (Ioannidis et al., 2002).

Additionally, proteins which are usually sequestered within cells, such as phospholipids and mitochondrial proteins, are recognised by the complement system and are able to activate the cascade if they become exposed by directly binding C1q or natural antibodies (Nauta et al., 2004). This activation leads to increased inflammation and recruitment of cells that further contribute to the inflammatory phenotype.

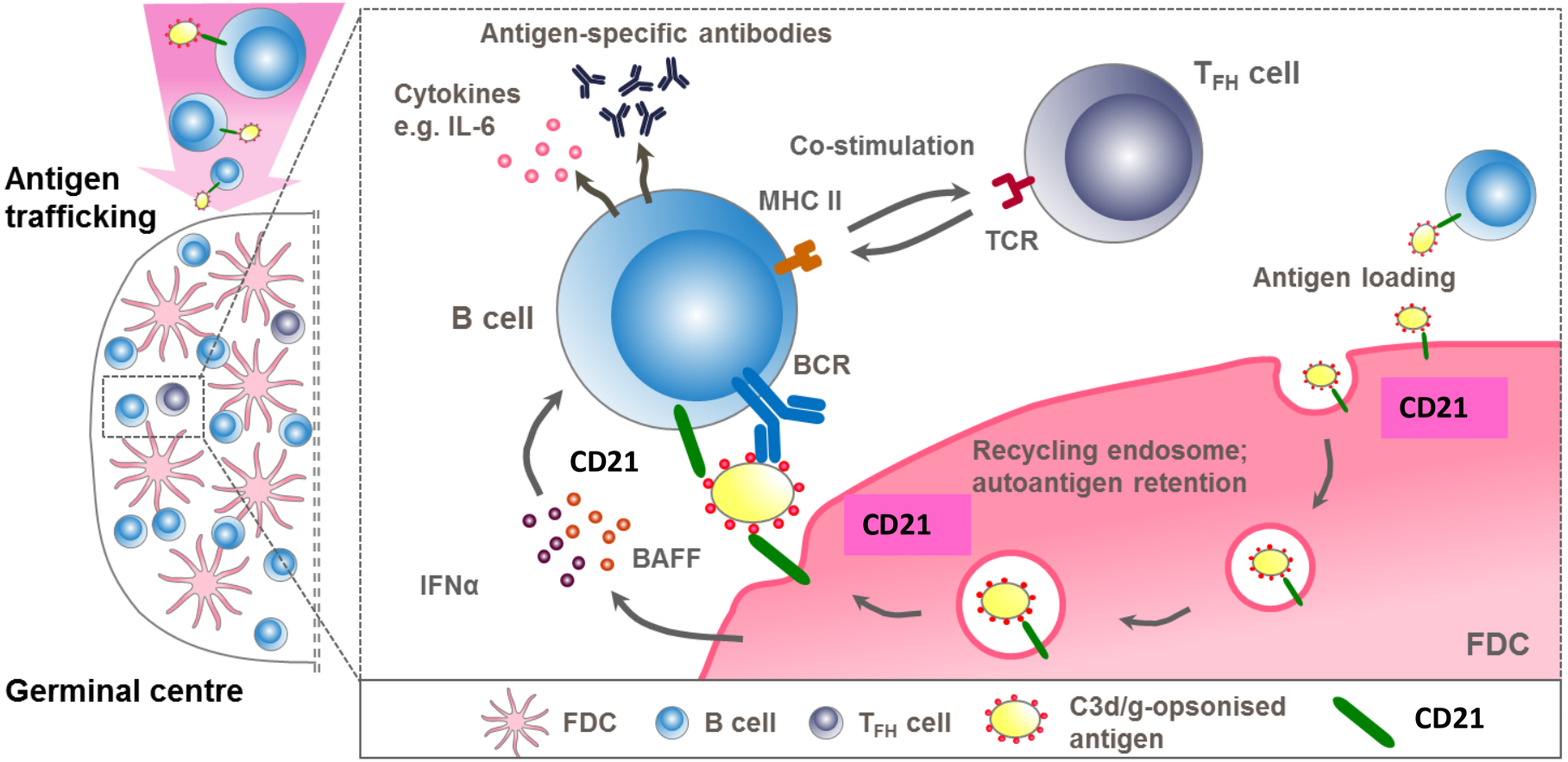

Figure 7. 7: Summary of the role of CD21 on FDCs and B cells

C3dg-opsonised immune complexes bind to CD21 expressed on B cells and cells traffic antigen to the germinal centre. Unidirectional transfer of the antigen occurs between CD21 on the B cell and CD21 on the FDC. FDCs internalise antigen-bound CD21 receptors and represent receptors to B cells expressing antigen-specific BCRs. This leads to antigen-specific antibody production when co-stimulation with T helper cells occurs.

7.6 Summary, thesis hypotheses and overall aims

Secondary lymphoid organs are essential for development of high specificity antibody responses. These responses primarily occur due to the germinal centre reaction, in which FDCs and B cells are the cells responsible for antigen presentation and subsequent high affinity antibody production, respectively. Interactions between these two cells types are essential for humoral immunity, but most published studies are carried out within mice due to the lack of a robust isolation protocol for human FDCs. FDCs and B cells within the germinal centre interact by the CD21 receptor which allows transfer of antigen from B cells to FDCs where it is retained and presented allowing recognition by antigen-specific B cells and subsequent antibody production. CD21 deficient mice do not develop GCs and have impaired antigen-specific immune responses (Carroll et al., 2012), therefore highlighting the essential function of this receptor in the development and function of the GC reaction. Due to these observations this receptor is the focus of this thesis. Little is known however about the exact mechanism of C3dg-opsonised antigen transfer between CD21 expressed on human B cells and FDCs.

Therefore this work aims to investigate the **hypothesis** that**:** *antigen transfer is due to (1) receptor number on the cell surface or (2) CD21 isoform expression on the different cell populations.*

CD21 and the complement pathway, including C3 and its derivatives, have been implicated in autoimmune diseases such as Rheumatoid Arthritis. The third results chapter in this thesis investigates the **hypothesis** that: *a soluble form of the CD21 receptor inhibits C3dg antigen complex binding to B cells, consequently dampening C3dg-mediated immune responses, therefore acting as a break on the immune response, which does not occur in autoimmune disease.*

The overall aims of this work are to:

1) Isolate and characterise human FDCs from human tonsil. Assess CD21 absolute receptor number on FDCs (tonsil derived), T and B cells (tonsil and blood derived).
2) Assess C3dg binding capacity of CD21 on FDCs (tonsil derived) and B cells (tonsil and blood derived), investigating potential differential C3dg binding between CD21S and CD21L isoforms.
3) Further understand the function and role of sCD21 in healthy volunteers and disease patients.

8. Materials and Methods

All human biological samples were sourced ethically and their research use was in accord with the terms of the informed consents under an IRB/EC approved protocol. Fresh healthy volunteer blood was derived from GSK BDU (Stevenage) under the Hertfordshire Ethics Committee (Ethics approval code: 07-H0311-103). Tonsil tissue was sourced from surgical discard at Lister Hosptial under the Cambs and Herts REC (Ethics approval code: 06/Q0204/25). Tonsils collected at the University of York were collected at York Teaching NHS Trust, ethically approved and informed consent was obtained from all participants. These tonsils were collected under NRES REC 12/NE/0360 approved study (IRAS: 114771) to Prof. Mark Coles and Prof. Charles Lacey.

Hepatic lymph nodes were collected during multi-organ donation procedures, after approval by the Medical Ethical committee of the Erasmus MC (MEC-2014-060) to Prof. Tom Cupedo by Prof. Wojciech G. Polak.

Human serum samples were used from the BEACON cohort at the University of Birmingham. The ethics for this study was from the West Midlands Black Country (Ethics approval code: 12/WM/0258).

All animal studies were ethically reviewed and carried out in accordance with Animals (Scientific Procedures) Act 1986 and the GSK Policy on the Care, Welfare and Treatment of Animals. Animals were kept under specific pathogen free facility at the University of York. All procedural work was done under a home office licence to Mark Coles.

8.1 Immunofluorescent Staining of Frozen Tissue

Snap frozen tissue was sectioned using a CryoStat (Leica) into 20 µm slices and stored on polylysine slides at -20°C until further use. For staining, sections were incubated at room temperature for 30 min and each section drawn around using a wax ImmEdge pen (Vector Laboratories). Samples were fixed in 4% paraformaldehyde for 10 min at room temperature before rehydration with PBS for a total of 15 min with changes of PBS wash every 5 min. Sections were incubated in a blocking buffer of PBS, 0.1% Tween-20 (Sigma-Aldrich), 0.1% Trition X-100 (sigma-Aldrich) and 5% serum (the serum of the host the secondary antibody was raised in) at room temperature (RT, 24°C) for 1 hour, this step significantly reduces non-specific antibody staining. Block was removed and, without any washing steps, primary antibody mix, made in blocking buffer, added (concentrations can be found within Table 1). Sections were incubated for 1 hour at RT. Slides were washed as above and secondary antibody added (as required), incubating for 30 min at RT. Slides were washed and a drop of Prolong gold (Invitrogen) was added to each section. To mount, a No 1.5 glass coverslip (Fisher) was added on top of the slide and incubated overnight at 4°C. Slides were sealed using nail varnish the next day. Stained slides were stored at 4°C prior to image analysis.

8.1.2 Confocal Microscopy

Immunofluorescent stained sections were imaged using the Zeiss LSM 880 confocal microscope. Samples were excited with 405, 488, 561 and 633 nm lasers and images acquired using either the 20X lens or 63X oil objective. Using the Zen acquisition analysis functions, tile scans and Z stacks were performed to image large tissue sections at high-resolution.

For comparability across experiments, laser power, pinhole and detector voltage gain & digital offset were kept constand. Each fluorophore was imaged on separate tracks to

minimise spillover and single colour controls were performed to ensure accuracy. Images were taken at 1024 x 1024 pixels and line averaging of 4.

For imaging chemokines (Figures 9.3.2, 9.3.3 and 9.3.4), the Airyscan module was used to increase spatial resolution beyond the diffraction limit of light. On a standard confocal microscope out of focus emission light is excluded through use of a pinhole at the focal plane. Image resolution is increased by decreasing the pinhole, but with the caveat of losing light energy. Airyscan deals with this issue using a hexagonal array of 32 detectors. Each detector acts as a small pinhole with positional information, this facilitates increased signal to noise ratio and spatial resolution in comparison to a standard confocal microscope (Huff, 2015).

Images were processed using ImageJ (Fiji), where z stack was merged at maximum intensity.

Antibody	Clone	Manufacturer	Conjugated	Concentration used
Anti-human CD19	HIB19	Biolegend	Alexa 488	1 in 200
Anti-human CD35	Ber-MAC-DRC	Santa Cruz	Unconjugated	1 in 200
Anti-human CD21	Bu32	Biolegend	Alexa 647	1 in 200
Anti-human CD21	R4/23	Origene	Unconjugated	1 in 200
Anti-human CD21	Bu32	Biolegend	Unconjugated	1 in 200
Anti-human CXCL13	53610	R&D Biosystems	Unconjugated	1 in 300
Anti-human CD3	HIT3a	Biolegend	Alexa 488	1 in 200
Anti-mouse CD3	17A2	Biolegend	Alexa 488	1 in 200
Anti-mouse CD21/CD35	7E9	Biolegend	Alexa 647	1 in 200
Anti-mouse CD19	6D5	Biolegend	Alexa 488	1 in 200
Secondary antibodies				
Goat anti-Mouse IgG (H+L) Cross-Adsorbed	IgG	Thermofisher Scientific	Alexa 488	1 in 2000
Goat anti-mouse IgG Cross-Adsorbed	IgG	Thermofisher Scientific	Alexa 647	1 in 2000

Table 1: Antibodies used for immunohistochemistry

8.2 Human Tonsil Tissue Digestion and FDC isolation

Tonsils were obtained from routine tonsillectomies from Lister Hospital, Stevenage and York Teaching Hospital, York (Andrew Coatsworth, Charles Lacey, Becky Wiggans). Using a protocol adapted from Karin Tatre (University of Rennes), the tonsils were briefly dipped in 70% ethanol and rinsed with PBS before being cut into small pieces (approximately 2 mm x 2 mm x 2 mm) using scissors and the tissue transferred to a 50 ml Falcon tube. Pre-warmed digestion buffer (Leibovitz's L15 Medium supplemented with L-Glutamine + 200 µg/ml + 800 µg/ml Dispase II + 100 µg/ml Dnase I) was added to cover the tissue to the 25 ml mark. The suspension was pipetted carefully up into a sterile 25 ml strippette and expelled fast against the side of the tube to help disperse the tissue; this was repeated a total of four times. The tube was incubated at 37°C in a water bath for 20 min, repeating the dispersion step half-way through the incubation. The supernatant was aspirated using a sterile Pasteur pipette and transferred to a 70 µm cell strainer placed onto a 50 ml Falcon tube. The cell suspension was made up to 35 ml with digestion buffer and centrifuged for 5 min at 200 xg, RT. Supernatant was removed, and the pellet resuspended in 25 ml of culture medium (RPMI1640 supplemented with 10% HI FCS, Glutamine and Penicillin/Streptomycin). Cells were counted using a Nucelocounter and cells pelleted as above. Cells were then either used for flow cytometry analysis, undergoing selective extraction through CD45 depletion and sorting for FDCs or frozen for future use.

For freezing, the cell pellet was gently resuspended in 1 ml of ice-cold HI-FBS per cryovial and transferred to vials. 150 µl of 100% DMSO was then added per vial and mixed gently by pipetting. The vials were transferred to a cooled Mr Frosty filled with 99.9% isopropanol and placed at -80°C for 72 hours; vials were then stored at -140°C for long term storage.

8.3 Fluorescence-activated Cell Sorting (FACS) from Tonsil Derived Human FDCs, T and B cells

Human tonsil digests were stained as described in section 8.8 with antibodies for identification of FDCs or T and B cells. Cells were sorted using a MoFlow (Beckman Coulter) or Aria (BD Biosciences). Cells were sorted through a 70 µm nozzle and separated by two-way separation. Cells were identified using FSC/SSC, doublets excluded using SSC-H vs SSC-W, and live cells selected. For the FDC panel, FDCs and FRCs were collected using lineage$^-$gp38$^+$CD35$^+$ (FDCs) and lineage$^-$gp38$^+$CD35$^-$ (FRCs) gating respectively (Figure 9.3.9). Lineage markers include CD34, CD11b, CD31 and CD45. For sorting T and B cells, cells were collected using CD3$^+$CD19$^-$ (T cells) and CD3$^-$CD19$^+$ (B cells) gating (Figure 9.3.10). Cells were collected into eppendorfs or FACS tube containing a small volume of FACS buffer (PBS with 0.1% BSA, Sigma, and 2mM EDTA, Invitrogen). Sorted cells were pelleted by centrifugation for 5 min at 450 xg and subsequently processed as desired.

Antibody	Clone	Manufacturer	Conjugated	Concentration used
FDC sorting				
Anti-human CD21	Bu32	Biolegend	PE	5 µl per 100 µl sample
Anti-human CD35	Ber-MAC-DRC	Santa Cruz	Unconjugated	5 µl per 100 µl sample
Anti-human CD34	581	Biolegend	FITC	5 µl per 100 µl sample
Anti-human CD31	WM59	Biolegend	FITC	5 µl per 100 µl sample
Anti-human CD11b	ICRF44	Biolegend	FITC	5 µl per 100 µl sample
Anti-human gp38	NZ-1.3	eBioscience	PerCP eFluor710	5 µl per 100 µl sample
T and B cell sorting				
Anti-human CD19	HIB19	Biolegend	PerCP Cy5.5	5 µl per 100 µl sample
Anti-human CD3	APC/Cy7	Biolegend	Alexa488	5 µl per 100 µl sample
Isotype antibodies				
PE IgG1	MOPC-21	Biolegend	PE	5 µl
PerCP IgG1	MOPC-21	Biolegend	PerCP	5 µl
APC/Cy7 IgG2a	MOPC-173	Biolegend	APC/Cy7	5 µl
Alexa488 IgG2b	MOPC-154	Biolegend	Alexa488	5 µl
FITC IgG1	MOPC-21	Biolegend	FITC	5 µl

Table 2: Antibodies used for cell sorting

8.4 qPCR of Human Tonsil Tissue Derived Cell Populations

8.4.1 RNA Isolation

RNA from isolated cells was extracted using the miRNAeasy Mini Kit (Qiagen). Cells were pelleted by centrifugation at 300xg for 5 min and resuspended in 350 µl QIAzol Lysis reagent and placed at room temperature for 5 min (NB: homogenate could be frozen at -80°C at this step). 140 µl chloroform was added to the homogenate and the tube shook vigorously for 15 seconds. The tube was rested at room temperature for 2 minutes before centrifugation at 4°C at 12000xg for 15 minutes. The aqueous phase was transferred to a new collection tube and 1.5 volumes of 100% ethanol added and thoroughly mixed by pipetting. 700 µl of the sample was immediately transferred to a Rneasy Mini spin column in a 2 ml collection tube and spun above 8000xg for 15 seconds at room temperature. The flow-through was discarded and step repeated with any remaining sample. 500 µl of Buffer RPE was added to the column and centrifuged for 2 minutes above 8000xg, discarding the flow-through. This step was repeated as above. The Rneasy Mini spin column was transferred to a new 2 ml collection tube and centrifuged at full-speed for 1 minute to dry the membrane. The column was then transferred to a 1.5 ml collection tube and 30-50 µl of RNase-free water added directly to the spin column membrane. The tube was centrifuged for 1 minute above 8000xg to elute the RNA.

8.4.2 Quantitative Real Time PCR

8.4.2.1 Complementary DNA (cDNA) synthesis

RNA samples were diluted to a known concentration in nuclease free water to a final volume of 10 µl in a 0.2 ml thin walled microcentrifuge tube. Using the high capacity cDNA reverse transcription kit (Applied Biosciences), a master mix was prepared containing (per 10 µl): 4.2 µl nuclease free water, 2 µl 10X Reverse Transcription buffer, 0.8 µl 25X dNTPs, 2 µl 10X RT random primers and 1 µl Multiscribe® Reverse Transcriptase. Per sample 10 µl of

master mix was added to the 10 µl RNA sample and transferred to a thermocycler PCR machine (SensoQuest) for reverse transcription. PCR conditions were as follows: 25°C 10 minutes, 37°C 2 hours, 85°C 5 minutes and then maintained at 4°C. cDNA was stored at -20°C or diluted to a known concentration using nuclease free water for further use.

8.4.2.2 qRT-PCR reaction

Two methods were used for qPCR, either Power SYBR® Green PCR Master mix or TaqMan Fast Universal PCR Master mix, no Amperase UNG (Applied Biosciences), depending on the genes to be analysed.

Primers were designed to amplify the DNA region additional exon within the long isoform of CD21 (Table 3), as commercial primers were not available.

For primers compatible with SYBR® Green, a master mix containing: 10 µl of Power SYBR® Green with 0.6 µl of primer mix, containing 10 µM forward and reverse primer, and 5.4 µl nuclease free water was added to a 96-well MicroAmp Optical reaction plate (Applied Biosciences), along with 4 µl of target cDNA. Alternatively, for TaqMan probes, a master mix containing: 10 µl TaqMan Fast Universal PCR Master mix, 5 µl nuclease free water and 1 µl of appropriate gene expression assay probe was added to plates with 4 µl target cDNA. Samples were added to the plate in duplicate and control wells containing 4 µl nuclease free water in replacement for target cDNA were included on each plate. Reactions were carried out using an Applied Biosystems 7300 Real-Time PCR System using the following programs. For TaqMan probes the program consisted of 50°C for 2 minutes, 95°C for 10 minutes and 40 cycles of 95°C for 15 seconds before 1 minute at 60°C. For reactions containing SYBR® green primers the program performed was as follows: 95°C for 10 minutes followed by 40 cycles of 95°C for 15 seconds and 60°C for 1 minute. At the end of each program, the temperature was increased from 50°C to 95°C during which the fluorescence is analysed to produce a melt curve to assess the specificity of amplicon

production. Upon separation of double stranded DNA fluorescence is reduced; primers producing a single peak are considered specific.

Gene	Forward Primer Sequence	Reverse Primer Sequence
CD21L	CTACACTTGTGACCCTGGCT	CTGGCATGTTTCTTCACACC
GAPDH	CAACTACATGGTTTACATGTTCCAA	TGGAAGATGGTGATGGGATT
Gene (Taqman probes)	**Assay ID**	**Company**
CD21	Hs00153398_m1	Thermofisher Scientific
CD19	Hs01047413_g1	Thermofisher Scientific
CXCL13	Hs00757930_m1	Thermofisher Scientific
CD3	Hs00174158_m1	Thermofisher Scientific
CD35	Hs00559348_m1	Thermofisher Scientific
CCL21	Hs00171076_m1	Thermofisher Scientific
GAPDH	Hs02786624_g1	Thermofisher Scientific

Table 3: Primer and probe information

8.4.2.3 qRT-PCR analysis

An automatic threshold (fluorescence normalised to reference dye) of 0.2Rn was set in the linear phase of the curve so that threshold cycles (C_t) could be determined for target genes and endogenous control genes. C_t is defined as the cycle number at which the fluorescence from the reporters passed the threshold. The mean C_t of the target gene from duplicate samples was calculated and normalised to the mean C_t for the endogenous control wells, this number is ΔC_t. From this, the $\Delta\Delta C_t$ was calculated by subtracting the ΔC_t of the sample from the ΔC_t of a calibrating sample (e.g. an untreated control). Finally, $2^{-\Delta\Delta Ct}$ calculated to measure relative expression in each sample. Data was plotted using Prism 7 (GraphPad).

8.5 PCR

Reactions were carried out using GoTaq® Green Master Mix (Promega). Each reaction contained a Master mix of: 12.5 µl GoTaq® Green 2X Master Mix, 1 µl primer mix, containing 10 µM of forward and reverse primer. This was added to 5 µl of cDNA template and the reaction made to a final volume of 25 µl using Nuclease-free water. The reaction was undertaken using a thermocycler PCR machine (SensoQuest) starting with 95°C for 2 minutes and then cycling through 95°C for 1 minute, 65°C for 1 minute, 72°C for 1minute/kb of target product, for 35 cycles. The final extension was carried out at 72°C for 5 minutes and the reaction held at 4°C indefinitely.

Gene	Forward primer	Reverse primer
CD21 (long vs short primers)	CAGATTCGTTGCAAAGCTGA	AATCACTGGTGGAGGGTGAC
pQXCIN cloning primers	CTTAATTAACGGATCATGGGC GCCGCGGGCCTG	GAGAGGGGCGGAATTTCAGCTGGCT GGGTTGTATGG

Table 4: Primers for PCR. All produced by IDT technologies

8.5.1 Agarose gel electrophoresis

Typically, a 0.8% agarose gel was prepared by dissolving agarose (Sigma) into 1X Tris-acetate-EDTA (TAE) buffer (Thermofisher) by heating using a microwave. The solution was allowed to cool to around 60°C before addition of ethidium bromide (10 µl per 100 ml) and subsequently poured into a gel cast. The gel was allowed to set and then placed in a gel tank filled with 1X TAE buffer.

PCR samples were prepared by the addition of 6X DNA Gel loading dye (Thermofisher) and 25-50 µl of the sample loaded into the wells. 10 µl of ladder GeneRuler 1Kb Plus (Thermofisher) was also loaded to each well. Gels were typically run at 100V for 30 minutes before visualisation with a UV light box (Thermofisher). Exposure time was dependent on intensity of band products.

8.5.2 DNA extraction from agarose gel

For extraction of PCR products, the QIAquick gel extraction kit (Qiagen) was utilised. Firstly, using a UV light box, the DNA band of interest was excised from the agarose gel with a scalpel and the gel slice weighed. Next the gel slice was added to a 1.5 ml eppendorf tube and 3 volumes of Buffer QG added to 1 volume of gel (i.e. 100 mg ~ 100 µl); for gel slices above 400 mg, extraction proceeded in two eppendorfs/columns. The tubes were incubated at 50°C for 10 minutes with mixing by vortex every 2-3 minutes during the incubation. 1 gel volume of isopropanol (Sigma-Aldrich) was added to the sample, the sample mixed by pipetting and loaded into a QIAquick spin column. The column was centrifuged at 17900xg for 1 minute to bind DNA and the flow-through discarded. A maximum of 800 µl was loaded to each column, for samples larger than this, this step was repeated with the remaining volume. 500 µl of Buffer QG was added to the column and centrifugation repeated as above. To wash the column, 750 µl of Buffer PE was added to the column and the tubes left to stand at room temperature for 2-5 minutes before centrifugation for 1 minute at 17900xg. The flow-through was discarded and the column centrifuged for a further 1 minute to remove

residual liquid. The column was placed in a clean 1.5 ml microcentrifuge tube and 50 µl of Buffer EB added to the centre of the column and incubated at room temperature for 1 minute before centrifugation for 1 minute to elute DNA. DNA concentration was determined using a nanodrop (Thermofisher) and used for downstream applications.

8.6 PBMC Isolation from Peripheral Blood

Accuspin tubes (Sigma-Aldrich) were prepared by the addition of 15 ml Ficoll (GE Healthcare Life Sciences) and spun at 1000 xg for 1 min. PBS was added to the blood sample to a total volume of 50 ml and split between two Ficoll Accuspin tubes. Tubes were centrifuged at 1000 xg for 10 min at RT without the brake. Using a Pastuer pipette, PBMCs at the interface were transferred to a fresh 50 ml polypropylene centrifuge tube. The contents of each tube were made to 50 ml with culture medium (RPMI1640 supplemented with 10% HI FCS, Glutamine and Penicillin/Streptomycin) and centrifuged at 250 xg at RT for 10 min to wash. Supernatant was removed, and pelleted cells gently re-suspended in 10 ml culture medium. 100 µl of cell suspension was added to 400 µl PBS and cell counting performed using a NuceloCounter. Subsequently, cells were resuspended in appropriate buffer, concentration depending on experimental need.

8.7 Thawing and Preparation of Tonsil cells for Flow Cytometry

Vials of frozen cells were thawed in a water bath with gentle agitation until only a small ice pellet remained and transferred into 20 ml of pre-warmed culture medium (RPMI1640 supplemented with 10% FI FCS, Glutamine and Penicillin/Streptomycin). Cell suspension was centrifuged at 200 xg for 5 min at RT and resuspended in isolation buffer (PBS with 0.1% BSA, Sigma, and 2mM EDTA, Invitrogen). 100 µl of cell suspension was added to 900 µl PBS for counting using a Nucleocounter and the centrifugation step repeated. Cells were resuspended in at $20x10^6$ cells/ml in isolation buffer based on the previous cell count. For analysis of T and B cells, cells were transferred into a V-bottom 96 well plate for antibody

staining. For analysis of FDCs, CD45 depletion was performed using CD45 depletion beads (Thermofisher – Dynabeads). Using isolation buffer, 12% volume of beads that there are cells, were washed and subsequently added to the cell suspension. Cells were incubated at 4°C with gentle agitation for 20 min. Then the tube was placed in a magnet for 2 min and supernatant transferred to a clean tube; this step was repeated. Cells were counted as above and pelleted by centrifugation at 200 xg for 5 min. Cell pellet was resuspended to a concentration of $20x10^6$ cells/ml and transferred to a V-bottom 96 well plate for antibody staining.

8.8 Surface Marker Antibody Staining for Flow Cytometry

Flow cytometry staining was performed in a V-bottom 96 well plate. Cells were typically plated at a density of $2x10^5$ cells/well for T and B cell staining and $2x10^6$ cells/well for FDCs as there are fewer FDCs within the samples. Plates were spun at 400 xg for 3 min at 4°C to pellet cells and resuspended in 50 µl of antibody mix (concentrations found in Table 2). The plate was incubated for 20 min at 4°C. For live/dead discrimination, 5 µl per well of DAPI (1in90 pre-diluted stock) was added, the plate mixed briefly on a plate rotator and incubated for 10 min at 4°C in the dark. The cells were washed three times with 150 µl FACS buffer (PBS with 0.1% BSA, Sigma, and 2mM EDTA, Invitrogen) by spinning at 400 xg for 3 min and resuspending in a further 150 µl FACS buffer. After the final wash cells were resuspended in 200 µl FACS buffer.

The samples were run using a Canto II or X-20 (BD Biosciences) flow cytometer. After running CS&T, voltages were set using single stained cells so that positive populations appeared around $log10^4$ where possible and ensuring all stains were brightest in their own channel with limited bleed into other channels. Compensation was carried out using Ultracomp beads (Thermofisher Scientific); 3 µl of antibody was added to 1 drop of beads and incubated for 10 min in the dark. 300 µl of PBS was added and the beads read on the

Canto. Compensation was applied prior to sample acquisition. Cells were identified by FSC/SSC, doublets were excluded, and live cells selected. Cells were further gated according to the staining panels used (Table 5). Data was analysed using the FlowJo (Treestar) software package.

Experiment	Gating strategy	Figure
Human tonsil derived FDC sorting	FDCs: lineage$^-$gp38$^+$CD35$^+$ FRCs: lineage$^-$gp38$^+$CD35$^-$	Figure 9.3.9
Human tonsil derived T and B cell sorting	B cells: CD19$^+$CD3$^-$ T cells: CD19$^-$CD3$^+$	Figure 9.3.10
Identification of CD21$^+$ FDCs	FDCs: lineage$^-$gp38$^+$CD21$^+$	Figure 9.3.11
Identification of CD21$^+$ T and B cells	B cells: CD19$^+$CD3$^-$CD20$^+$CD21$^+$ T cells: CD19$^-$CD3$^+$CD21$^+$	Figure 9.3.12
FE8 blockage of C3dg binding on FDCs	FDCs: lineage$^-$gp38$^+$CD21$^+$C3dg$^+$	Figure 10.3.2
FE8 blocking of C3dg binding on T and B cells	B cells: CD19$^+$CD3$^-$ CD20$^+$CD21$^+$C3dg$^+$ T cells: CD19$^-$CD3$^+$CD21$^+$C3dg$^+$	Figure 10.3.3
sCD21 blockage of C3dg binding on peripheral blood derived B cells	B cells: CD20$^+$C3dg$^+$	Figure 11.3.17
Activation of peripheral blood derived B cells using C3dg/anti-IgM complexes	B cells: CD20$^+$pERK$^+$	Figure 11.3.24

Table 5: Identification markers used for each cell type

Antibody	Clone	Manufacturer	Conjugated	Concentration
Anti-human CD21	Bu32	Biolegend	PE	5 µl per 100 µl sample
Anti-human CD35	E11	eBioscience	APC	5 µl per 100 µl sample
Anti-human CD34	581	Biolegend	FITC	5 µl per 100 µl sample
Anti-human CD31	WM59	Biolegend	FITC	5 µl per 100 µl sample
Anti-human CD11b	ICRF44	Biolegend	FITC	5 µl per 100 µl sample
Anti-human gp38	NZ-1.3	eBioscience	PerCP eFluor710	5 µl per 100 µl sample
Anti-human CD19	HIB19	Biolegend	PerCP Cy5.5	5 µl per 100 µl sample
Anti-human CD3	HIT3a	Biolegend	APC/Cy7	5 µl per 100 µl sample
Anti-human CD20	2H7	Biolegend	Alexa488	5 µl per 100 µl sample
Anti-human CD21	7D6	Novus Biologicals	Unconjugated	5 µl per 100 µl sample
Anti-human CD21	R4/23	Origene	Unconjugated	5 µl per 100 µl sample
Anti-human IgM	MHM-88	Biolegend	FITC	5 µl per 100 µl sample
Anti-human pERK	4B11B69	Biolegend	Alexa 488	5 µl per 100 µl sample

Table 6: Antibodies used for flow cytometry

Antibody	Clone	Manufacturer	Conjugate	Volume used
PE IgG1	MOPC-21	Biolegend	PE	5 µl
PerCP IgG1	MOPC-21	Biolegend	PerCP	5 µl
APC/Cy7 IgG2a	MOPC-173	Biolegend	APC/Cy7	5 µl
Alexa488 IgG2b	MOPC-154	Biolegend	Alexa488	5 µl
FITC IgG1	MOPC-21	Biolegend	FITC	5 µl

Table 7: Isotype antibodies used for flow cytometry

8.9 Receptor Quantification on FDCs, T and B cells

Tonsil derived FDCs and peripheral blood and tonsil derived T and B cells were stained with their respective antibody staining panels as previously described using a range of Bu32 (CD21 clone) concentrations, starting at 10 µg/ml and serially diluted 3-fold, to identify a saturating antibody concentration appropriate for use in receptor numeration.

Quantibrite-PE beads (BD Biosciences) were used to calculate the absolute CD21 receptor number on the cell membrane of FDCs (tonsil derived), T and B cells (blood and tonsil derived). Following antibody staining with 1 µg/ml Bu32-PE, the determined saturating concentration, and respective antibody panels as described, cells were resuspended in 200 µl FACS buffer and run on the cytometer using the appropriate voltage settings.

CD21 positive cells were identified in each cell type. Cells were identified using FSC/SSC, doublets excluded, and live cells selected. FDCs were identified as lineage$^-$gp38$^+$CD21$^+$ (Figure 9.3.11), B cells were identified as CD19$^+$CD20$^+$CD21$^+$ (Figure 9.3.12) and T cells identified as CD3$^+$CD21$^+$ (Figure 9.3.12). All gates were drawn using FMO and isotype controls.

After collection of sample data, a single vial of Quantibrite beads were resuspended in 300 µl PBS and beads were run using the same settings as respective sample data; PE voltage varies from cell type. Beads contain four populations, each with a known average number of

PE molecules (Figure 8.1A). Geometric mean of these populations was plotted against the number of PE molecules to create a standard curve (Figure 8.1B) from which the number of PE molecules on each cell type could be interpolated using the PE geometric mean of each sample. Two standard curves were drawn for the different voltages used for FDCs and T/B cells and number of CD21 molecules were interpolated from respective curves. The number of PE molecules was then divided by 2.1, due to this being the number of PE molecules present on each CD21-PE antibody (Biolegend, confirmed by company using lot numbers), therefore normalising the data between each labelling protocol.

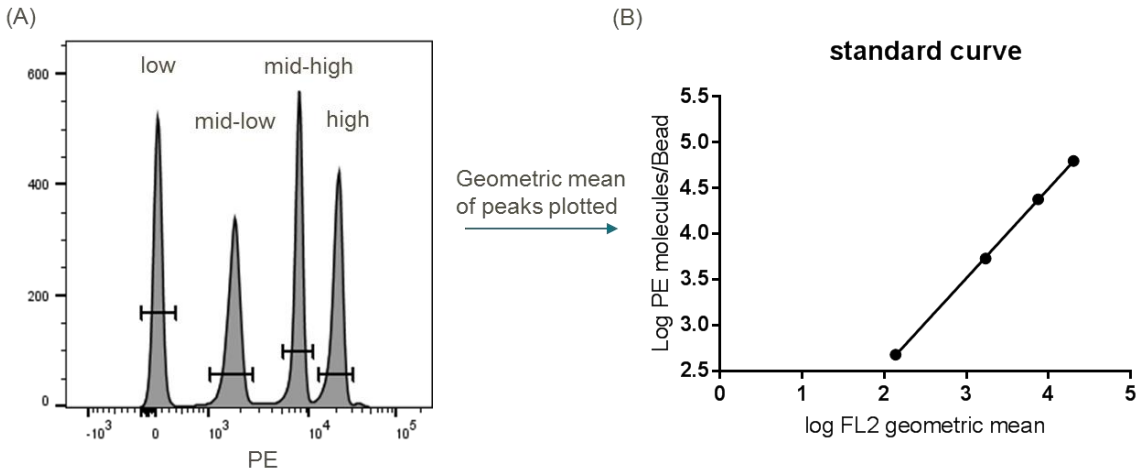

Figure 8. 1: Absolute receptor number using Quantibrite-PE beads

(A) The geometric mean of each of the PE-bead populations was calculated using FlowJo. (B) Log geometric mean is plotted against the known number of PE molecules on respective bead populations

8.10 Making C3dg-Strep(APC) Complexes

In separate 1.5 ml microcentrifuge tubes, the stock solutions of Streptavidin-APC (Prozyme) and biotinylated C3dg (provided by GSK) were diluted to form 20X concentrations, 400 µg/ml and 462.4 µg/ml respectively. 400 µl of 20X Streptavidin-APC was added to 400 µl 20X C3dg to generate 800 µl of 10X concentrated C3dg:Streptavidin-APC complexes. 200 µl of PBS was added to the remaining streptavidin to generate a 10X stock of a "No C3dg" control, i.e. streptavidin alone. The microcentrifuge tube was incubated at RT in the dark for 30 min to promote complex formation, then stored on ice in the dark until required.

8.11 Blocking C3dg binding to CD21 using FE8 on tonsil derived FDCs and blood and tonsil derived B cells

Cells were prepared from fresh blood and frozen tonsil digests as previously described (sections 8.6 and 8.2 respectively) and stained for extracellular flow cytometry analysis as above (section 8.8). To determine an appropriate C3dg-Strep(APC) concentration, cells were stained with a range of concentrations starting at 10 µg/ml and 3-fold serial dilutions made.

Cells were then stained with Bu32 and C3dg, Bu32 and FE8 or FE8 (CD21 clone) and C3dg (1 µg/ml) and incubated for 20 min in the dark at 4°C. Appropriate antibody staining panels were subsequently added and staining protocol continued as above (Section 8.8). Costaining confirmed whether the nature of the antibodies were competitive for the ligand binding site of CD21.

For the final assay FE8 was used to block C3dg binding to CD21 on FDCs and B cells. Samples were prepared and before staining for flow cytometry, were preincubated with a range of FE8 concentrations starting at 2 µg/ml then 3-fold serially diluted. Isotype antibody was also used to stain control samples using the same range of concentrations. Samples

were incubated for 20 min at 4°C and subsequently stained following the extracellular staining protocol previously described with the addition of 1 µg/ml C3dg to each well.

Samples were read using the Canto II and voltages set according to single stained controls. Analysis was undertaken by gating on $CD21^+$ cells and assessing C3dg-APC geometric mean of this population. Data values were normalised by performing the following calculation:

FE8 geometric mean/isotype geometric mean x100

This value was plotted against FE8 concentration to obtain a binding response curve.

8.12 Making retroviral vectors to express CD21 isoforms in Human Epithelial Kidney cells (HEKs)

8.12.1 In-Fusion® Cloning

8.12.1.2 Primer design

Primers were designed using In-Fusion® online cloning tools Primer Design. The vector sequence, in this case pQXCIN (Figure 8.4), and the insert sequence, CD21 and CD21L, is analysed by the program. Restriction enzymes are chosen depending on where the gene is wished to be inserted and the program designs primers that will add 15 bp extensions onto the insert sequence, allowing for insertion of the gene of interest into the vector.

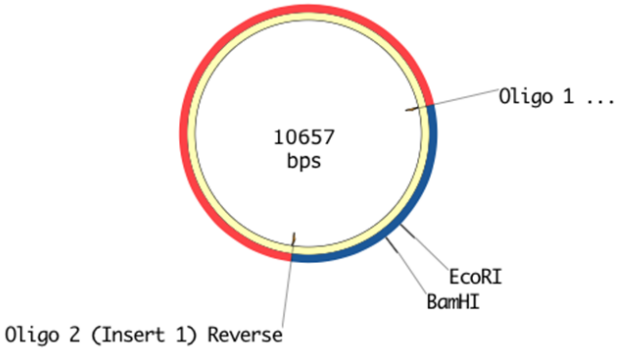

2 PCR Fragment Overlaps

```
Destination Vector(+): ...TCGTACGCTTAATTAACG      -3'          5'- AATTCCGCCCCTCTCCCTCCCC...
Destination Vector(-): ...AGCATGCGAATTAATTGCCTAG -5'          3'-     GGCGGGGAGAGGGAGGGG...
Insert 1(+)          :       5'- CTTAATTAACGGATCATGGGCG...CAGCTGAAATTCCGCCCCTCTC -3'
Insert 1(-)          :       3'- GAATTAATTGCCTAGTACCCGC...GTCGACTTTAAGGCGGGGAGAG -5'
```

Figure 8. 2: In-Fusion primer design programme

The plasmid and insert sequences are entered into the online programme and the restriction enzymes to cut the DNA selected. Primers are designed automatically by the programme (2). This was done for pQCXIN with CD21S and CD21L cDNA.

8.12.1.3 Vector linearisation

Vector pQXCIN was linearized with EcoRI-HF (New England Biolabs) and BamHI-HF (New England Biolabs). On ice, vector was diluted to 0.3 µg/µl and 3 µl, i.e. 1 µg, of plasmid DNA added to each reaction (3 reactions were set up in total, a total of 3 µg plasmid DNA was linearised). 10 units of each enzyme (1 µl in this case) was added to the reaction with 5 µl 10X CutSmart buffer (New England Biolabs) and the final reaction volume made up to 50 µl with nuclease free water. Reactions were run at 37°C for 15 minutes in a thermocycler (SensoQuest) and then loaded onto an 0.8% agarose gel for electrophoresis separation of products following the protocol above (Section 8.5.1). Linearised plasmid was extracted from the gel following the protocol described above (Section 8.5.2).

8.12.1.4 PCR amplification of the target gene

In-Fusion® PCR Premix (Clontech) was used to amplify the CD21 (SinoBiological) and CD21L (cDNA provided by GSK) insert from carrier vectors (Figure 8.3). 12.5 µl of PCR premix was added to 0.5 µl of the forward and backwards primers, designed for In-Fusion® cloning. 150 ng (1.5 µl in this case) of cDNA was added to each reaction and the nuclease-free water added to a final volume of 25 µl. The reactions were run using a thermocycler (SensoQuest) using the following conditions: 98°C for 10 seconds, 55°C for 10 seconds, 72°C for 15.5 seconds; this cycle was repeated 35 times. Samples were loaded onto a 0.8% agarose gel and products separated using electrophoresis following the protocol described in section 8.5.1. Insert was extracted from the gel following protocol detailed in section 8.5.2.

8.12.1.5 In-Fusion® cloning reaction

The ratio of vector:insert to be used in the cloning reaction was calculated by analysis of plasmid and vector DNA sequences by the online Clontech ratio calculator (https://www.takarabio.com/learning-centers/cloning/in-fusion-cloning-tools). In this case 200 ng of vector was used and 189.2 ng of each insert used. 4 µl of the In-Fusion® enzyme was added to DNA mix and nuclease free water added to a final volume of 20 µl. Reactions were placed in a thermocycler (SensoQuest) and heated at 50°C for 15 minutes and subsequently placed on ice.

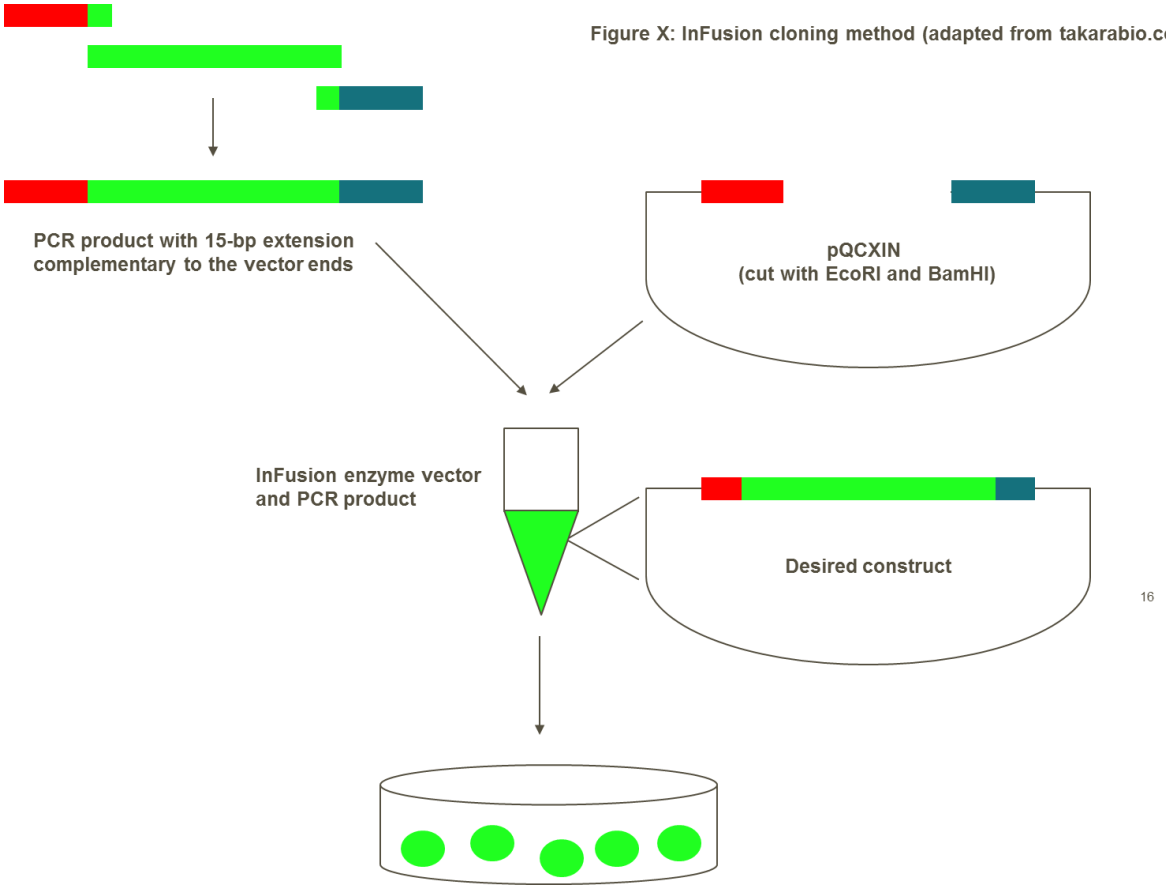

Figure 8. 3: InFusion cloning method (adapted from takarabio.com)

8.12.1.6 Transformation of cloning reaction into competent E.coli

Reactions were transformed into Stellar Competent bacteria (Clontech) by the addition of 2.5ul of the In-Fusion® cloning reaction to 50 µl bacteria on ice. A vector only control was also performed for each transformation. Cells are rested on ice for 30 minutes before heat-shock at 42°C for 40 minutes. Cells are placed back on ice for 1-2 minutes before the addition of 450 µl SOC (Clontech), prewarmed to 37°C, and incubated at 37°C for 1 hour with gentle, continuous mixing.

Cells were spread on LB/ampicillin plates, made with sterile LB broth (Sigma-Aldrich) and Bacto agar (Sigma-Aldrich) and the addition of 50 µg/ml ampicillin (Sigma-Aldrich). Plates were incubated overnight at 37°C and colonies picked the next day.

8.12.1.6 Miniprep of bacterial colonies

Bacterial colonies were picked and placed in 4 ml of LB media containing 50 µg/ml ampicillin and allowed to grow at 37°C for 4 hours with constant mixing. Cells were pelleted by centrifugation at 6000 rpm for 5 minutes. Cells were then mini-prepped using the QIAprep spin miniprep kit (Qiagen). Pelleted bacteria was resuspended in 250 µl of Buffer P1 and transferred to a microcentrifuge tube. 250 µl of Buffer P2 was added to the tube and mixed thoroughly by inverting the tube 4-6 times. Immediately afterwards, 350 µl Buffer N3 was added and thoroughly mixed by inversion. The tubes were centrifuged for 10 minutes at 13000 rpm in a table-top microcentrifuge (Eppendorf). The supernatants of samples were applied to a QIAprep spin column and centrifuged for 40 seconds. This flow-through was discarded. The column was washed by the addition of 500 µl Buffer PB and centrifugation as above. The column was then washed with 750 µl Buffer PE and centrifugation repeated. The columns were spun for an additional 1 minute to remove any residual wash buffer before addition of 50 µl of Buffer EB. The column was left to stand at room temperature for 1 minute before centrifugation for 1 minute at 13000 rpm to elute DNA.

Eluted DNA was quantified using a nanodrop and then digested with EcoRI-HF and BamHI-HF using the protocol described in section 8.12.1.3 and subsequently run on an agarose gel (as described in section 8.5.1) to check isolated DNA was the vector pQXCIN containing the insert, CD21 or CD21L.

8.12.1.7 Maxiprep of bacterial colonies

Colonies were picked from LB-agar plates and placed into 100 ml LB plus 50 µg/ml ampicillin and grown overnight at 37°C whilst shaking. Glycerol stocks were made of the cultures by taking 500 µl of the cell solution and adding 500 µl of 50% glycerol in PBS. Stocks were stored at -80°C.

For Maxipreps, 35 ml of bacteria was pipetted into a 50 ml Falcon tube and spun at 3200xg for 30 minutes to pellet cells. Supernatant was removed and 4 ml of cold P1 buffer was added to each falcon and pellet resuspended. 4 ml of P2 buffer was added to the tube and inverted to mix before the addition of 4 ml P3 and mixing again. The lysate was poured into the barrel of a QIA filter cartridge and incubated at room temperature for 10 minutes. During this time, 4 ml of QBT buffer was added to Qiagen-tips and allowed to flow-through to equilibrate the column. The cap of the QIA filter cartridge outlet nozzle was removed, and the plunger inserted. The lysate was filtered into the equilibrated Qiagen-tip and allowed to flow through. The column was washed twice with 10 ml of Buffer QC and then DNA eluted with 5 ml of Buffer QF, prewarmed to 55°C into a fresh 15 ml falcon tube. DNA was precipitated by adding 3.5 ml of room temperature isopropanol to the eluted DNA and centrifugation at 3200 xg for 45 minutes. The supernatant was discarded, and the pellet washed with 2 ml of 70% ethanol (Sigma-Aldrich) by centrifugation at 3200xg for 20 min at 4°C. The supernatant was discarded, and the pellet allowed to dry for 5 minutes. Samples were resuspended in 250 µl nuclease-free water and quantified with a nanodrop (Thermofisher) before being stored at -20°C.

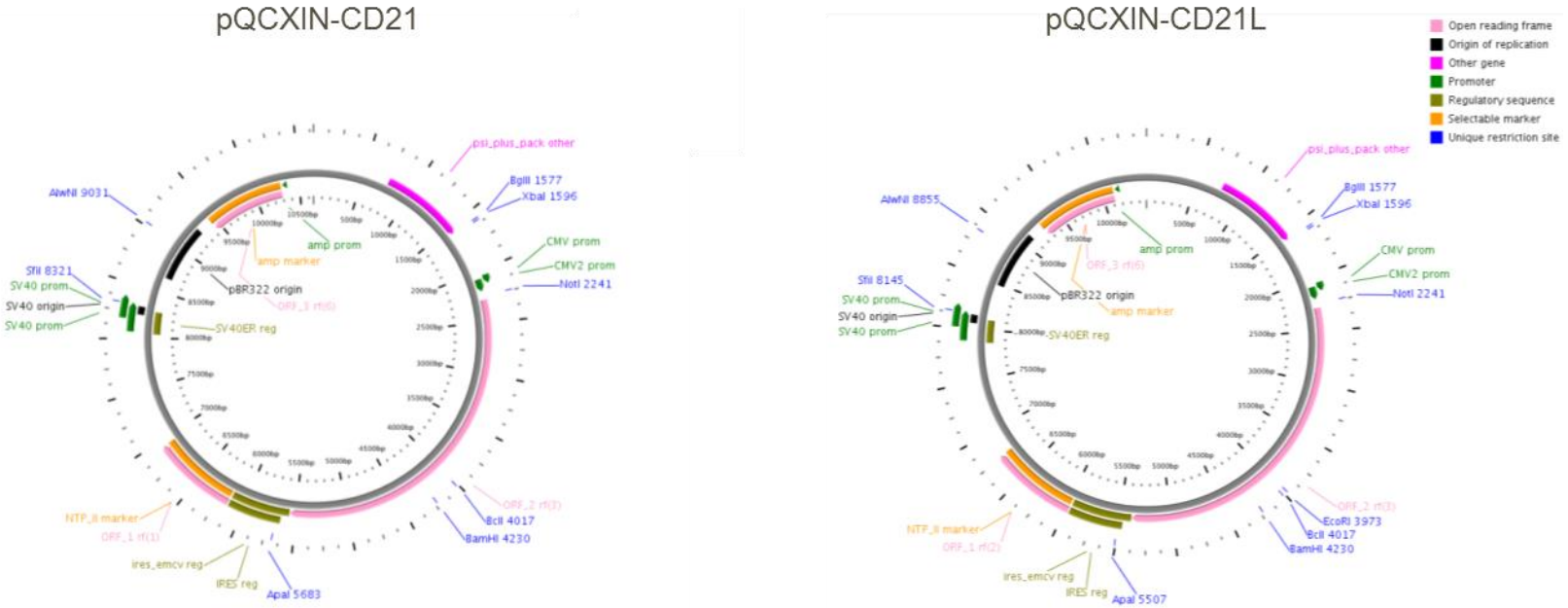

Figure 8. 4: Plasmid maps of cloned pQCXIN-CD21 and pQCXIN-CD21L

Open reading frame = pink

8.13 Cell culture of Human Epithelial Kidney cells (HEKs)

8.13.1 Cell culture

HEK cells were sourced from ATTC and cultured in Dulbecco's modified eagle medium (DMEM; Sigma-Aldrich) supplemented with 2mM L-glutamine, 15% FCS and 1% pen-strep. Complete media is termed as D15%.

8.13.2 Cell subculture

Upon reaching confluency (~80-90%), media was removed, and cells washed twice in Dulbecco's-PBS (D-PBS; no $CaCl_2$, no $MgCl_2$; PAA) and 2ml or 5ml 1X Trypsin-EDTA added to a T75 flask or T175, respectively. Cells were incubated at 37°C for up to a maximum of 7 minutes with constant monitoring for rounding and detachment. Once cells were detached, flasks were tapped to remove cells and 5ml warm D15% added to terminate trypsin activity and cells collected. The cells were centrifuged for 5 min at 300xg and resuspended in 5ml D15% for cell counts using a ViCell cell counter. Depending on experimental requirements, cells were seeded in 12 and 6 well plates (VWR). Table 8 was used for calculating number of cells to be seeded in different culture plates. For routine passage, cells were split 1:3. At least 1 vial of cells was frozen from each passage.

Dish	Surface Area cm^2	Seeding density (~25%) ($x10^6$)	Seeding density (~60%) ($x10^6$)	Confluency ($x10^6$)	Growth media
T75	75	0.375	0.9	1.5-20	10ml
T25	25	0.125	0.3	0.5-0.7	4ml
T160	162	0.8125	1.95	3.5-4.0	17ml
6-well	9	0.05	0.12	0.2	3ml
12-well	4	0.02	0.048	0.08	1ml
24-well	2	0.01	0.024	0.04	0.5ml

Table 8: Determining the approximate cell number for seeding at particular densities

8.13.3 Cryopreservation

Cells were resuspended at $1x10^6$ cells/ml in D15% culture media after detaching and quantifying cells. 500 µl of freezing media ($0.5x10^6$) were transferred to cryovials (Corning) with the addition of 500 µl of freezing media (FCS, 20% dimethyl sulfoxide; DMSO; Sigma-Aldrich), added drop-wise. Vials were immediately transferred to a Mr Frosty (Nalgene) and stored at -80°C. For long-term storage vials were deposited in liquid nitrogen.

For revival of frozen cells, vials were removed from liquid nitrogen storage and transferred to a 37°C water bath until only a small portion of the cell mix remained frozen. Cells were added to 3 ml of pre-warmed media and pelleted by centrifugation at 300xg for 5 min. The pellet was resuspended in 10 ml of warm media and transferred to a T75 flask. The next day media was replaced with fresh warm media so as to discard dead cells.

8.14 Transfection of Human Epithelial Kidney cells (HEKs)

Cells were seeded into a 6-well plate (Section 8.13.1) so that they were 50-80% confluent on the day of transduction. The next day, transduction was carried out using lipofectamine LTX (Thermofisher). For each well, 35 µl lipofectamine was diluted in 500 µl Opti-MEM (Thermofisher). A total of 15 µg DNA for interest was diluted into 500 µl Opti-MEM and PLUS reagent (Thermofisher) added at a 1:1 volume as total DNA added. Each tube was incubated separately for 5 minutes at room temperature before addition of the DNA to the lipofectamine reagent. This solution was incubated at room temperature for 25 minutes. Meanwhile, the HEK cells were prepared by aspirating media and subsequently washed twice with PBS. After the second wash, 9 ml of Opti-MEM was added to the cells and the transfection reagent/DNA mix added dropwise. Plates were incubated for 24 hours at 37°C before removing Opti-MEM and replacing media with D15%. Cells were harvest 48-60 hours later, when 70-90% confluency was reached.

To harvest cells, media was removed from the cells and frozen at -80°C as CD21/CD21L containing supernatant. Cells were lifted by the addition of 1 ml 1X Trypsin-EDTA and

incubated for up to 5 minutes at 37°C. 1 ml D15% was added to stop the reaction and cells collected from wells and pelleted by centrifugation at 350xg for 5 minutes. Cells were resuspended in media and counted using a ViCell cell counter and resuspended at an appropriate density for subsequent use.

8.15 C3dg binding/blocking experiments

HEK293T cells were transfected with CD21S or CD21L and harvest as described in Section 8.13.1. Cells were resuspended in flow buffer at a final cell density of $0.5x10^6$ cell/ml and 100 µl of cells were added to each well in a 96 well plate.

C3dg-strepavidin-APC complexes were prepared to a final concentration of 1 µg/ml and 10 µg/ml as in Section 8.10. During the incubation of the complex, FE8 (provided by GSK) and isotype (Biolegend) antibodies were titrated starting at a final assay concentration of 6 µg/ml, 3-fold dilutions were made to gain the full dilution series. After the complex incubation period, a serial dilution of C3dg-strepavidin was made with a starting concentration of 10 µg/ml, making 3-fold dilutions to complete the series.

Plates containing cells were spun at 400 xg for 3 minutes to pellet cells and were resuspended in 50 µl of FE8/isotype antibody titration or flow buffer. Cells were incubated for 20 minutes at room temperature before the addition of C3dg-strepavidin, 1 µg/ml for those samples preincubated with antibody titration, or titration series for those samples resuspended in flow buffer. CD21-PE (Bu32, Biolegend) was also added to samples to a final concentration of 1 µg/ml. The plate was mixed briefly by a plate rotator before incubation for 20 minutes at 4ºC. DAPI stain (Biolegend) was added to each well, the plate mixed briefly and incubated for a further 10 minutes at room temperature. Samples were washed three times with 150 µl flow buffer (PBS, Dibco, plus 0.2 mM EDTA, Invitrogen, and 2% BSA, Sigma) by spinning the plate at 400 xg for 5 min, removing the contents of the well and resuspending the pellet in flow buffer.

Samples were read using the BD Canto II. After running CS&T, voltages were adjusted using single stained cells, making sure all stains were brightest in their own channel. Compensation was set up using Ultracomp beads (BD Biosciences) and then data collected.

In addition to binding data, CD21 absolute receptor number expression in each transfection was calculated using Quantibrite-PE beads (BD Biosciences) following the protocol detailed in Section 8.9.

8.16 Western blot for CD21 protein

HEK293T cells transfected with CD21S and CD21L DNA as described above (Section 8.14) were lysed using RIPA buffer (Sigma) plus protease inhibitor cocktail (Sigma). Cell lysate was left on ice for 30 minutes and then centrifuged at 13,000 xg for 2 minutes to pellet insoluble proteins. 4X LDS + DTT was added to each sample and then boiled at 90ºC for 10 minutes before repeating the centrifugation step above. Cells were placed on ice until loading onto gels.

20 µl of each sample and 4 µl ladder (LiCor) was loaded onto an 8% Bris-Tris SDS gel (Invitrogen). The gel was run in 1X MOPS buffer (Thermofisher Scientific) at 180V for 45 minutes. The gel was removed from the cassette and transferred to nitrocellulose using the iBlot transfer (Invitogen), run time was 7 minutes using the standard manufacturers protocol. The blot was blocked for 60 minutes at room temperature in Odessey blocking buffer (LiCor) before the addition of primary antibody made to a concentration of 1 in 1000 in Odessey blocking buffer and incubated at room temperature for 60 minutes on a rocker. The blot was washed briefly with PBS + 0.05% Tween three times and then washed for 3 minutes three times. Secondary antibody, rabbit anti-mouse IgG-HRP (Invitrogen) was made to a concentration of 1 in 5000 in PBS + 0.05% Tween and incubated at room temperature for 60 minutes on a rocker. The blot was washed as above before addition of ECL and imaged using an imaging box (Biorad). Blots were each exposed for around 40 seconds before

further downstream processing, i.e. greyscale and intensity adjustments, to gain the best visualisation of the bands present.

8.17 Validation of a human CD21 ELISA and measuring soluble CD21 levels in healthy volunteer and Rheumatoid Arthritis patient serum

A commercial CD21 ELISA (abcam) was first validated for use with serum samples (details within results section 11.3.1) and subsequently used to measure sCD21 levels within healthy volunteer and Rheumatoid Arthritis patient serum.

All reagents were made to the manufacturer's instructions, the volumes prepared determined by the number of wells required for each assay (see table). A 1X standard diluent buffer was made by diluting the 10X stock in distilled water. Standards were made within 1in4 diluted serum, due to matrix interference; therefore human serum was diluted with 1X standard diluent. Recombinant CD21 (R&D systems) was added to the first standard at a final concentration of 600 µg/ml and serially diluted 2-fold into the remaining 6 standards. For the blank standard 1in4 diluted serum alone was used. 1X Biotinylated anti-CD21 and 1X Streptavidin-HRP solution was made by dilution in their respective diluent buffers according to the number of wells used in the assay (see table 9). All serum samples were diluted 1in4 in a separate 96-well plate before addition to the ELISA plate.

100 µl of all samples and standards were loaded into the appropriate wells and 50 µl of 1X Biotinylated anti-CD21 added to all wells before incubation at RT for 1 hour. The plate was washed three times using PBS + 0.05% Tween using an automatic plate washer. 100 µl of 1X Streptavidin-HRP solution was added to each well and the plate incubated at RT for 30 min. The wash step was repeated as described above. 100 µl of Chromogen TMB substrate solution was added to each well and incubated in the dark for 12 min at RT. 100 µl of Stop Reagent was added to each well and absorbance read immediately on a spectrophotometer using 450 nm.

For data analysis, the absorbance of the blank measurements (1in4 diluted serum alone) was subtracted from each of the samples. A standard curve was drawn using the background corrected absorbance values and the known CD21 concentrations; curves were drawn using a log-4 parameter fit. sCD21 concentration of samples was interpolated from this curve and interpolated value multiplied by 4 to account for the dilution made.

Each time the assay was performed quality control samples were run on the plate, samples were made from 1in4 diluted human serum in 1X standard diluent, spiked with a known concentration of rc-CD21. These samples were made by spiking recombinant CD21 into neat serum 4-fold the desired concentration and subsequently diluting serum 1in4 in 1X standard diluent buffer. The final CD21 concentration within these samples was 20 ng/ml, 50 ng/ml and 100 ng/ml. Samples were loaded onto the plate and analysed as above.

Humanised mouse serum was also analysed for sCD21 content, using the protocol as detailed above.

Number of well strips used	Volume of reagent	Volume of Diluent
	Biotinylated anti-CD21	
Number of well strips used	**Volume of Biotinylated anti-CD21 (µl)**	**Volume of Biotinylated Antibody Diluent (µl)**
2	40	1060
3	60	1590
4	80	2120
6	120	3180
12	240	6360
	Strepavidin-HRP	
Number of well strips used	**Volume of Strepavidin-HRP (µl)**	**Volume of HRP-Diluent (ml)**
2	30	2
3	45	3
4	60	4
6	75	5
12	150	10

Table 9: Volume of CD21 ELISA reagents used

8.18 Using soluble CD21 to block binding of C3dg to peripheral B cells

Soluble CD21 was titrated with a starting concentration of 5000nM and serially diluting 2-fold. Two soluble CD21 reagents were used, recombinant CD21 (R&D Systems), the full-length protein, and a protein construct consisting of only SCR's 1 and 2 (GSK), the ligand binding site of CD21. 0.2 µg/ml C3dg-StrepAPC complexes, made as above, were added to soluble CD21 and incubated at RT for 20 minutes. Using this concentration of C3dg creates a molar ratio of 10,000 sCD21:1 C3dg at the top titration point.

Meanwhile, PMBCs were isolated from blood donated at the BDU, GSK (Stevenage), using the method described above (Section 8.6) and plated into V-bottom 96-well plates at a cell density of $1x10^5$ cells/well. Cells were pelleted by centrifugation at 450 xg for 3 minutes and resuspended in the sCD21/C3dg titration. The cells were then stained for extracellular flow cytometry analysis following the protocol described in Section 8.8.

B cells were identified as $CD19^+$ and C3dg binding assessed (Figure 11.4.18). Percentage of C3dg binding was assessed by recording C3dg-strepAPC MFI and normalising this value to the MFI of samples containing 0 nM sCD21. A binding response curve was created by plotting these values against log sCD21 concentration.

8.19 Culture of B cell lines (Raji and Ramos)

8.19.1 Cell culture of B cell lines

Cell lines, Raji (ATCC number CCL-86) and Ramos (ATCC number CRL-1596) were cultured in RPMI medium 1640 (GIBCO) supplemented with 2mM L-glutamine, 10% FCS and 1% pen-strep (provided by Sodexo, GSK).

8.19.2 Thawing B cell lines

Raji and Ramos cells were thawed after removal from liquid nitrogen in a 37ºC water bath and suspended in 10 ml growth media. Cells were spun at 300 xg for 4 minutes and media discarded. Cells were resuspended at a density of $0.5x10^6$ cells/ml.

8.19.3 Subculture of B cell lines

Every 2 to 3 days, medium was changed, and cultures spilt to a density of $0.5x10^6$ cells/ml by transferring cells into centrifuge tubes and spinning for 4 minutes at 300 xg. The supernatant was aspirated, and 10 ml of culture media added. Cells were counted using a ViCell cell counter and the spin repeated. Finally, cells were resuspended to the required density and transferred to a new culture vessel.

8.20 Activation of peripheral B cells with C3dg-anti-IgM complexes

The day before performing activation assays, cell lines were fed as described in Section 8.19.3 and replated at a density of $0.5x10^6$ cells/ml.

In advance of cell preparation, proteins for stimulation cocktails were prepared at 30x final assay concentration. Anti-human IgM (FC5MU), F(AB')2 Fragment (Sigma) was prepared by dilution in PBS to 300 µg/ml and serially diluted to gain an anti-IgM titration. Biotinylated C3dg (provided by GSK) was prepared to a concentration of 9 µg/ml and neutravidin (Sigma) was diluted to a concentration of 30 µg/ml. Stimulation reagents were mixed to a ratio of 1:1:1 so the cocktail was at a 10X final concentration and left at room temperature for 30 minutes and then placed on ice 5 minutes prior to cell stimulation.

Cell lines were removed from flasks and pelleted by centrifugation at 350 xg for 5 minutes. Cells were resuspended in RPMI and counted using a ViCell cell counter. The spin was repeated, and cells resuspended in complete RPMI at a density of $0.5x10^6$ cells/ml before allowing the cells to rest for an hour.

Meanwhile Phospho fix/lyse solution (BD Biosciences) was diluted to create a 1X solution and prewarmed to 37ºC in a water bath and Perm-buffer III (BD Biosciences) was chilled on ice.

Next, 180 µl of rested cells were added to 20 µl of chilled stimulation cocktail and transferred to a 37ºC humidified CO_2 incubator for 10 minutes. After the stimulation period, the cells were fixed immediately by adding 1-fold volume of 1X Phospho fix/lyse buffer. The incubation period was repeated as above. Plates were then centrifuged at 600 xg for 5 minutes and the supernatant aspirated, leaving no greater than 50 µl of residual volume. Pellets were vortexed to disrupt the cells and permeabilised by the addition of 200 µl of pre-chilled Perm buffer III (BD Biosciences), resuspended thoroughly by pipetting up and down, and then transferring into a 2 ml deep well plate containing 200 µl of pre-chilled Perm buffer I, making the total volume 400 µl. The plate was then stored at -20ºC for 30 minutes. After

the incubation period, the plate was centrifuged at 600 xg for 5 minutes and supernatant removed. The cells were resuspended in 200 µl of flow buffer (PBS, Dibco, plus 0.2 mM EDTA, Invitrogen, and 2% BSA, Sigma) and transferred to a V-bottom plate. The centrifugation step was repeated three times to wash the cells. After the final wash, cells were resuspended in 50 µl of antibody mix. Antibody mix contained flow buffer, anti-CD20-PE (Biolegend) and anti-pERK-APC (Invitrogen). Cells stained with single antibodies were prepared for compensation. Samples were mixed and incubated at 4ºC for 30 minutes in the dark. Cells were washed 3 times in 150 µl flow buffer.

Samples were read using a Canto flow cytometer (BD Biosciences). Voltages were adjusted based on negative and positive cells and compensation calculated with single stained compensation beads (Invitrogen) applied using the compensation wizard. Approximately 10,000 events were collected for each sample. Events were imported into FlowJo (version 10) and CD20 events were plotted as a scatter plot against side scatter to reveal CD20 positive events (Figure 11.3.23). CD20 positive events were gated and pERK+/- events were plotted as histograms within this gate. Percent positive phospho-protein content was calculated using gating on unstimulated and isotype control stained cell samples.

8.21 Blocking B cell line activation with FE8 and sCD21

The day before performing activation assays, cell lines were fed as described in Section 8.19.3 and replated at a density of $0.5x10^6$ cells/ml.

Ahead of cell preparation, stimulation complexes were prepared at 4x final assay concentration. Anti-human IgM (FC5MU), F(AB')2 Fragment (Sigma), biotinylated C3dg (provided by GSK) and neutravidin (Sigma) were prepared to a concentration of 12 µg/ml, 40 µg/ml and 12 µg/ml respectively and incubated together for 30 minutes at room temperature and then placed on ice. Final concentrations of reagents in the complex were as follows: 1 µg/ml neutravidin, 0.3 µg/ml C3dg and 0.3 µg/ml anti-IgM.

A titration of FE8 antibody (provided by GSK) was made starting at 72 µg/ml (4x final assay concentration,18 µg/ml) and subsequent 3-fold log serial dilutions made in PBS. The same titration series was made with an isotype control antibody (Biolegend). Recombinant CD21 (R&D systems) was titrated, starting at 500 µg/ml (4x final assay concentration, 125 µg/ml) and serially diluted using 3-fold log titrations into PBS. To control for protein addition into the assay, the equivalent dilution series was made using recombinant IL7R (R&D systems).

Cell lines were removed from flasks and pelleted by centrifugation at 350 xg for 5 minutes. Cells were resuspended in RPMI and counted using a ViCell cell counter. The spin was repeated, and cells resuspended in complete RPMI at a density of $2x10^6$ cells/ml before allowing the cells to rest for an hour.

Before the addition of any stimulation reagents to plates, 50 µl of RPMI was added to each well. For the FE8 assay, 50 µl of the FE8 or isotype antibody titration was added to appropriate cells along with 50 µl of rested cells. For the rc-CD21 assay, 50 µl of rc-CD21 or rc-IL7R was added to 50 µl of 4x stimulation complex. Both assays were incubated at room temperature for 20 minutes. After this preincubation period, 50 µl of cells was added to the rc-CD21 assay wells and 50 µl of stimulation complex added to the FE8 assay wells. The total assay volume was 200 µl.

The samples were transferred to a 37ºC humidified CO_2 incubator for 10 minutes. After the stimulation period, the cells were fixed immediately by adding 100 µl of Phospho fix/lyse buffer (BD Biosciences), prewarmed to 37ºC. Cells were incubated at 37ºC for 10 minutes before centrifugation at 600 xg for 5 minutes. Supernatant was removed, leaving no greater than 50 µl of residual volume. Pellets were vortexed to disrupt the cells. Cells were permeabilised by the addition of 200 µl of pre-chilled Perm buffer III (BD Biosciences), resuspended thoroughly by pipetting up and down, and then transferred into a 2 ml deep well plate containing 200 µl pre-chilled Perm buffer III, making the total volume 400 µl. Plates were stored at -20ºC for at least 30 minutes. After this time, plates were centrifuged at 600 xg for 5 minutes and the supernatant removed. Cells were resuspended in 200 µl flow buffer

(PBS, Dibco, plus 0.2 mM EDTA, Invitrogen, and 2% BSA, Sigma) before transfer to a V-bottom plate. The plate was centrifuged at 600 xg for 5 minutes and the wash step was repeated three times. After the final wash, the cells were resuspended in 50 µl of antibody mix. Antibody mix contained flow buffer, anti-CD20-PE (Biolegend) and anti-pERK-APC (Invitrogen). Cells stained with single antibodies were prepared for compensation. Samples were mixed and incubated at 4ºC for 30 minutes in the dark. Cells were washed 3 times in 150 µl flow buffer as above.

Samples were read on a BD Canto flow cytometer. Voltages were adjusted based on negative and positive cells before collecting samples. For each sample around 10,000 events in the CD20+ gate were collected. Events were imported into FlowJo (version 10) and CD20 events were plotted as scatter plots against side scatter to reveal CD20 positive events. CD20 positive events were gated and pERK+/- events were plotted as histograms within this gate. pERK+ gate was set using isotype control antibody stained and unstimulated cell samples.

8.22 Statisical analysis

Statistical analysis was done using GraphPad Prism. When comparing two data-sets a two way T-test was used, using multiple comparisons if the data-set was to be compared to more than one other factor. Data was plotted on graphs with bars illustrating the mean values and error bars representing the standard deviation of the mean (SD) (GraphPad).

9. Results chapter 1: Identification and characterisation of human Follicular Dendritic Cells

9.1 Introduction

9.1.2 Human FDCs and their identification

FDCs are shown to express complement receptors CD21 and CD35 (Imai et al., 1996) in both primary and secondary follicles within the light zone of the germinal centre. FDCs are also critical for germinal centre formation; mice deficient in CD21/CD35 (no FDCs) have unorganised germinal centres and are unable to retain antigen. Ablation of FDCs in mice lead to rapid loss of the primary follicles structure leading to unorganised bands of cells and T cell-zones (Wang et al., 2010), highlighting the importance of these cells' role in the microarchitectal organisation of secondary lymphoid organs (Wang et al., 2011). Expression of CXCL13 by FDCs contributes highly towards this organisation (Cyster et al., 2000). This chemokine is essential for the attraction of $CXCR5^{+}$ B cells from the dark zone to the light zone of the germinal centre. CXCL13 expression has been previously detected in FDC-enriched cell preparations (Tjin et al., 2005), during the culture of FDC cell lines (Murakami et al., 2007), and FDCs within inflammation-induced ectopic lymphoid follicles (Shi et al., 2001). Expression of this chemokine is dependent on LTα1β2 and directly induces expression of this molecule by naïve B cells, therefore a positive feedback loop to augment CXCL13 production (Ansel et al., 2000).

FDCs express low affinity antibody receptors, CD23 for IgE (Maeda et al., 1992) and FcγRIIb for IgG (Qin et al., 2000). It has been suggested that although these receptors are not as important as complement receptors for immune complex trapping, they do enhance long-term retention of these complexes by the FDC. In addition to this observation, FDCs lacking FcγRIIB are unable to convert poorly immunogenic immune complexes into an immunogenic form for presentation to B cells (Qin et al., 2000). The direct interaction of the immune complex with FcγRIIB on FDCs causes upregulation of the receptor, as well as ICAM-1 and

VCAM-1, suggesting this engagement is important in initiating pathways leading to FDC activation (El Shikh et al., 2006). Interactions between FDCs and B cells are facilitated by the expression of integrin ligands VCAM-1 and ICAM-1 on FDCs (Koopman et al., 1991). This close interaction allows B cells to encounter the opsonised antigen presented by FDCs on CD21, a receptor common between both cell types (Bradbury et al., 1992).

Human FDCs have been shown to express CD14, CD10 and CD21, but not CD45 (Munoz-Fernandez et al., 2006) using flow cytometry. These results, along with the immunohistochemical observation of smooth muscle-actin expression in the cytoplasm of the cell, suggested that FDCs were related to bone marrow stromal cell progenitors and myofibroblasts and were not derived from haematopoietic origin. Other markers which identify FDCs include CD40 and BAFF known to promote B cell responses. BAFF is needed for maintaining B cell homeostasis and FDCs have been identified as a major source of this factor (Gorelik et al., 2003). This evidence came from the observation that FDC cell lines and freshly isolated FDCs from human tonsils, express BAFF mRNA (Zhang et al., 2005) as well as immunohistochemical analysis showing BAFF staining within the germinal centre (Hase et al., 2004). CD40 signalling of B cells promotes germinal centre formation, immunoglobulin isotype switching, somatic hypermutation and long-lived plasma and memory B cells (Danese et al., 2004), therefore this pathway is essential to germinal centre reaction as absence of CD40 stimulation eradicates the germinal centre response (Paus et al., 2006).

Several monoclonal antibodies are available that are reported to bind to specific FDC antigens. The antigen FDC-M1 is also abundant on tingible body macrophages in germinal centres but its molecular identity remains undetermined. However, the FDC-M2 antigen has been identified as complement component C4 in immune complexes, this observation is consistent with the knowledge that deposition of immune complexes and complement components are observed on FDCs within the germinal centres (Imai et al., 1996). Other antibody clones specifically against CD21 expressed on FDCs have been reported, but this will be discussed later in the thesis.

FDCs can be isolated from irradiated mice using collagenase and DNaseI (Sukumar et al., 2005). However, isolation of human FDCs is more challenging and, despite it being achieved in the past (Schriever et al., 1989), there is no standardised protocol. Due to this, the vast majority of published *in vivo* studies are carried out within murine models and were discussed within the main introduction to this thesis. In mice, both CR1 and CR2 (CD35 and CD21 respectively) are transcribed from the same gene and then alternatively spliced from this mRNA, while in human these proteins are derived from two distinct but closely related genes on chromosome 1 (Boackle et al., 2003). Alternative splicing of a single exon generates two isoforms in human (Fujisaku et al., 1989) which do not exist within mice. Expression of CD21 is exclusive to murine B cells and FDCs, whereas in human expression extends to a broader distribution of cell types. Mouse CR2 is 67% homologous to the human equivalent and binds with similar affinities to human and mouse C3d (Fang et al., 1998). Despite this similarity, interspecies differences lead to little translatability of murine studies to human biology.

9.1.3 Human FDC cell lines

Many FDC-like cell lines have been reported within the literature, however their use to collect reliable information about the human FDC characteristics and function is questioned due to phenotypical and functional discrepancies between these lines and primary cells.

An early study showed how long-term culture of primary FDCs could be achieved and that the resultant cell line expressed FDC markers CD14, CD40, ICAM-1 and VCAM-1 (E. Clark et al., 1992). These cells where shown to bind human B cells but not T cells and augment B cell proliferation together with anti-μ sera and/or CD40 mAb, both characteristics important to FDC function. A small population of cells were shown to express CD35 early after culture, but expression decreased over time and CD21 expression was neither detected nor could be induced by culture using cytokines. Expression of CD21 is essential for FDC functionality;

therefore the ability of the cultured cells to act in the same way as primary FDCs is questionable. These cells, now termed the FDC-1 cell line, were used in a further study detailing the cells ability to activate B cell maturation. As few as 50 to 100 FDC-1 cells were shown to increase B cell IgM production by 10 to 100-fold (E. Clark et al., 1995). This augmentation of FDC-dependent IgM production was shown to depend on either IL6 or IL7 and was inhibited with IL4. For this stimulation to occur, cells did not require contact with B cells, another discrepancy between primary FDCs and this FDC-like cell line. Primary FDCs activate B cells through interactions between C3dg-opsonised antigen and CD21 receptors expressed by both cells, hence it is necessary for cell-cell contact to occur. Supernatants from cultured FDC-1 cells could also stimulate B cells to produce IgM, suggesting cells were generating a soluble molecule with the ability to activate B cells, rendering the need for cell-cell contact unnecessary. Additionally, human foreskin fibroblasts were also shown to induce production of IgM by B cells, suggesting the mechanism of activation used in this study was not FDC-dependent.

There are reports of another cell line derived from EBV transformed FDC-enriched cell populations (Lindhout et al., 1994). This study obtained cell lines (FLCs) consisting of slowly duplicating, large cells with a fibroblast-like morphology. These cells could be distinguished from other human fibroblast cell lines by displaying a phenotype including expression of ICAM-1, CD40 and CD75, however expression of CD21 was not reported. These FDC-like cells were also shown to bind nonautologous B cells and preserve them from apoptosis, another important function of FDCs.

A study comparing these two cell lines showed that primary cultured FDCs did not enhance the CD40-dependent proliferation of germinal centre B cells however; FLCs augmented it (Tsunoda et al., 1996). Characteristic to human FDCs, both cells were shown to produce a significant amount of cytokine-dependent IL6; however, out of the 72 long term cultures of FLCs, only 2 divided. As FDCs have been shown to readily de-differentiate in culture, this raises the question to whether these cells are still ruminant of primary human FDCs in vivo.

Another FDC-like cell line, HK cells, was also shown to have the ability to stimulate germinal centre B cell proliferation resulting in memory B cells (H. Kim et al., 1995). Similar to studies using the other reported FDC cell lines discussed above, this proliferation was also dependent on the presence of anti-μ or anti-CD40. Cell-cell interaction between the HK cell line and germinal centre B cell was also shown to rescue the cells from apoptosis, a characteristic of primary FDCs in vivo. Although long term culture did not affect the ability of the cells to bind B lineage cells, characteristic phenotypes of FDCs were not detectable by FACs, suggesting again the cells had de-differentiated.

Considering the phenotypes and functional abilities of the cell lines discussed, it is clear that work towards further understanding the function of FDCs must be undertaken on primary human FDCs, highlighting the importance of developing a robust isolation protocol for these cells to enable this work.

9.1.4 CD21 expression on Germinal Centre cell types

It is known that both FDCs and B cells express CD21; a receptor essential for the function and interaction between both cell types. An impaired humoral immune response is found in *Cr2*$^{-/-}$ mice (Fang et al., 1998) verifying the essential nature of this receptor for the germinal centre reaction and strong antigen-specific IgG responses. These effects are presumably due to impaired antigen trapping by FDCs which could affect B cell maturation into plasma or memory B cells and the absence of complement receptors resulting in the lack of B cell activation. In addition, it was reported that antibody responses from B cells were dramatically enhanced by the addition of FDCs to cultures (Qin et al., 1998) and therefore FDCs were providing an important costimulatory signal to B cells, shown to be CD21. A ligand blocking antibody against CD21 dramatically reduced these responses, demonstrating a role for the receptor within this system (Qin et al., 1998).

The essential function of CD21 on FDCs is antigen retention, in the absence of this receptor FDCs are unable to present antigen and the size of germinal centres appear reduced (Fischer et al., 1998). To preserve antigen for long time periods, FDCs trap the CD21 bound antigen in recycling endosomal compartments, protecting the antigen from degradation (Heesters et al., 2013). Delivery of said antigens to secondary lymphoid organs occurs in multiple ways dependent on size of antigen and opsonisation with complement. Lymph-borne antigen smaller than 70 kDa can flow directly to FDCs via the conduit network, alternatively larger complexes are captured by SCS macrophages and transported across the SCS to FDCs (Gretz et al., 2000). If the antigen is opsonised with C3-derived complement fragments, naïve B cells can capture these molecules using CD21 expressed on their surface and shuttle it to FDCs where unidirectional transfer of the antigen-complex between the CD21 molecules occurs (Heesters et al., 2013).

CD21 on B cells is non-covalently complexed with CD19, CD81 (TAPA-1), and Leu-13 (Matsumoto et al., 1991). Engagement of this receptor synergistically enhances signalling through the B cell antigen receptor (BCR) and lowers the threshold for B cell activation (Cherukuri et al., 2017). Co-ligation of the CD21/CD19 complex to the BCR occurs through binding of C3dg-tagged antigen that serves as a bridge between CD21 and the BCR (Fearon et al., 1995) causing Ca^{2+} flux and drives cells into cell cycle (Carter et al., 1988). This crosslinking also enhances BCR-mediated antigen processing. In addition, studies were undertaken in murine B cells that showed CD21 and CD19 uncoupling significantly diminishes survival of germinal centre B cells and antibody titres (Barrington et al., 2009).

Interestingly, FDCs also express low levels of CD19 (Barrington et al., 2009); however the role of this receptor in this cell type is unclear. Transfer of immune complexes between murine naïve B cells and FDCs, and antigen retention on FDCs, was shown to be CD19-independent (Barrington et al., 2009). As CD21 is expressed in molar excess to CD19 on FDCs, it is thought that the majority of CD21 is not contained within the CD19/CD21 complex, unlike in murine B cells where CD19 was shown to be expressed in molar excess

to CD21 at all stages of development (Fearon et al., 2000). Coligation of CD19/CD21 in B cells lowers the threshold for cell activation (Carter et al., 1992), however it is unlikely that CD19 on FDCs has a role in activation as the CD19/CD21 complex is unlikely to form due to low levels of CD19 expression, although this has not been studied within the current literature. Single cell RNA sequencing revealed that murine FDCs express high levels of CD81 (Rodda et al., 2018), the tetraspanin protein involved in the anchoring of the CD19/CD21 complex in B cells. Tetraspanins are known to regulate trafficking of their partner proteins (Charrin et al., 2014). Specifically, CD81 has been shown to traffic CD19 along the secretory pathway at the post-ER compartment and is essential for normal CD19 expression in murine B cells (Shoham et al., 2003). CD81 or CD19 deficient mice express normal levels of CD21 (Tsitsikov et al., 1997) suggesting this receptor is not regulated by CD81 in the same way as CD19. However, as this has not been studied within humans, and CD19 expression is much lower on FDCs than B cells, a role for CD81 in internalisation of CD21 into recycling endosomal compartments within human FDCs cannot be completely discarded.

Published data has shown that a small subset of peripheral T cells (Fischer et al., 1991) and early $CD4^{++}$ and $CD8^{++}$ human thymocytes (Tsoukas et al., 1988) express CD21. Knowledge of the physiological role of CD21 on T cells is limited but it has been reported that HIV-1 can mediate infection of T cells via CD21 independently of CD4 (Boyer et al., 1991). It has been hypothesised that CD21-C3dg interactions may be a mechanism of enhancing T cell adhesion as $CD21^{+}$ T cells have been shown to have increased cell-cell interactions (Levy et al., 1992), however further evidence for this does not currently exist.

9.2 Summary and aims:

The focus of this chapter is the identification, isolation and characterisation of FDCs from human tonsil compared to tonsil lymphocytes and stromal fibroblasts. Isolation of these cell types allows the potential for downstream functional assays to be undertaken focusing on the role of the CD21 receptor. As both FDCs and B cells express this receptor and its role is essential for the germinal centre reaction it is important to further understand its different functions on both cell types.

This chapter also addresses the first component of the overall hypothesis described in the introduction to this thesis. The literature describes C3dg opsonised antigen complex transfer between the CD21 receptor on B cells to CD21 on FDCs. We hypothesise this transfer could occur due to multiple factors, one of which is due to the number of CD21 receptors on the surface of FDCs compared to B cells. To address this idea, absolute quantification of surface receptor number on these cells will be analysed which has not previously been investigated. Expression of CD21 on both tonsil and blood derived human T and B cells will also be compared. In brief the aims of this chapter are:

1. Characterise germinal centre cells within human secondary lymphoid organs (tonsil and lymph node) using immunohistochemistry and established cell surface receptors.
2. Develop a protocol to isolate human FDCs from tonsil tissue.
3. Identify and isolate human FDCs from tonsil tissue and confirm the identity of sorted cells using qPCR for well characterised markers of the cell populations.
4. Determine absolute CD21 receptor number on the surface of FDCs, T and B cells in tonsil.
5. Compare CD21 receptor expression in T and B cells from tonsil compared to circulating lymphocytes.

9.3 Results

9.3.1 IHC characterisation of Secondary lymphoid organs

It was important to first identify FDCs within human tonsil and lymph node tissue and confirm expression of key markers before isolation of these cells could occur; therefore, to visualise the cells within these micro-structures, immunohistochemistry of human tonsil and lymph node tissue was undertaken.

Frozen human and lymph node tissue sections were stained confirming that germinal centres can be found within these tissues and FDCs ($CD35^+$) and B cells ($CD19^+$) that can be visualised within these microstructures (Figure 9.3.1). The cells are tightly packed suggesting the potential for a high incidence of interactions between the two cell types. $CD35^+$ cells are in a tight structure forming the light zone of the germinal centre, confirming these tissues contain FDCs (Figure 9.3.1). $CD19^+$ cells are seen within this light zone but is also seen outside of this zone, the dark zone, confirming B cells can be identified within these organs.

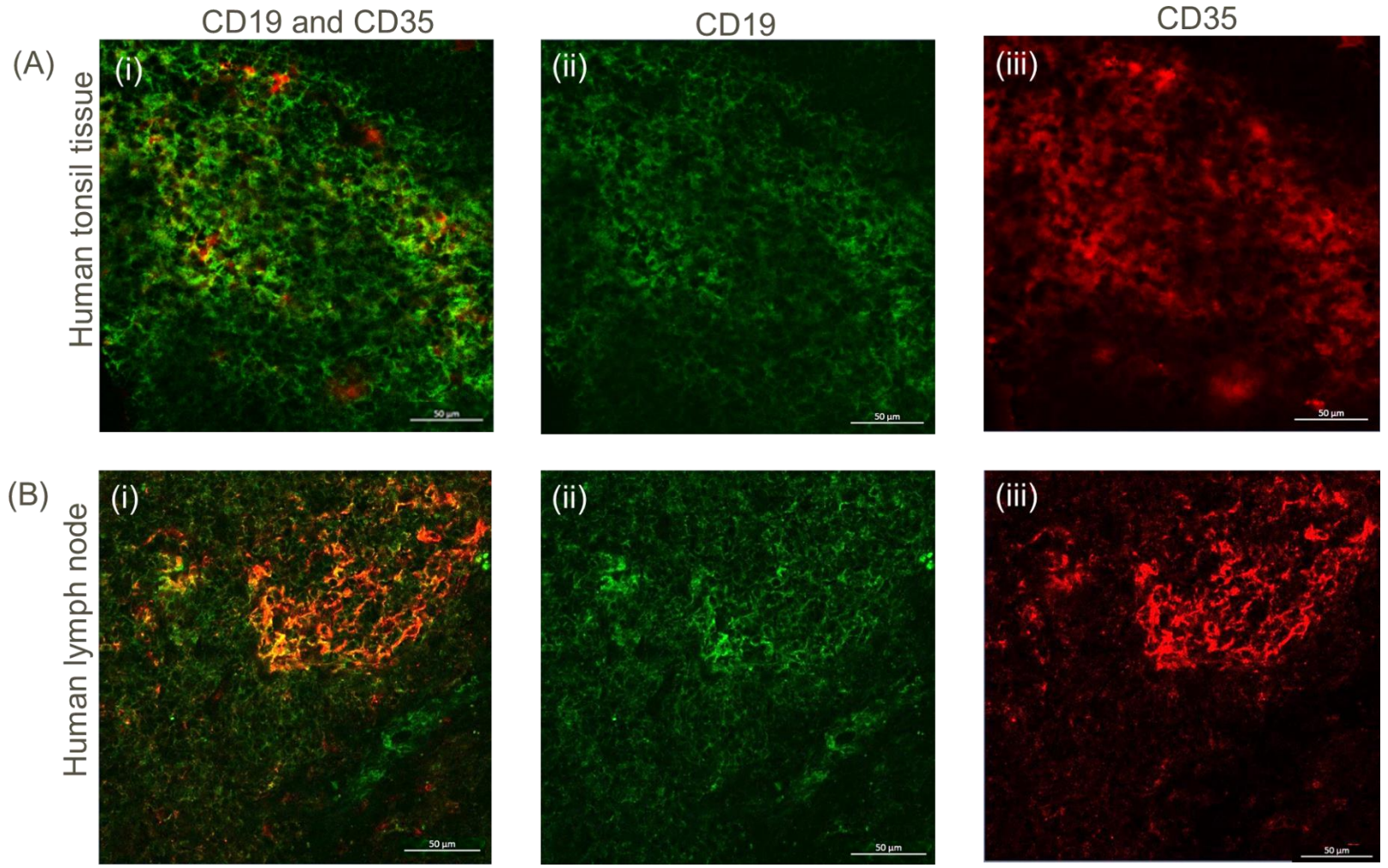

Figure 9.3.1: Germinal cenres in human tonsil and lymph nodes are CD19+CD35

(A) human tonsil tissue stained for CD19 (A488-green) and CD35 (A647-red), x63 magnification, scale bar = 50um. (i) DAPI, CD19 and CD35 overlay. (ii) CD19 only. (iii) CD35 only. (B) Human lymph node stained for CD19 (A488-green) and CD35 (A647-red), x63 magnification, scale bar = 50um. (i) CD19 and CD35 overlay. (ii) CD19 only. (iii) CD35 only. This image is representive of 3 patients, from which 3 sections were examined and mutliple images taken of germinal centres in each section.

To extend these observations, tonsil tissue was stained with antibodies against CD35 and CXCL13 (Figure 9.3.2). This analysis shows that CXCL13 is tightly associated with the $CD35^+$ cells, previously identified as FDCs (Figure 9.3.3). CXCL13 is the ligand for CXCR5, a receptor expressed by B cells and this causes B cells to migrate to the light zone within the germinal centre (Tjin et al., 2005), which may explain the close association of the chemokine with FDCs. Within lymph node tissue, a large proportion of FDC networks were seen to be inactivated; smaller, less connected cells, with little CXCL13 signal (Figure 9.3.2), suggesting CXCL13 production is higher in activated FDCs. Increased CXCL13 expression in mature networks during an immune response occurs to attract more B cells to the dark zone and undergo high affinity antigen selection, therefore producing a larger immune response when required. As human tonsil tissue is obtained from tonsillectomy patients it is reasonable to suggest that their FDC networks are activated and undergoing an immune response, unlike the lymph node tissue derived from donor liver transplants used in this investigation and thus thought to be naïve. This may be the reason all networks imaged here, within tonsils, are activated.

Costaining of tonsil and lymph node tissue with antibodies against CD21 and CD35, confirmed FDCs are $CD21^+CD35^+$ (Figure 9.3.5); suggesting both are suitable markers for FDC identification.

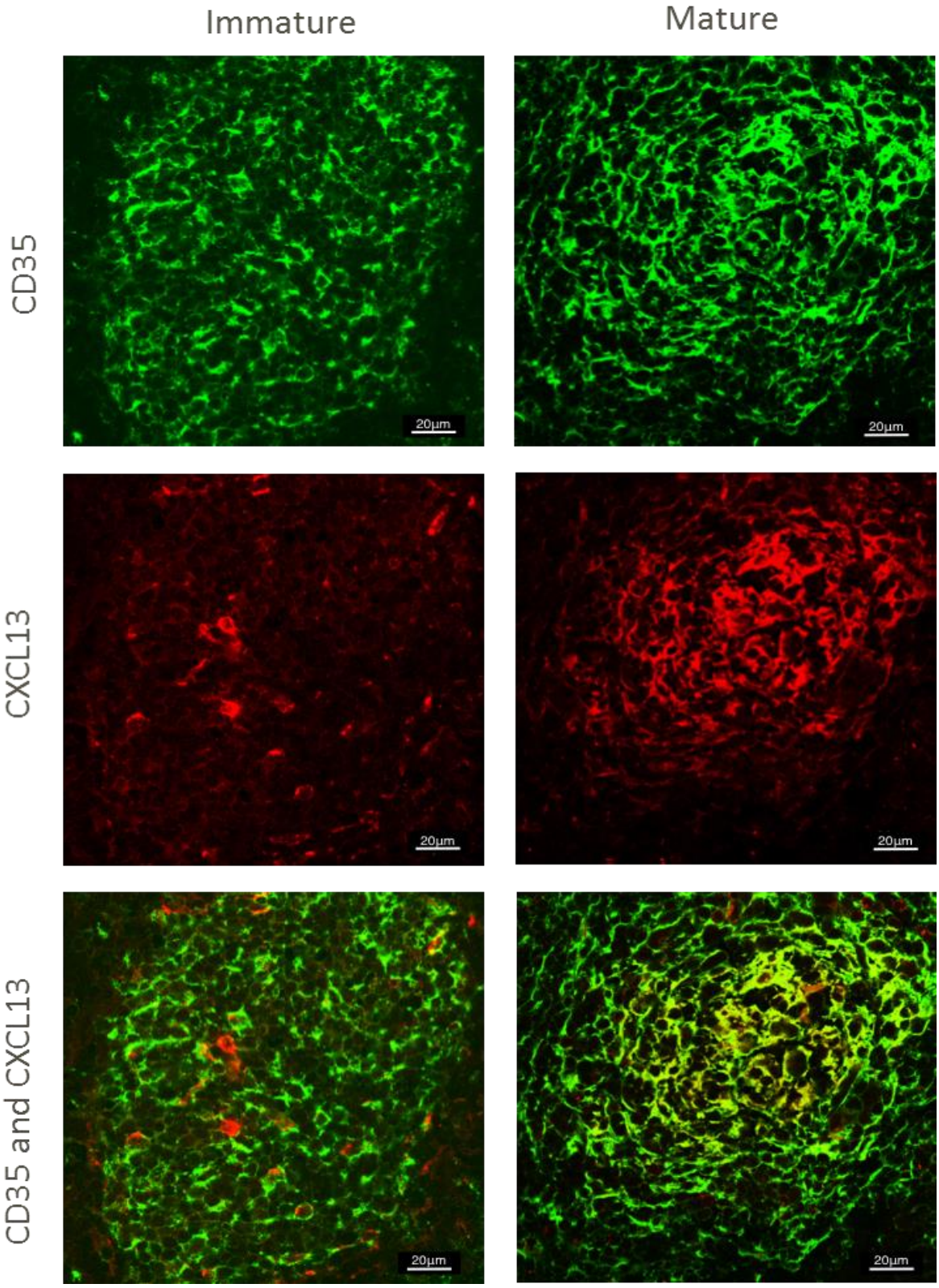

Figure 9.3. 2: CXCL13 expression in human lymph nodes

The left hand side shows an immature FDC network with relatively low expression of CD35 (green) and CXCL13 (red). The right hand side shows a mature FDC network with upregulated CD35 and CXCL13. Scale bar = 20um. This image is representive of 3 patients, 3 sections were stained from each patient and multiple images taken of germinal centres within each section.

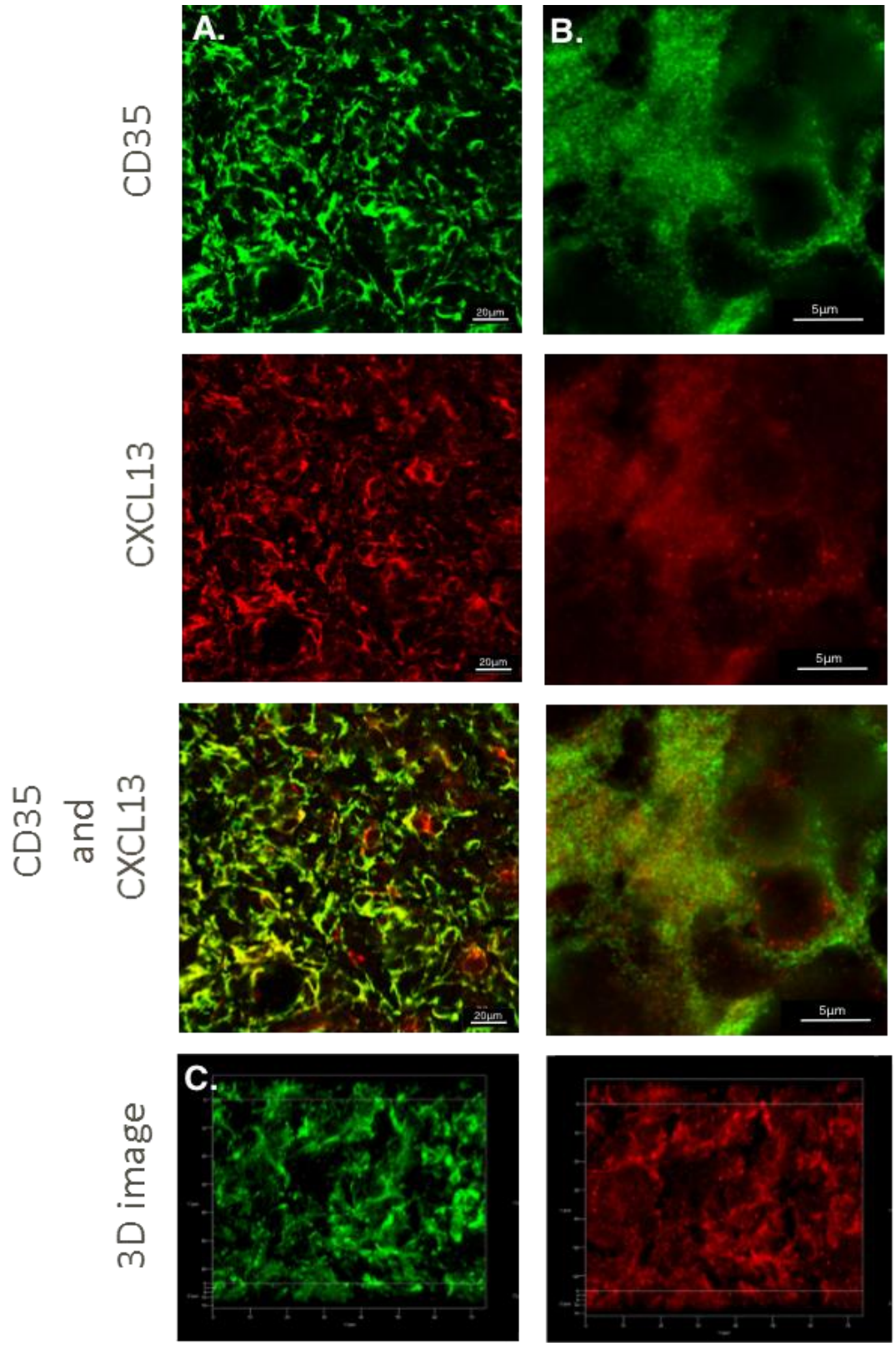

Figure 9.3. 3: 2D and 3D images of CXCL13 expression in human tonsil tissue

(A) CD35 (green) and CXCL13 (red) expression in human tonsils, scale bar = 20um. (B) Close up of CXCL13 and CD35 expression, scale bar = 5um. (C) Z=stack of CD35 and CXCL13 in human tonsils. These images are representive of 3 patients investigated. 3 sections were stained from each patient and multiple images were taken of germinal centres for each section.

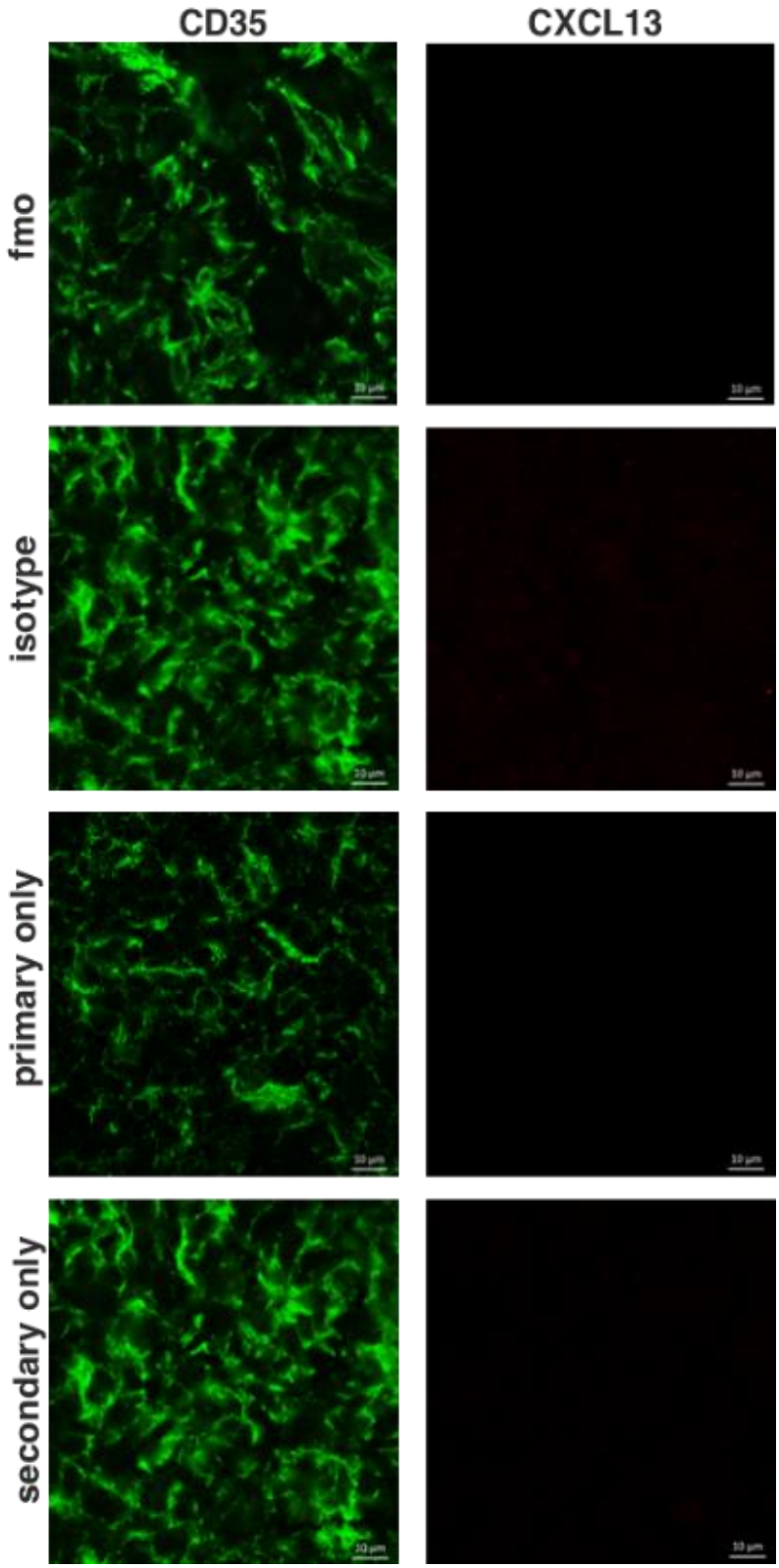

Figure 9.3. 4: IHC controls for CXCL13 expression

Scale bar = 10um

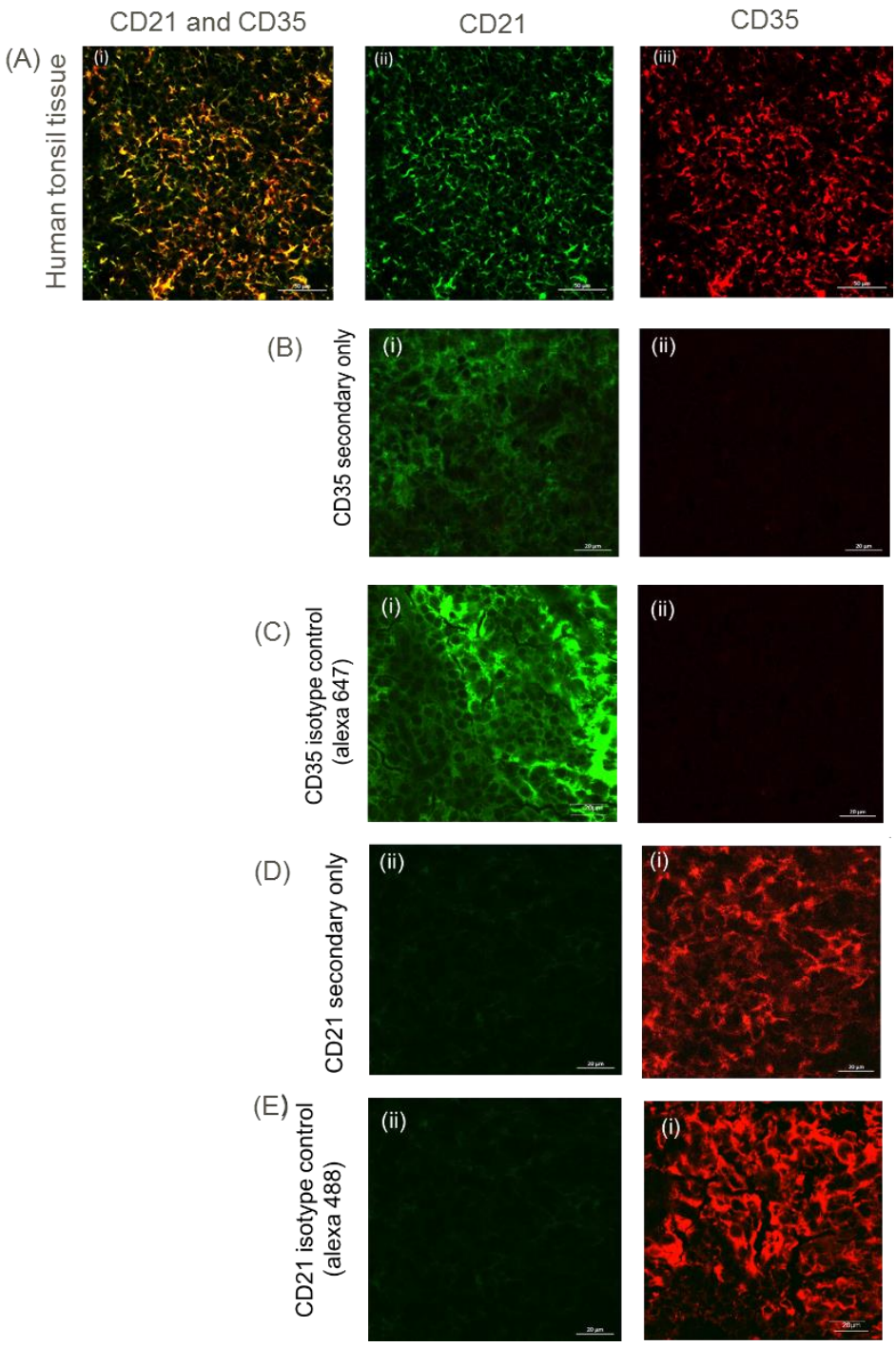

Figure 9.3. 5: Human FDCs in the tonsil and lymph node are CD21 and CD35 positive

(A) Human tonsil tissue stained for CD21 (A488-green) and CD35 (A647-red), x63 magnification, scale bar = 50um. (i) CD21 (green) and CD35 (red) overlay. (ii) CD21 only. (iii) CD35 only. (B) A647 secondary only control shows no signal in the red channel, therefore staining is specific for CD35, scale bar = 20um. (i) CD21 (green channel) and A647 secondary (red channel). (ii) Red channel only. (C) CD35 isotype control antibodies show no non-specific staining, x63 magnification, scale bar = 20um (i) green and red channel. (ii) red channel only. (D) A488 secondary only control shows no signal in the green channel; antibody is specific for CD21, x63 magnification, scale bar = 20um. (i) green channel only. (ii) green and red channel. (E) CD21 isotype control antibodies show no non-specific staining, x63 magnification, scale bar = 20um. (i) green channel only. (ii) green and red channel. These images are representiative of 3 patients, 3 sections were stained from each patient and each section was imaged multiple times.

Staining both tonsil and human lymph node tissue sections with antibodies against CD21 identifies the stromal-like cells within the germinal centre known to be FDCs (Figure 9.3.5). Antibodies against CD19 confirm B cells are present within the section but staining does not overlap with the measured CD21 signal. It is known that CD21 is expressed by B cells, however it does not appear to be detectable using this method. Reasons for this discrepancy could be due to the bright signal seen on the stromal cells (assumed FDCs) for CD21 staining. Similarly, FDCs are reported to express low levels of CD19 at the mRNA level (Barrington et al., 2009), however IHC staining performed within the current study suggests they are negative for this marker. This observation supports the hypothesis of bright versus dim cells and the ability to detect expression on both cells by IHC when both cell types are present in the tissues. Other explanations could include differences in receptor expression by the cell types; it is known that CD21 on B cells is in a co-complex with CD19 (Bradbury et al., 1992) which could be masking the epitope recognised by the antibody clone chosen. Additionally, as CD21 has two isoforms, named short and long, and it is reported FDCs express the long form, this could also be a reason for this discrepancy. Although the antibody clone Bu32 binds both isoforms, it is possible it may have a higher affinity for one isoform over the other.

In summary this immunohistological imaging of human secondary lymphoid organs shows FDCs can be identified as $CD35^{+}CD21^{+}CXCL13^{+}$ in contrast to $CD19^{+}$ B cells. Both cell types are found to have tight interactions within the germinal centres of these tissues. Interestingly, where both cell types are reported to be $CD21^{+}$, only FDCs are identifiable by this marker in an IHC setting, possibly due to differing expression levels by the two cell types.

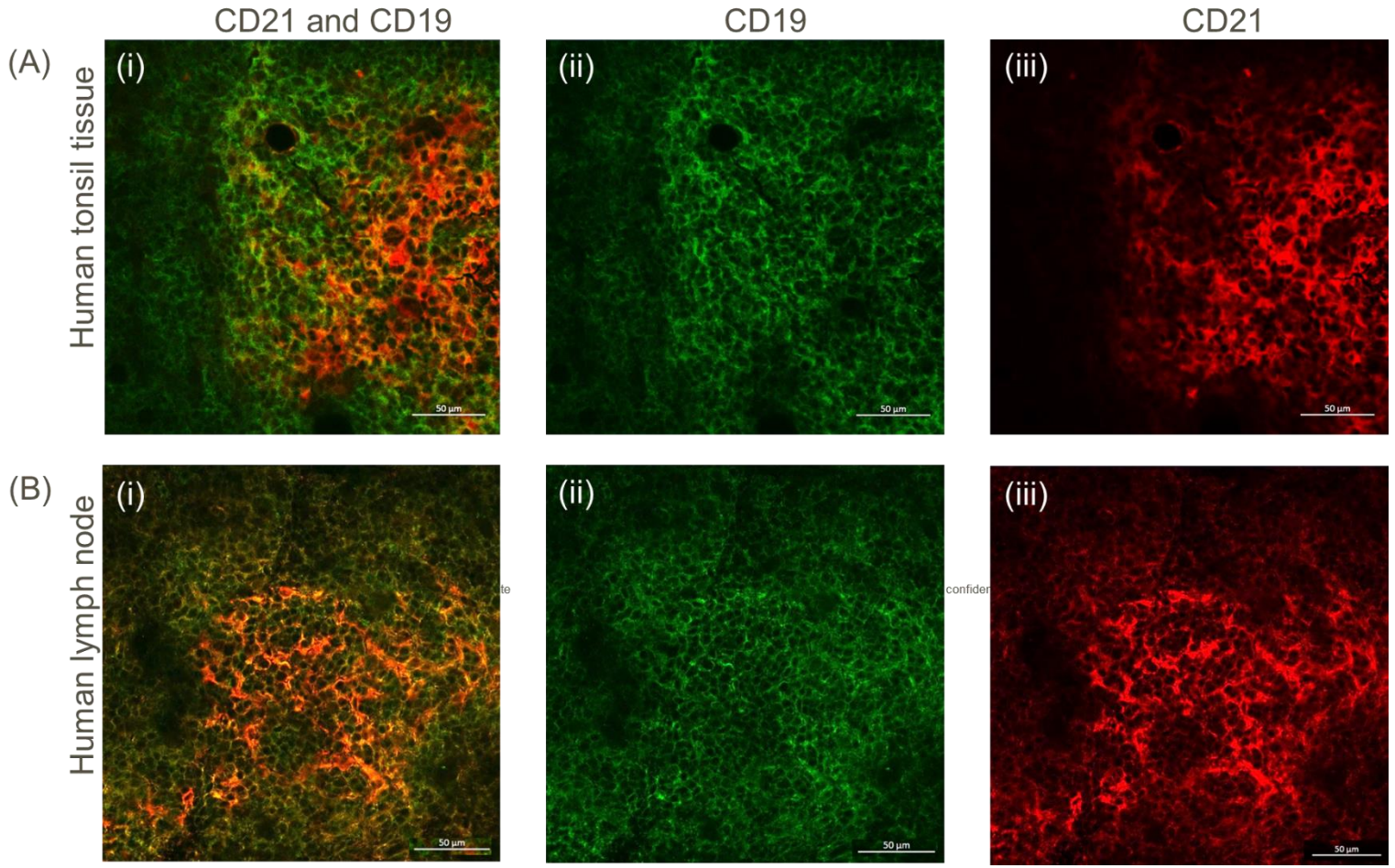

Figure 9.3. 6: Human tonsil and lymph nodes contain CD21+ FDCs

(A) Human tonsil tissue staining for CD21 (A647-red) and CD19 (A488-green), x63 magnification, scale bar = 50um. (i) CD21 (red) and CD19 (green) overlay. (ii) CD19 only. (iii) CD21 only. (B) Human lymph node staining for CD21 (A647-red) and CD19 (A488-green), x63 magnification, scale bar = 50um. (i) CD21 (red) and CD19 (green) overlay. (ii) CD19 only. (iii) CD21 only. These images are representivative of 3 patients, 3 sections were stained from each patient and miltiple images taken of germinal centres within the section.

9.3.2 Isolation of primary human FDCs from tonsil tissue

FDC development and function has been extensively studied using murine models both *in vivo* and *in vitro*, however far less is understood about human FDCs. As no standardised protocol exists for their isolation, work was undertaken to develop a reproducible and robust isolation method for human FDCs from readily available tonsil tissue.

There are few literature-based protocols for human FDC isolation but attempts to reproduce these methods were unsuccessful from human tonsils. Therefore, efforts began to develop a reliable FDC isolation protocol. Initially, many different collagenase enzymes were tested for their ability to digest tonsil tissue. Multiple liberase blends were used to digest tonsil tissue with varying results; liberase was chosen due to reports describing the enzyme as a collagenase with increased specificity, resulting in more efficient cleavage and digestion of tissue. Using this enzyme, stromal-like cells were isolated and could be cultured *in vitro* but flow cytometry analysis for FDC markers (CD21, ICAM-1 and CD35) revealed FDCs were not present within these cell cultures (data not shown). Engagement with collaborators in the Tarte lab (unpublished, University of Rennes) and the C3 DPU at GSK (Stevenage), lead to development of the resulting protocol. During method development, samples were taken at different time points during the tissue digestion steps for flow cytometry analysis to investigate the optimal time conditions for the extraction of FDCs from tissue. Incubation at 37ºC for 20 minutes was determined as the optimal digestion time for extraction of FDCs from human tonsil tissue with the final cocktail of enzyme chosen. Additional incubation time also allowed the increased isolation of FRCs, but as FDCs were the cell of interest for this study, incubation time was kept to 20 minutes.

The final protocol used for FDC isolation is detailed within Materials and Methods Section 8.2. In brief, tonsil tissue was digested using a cocktail of DNase I, Collagenase IV and Dispase and subsequently CD45 depleted to remove $CD45^+$ lymphoid cells. An antibody staining panel was developed to correctly identify FDCs within the tonsil digests (Figure 17). FITC was used as a “lineage” channel containing markers; CD45 (lymphoid cells), CD11b

(macrophage), CD31 (endothelial cells) and CD34 (progenitor cells). Markers within this channel exclude cells of hematopoietic lineage such as T and B cells. Germinal centre stromal cell populations, FDCs and FRCs, express gp38, therefore lineage$^-$gp38$^+$ cells contain these cell types. On average, when using this protocol, 300 FDCs were isolated from each sample per 2x10^6 cells. Finally, to separate the stromal cell types, CD21 or CD35 was used. FDCs are positive for both these receptors but they are not expressed on FRCs. Therefore, FDCs were identified as lineage$^-$gp38$^+$CD35/CD21$^+$. Identification and isolation of this cell population allows downstream analysis of function and characterisation using mRNA and protein analysis tools.

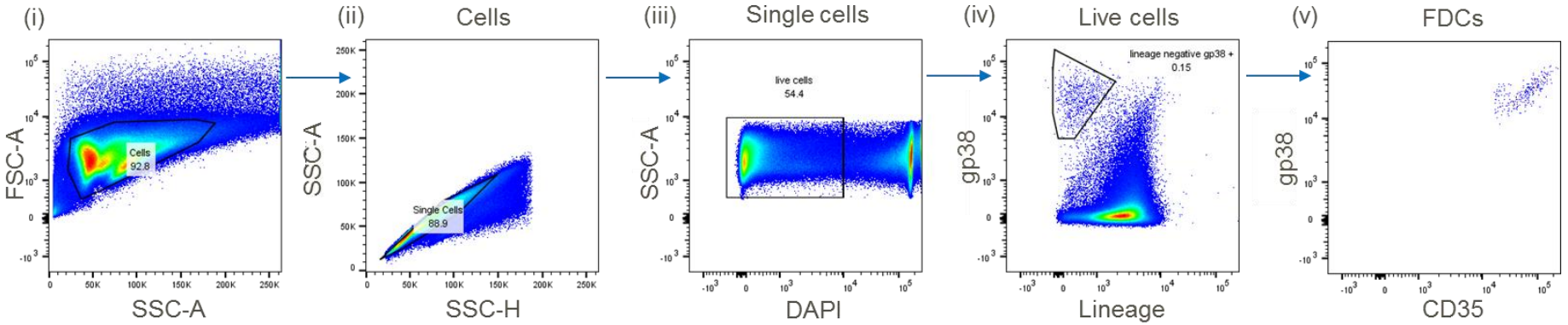

Figure 9.3. 7: FDCs can be successfully isolated from human tonsil tissue

(i) cells were gated, followed by (ii) single cells and (iii) live cells. (iv) FDCs are identified by lineage negative and gp38 positive cells. Lineage gate includes markers CD31, CD11b, CD45 and CD34. (v) FDCs are further characterised by the expression of CD35. The number of FDCs from each patient varies, on avaerge around 300 cells are collected per sample, a small fraction of the initial ~12X10^6 cells run. This figure is an example of one FDC isolation, isolation was carried out in many patients (above 100 samples) and results were consistent between patients.

Data presented above confirmed that FDCs within the germinal centre can be identified using CD35 or CD21 by immunohistochemistry (Figure 9.3.6). To further confirm the interchangeability of the two receptors as FDC markers using flow cytometry, FDCs derived from human tonsil tissue were costained with antibodies against CD21 and CD35. A single FDC population (lineage$^-$gp38$^+$CD35$^+$CD21$^+$) is seen, therefore the same population will be analysed whether cell identification uses CD35 or CD21 (Figure 9.3.8). For isolation by cell sorting, CD35 was used to identify FDCs, described as a lineage$^-$gp38$^+$CD35$^+$ population. In later investigations focusing on CD21 biology, it is important to confirm cells of interest are CD21$^+$, therefore CD21 was chosen to identify FDCs, described as a lineage$^-$gp38$^+$CD21$^+$ population.

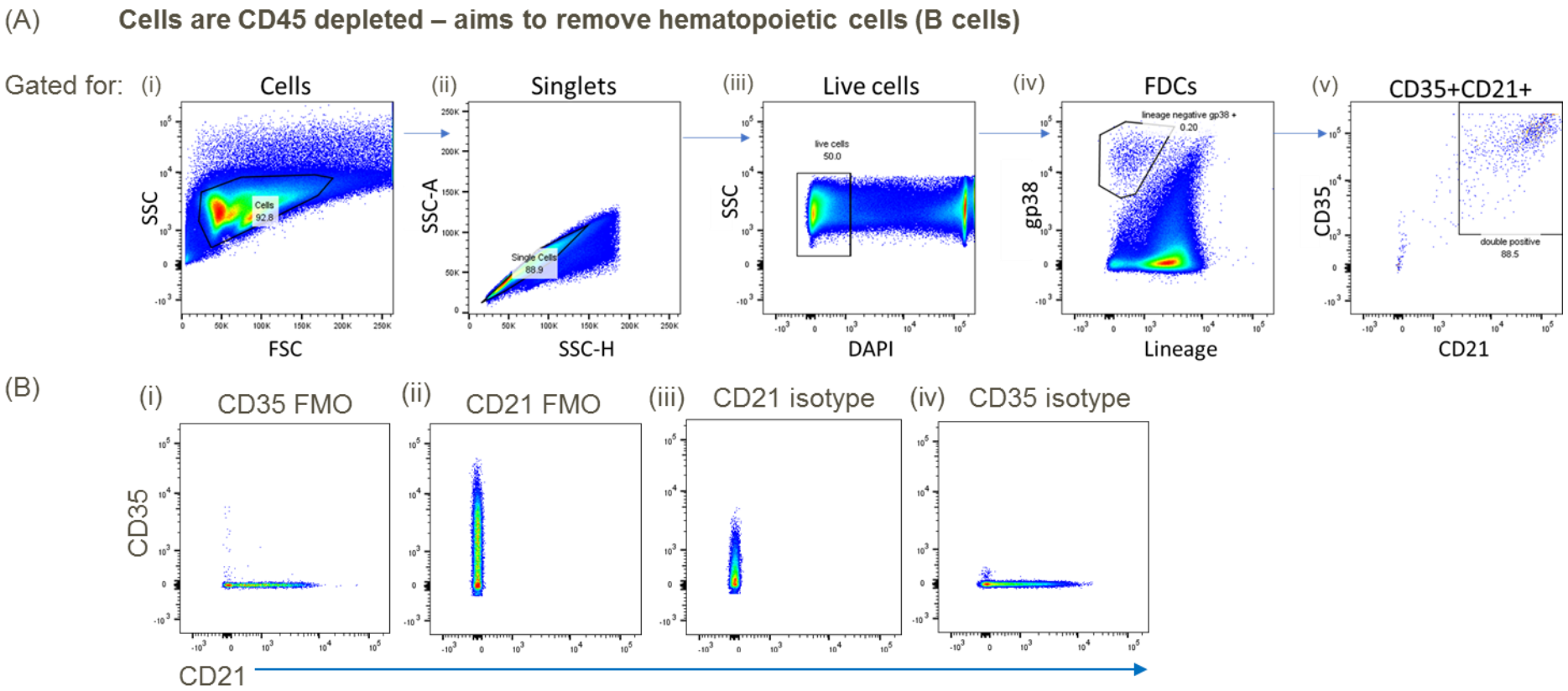

Figure 9.3. 8: FDC populations can be identified as CD35 or CD21 positive

(A) (i) human tonsil tissue cells are gated on, (ii) doublets and (iii) dead cells are removed from the analysis. (Iv) FDCs are gp38 positive and lineage negative (lineage gate = CD45, CD11b, CD34 and CD31). (v) FDC population is double positive for CD35 and CD21. (B) Staining panel controls. (i) CD35 fluorescence minus one, sample stained with full staining panel minus CD35 antibody. (ii) CD21 fluorescence minus one, sample stained with full staining panel minus CD21 antibody.(iii) CD21 isotype stained sample, sample stained with full antibody panel with CD21 antibody replaced with isotype control antibody. (iv) CD35 isotype stained sample, sample stained with full antibody panel with CD35 antibody replaced with isotype control antibody.

As B cells also express CD21 and are tightly associated with the stromal cells of the germinal centre within tonsil tissue; showed in this investigation by IHC (Figure 9.3.1). CD35 was chosen as the FDC identification marker for cell sorting to ensure collection of FDCs only. When assessing $CD21^+$ cells, it was confirmed that the FDC population identified were not an FRC/B cell doublet, which would also be $lineage^-gp38^+CD21^+$ when assessed by flow cytometry. Although the FDC population is positive for CD19 (Figure 9.3.9A), which is highly expressed by B cells, staining with CD20 reveals the FDCs are $CD20^-$ therefore do not have B cells attached (Figure 9.3.9B). Low levels of CD19 surface expression by FDCs has been previously reported, the function of which is unknown (Barrington et al., 2009). Expansion of the $lineage^+$ population shows the expected high $CD20^+$ staining of the B cells contained in this gate (Figure 9.3.9C), confirming the antibody staining with CD20 was successful and FDCs are truly negative for this marker.

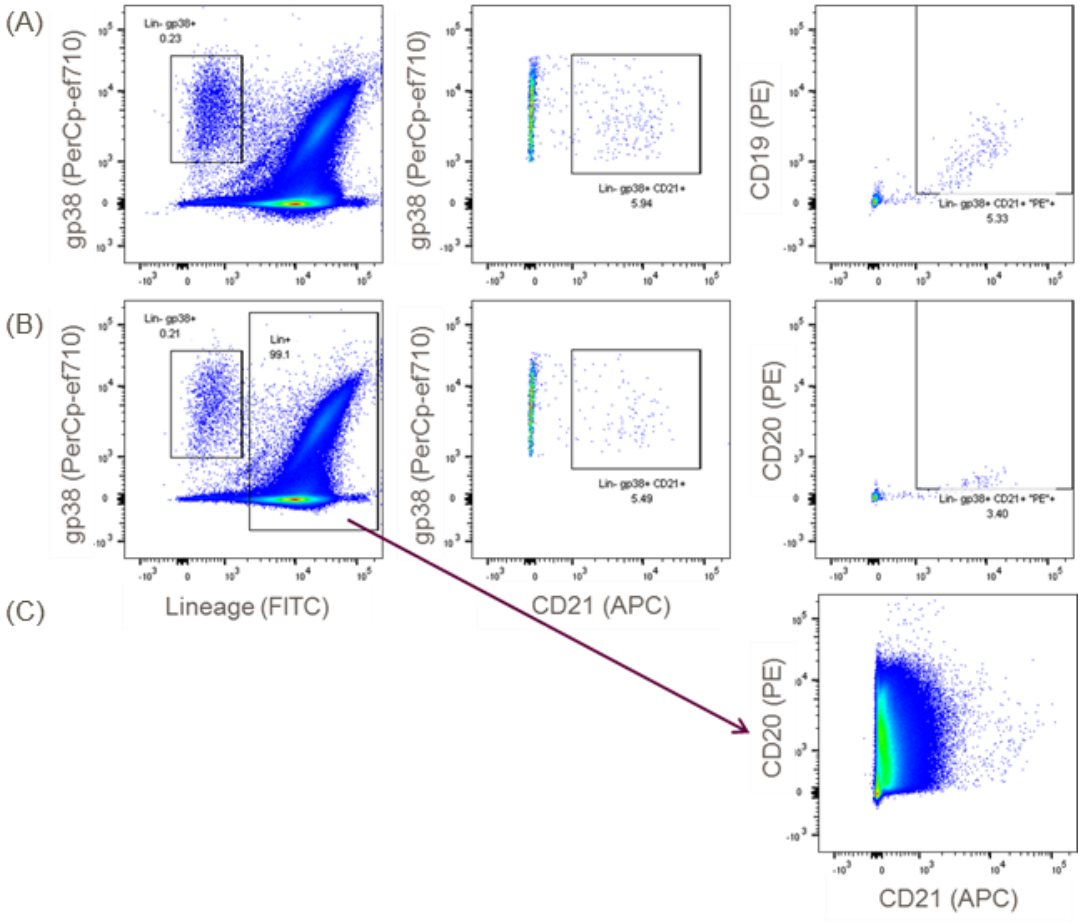

Figure 9.3. 9: FDCs isolated from human tonsil are CD19 positive and CD20 negative

(A) Lineage negative, gp38 positive cells are gated for CD21. CD21 positive cells are also CD19 positive (B) but CD20 negative, therefore are not FRC/B cell doublets. (C) Lineage positive cells are both CD20 and CD21 positive; this gate contains B cells. Data collected by Laura Rapley (GSK).

It was then possible to isolate FDCs (lineage$^-$gp38$^+$CD35$^+$ gated cells) using cell sorting (Figure 9.3.7). FRC/MRCs (lineage$^-$gp38$^+$CD35$^-$ cells) were also collected to use as controls in further experiments. Tonsil samples that had not undergone a CD45 depletion were used to isolated T cells (CD3$^+$) and B cells (CD19$^+$) by cell sorting (Figure 9.3.10). Identification by flow cytometry of these cell types is important for downstream functional assays investigating antigen carriage on FDCs and B cells and isolation allows assessment of CD21 mRNA and protein expression within the cells.

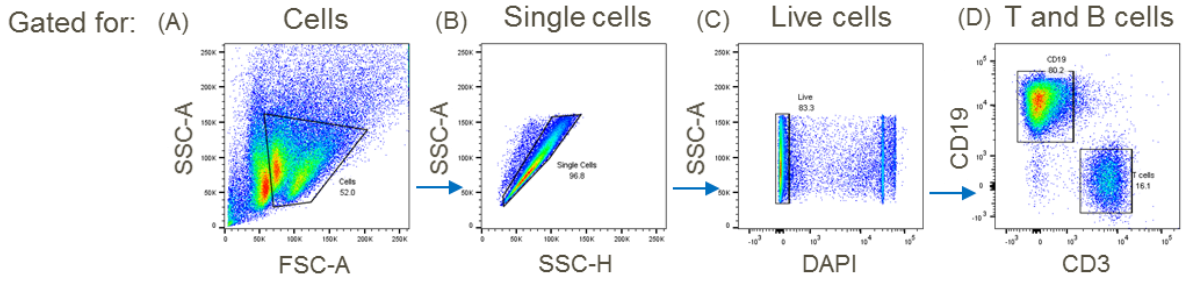

Figure 9.3. 10: Sorting T and B cells from human tonsil tissue

A) Cells are gated for PBMCs (B) and single cells. (C) Live cells are selected and (D) separated into T and B cells using CD3 and CD19 staining respectively.

To further characterise the sorted cell populations and confirm their identity, qPCR was performed for key cell markers (Figure 9.3.11), similar to those used previously in IHC and flow cytometry analysis of the cell populations. The isolated lineage$^-$gp38$^+$CD35$^+$ cell population was shown to express CD35, CD21 and CXCL13 mRNA, consistent with the protein expression seen using IHC in this investigation, confirming this population are FDCs. B cells express CD21 and CD19, which is also confirmed here by qPCR at the mRNA level (Figure 9.3.11C and 9.3.11B). T cells were identified by expression of CD3 mRNA (Figure 9.3.11F). The lineage$^-$gp38$^+$CD35$^-$ sorted population, are CCL21$^+$ but negative for the other markers investigated here (Figure 9.3.11E), confirming they are the stromal cell FRC/MRCs. Interestingly, FDCs express much higher levels of CD21 at the gene level than B cells and T cells express low levels of CD21. These data support the previous observations seen by IHC where FDCs are bright for CD21 and mask the dimmer staining for CD21 on B cells.

These data confirm that FDCs from human tonsil tissue can be identified and continue to express key cell markers after FACS sorting using the developed protocol.

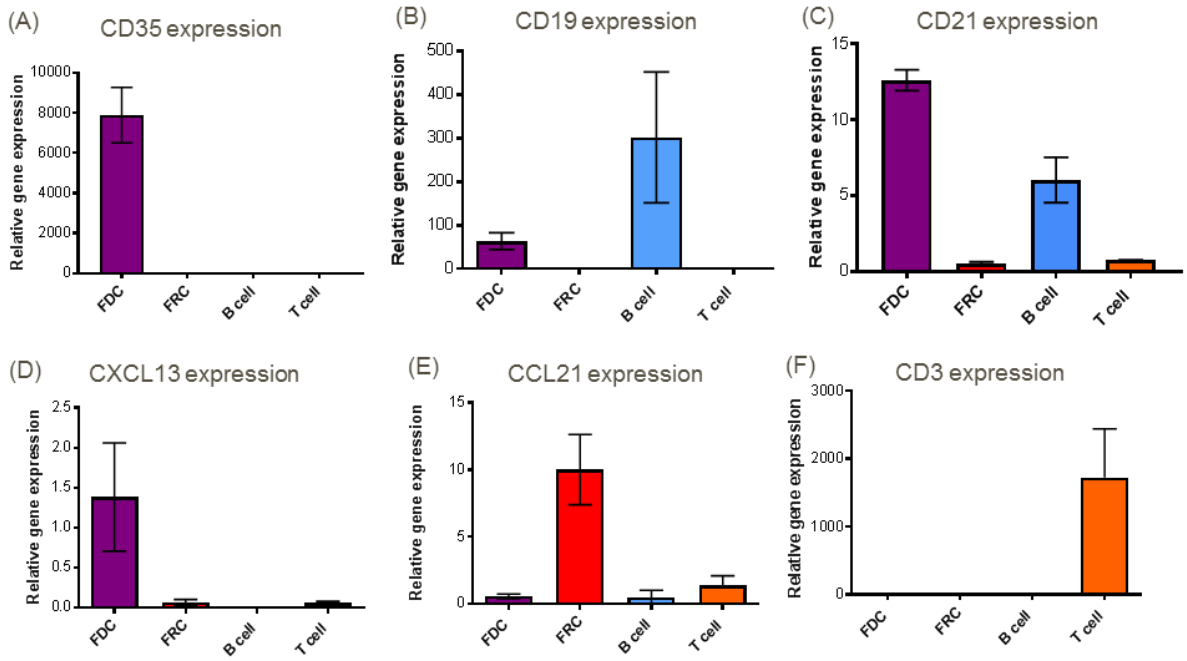

Figure 9.3. 11: qPCR for known markers of germinal centre cell populations

n=3, bars represent SD (A) CD35 expression; FDC population expresses high levels. (B) CD19 expressed by B cells and low levels expressed in FDCs. (C) CD21 expressed highly in FDCs, B cells and low levels expressed in T cells. (D) CXCL13 expressed in FDCs. (E) CCL21 expressed in FRC population. (F) CD3 expressed highly by T cells.

9.3.3 Absolute CD21 receptor number on the surface of germinal centre cells

As CD21 is a critical receptor within the germinal centre reaction expressed by these cells, the remainder of this work focuses on the role of CD21 within biology. Although it is well accepted that FDCs, T and B cells express CD21, absolute receptor number on these cell types has not previously been investigated. Consistent with published data, this investigation has shown that FDCs express CD21 by IHC and qPCR, however B cells are not $CD21^+$ by IHC analysis but can be identified as $CD21^+$ by flow cytometry and qPCR. These observations suggest a higher expression of CD21 receptor by FDCs, a phenomenon that could lead to transfer of C3dg-bound antigen between the two cells as hypothesised. This discrepancy was the driver for this work which aimed to quantify and compare the number of CD21 receptors expressed on the surface of human tonsil derived FDCs, B cells and T cells, as well as comparing peripheral and tonsil derived T and B cells.

CD21 expression on T and B cells was assessed by flow cytometry. B cells were $CD19^+CD20^+CD21^+$ cells (Figure 9.3.13); both CD19 and CD20 were used as markers in this analysis to demonstrate that either receptor can be used as a marker for B cells. FDCs have low level expression of CD19 (Figure 9.3.9A), therefore CD20 staining confirms these cells are B cells. T cells were identified using CD3; only a small population of these cells are CD21 positive (Figure 9.3.13A viii). This data was collected on a higher voltage than that for FDC data collection due to the brightness of CD21 signal on the cell surface (Figure 9.3.15). This was thought to be due to receptor number; this is further discussed in later experiments. For this investigation, FDCs were identified as $lineage^-gp38^+CD21^+$ as described above (Figure 9.3.12).

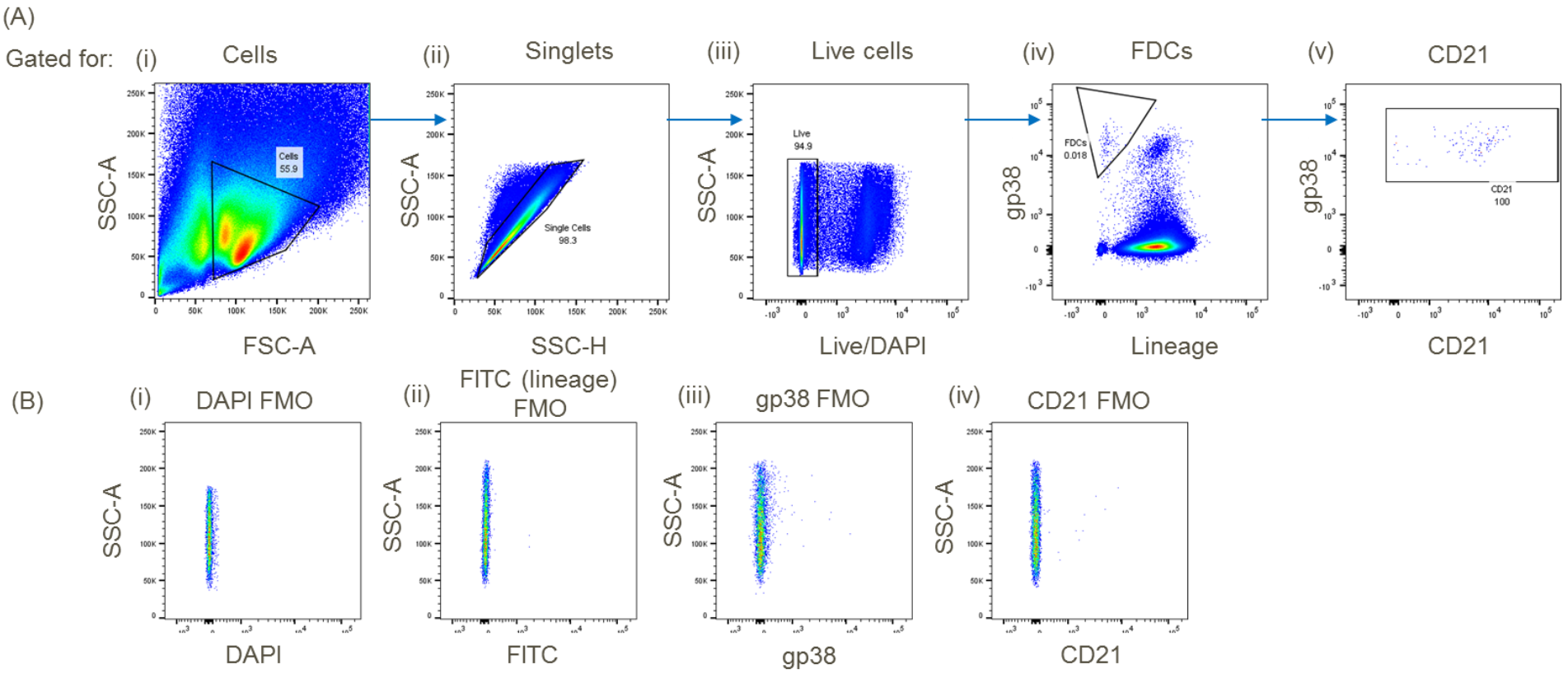

Figure 9.3. 12: Flow cytometry identification of FDCs using CD21

(A) Identification of CD21 positive FDCs. (i) Cells are gated on, (ii) followed by singlets and (iii) live cells. (iv) FDCs as lineage negative (lineage gate includes markers CD45, CD34, CD11b and CD31) and gp38 positive. (v) all cells are CD21 positive confirming they are FDCs.

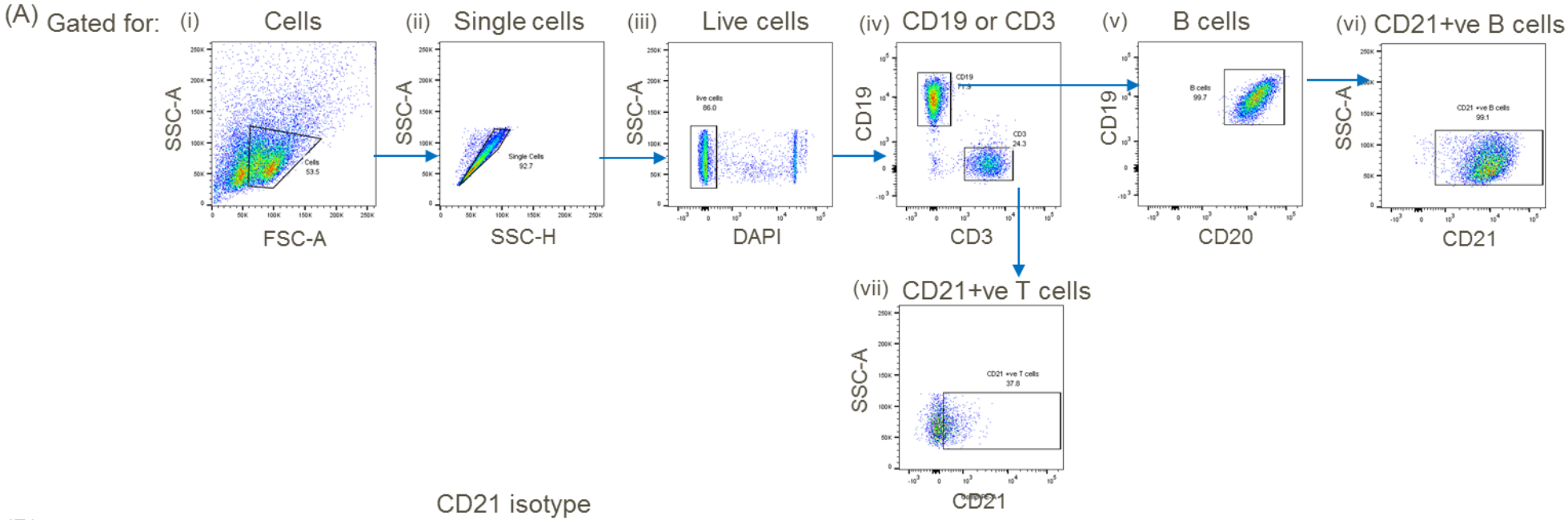

Figure 9.3. 13: Flow cytometry gating strategy for CD21 positive T and B cells

(A) Examples of gating strategy from blood; tonsil and blood derived T and B cells were gated in the same way. (i) PBMCs are selected and (ii) doublets and (iii) dead cells excluded. (iv) Cell populations were split into T and B cells using CD3 and CD19 markers respectively. (v) B cells were further gated for CD20 and (vi) CD21 positive cells resolved. (vii) CD21 positive T cells were gated on using (Bi) FMO and (Bii) CD21 isotype control samples as only a small population is positive for this marker.

In order to accurately calculate the number of CD21 receptors on the cell surface, antibodies were used at saturating concentrations to ensure all receptors are bound and therefore counted. Starting at 10 µg/ml, a serial dilution of CD21 antibody, clone Bu32, was undertaken on FDCs (tonsil derived), T and B cells (tonsil and blood derived). Bu32 binds to all cell types in a concentration dependent manner (Figure 9.3.14) and saturating concentrations are reached at 1 µg/ml for all cells of interest. Bu32 MFI on T cells is lower than the other cell types investigated; saturating concentrations of the antibody are still reached at 1 µg/ml (Figure 9.3.14A and B iii) perhaps influenced by the presence of B cells within the sample compared to if the population had been isolated previous to performing the saturation curve.

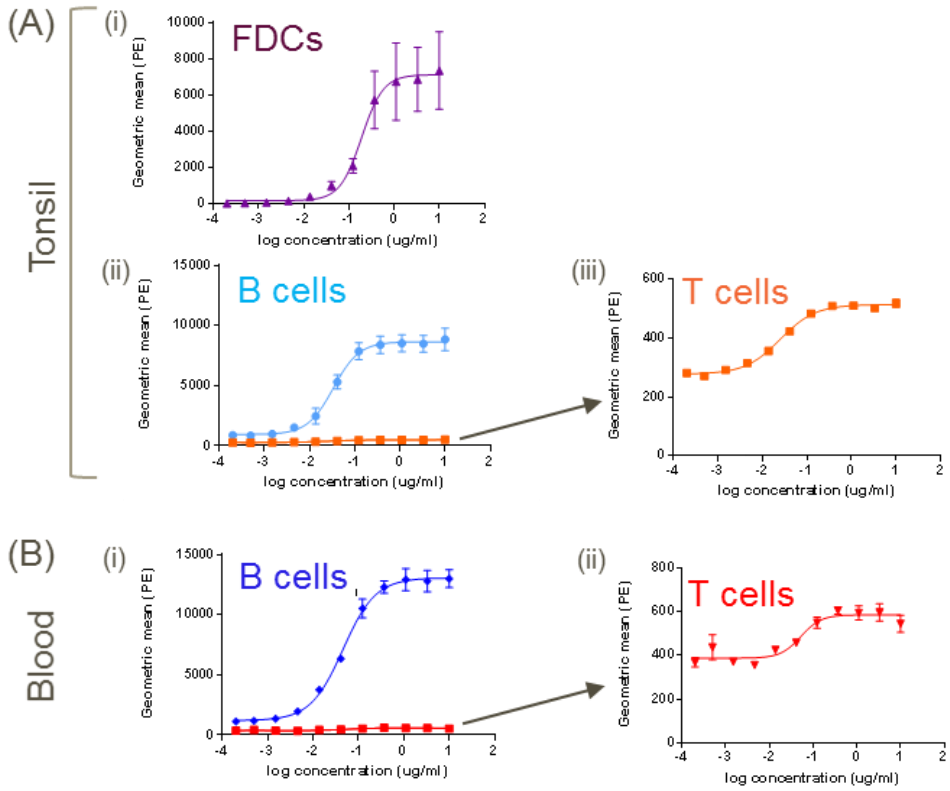

Figure 9.3. 14: Bu32 binds to FDCs, T and B cells in a concentration dependent manner

(A) Tonsil derived FDCs, T and B cells, saturating concentrations of Bu32 are reached at 1ug/ml, n=3, bars represent SD. (i) Bu32 binds to FDCs in a concentration dependent manner. (ii) Bu32 binds to tonsil derived B cells in a concentration dependent manner. (iii) Bu32 binds to the small population of CD21 positive, tonsil derived T cells in a concentration dependent manner. (B) Blood derived B and T cells, saturating concentrations of Bu32 are reached at 1ug/ml, n=3. (i) Bu32 binds to peripheral B cells in a concentration dependent manner. (ii) Bu32 binds to peripheral T cells in a concentration dependent manner.

Using the saturating concentration of Bu32-PE (1 µg/ml) , the MFI of CD21 on the different cell types was converted to absolute receptor number using Quantibrite-PE beads. Quantibrite beads are conjugated with a known quantity of PE molecules which can be plotted against the measured MFI of each bead set to create a standard curve (Figure 8.1). Using the $CD21^+$ population of each cell type, the number of receptors on the cell surface is then interpolated from the standard curve using the MFI of each sample. Similar to IHC staining, CD21 staining on FDCs is brighter than that of B and T cells; therefore, FDC CD21 quantitation data was collected using lower PE voltages than those used for T and B cell CD21 quantitation (Figure 9.3.15). Receptor number was interpolated from standard curves drawn from data collected on respective voltages (Figure 9.3.15). 100% of FDCs and 99.6% of B cell populations were CD21 positive. FDCs express >30-fold higher CD21 on their cell surface than B cells (Figure 9.3.16), an average of 140000 on FDCs compared to 5500 on B cells. As FDCs are much larger than B cells, approx. 3000 μm^3 compared with 300 μm^3 respectively, the increase may be due solely to cell size, but this is unknown as receptor density was not investigated. B cells express higher numbers of CD21 than $CD21^+$ T cells, of which ~20% of the T cell population express CD21. $CD21^+$ T cells express an average of 200 receptors per cell, significantly lower than the other cell populations investigated (FDCs and B cells), of which 99% of cells were $CD21^+$.

It is noted that B cells isolated from blood express higher numbers of receptors than those isolated from tonsil; this may be reflective of biology or alternatively may be due to how the samples were processed. PBMCs from blood were isolated by Ficoll, tonsil derived cells have been isolated from the tissue both mechanically and using enzymes, cells have also been through one freeze/thaw cycle, this tissue processing may cause the cells to lose some level of surface receptors.

In summary, data shows FDCs express high numbers of CD21 receptors on their cell surface, >30-fold higher than B cells which also express many CD21 receptors. Both FDCs

and B cells are 99% CD21^{+} whereas only 20% of T cells express CD21 on their cell surface at low numbers.

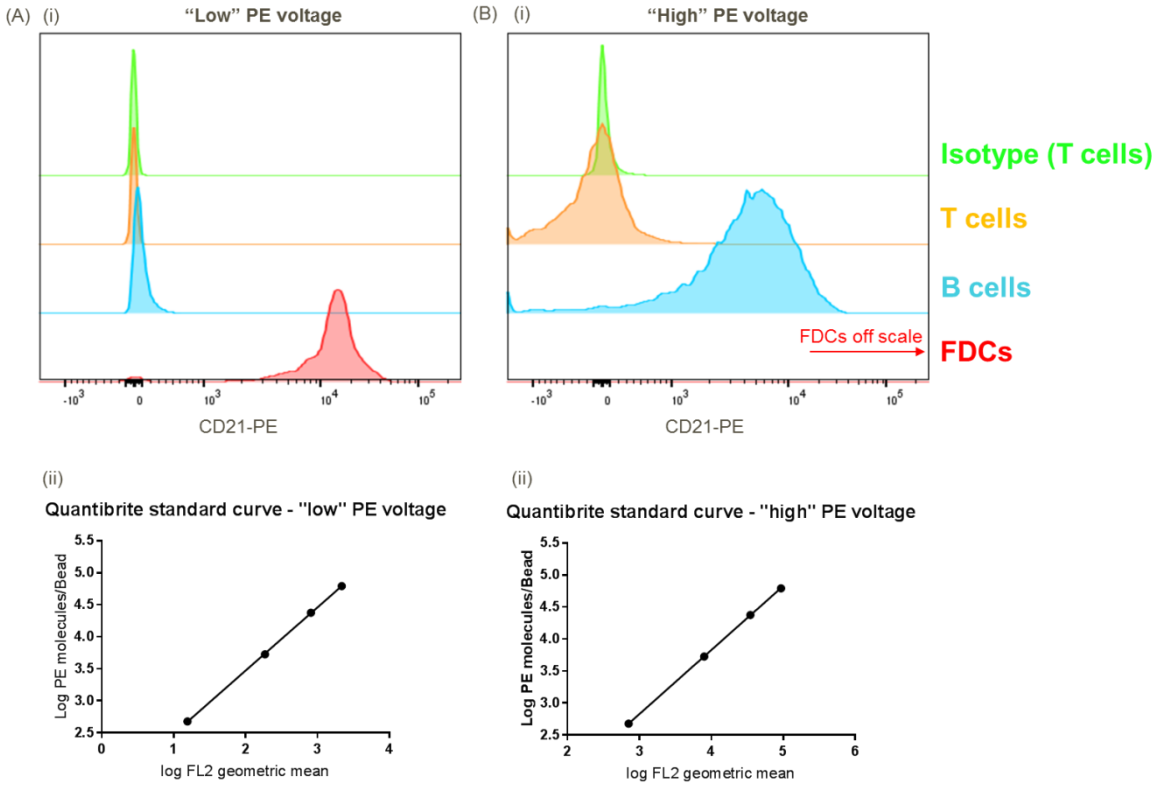

Figure 9.3. 15: CD21 data is collected at different voltages for FDCs and T/B cells

Orange – T cells, Blue – B cells, Red – FDCs, Green – isotype (T cell representative image). (A) (i) CD21 staining on FDCs is brighter than that of T and B cells therefore a lower PE voltage is used to collect this data. T cell CD21 positive cells are not visible above isotype staining (ii) Quantibrite beads standard curve derived from "low" PE voltage data. FDC receptor numeration was calculated from this curve. (B) (i) At higher PE voltages T cell and B cell data is spread to show B cells express higher levels but FDC data is off-scale. T cell CD21 positive cells are now visible above isotype staining. (ii) Quantibrite beads standard curve derived from "high" PE voltage data. T and B cell receptor numeration was calculated from this curve.

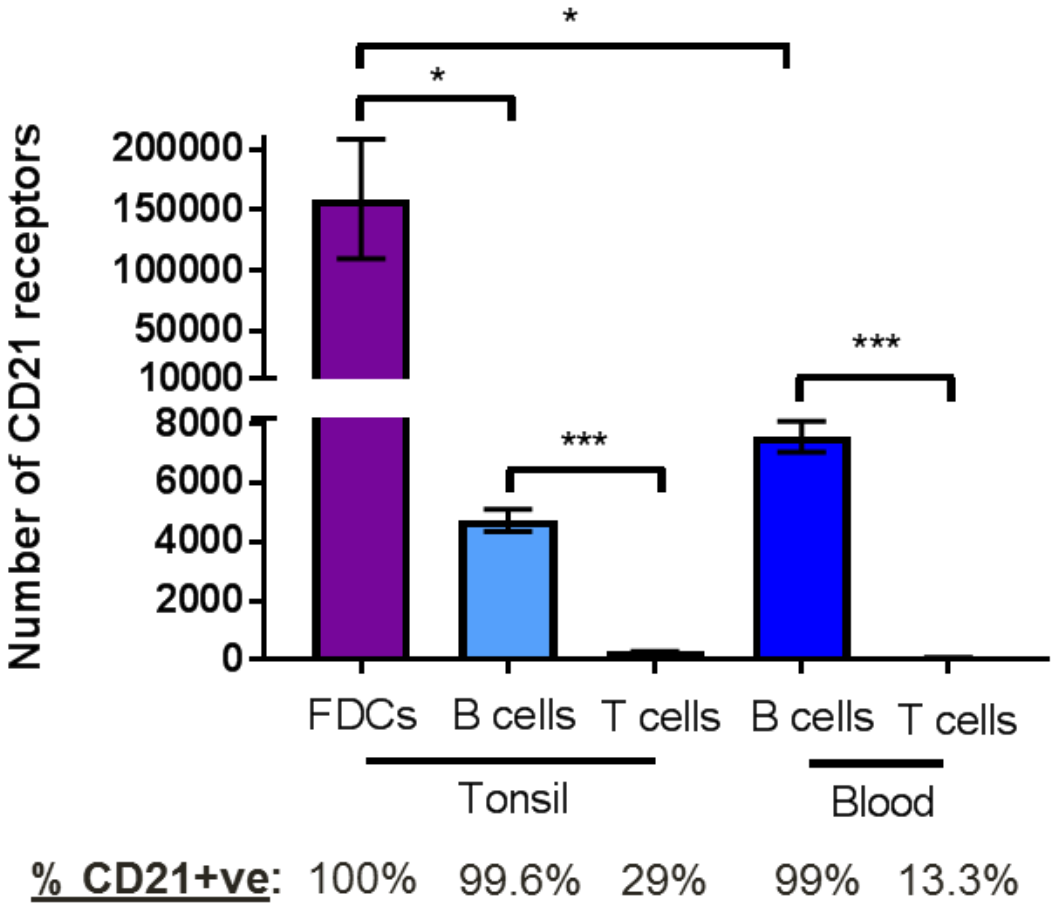

Figure 9.3. 16: Absolute receptor numeration of CD21 molecues on the cell surface

Quantibrite beads were used to calculate the number of CD21 receptors on the cell surface of human tonsil derived FDCs, T and B cells and peripheral T and B cells. FDCs express 33-fold higher CD21 on their cell surface than B cells; B cells express more CD21 than T cells. Significant using a multiple comparisons ANOVA test. n=3, bars represent SD.

9.4 Discussion:

The literature reports unidirectional transfer of C3dg-opsonised antigen complexes between CD21 on B cells and CD21 on the surface of FDCs. The mechanism for transfer is not fully understood, therefore this chapter explores the hypothesis that transfer occurs due to an increased number of CD21 receptors expressed on the surface of FDCs compared to B cells. In order to calculate the absolute receptor expression on these cells types, it was necessary to develop a robust method for human FDC isolation from tonsil tissue, as published methodologies proved unreliable and unsuccessful. Therefore the first aim of this chapter was to identify and isolate human FDCs from secondary lymphoid tissue to allow for downstream analysis of CD21 expression and function of this receptor in further work.

Histological studies give context to cell specific expression of known surface markers in 3D space as well as cellular interactions within the germinal centre microarchitecture. These techniques allowed identification of FDCs and B cells within secondary lymphoid organs, confirming FDCs as $CD35^{+}CD21^{+}CXCL13^{+}$ cells (Figure 9.3.1, 12 and 15) and B cells as $CD19^{+}$ cells (Figure 9.3.1). In alignment with published data (Naiem et al., 1983), B cells are not $CD21^{+}$ when identified using IHC (Figure 9.3.5) but qPCR and flow cytometry analysis (Figure 9.3.11 and 23 respectively) reveals CD21 expression by these cells, something that is well documented in the literature. This discrepancy was the first indication that CD21 expression on FDCs may be greater than that on B cells; therefore it is thought that the high number of receptors bound by antibody on the FDCs in tissue sections causes a bright signal masking any signal from the CD21 on the B cells. This observation is not considered in the literature when assessing specificity of antibody clones by IHC. Both CD21 antibody clones R4/23 (Naiem et al., 1983) and 7D6 (Liu et al., 1997) were reported to bind only to FDCs within tissues, with weak reactivity to B cells outside of FDC zones. These results were interpreted as antibody specificity for FDCs rather than considering levels of epitope expression. Weak staining of B cells with the CD21 antibody clone Bu32 (the clone used within this study) is observed, consistent with the reports discussed above; but staining

within areas devoid of FDCs is likely to reveal strong CD21 signal on the surface of these cells, however this was not undertaken in this investigation.

Human FDCs were successfully isolated from tonsil tissue and identified using lineage$^-$ gp38$^+$CD35$^+$ gating by flow cytometry (Figure 9.3.7). The standardised method developed allowing reliable exclusion of FDCs from human tonsil tissue is detailed in Methods Section 8.2. It was important to establish these methods and identification of this cell type to allow for further experiments using human FDCs to occur. qPCR analysis confirmed isolated populations were FDCs (CXCL13$^+$CD21$^+$CD35$^+$CD19$^+$), FRCs (CCL21$^+$), B cells (CD19$^+$CD21$^+$) and T cells (CD3$^+$) as widely reported in the literature (Figure 9.3.11).

After successful isolation and characterisation of human FDCs and B cells was achieved, absolute numeration of CD21 receptors on the cell surface was undertaken with the hope that this information may help understanding of antigen transfer between CD21 of B cells and CD21 on FDCs. Absolute receptor numeration confirmed FDCs express CD21 at higher levels than B cells on their cell surface (Figure 9.3.16). FDCs express over 30-fold more receptors than B cells. B cells were shown to express ~8000 CD21 receptors per cell; cells typically bear 10,000 – 20,000 receptors for a particular ligand (Lodish et al., 2000), therefore the number of CD21 molecules on B cells is around average. In contrast, FDCs express ~150,000 CD21 receptors per cell. As FDCs are ~10 times larger than B cells (~3000 µm FDCs versus ~300 µm B cells), the number of CD21 receptors expressed by these cells are also thought the be around average levels due to their size. Bearing this in mind, although receptor density was not thoroughly investigated, as the size difference between FDCs and B cells is around 10-fold, it is reasonable to suggest receptor density on FDCs is ~3-fold higher than that on B cells. This increased density of CD21 receptors and the larger cell size in comparison to B cells may allow FDCs to bind a greater proportion of C3dg molecules present on the C3dg-immune complexes bound by B cells, thus rapidly sequestering the immune complexes by endocytosis into endosomal compartments would allow unidirectional transfer of complexes from B cells to FDCs. This concept was previously

suggested in the literature (Heesters et al., 2014), in which they proposed that is was the size of the FDC that allowed for unidirectional transfer of C3dg-antigen complexes, however this was not investigated further in this particular study. Previous studies visualising antigen transfer between B cells and FDCs using a mouse model also suggested that one mechanism of action for this transfer could be receptor number (Phan et al., 2007). Murine FDCs have also been shown to express higher levels of CD21/CD35 on their surface than B cells, although absolute quantification has not been reported. This study suggested that this increased receptor expression may be potentially important in the successful competition with migrating B cells for the capture and retention of noncognate immune complexes.

Electron microscopy studies have been utilised to visualise the spacing of antigen complexes, and hence CD21, on the FDC membrane (Shikh et al., 2010). Antigen complexes were found to be periodically arranged on the FDC cell membrane, spaced 200 to 500 Angstroms apart. This spacing is likely optimal for multimerised FDC-immune complexes to simultaneously engage multiple BCRs and induce B cell activation. These findings further support the hypothesis that greater CD21 receptors allow for antigen transfer to FDCs as the spacing observed here suggests that FDCs would are able to bind to multiple C3dg molecules on the immune complexes, creating greater contacts to the complex than the B cell, again resulting in successful competition within transfer.

To conclude, immunohistochemical studies allowed visualisation and identification of FDCs and B cells within the germinal centre of secondary lymphoid organs, tonsil and lymph node; revealing CD21 staining occurs only on FDCs due to high expression of this receptor compared with B cells. Development of a robust FDC isolation protocol from tonsil tissue allowed for CD21 receptor numeration on human FDCs as well as tonsil and blood derived T and B cells. Receptor numeration revealed a small population of T cells expressing a low number of CD21 receptors, approximately 200 receptors per $CD21^+$ cell. This experiment also confirmed that FDCs express >30-fold higher CD21 receptor numbers on their cell surface than B cells. When considering the relative size of FDCs and B cells, it is thought

that CD21 expression on FDCs is ~3-fold denser than that on B cells. Therefore this data suggests the increased cell size and CD21 receptor density may be a mechanism for unidirectional transfer of C3dg-antigen complexes from B cells to FDCs.

A second hypothesis regarding another possible mechanism for antigen transfer is that transfer occurs due to differential CD21 isoform expression on B cells and FDCs. The FDC isolation method developed here will further allow investigation into this second hypothesis and reveal a greater insight into the mechanism for antigen transfer. Therefore the remainder of the thesis will focus on CD21 C3dg-binding functionality and the receptors role in health and disease, determined by the vast difference in receptor number expressed on the cell surface and the essential role CD21 has within the germinal centre reaction.

10. Results chapter 2: CD21 function and isoforms in biology

10.1 Introduction

CD21 is an essential receptor involved in the initial formation and function of the germinal centre reaction. It is expressed on both FDCs and B cells and is responsible for C3dg-antigen complex binding and transfer of said complexes between B cells and FDCs.

The CD21 protein is formed of sushi domains, also known as complement control protein (CCP) modules, or short consensus repeats (SCR). These domains exist in a variety of complement and adhesion proteins; the structure is based on a beta-sandwich arrangement, one face made of three β-strands (Campbell et al., 1991). The complete structure of the CD21 molecule, 15 SCRs, (Gilbert et al., 2006) and the structure of the first two SCRs complexed with C3d, the binding domain of the receptor and its ligand, have been solved by X-ray crystallography (van den Elsen et al., 2011). The structure for the first two SCRs was solved as an asymmetric unit containing four molecules: two CD21(SCR1-2) and two C3d molecules forming CD21(SCR1-2):C3d complexes. The interactions between the SCR domains and C3d are in the acidic pocket on the concave surface of C3d and most contacts are between C3d and SCR1.

The structure of all 15 SCRs (CD21S) shows there are flexible linkers between the SCR domains suggesting the role of these structures is to enable reorientation of CD21 and effective C3dg binding independent of the surface topology of the antigen (Gilbert et al., 2006). Conservation of the six longest linkers in CD21 across species including murine and ovine, suggests some immunological importance of this structure. These linkers are distributed throughout the length of the CD21 receptor and appear to act as conformational variable joints (Gilbert et al., 2006).

During development of B cells, CD21 expression is tightly regulated; demonstrated using immunofluorescence analysis with the human CD21 monoclonal antibody clone HB5 (Tedder et al., 1984). This study revealed that, within the foetal bone marrow and liver, preB

and immature B cells do not express CD21. However, there was a small population, approximately 25%, of B cells in the foetal spleen that were $CD21^+$. In contrast, 50% of B cells within the adult bone marrow were shown to express CD21. Mature B cells in the blood from both new-borns and adults, and in the peripheral lymphoid tissue of adults, uniformly express CD21. In addition, activated B cells, which were responsive to T cell-derived differentiation factors were $CD21^+$, whereas plasma cells did not express CD21. These findings suggest that loss of CD21 expression at the message and protein level has a key role in B cell development and maturity.

In CD21 knockout mice germinal centre formation is still retained, although the size is reduced and lack of CR1 and CR2 on both B cells and FDCs reveals an essential function for these receptors in germinal centre phenotype and immune function (Y. Fang et al., 1998).

Interestingly CD21 also has a role in many diseases. FDCs have been shown to be a reservoir for HIV infectious particles and blockade of C3d binding to CD21 prevented transmission of virus to CD4 T cells (Heesters et al., 2015). Viral complexes have been opsonised allowing binding to CD21 expressed on FDCs and B cells, blocking C3dg binding to the receptor prevents virus from entering the cell and being transmitted to other cell types. CD21 is also named the Epstein-Barr virus (EBV) receptor as the virus is able to initiate infection of B cells by binding SCRs 1 and 2 of the receptor, similar to C3dg (Fearon et al., 1995). After binding, within minutes the virus undergoes passive endocytosis, de-envelopment, and passage of the viral nucleocapsid to the cytoplasm and vectoral movement of the nucleocapsid to the nucleus (Nemerow et al., 1984).

CD21 deficiency in humans has been associated with hypogammaglobulinemia (Thiel et al., 2012). The first patient described with this deficiency suffered from recurrent upper respiratory tract infections in early childhood and gastrointestinal infections later in life. Within this study, the patient's B cells were completely devoid of CD21 surface protein, no intracellular CD21 protein was detectable and there was no sCD21 present within the patient sera (Thiel et al., 2012), however expression of CD19 and CD35 was normal within these

cells. Analysis of the patient's family found consistent decreased CD21 expression on B cells compared with healthy controls, suggesting the deficiency was genetic (Figure 10.1.1). Sequencing of the patient's genomic DNA revealed a heterozygous mutation disrupting the highly conserved "GT" splicing donor site of exon 6, causing a frame shift of the entire exon and resulting in shorter CD21 mRNA, coding for a truncated CD21 protein. A second mutation was found within exon 13 introducing a premature stop codon and presumably causing nonsense-mediated mRNA decay. The patient's father and sister are carriers of the exon 6 mutations and the mother carries the exon 13 mutation; neither mutation was found within 100 healthy control subjects. Because of this deficiency the patient's B cells exhibited only one tenth of the immune complex binding observed with normal B cells (Figure 10.1.1) and complex binding could not be inhibited using CD21 blocking mAb FE8, unlike in healthy B cells (Theil et al., 2012). However, CD21 deficiency did not prevent EBV infection of the patients B cells, indicating although CD21 is a receptor for EBV binding, entry via CD21 is not absolute.

Studies on a second patient with a compound heterozygous CD21 deficiency, also resulting in hypogammaglobulinemia, showed that CD21 deficient B cells had a normal BR mediated signalling upon stimulation *in vitro*, but slightly reduced SHM frequency and class switch recombination (Wentink et al., 2015).

Subject	CD21 mutation	CD21 expression	Disease phenotype	C3dg binding capacity of patient B cells
Healthy control	N/A	Normal	Healthy	++
Patient	Heterozygous mutation in exon 6 and mutation in exon 13	No expression	Hypogammaglobulinemia	-
Sister	Mutation in exon 6	Lower expression	Healthy	+
Father	Mutation in exon 6	Lower expression	Healthy	+
Mother	Mutation in exon 13	Lower expression	Healthy	+

Figure 10.1. 1: Genetic CD21 deficiency is associated with hypogammaglobulinemia

Data from Thiel et al., 2012. (A) Family members have decreased CD21 expression and patient is completely devoid of CD21 expression and subjects have defective binding of C3d-containing immune complexes compared with healthy controls.

10.1.2 CD21 isoforms in human biology

Alternative splicing within the human CD21 gene generates two isoforms termed CD21 short (CD21S) and CD21 long (CD21L) (Fujisaku et al., 1989). The short form of CD21 contains 15 SCRs and the long form differs by the insertion of one additional SCR; this SCR is known as SCR11 or SCR10a and is located in the middle of the protein (Figure 10.1.2). Although the crystal structure of CD21S has been published (Gilbert et al., 2006), to date, there is no known structure of CD21L. The published structure of the SCR1/2 binding site of CD21 and its ligand C3d suggests that the additional SCR within the long isoform of CD21 does not directly affect the binding of C3d to the receptor as only SCR1 and 2 interactions are involved. However, this does not rule out that this isoform may have a greater affinity for C3dg binding using an alternative mechanism.

Figure 10.1. 2: CD21 is found in two isoforms

CD21 short (CD21S) is made of 15 SCRs, CD21 long (CD21L) has an additional SCR, named SCR10, in the middle of the protein. It is unknown what the function of this additional SCR has at present.

FDCs have been shown to specifically express CD21L whereas B cells express the short form (Liu et al., 1997). An early study used amplified CD21 cDNA derived from human B cells and FDCs, revealing a larger band product for the FDCs (Liu et al., 1997). The products were sequenced revealing a 177bp insertion encoding SCR10a in the FDC samples which was absent from the B cell derived shorter PCR product. The function of this additional SCR is as yet unknown. It is interesting that SCR10a would create another SCR within the folded region of the protein (Figure 10.1.2). The addition of this protein unit could alter the structure of CD21 completely, potentially making the protein more stable, but as there is no published CD21L structure, this is unknown.

A study analysing the CD21 exon-intron junctions revealed the presence of three types of exons in the SCR region of CD21 (Fujisaku et al., 1989). The types of exon occur in the following order; four exons each of which encode two SCRs, five exons that together encode a single SCR, followed by six exons which encode SCRs which are split in identical positions, this position being after the second guanidine of a glycine codon three amino acids past the second cysteine. This exon order is repeated for each group of four SCRs within the CD21 receptor, indicating the CD21 gene likely evolved from duplication of a gene containing four SCRs. As CD21L has 16 SCRs it suggests the short form of CD21 changes the repetitive conformation of the 4 SCR units, potentially changing the functionality of the receptor.

Interestingly, many antibody reagents have been utilised to demonstrate CD21L expression by FDCs. One of the first reported was a murine monoclonal antibody clone, R4/23, was shown to react strongly with FDCs using immunohistochemical techniques (Naiem et al., 1983). Due to this observation, and only weak staining of B cells outside of zones containing FDCs, the antibody was reported to be CD21L and thus FDC specific. Another monoclonal antibody, 7D6, was also reported to specifically recognise human FDCs (Liu et al., 1997). Again, this was determined using staining patterns of human tonsil sections; 7D6 was shown to bind to FDCs but not B cells, therefore it was concluded from this study the antibody was

specific for CD21L. Within the same study, expression cloning was utilised allowing the production of a cDNA clone encoding the long human CD21 isoform, containing exon 10a. Transfection of mouse Ltk^- cells with this cDNA further showed that the other FDC mAbs, DRC-1 and KiM4, also recognise CD21L (Liu et al., 1997). Weak cross reactivity with B cells was reported for all of these antibodies; raising the question as to whether it is isoform expression that's responsible for these observations. In addition, it was noted that the B cell lymphoma line, Raji, among others, also expressed the 7D6 antigen (Liu et al., 1997).

10.1.3 CD21 dependent antigen presentation

Antigen transfer occurs between CD21 on B cells and CD21 on the surface of FDCs within germinal centres.

Delivery of antigen to secondary lymphoid organs is dependent on size. Large antigen-complexes are bound by subcapsular sinus macrophages, whereas small antigens (under 70 kDa) are rapidly channelled into follicles via the conduit system. The latter pathway provides a directed flow of small antigen to the FDC resulting in transient antigen retention or, in the presence of antigen and complement, long term binding with CD21 receptors. FRCs secrete collagen-rich fibres that form this network in the paracortical region; imaging studies revealed trafficking of T and B cells within the peripheral lymph nodes through directed migration along these stromal "highways" (Bajenoff et al., 2006). A study on neonatal lymph nodes revealed an absence of B cell follicles, but these SLOs do have a developed T cell zone and a dense conduit network (Bajenoff et al., 2009). It was shown that as new T and B cells enter the developing lymph node, the conduit network density is maintained in the T cell zone, but not the B cell zone. B cell accumulation leads to remodelling of the follicular network, a process dependent on both FDC dendritic processes and the network of FRC fibres (Gonzalez et al., 2010). In adults, the residual follicular conduits are then able to transport low molecular weight soluble antigen to FDC regions,

allowing the capture of soluble antigens draining from subcutaneous sites by antigen-specific B cells even in the absence of Ag-specific antibodies.

Studies investigating delivery of larger lymph-borne particulate antigens, such as vesicular stomatitis virus, demonstrated a mechanism for antigen transfer via uptake of antigen by macrophages lining the sub-capsular sinus (SCS) (Junt et al., 2007). Antigen is shuttled to the underlying surface where it is made available to cognate B cells. Experiments using large protein antigens were showed to bind SCS macrophages after sub-cutaneous injection into passively immunised mice; this study also revealed antigen capture was complement-dependent (Phan et al., 2007). Formation of immune complexes activated the complement pathway resulting in C3-coated immune complexes that enhance uptake of antigen via CR3 and FcRIIb receptors expressed on the surface of the macrophage (Phan et al., 2007). C3-coated complexes are subsequently shuttled to B cell compartments and transferred to naïve B cells. It is possible that complexes are partially protected during the delivery phase; FcRIIb is known to recycle to the surface following internalisation and not go through a lysosomal compartment (Bergtold et al., 2005).

CD21 expressed on B cells is essential for transport of lymph-borne C3-coated immune complexes into the B cell follicles and transfer to FDCs. Marginal zone B cells acquire antigen complexes from SCS macrophages through CD21 receptors on their cell surface. These B cells have been shown to have a unique surface phenotype; expressing high numbers of CD21 and CD35 and the non-classical MHC molecule, CD1d3 (Cinamon et al., 2008). Uncoupling CD21/35 from CD19 in naïve B cells in mice still allowed for uptake of C3-coated immune complexes and delivery to FDCs, indicating the CD21/35 receptor includes a cytoplasmic domain that allows CD21 signalling after C3-immune complex uptake independent of CD19 and triggers B cells migration to the FDC (Barrington et al., 2009). Alternatively, the CXCL13 chemokine gradient created by FDCs may be enough to cause B cell migration within follicles; therefore, direct signalling by C3-IC may not be essential (Cinamon et al., 2008). Thus, B cells enter the peripheral lymph node, they cycle to the sub-

capsular sinus, attracted by chemokine gradients produced by marginal reticular cells, attain antigen from SCS macrophages before migrating to FDCs via an additional FDC-dependent chemokine gradient.

Antigen-complexes now bound by CD21 on the surface of B cells are transferred to FDCs. Transfer of C3dg-antigen complexes is dependent on CD21 and FcRIIb receptors. FcRIIb is upregulated following FDC activation; although these receptors appear to enhance long-term retention of immune complexes, as FcRIIb is not constitutively expressed, the initial capture and retention of these complexes is largely due to CD21 (El Shikh et al., 2006). In mice, it was shown that FDCs acquire complement-coated immune complexes from noncognate B cells via CD21 and rapidly internalise the co-ligated receptor/ligand complex using an actin-dependent pathway (Heesters et al., 2013). Immune-complexes were retained within a nondegradative cycling compartment and were displayed periodically on the cell surface where they were accessible to antigen-specific B cells. Endocytosis of antigen into these compartments, similar to that observed in macrophage antigen delivery, explains how they are protected from damage and how long-term retention is achieved by FDCs. This essential role of CD21 on FDCs concentrates antigen in the lymphoid tissues. It is not clear, however, whether antigen retention by FDCs is required for the initiation of the primary antibody response. Chimeric mice in with CD21 deficient FDCs are able to produce a normal IgM primary response; this suggests other sources of antigen may be sufficient to trigger early B cell activation (Ahearn et at., 1996) but presentation of antigen by FDCs is needed to produce a memory B cell response (Rossbacher et al., 2006). It is known that B cells acquire antigen and are most efficiently activated when it is attached to membrane; therefore, retention of antigen and C3dg on the FDC surface enhances antigen-specific B cell responses (Carrasco et al., 2004). Studies using multi-photon intravital microscopy support a role for FDCs as an essential source of antigen for B cells (Suzuki et al., 2009). Contact between FDCs and B cells were often brief but occasionally persisted for over 30 minutes. A prolonged display time of antigen ensures even rare B cells have the chance to encounter

antigen. These investigations also identify a role for CD21/CD35 in efficient uptake of medium affinity antigens in their murine model, demonstrating how CD21/CD35 deficient B cells acquired fewer antigens from FDCs. One potential model of transfer between receptors, is that unidirectional transfer occurs between CD21S and CD21L receptors, suggesting the complex is bound with low affinity to CD21S on B cells permitting efficient uptake of complexes to CD21L on FDCs. As these two isoforms differ in the expression of SCR10a, this sequence may modify the stability, membrane organisation or affinity for ligand of the CD21L isoform, allowing this unidirectional transfer of opsonised antigen-complexes to occur.

10.1.4 The role of C3dg

Another important role for CD21 is the binding of C3dg-opsonised antigen complexes allowing antigen-specific antibody responses to occur. The central component in complement activation is C3; when complement pathways are activated C3 is cleaved into two fragments: C3a and C3b (Merle et al., 2015). The C3b fragment is further cleaved by factor I into iC3b and subsequently to C3dg and C3c. C3a, the smallest fragment, has the shortest half-life, while C3dg, the larger fragment (37 kDa), has a plasma half-life of 4 hours (Teisner et al., 1983). CD21 binds to cleavage products C3dg and, with a lower affinity, iC3b, covalently attached to antigens. These proteins play a critical role in humoral immunity as blocking with antibodies, a soluble receptor or deletion of CD21 receptors leads to impaired humoral immunity to model protein antigens, bacteria and viruses.

Studies using animals depleted of C3 demonstrated a correlation between the concentration of C3 present and the humoral immune response elicited; depletion of C3 caused a reduction in the antibody response (Pepys et al., 1972). *In vivo* C3 depletion has a greater effect on the antibody response to T cell-dependent antigen than the T cell-independent antigen response. Studies in humans genetically deficient in C3 did not reveal defects in antibody responses after routine immunisations, however these studies used high doses of

antigen in adjuvant therefore may not be directly testing C3-dependent pathways (Alper et al., 1972). Studies using limiting doses of T-dependent antigen, bacteriophage ΦX 174, showed no switch from IgM to IgG antibody synthesis (Ochs et al., 1986). The same antigen was used to further highlight the role of C3 in humoral immunity using a C3-deficient dog model (O'Neil et al., 1988). The serum IgG levels of the dogs were within the normal range but significantly lower than compared with normal controls. Additionally, specific antibody production was defective upon primary response to antigen. After secondary immunisation with the T-dependent antigen, the total antibody titres were within normal ranges, but the animals made proportionately more IgM and less IgG antibody than that seen in control groups, indicating there was a defect in class switching in the C3 deficient model. These effects could not be rescued with an increase in the antigen dose. Memory B cell development was also impaired in mice depleted of C3 by treatment with cobra venom (Pryjma et al., 1975).

C3dg is known to lower the threshold of B cells for activation. C3dg bound to a primary protein antigen complex with natural antibody was shown to enhance recognition and specific immunoglobulin synthesis by antigen-specific B cells (Thornton et al., 1996). Interestingly, antigen was taken up and processed via CD21 by both antigen-specific and non-specific B cells. The C3dg-immune complexes induced expression of the B cell costimulatory molecule CD80 upon ligation to CD21; this was followed by FcγRII stimulation via the IgG antibody on the complex. This suggests that non-specific B cells may have the capacity to function as antigen-presenting cells for antigen-specific T helper cells in the same way as macrophages, promoting expansion of this subset of cells (Thornton et al., 1996). This study concluded that C3dg-mediated antigen recognition enhanced the immune response to antigen present at low levels, and hence is important when only a few antigen-specific B cells with low affinity to antigen are available due to the threshold of activation being lowered when antigen is complexed with C3dg. Preculture of tonsil B cells with 0.01 to 1 µg/ml polymeric C3dg caused a dose-dependent enhancement of proliferation, however

C3dg alone did not induce this effect; anti-IgM had to be present to cause activation of cells (Carter et al., 1989).

EBV and C3dg were mapped to binding a common domain of the CD21 receptor; antibody clone OKB-7 blocked uptake of both ligands (Clifford et al., 1989). By analysis of CD21 deletion mutants and chimeric mouse models, it was determined that the NH_2-terminal two SCRs (SCR1 and 2) are necessary and sufficient to bind gp350/220 (EBV) and C3dg with equal affinities. Molina et al., suggested that the SCR1 sequence 10-LNGRIS-15 and the SCR2 sequence 84-GSRPYRHGDSVTFA-97 contribute to C3dg binding; rat mAbs 7G6 and 4E3, which inhibit binding of mouse or human C3dg to mouse CD21 independently, have their epitopes corresponding to these sequences in the mouse CD21 protein (Molina et al., 1995). An IgG1 mouse mAb, FE8, was shown to interfere with the binding of both C3dg and EBV to CD21 expressed on human B cells. This antibody was subsequently found to bind a conformational epitope in the recess between SCR1 and SCR2, the ligand binding site of CD21 (Wolfgang et al., 1998). FE8 blocked binding of soluble C3dg or particles carrying multiple copies of surface bound C3dg to CR2 or induced complete removal of these ligands from the receptor. Removal of ligands by this antibody suggests a lower affinity of C3dg for its receptor than FE8. This phenomenon has also been demonstrated in additional models where administration of mAb against CD21/CD35 inhibited the primary and secondary *in vivo* response in mice (Gustavsson et al.,1995). This study utilised an ELISPOT assay to determine the number of antigen-specific, IgG-producing B cells, an indication of T cell priming within this model system. Data revealed a 99% suppression of the primary antibody response when CD21/CD35 is blocked, however the secondary response is only partially inhibited (82-93%) or has been shown to be unaffected in other studies (Thyphronitis et al., 1991). One explanation for this is that the initial primary reaction elicited is lower and, therefore, easier to supress than a secondary response; it is known that the complement system is required only in responses to suboptimal antigen doses, therefore works to enhance the primary immune response (Bottger et al., 1987).

Surface plasmon resonance has been utilised to study the interactions between CD21 and C3dg. Kd values for binding to SCR1-2 (ligand binding site) and SCR1-15 (full length protein) were determined as 22.4 nM and 27.1 nM, respectively (Ling et al., 1991). While the Kd values for each of the molecules are indistinguishable; the binding kinetics differed greatly. C3dg both associated and dissociated 10-fold slower from SCR1-15 than SCR1-2 (Sarrias et al., 2001). This suggests that the structure of the protein affects its binding kinetics, hence the additional exon in CD21L may modulate antigen-complex binding and maintenance on the surface of FDCs, and perhaps indicating Koff rates are the determining factor in antigen stability.

An additional function of C3d as a molecular adjuvant has been suggested, even in the absence of CD21. Studies carried out in a CD21/35$^{-/-}$ mouse model revealed immunisation with SA-C3dg tetramers produced primary and secondary antibody responses in these mice similar to wild-type mice (Karen et al., 2004). Thus, suggesting C3dg can function as a molecular adjuvant in the absence of CD21/35 expression. One mechanism in which C3dg could function as a molecular adjuvant could be through its known interactions with numerous serum proteins, cell surface receptors and membrane-associated regulatory proteins; said interaction could potentially result in enhanced humoral immune responses using CD21-independent mechanisms. Immunisation of CD21/35$^{-/-}$ mice with antigen only, no C3dg, resulted in impaired antibody responses, confirming the importance of CD21/35 expression in responses to antigens administered in the absence of adjuvants.

10.1.5 Tetramer biology

Interestingly, when examining the effect of monomeric, aggregated and latex-bound C3dg for their actions on tonsil B cells, the aggregated and latex-bound form of C3dg caused B cell activation, whereas C3dg in a monomeric form inhibited this response (Bohnsack et al., 1988). This phenomenon was also noted in additional studies in which use of polymeric

C3dg activated B cells; whereas incubation of cells with monomeric C3dg had no effect on the activation response (Carter et al., 1989).

The application of tetrameric complexes has transformed understanding of antigen specific T cell responses by permitting visualisation of weak but specific ligand interactions of TCR and MHC (Altman et al., 1996). This study utilised tetramers of human lymphocyte antigen A2 complexed to two different HIV-derived peptides or with a peptide derived from influenza A matrix protein bound to peptide-specific cytotoxic T cells *in vitro* and to T cells from the blood of HIV-infected individuals. Studies revealed the affinity to isolated, soluble monomeric MHC/peptide complexes for their specific TCR partners is weak and therefore use of these complexes had long hindered efforts to identify antigen-specific T cells by ligand binding methods using labelled, monomeric MHC/peptide complexes. Upon using tetrameric complexes, which engage more than one copy of the TCR on the surface of a T cell, thereby increasing the avidity of the interaction between receptor and ligand, allowed effective identification of antigen-specific T cells by flow cytometry, even those subsets present at low frequencies (Altman et al., 1996). Subsequent studies using defined oligomers of soluble antigen-MHC molecules of natural ligands for the TCR also revealed that monomeric stimuli failed to activate T cells, even at concentrations 20,000-fold higher than the doses of tetramer used (Boniface et al., 1998). The occupancy of the TCR using higher concentrations of the monomeric complexes would be much higher than using a lower concentration of tetrameric complexes, but the failure of T cells to respond excluded occupancy as the reason for the greater potency of tetramer versus monomer and dimer activation. Therefore, it is thought that tetramers allow colocalisation of TCRs, resulting in increased stimulation of cells.

These results are mirrored in studies using monomeric and tetrameric complexes of C3dg. Under physiological conditions, monomeric C3dg was unable to bind to recombinant CD21, whereas the HIV viral ligand, gp350/220, was saturable and univalent under the same conditions (Moore et al., 1989). These studies indicated the affinity of the C3dg monomer for

rCD21 under physiological conditions is approximately 10^4-fold less than that of the viral ligand. Applying what is known about the increased affinity of ligands with weak binding when they are found in a tetrameric complex, it is reasonable to suggest C3dg-tetramer complex binding to rCD21 may have been possible under physiological conditions. This concept was confirmed in a study using biotinylated C3dg create C3dg-immune complex tetramers with fluorochrome-conjugated streptavidin (Henson et al., 2001). Again, flow cytometry analysis showed monomeric C3dg was unable to bind CD21, whereas C3dg-tetramer complexes caused tight ligand-receptor interactions. This multimeric C3dg complex caused phosphorylation of the mitogen-activated kinase, p38, in mature B lymphoma cells and enhanced the activation of primary B cells in combination with sub-stimulatory concentrations of anti-IgM monoclonal antibody.

An investigation utilising diphtheria toxin (DT)-C3d fusion protein and C3dg-streptavidin (SA) tetrameric complexes to assess the role of CD21 during BCR-induced activation and *in vivo* immune responses, revealed monomeric DT-C3d inhibited immune responses (Youngkyun et al., 2005). Immunisation of mice with DT-C3d reduced DT-specific Ab responses independently of CD21 expression or signalling. This inhibition had previously been described in studies where anti-Ig-induced Ca^{2+} responses in human B cells were inhibited with monovalent C3dg (Tsokos et al., 1990). It was suggested that crosslinking of CD21 by multivalent ligands promotes the formation of domains of membrane Ig that have a conformation able to activate phospholipase C, resulting in increased Ca^{2+} responses. In contrast, immunisation with SA-C3dg tetramers dramatically enhanced antigen-specific responses, as well as enhancing BCR-induced Ca^{2+} responses (Youngkyun et al., 2005). As monomers should not be able to induce BCR crosslinking, it is thought that in order for B cell activation and antigen-specific antibody responses, multimeric C3dg-immune complexes must form in order to allow for this crosslinking effect to occur and allow downstream signalling resulting in increased humoral immune responses. Interestingly, stimulation with higher concentrations of SA-C3dg significantly inhibited BCR-induced Ca^{2+} responses.

Therefore, it was concluded that C3dg can enhance or inhibit antigen-specific humoral immune responses through both CD21-dependent and -independent mechanisms depending on the concentration and nature of antigen-C3dg complexes (Youngkyun et al., 2005). The concept of CD21 as both a positive and negative regulator of B cell signalling also provides explanation for phenotypic observations in CD21 deficient mice. CD21-/- mice are generally hyporesponsive to antigen challenge (Takahashi et al., 1997) whereas defective CD21 ligand binding in lpr/lpr mice contributes to the development of autoimmunity (Boackle et al., 2001). The lpr/lpr mouse model contains a mutation within the CD21 gene encoding a single polymorphism that introduces a glycosylation site located within the C3dg binding domain of the receptor, interfering with its ability to form dimers. This mutation reduces ligand binding and receptor-mediated cell signalling. This mutation may lead to autoreactive B cells being able to escape mechanisms that would normally render them tolerant to autoantigen. Alternatively, this mutation may affect antigen presentation by the receptor, binding and internalisation of autoantigen by the mutated receptor may result in the presentation of unique peptides which are recognised by autoreactive cells.

10.2 Summary and Aims

Within humans, the CD21 receptor exists in two isoforms, CD21S and CD21L. CD21S is reported to be expressed on B cells, whereas FDCs are said to express the long isoform, as determined using antibody staining patterns with specific CD21L antibody clones (Fujisaku et al., 1989). An essential role of CD21 elicited through the binding of C3dg-immune complexes, allowing presentation of antigen to B cells resulting in high affinity, antigen-specific antibody responses. The literature describes unidirectional transfer of these C3dg opsonised antigen complexes between CD21 receptors on B cells to CD21 on FDCs.

In the previous chapter, the hypothesis that receptor number on the cell surface was a contributor to the action of antigen transfer between cells was explored. Using tetrameric C3dg-immune complexes; a second hypothesis that CD21L expressed on FDCs has a higher affinity for C3dg binding allowing C3dg-opsonised antigen transfer from B cells to FDCs is assessed with this work (Figure 10.2.1).

Therefore, the specific aims of this chapter are:

1) To assess C3dg binding to CD21 on FDCs (tonsil derived) and B cells (tonsil and blood derived).
2) Investigate the potential differential binding of C3dg to CD21S and CD21L

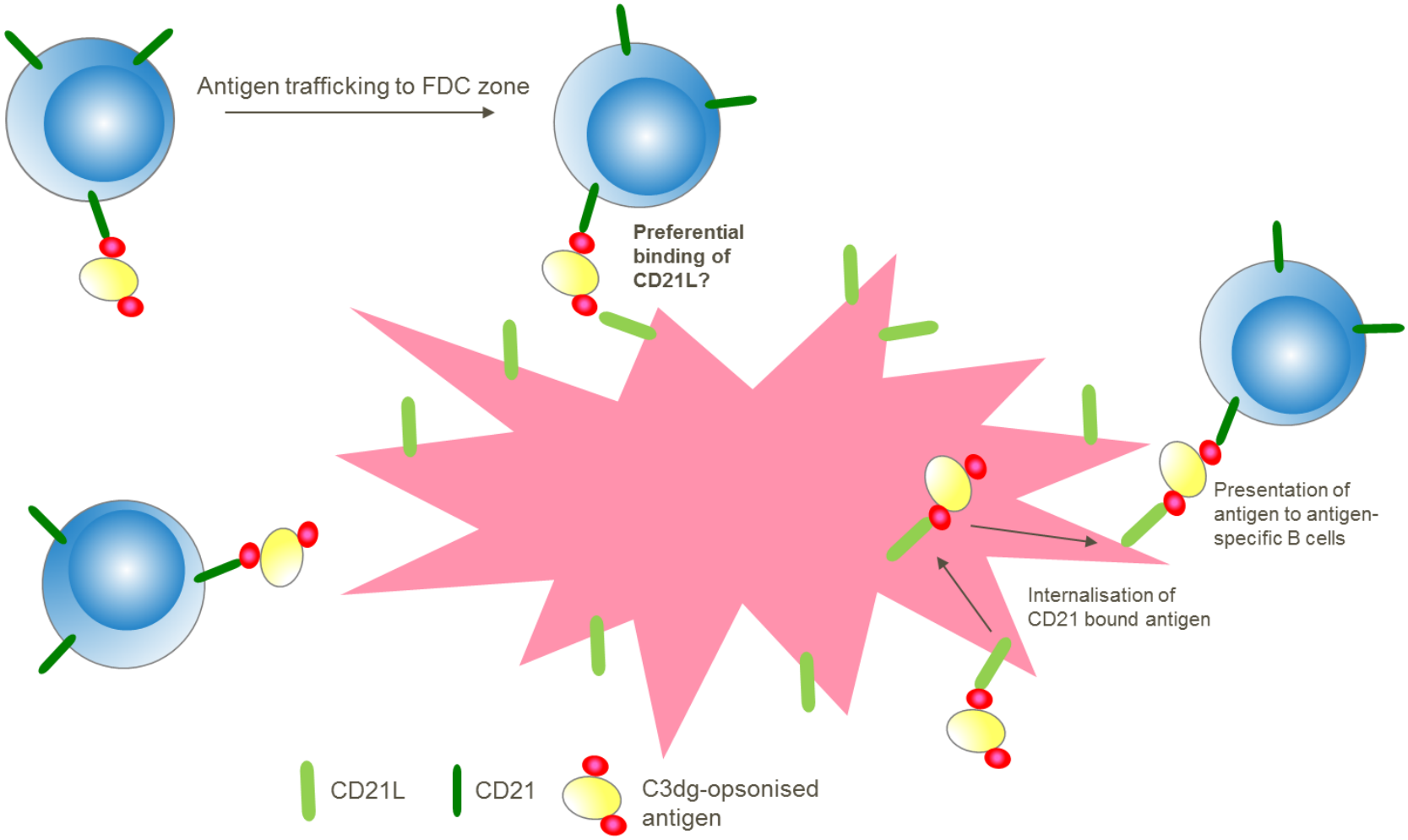

Figure 10.2. 1: : Proposed antigen transfer mechanism between B cells and FDCs

C3dg-opsonised antigen is trafficked to FDC zones bound to CD21 on the B cell surface. Antigen is presented to FDCs. C3dg preferentially binds to CD21L expressed on the FDC. Antigen-bound CD21 is internalised, pulling the immune complex from CD21 receptors on the B cell, and presented to antigen-specific B cells

10.3 Results

10.3.1 Assessing CD21 functionality through binding of C3dg-immune complexes on primary cells

In order to assess C3dg binding, first an “immune-complex” was established. The complex composed of 100% monobiotinylated C3dg bound to a streptavidin molecule, fluorescently labelled with an APC molecule. Theoretically the complex takes the form of a tetramer, as depicted in Figure 10.3.1A. A tetrameric form of the complex was used to allow visualisation of receptor binding with a greater assay window. Use of monomeric C3dg complexes, in which only one C3dg molecule is conjugated to the streptavidin-APC molecule, were shown to bind to $CD21^{+}$ cells, however signal obtained from this interaction is lower than that using tetrameric complexes, suggesting a lower affinity ligand-receptor interaction (Figure 10.3.1B).

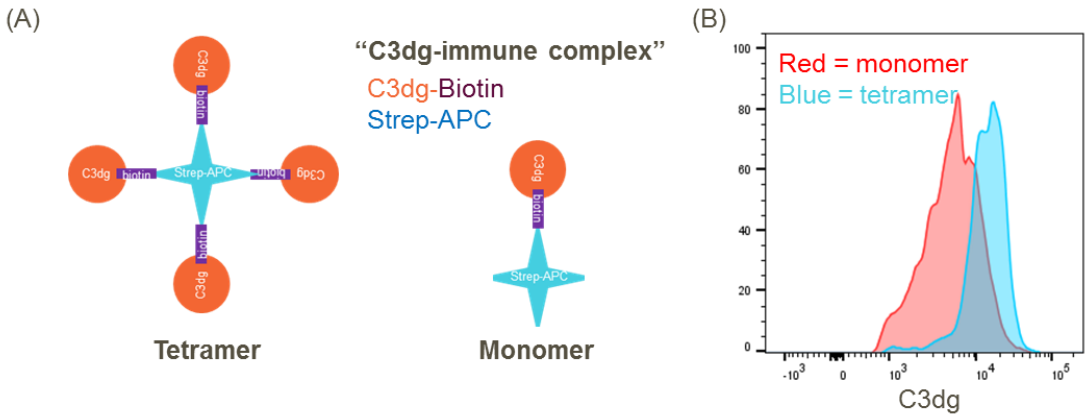

Figure 10.3. 1: Biotinylated C3dg is complexed to a streptavidin molecule to form "immune-complexes"

(A) Streptavidin is labelled with an APC molecule. C3dg is 100% mono-biotinylated. Tetrameric C3dg-StrepAPC complexes are formed from 4 biotinylated-C3dg molecules binding StrepAPC. Monomeric C3dg-StrepAPC complexes only have 1 C3dg molecule bound to the StrepAPC. (B) Tetramers bind to CD21+ cells with high affinity than monomeric complexes.

Binding of this “C3dg-immune complex” was assessed on primary FDCs (tonsil derived), B and T cells (blood and tonsil derived) using a titration of the complex, starting with a concentration of 10 µg/ml and serially diluting the reagent 3-fold. Binding was assessed on $CD21^+$ cells; important as the aim of this investigation was to assess CD21 functionality using its ability to bind C3dg. $CD21^+$ cells were gated as shown in Figure 10.3.3 for T and B cells and FDCs in Figure 10.3.2. Gates were set using CD21 isotype control samples and Streptavidin-APC alone (no biotinylated-C3dg) stained samples to ensure staining was specific for CD21 and C3dg respectively. C3dg was shown to bind to all cells in a concentration dependent manner (n=3 independent donors, Figure 10.3.4) however saturating concentrations of C3dg were not reached for any of the cell types investigated (Figure 10.3.4) as immune-complex concentrations higher than 1 µg/ml caused a high non-specific background signal on $CD21^-$ cells. Saturating concentration of C3dg are not essential for the final assay as long as sufficient signal can be measured with the concentration of C3dg used; therefore 1 µg/ml C3dg was used for the subsequent assays. Binding of complexes to $CD21^+$ T cells is in a concentration dependent manner; however MFI is lower than the other cell types investigated. This is due to only a small population of T cells expressing the CD21 receptor (Figure 9.3.16); hence no further investigation of CD21 functionality on T cells was carried out during this work.

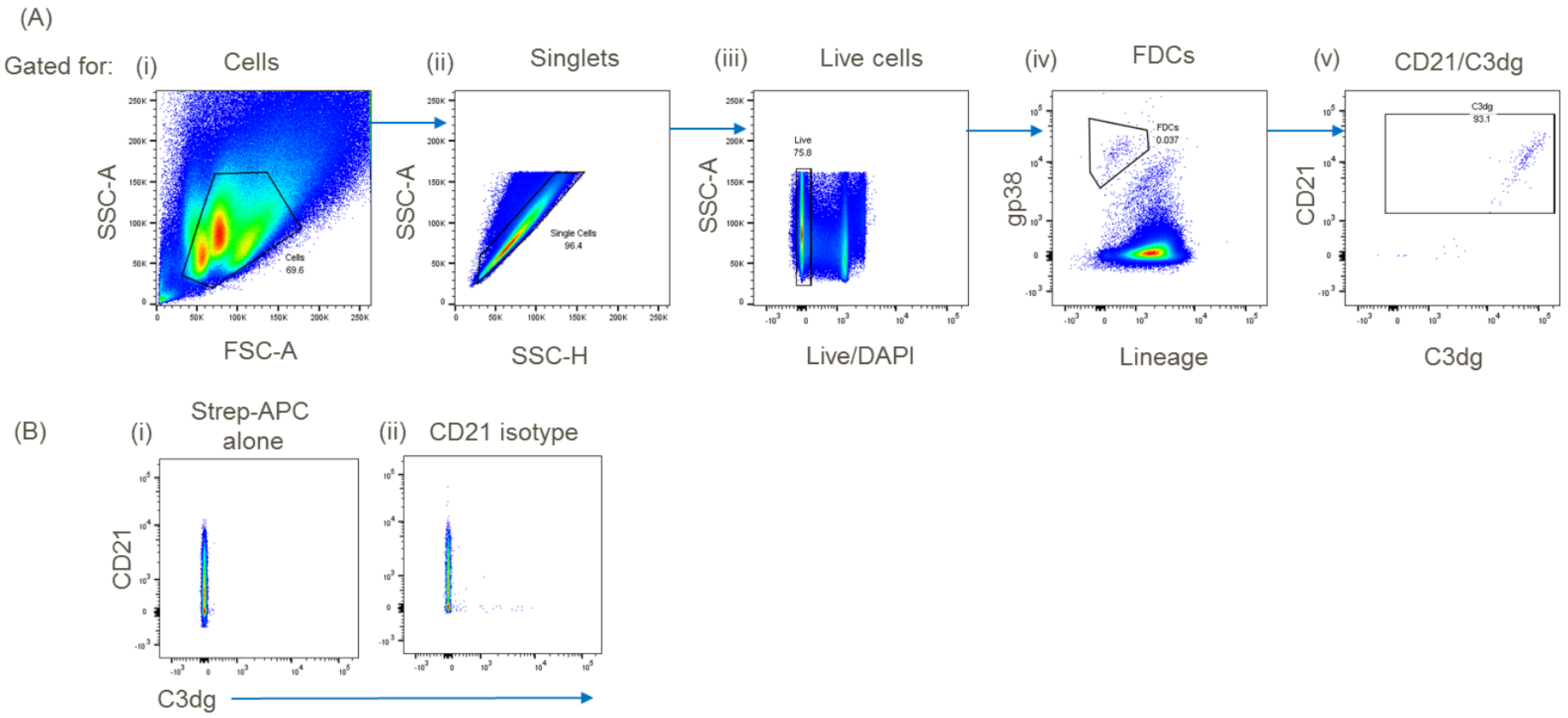

Figure 10.3. 2: Gating strategy for C3dg binding to FDCs

(A) (i) Cells are gated and doublets excluded (ii). Live cells are selected (iii) and a gate for gp38+ and lineage- cells drawn (iv). These cells are FDCs. FDCs are then gated on CD21+ and C3dg+ cells. Sample shown is stained with 1 µg/ml CD21 (Bu32) and 1 µg/ml C3dg-StrepAPC. (B) (i) Sample stained with full staining panel plus Strep-APC alone (no C3dg), lack of staining with the fluorophore only confirms staining seen is C3dg specific. (ii) Sample stained to identify FDCs and CD21 isotype antibody, confirms staining for CD21 is specific.

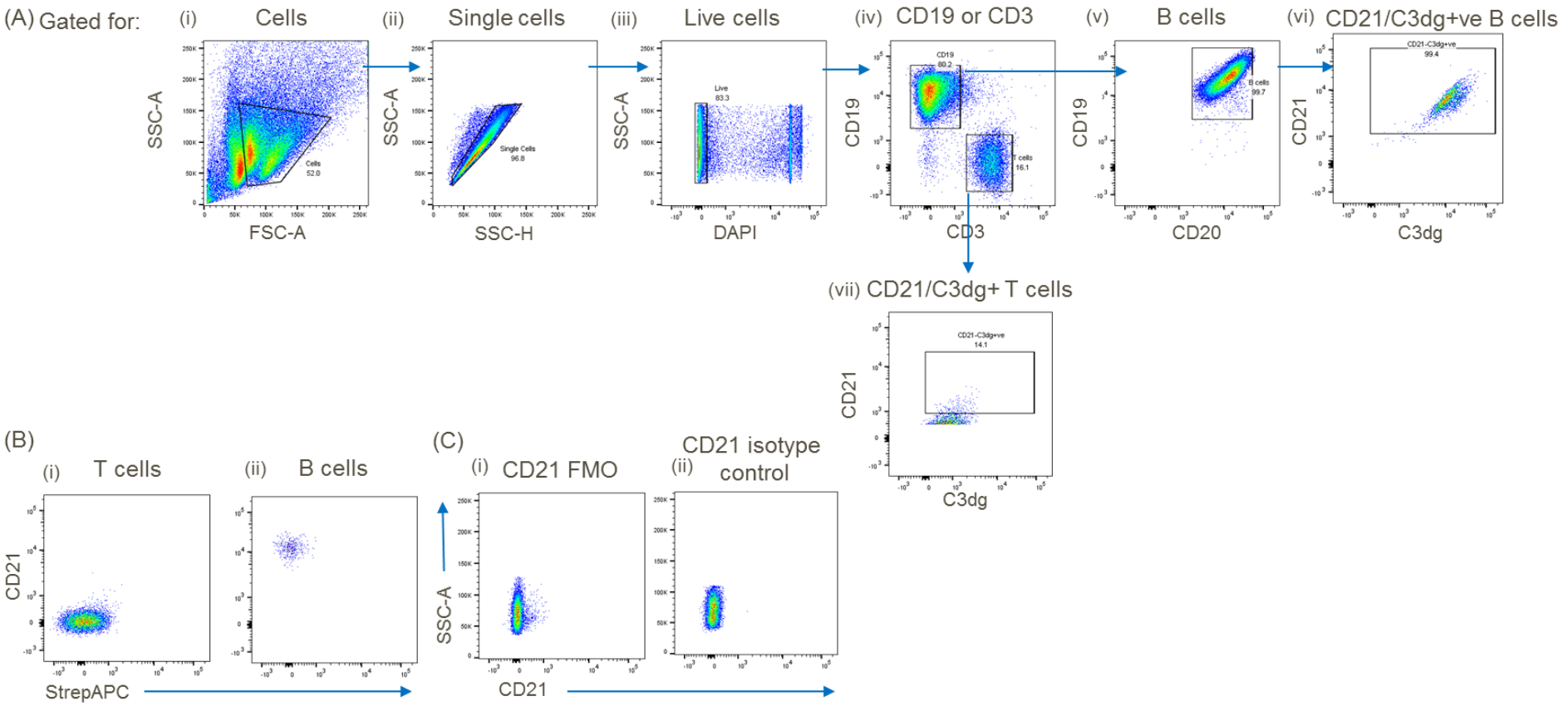

Figure 10.3. 3: Gating strategy for CD21/C3dg positive T and B cells

(A) (i) Cells are selected and doublets excluded (ii). Live cells are selected as DAPI negative (iii). T and B cells are separated using CD3 and CD19 staining respectively (iv). CD19 positive B cells are further gating using CD20 (v) and CD21/C3dg+ cells resolved. Samples shown are stained with 1 µg/ml CD21 (Bu32) and 1 µg/ml C3dg-StrepAPC (vi). CD21/C3dg+ T cells are resolved by further gating on CD3+ cells. Sample shown is stained with 1 µg/ml CD21 (Bu32) and 1 µg/ml C3dg-StrepAPC. (vii). (B) (i) T cells stained with CD21 and StrepAPC alone confirms staining is C3dg specific (ii) B cells stained with CD21 and StrepAPC alone confirms staining is C3dg specific. (C) (i) CD21 fluorescence minus one shows all signal in the CD21 channel is specific for the CD21 Bu32 antibody. (ii) CD21 isotype control stained sample shows the antibody staining seen using Bu32 is specific for the antibody binding to CD21.

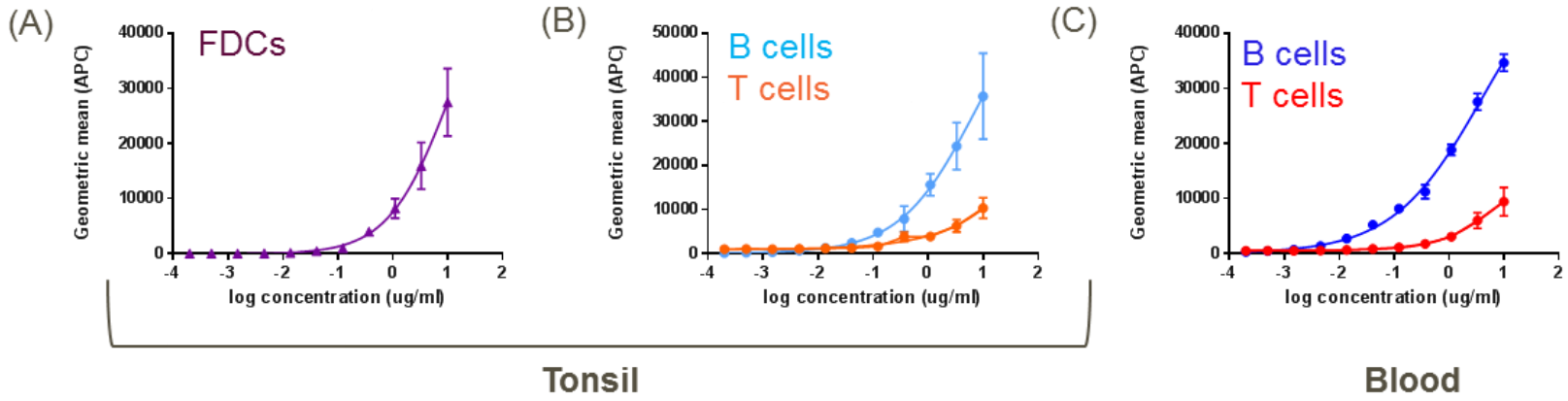

Figure 10.3. 4: C3dg binds to CD21+ve FDCs, T and B cells in a concentration dependent manner

n=3, bars represent SD. (A) C3dg binds to tonsil derived FDCs (B) T and B cells in a concentration dependent manner. (C) C3dg binds to peripheral T and B cells in a concentration dependent manner.

The CD21 antibody clone FE8 is known to block C3dg binding to the ligand binding site on the CD21 receptor. Before using this reagent in the final assay, all antibody clones and reagents were validated for their ability to co-stain or block binding of $CD21^+$ cells. Firstly, to assess the blocking ability of FE8, both C3dg and FE8 were added to cells simultaneously. The resultant data showed that in the presence of FE8, C3dg is unable to bind CD21 (Figure 10.3.5C). FE8 was also added prior to staining with C3dg-immune complexes; again, C3dg is unable to bind to CD21 in the presence of FE8 (Figure 10.3.5D). This data concludes that FE8 can be used as the blocking reagent within the final assay. It is important that $CD21^+$ cells can still be identified within this assay; therefore an antibody clone that binds to CD21 in the presence of C3dg and the blocking antibody FE8 was identified. The ability of the CD21 antibody clone Bu32 (used previously for receptor numeration in Chapter 1) to bind to the receptor in the presence of FE8 or C3dg was investigated. FDCs were shown to be double positive for Bu32 and FE8 or Bu32 and C3dg (Figure 10.3.5 A and B respectively) when reagents were added simultaneously; therefore, they can be used in the same assay in order to identify CD21 on cells (Bu32) while assessing biology of CD21 (FE8 or C3dg). It was concluded that Bu32 binds to an epitope away from the ligand binding site on CD21, while FE8 and C3dg compete for binding at this site (Figure 10.3.5E).

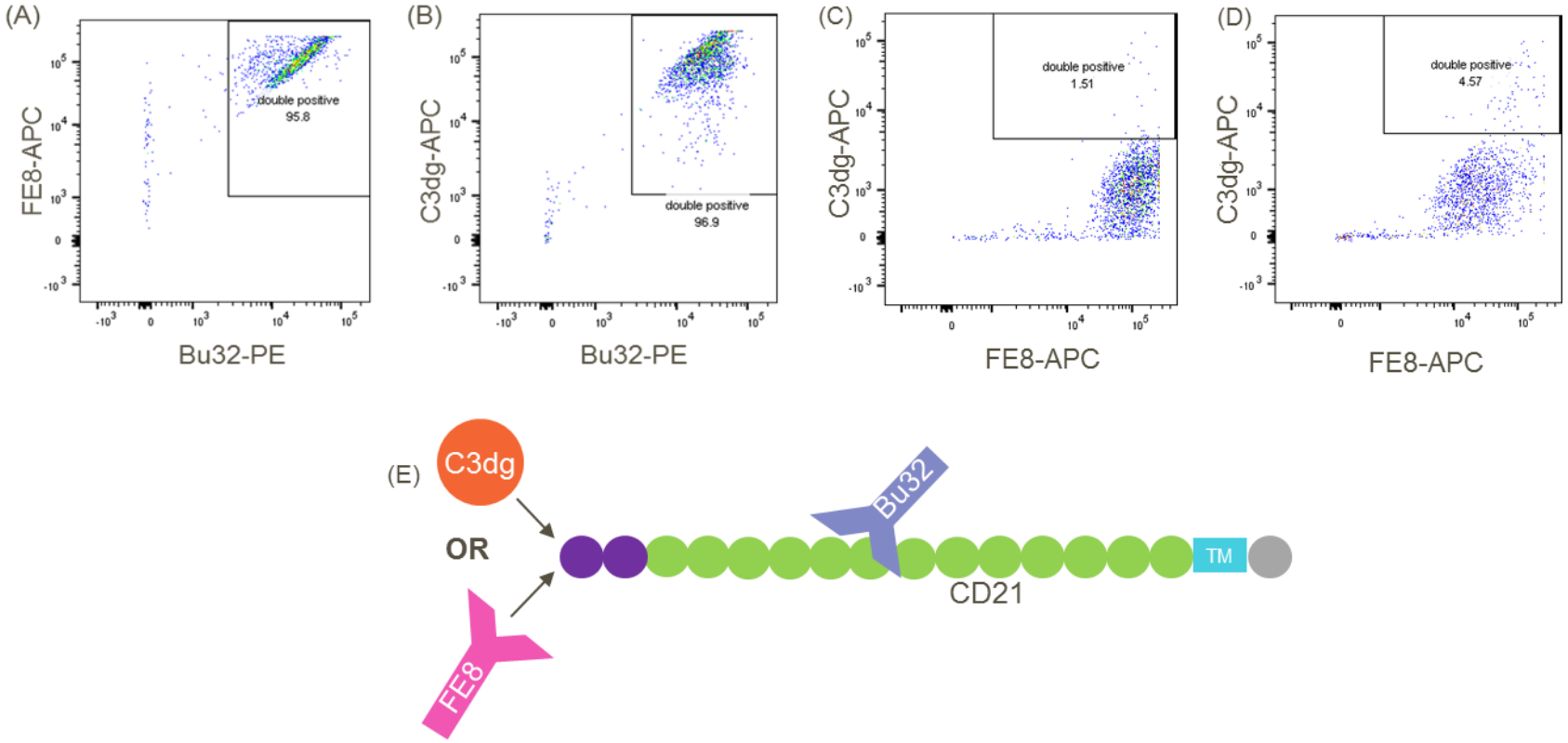

Figure 10.3. 5: Identification of blocking and non-competitive CD21 antibody clones

(A) FDCs (gated as in Figure X) can be simultaneously stained with both FE8 and Bu32 CD21 antibody clones. (B) C3dg can bind to the CD21 receptor in the presence of the Bu32 antibody clone for CD21, all cells are double positive for these markers. (C) C3dg is unable to bind to its ligand binding site on CD21 in the presence of FE8; cells are single positive for FE8 only. Reagents were added simultaneously. (D) C3dg is unable to bind to its ligand binding site on CD21 in the presence of FE8 when FE8 is added prior to C3dg staining. (E) Schematic of antibody clones and C3dg molecule binding to CD21 receptor

In the final assay to assess C3dg-immune complex binding to CD21, cells were preincubated with unlabelled FE8 (13 nM serially diluted 3-fold) before addition of a fixed concentration of C3dg-complex (1 µg/ml C3dg equivalent). FE8 blocked C3dg binding to CD21 on tonsil derived FDCs in a concentration dependent manner (IC_{50} 0.4 nM, n=3; Figure 10.3.6A). FE8 also blocks C3dg binding to tonsil and blood derived B cells in a concentration dependent manner (IC_{50} 0.07 and 0.06 respectively, n=3; Figure 10.3.6A). These data show that approximately 6-fold more FE8 is needed to block C3dg binding to FDCs than B cells. The literature suggests FDCs express the long form of CD21, whereas B cells express the short form. This raised the question as to whether the observed difference in blocking ability was due to the affinity of the receptor isoforms. However, as FDCs have over 30-fold higher CD21 receptors on their cell surface compared with B cells (Figure 9.3.16) it would be expected that if the receptors expressed on the surface of the FDC had higher affinity, a fold-change in the amount of FE8 needed to block C3dg binding would be more comparable to this change in receptor expression rather than the 6-fold change observed. Therefore, it is reasonable to suggest that more FE8 is needed because of the increase in receptor number, and this data suggests that CD21 on FDCs does not have a higher affinity for C3dg than the receptor on B cells. Isotype control antibodies had no effect on C3dg binding at any of the concentrations tested (n=3, Figure 10.3.6B).

The IC_{50} of B cells from blood and tonsil are comparable; however, there is a difference in the shape of the FE8 blocking response curves. Using the same high concentrations of FE8, C3dg binding can be blocked completely on blood derived B cells (0% C3dg binding), however in B cells (and FDCs) from tonsil, blocking at the highest concentration of FE8 used is incomplete. This may be influenced by the different cell isolation methods; tonsil cells had undergone a tissue digestion protocol (Methods section 8.2) whereas blood derived cells were isolated using a Ficoll gradient, a gentler method of isolation. Additionally, the source of the cells may be a reason for the differences observed.

In summary, this work shows that C3dg-immune complexes bind to $CD21^{+}$ FDCs and B cells in a concentration dependent manner and that this binding can be blocked using the CD21 blocking antibody clone, FE8, also in a concentration dependent manner. Blocking of C3dg requires an antibody concentration 6-fold higher for FDCs than that of B cells, suggesting CD21L, reported to be expressed on FDCs, does not have a higher affinity for C3dg than CD21S expressed on B cells due to the observation that FDCs express 33-fold higher CD21 receptors on their cell surface (Figure 9.3.16). This concept was further investigated in the following experiments.

(A)

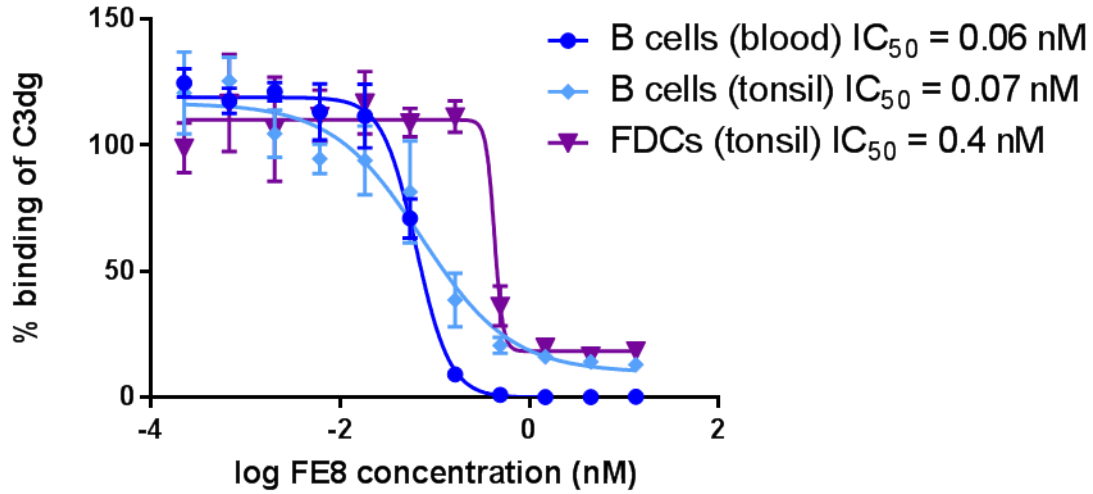

(B)

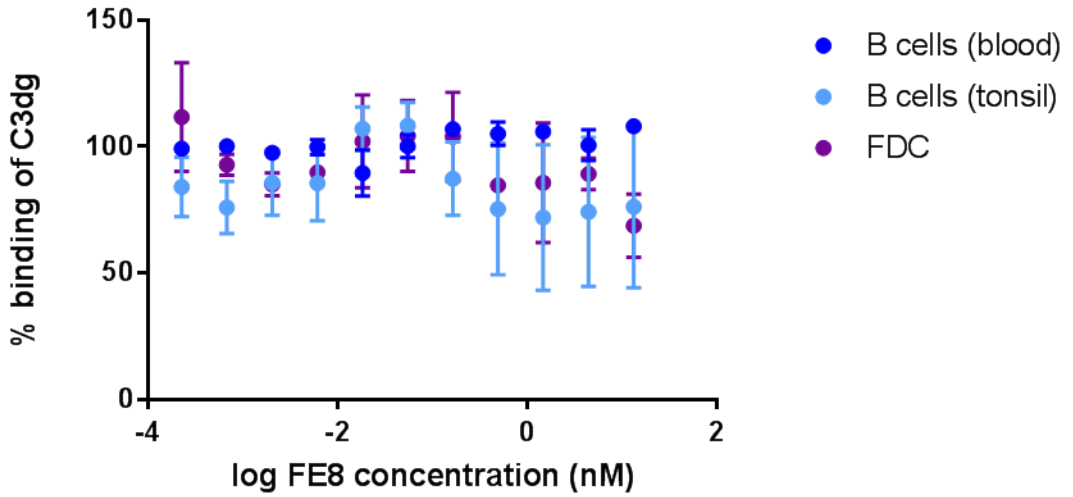

Figure 10.3. 6: FE8 blocks C3dg binding to FDCs and B cells in a concentration dependent manner

(n=3, bars represent SD). (A) FE8 titration, starting at 13.3 nM and serially diluted 3-fold. C3dg was added to all samples to a final concentration of 1 µg/ml. Blocking occurs on tonsil derived B cells at an IC50 of 0.07 nM and blood derived B cells at 0.06 nM. Blocking occurs on FDCs at an IC50 of 0.4 nM, a 6-fold greater concentration of FE8 than that on B cells. (B) No effect on C3dg binding is seen using IgG1 isotype antibody (unlabelled) on any cell type at any concentration tested.

10.3.2 Investigating the presence of the long isoform of CD21 in biology

Expression of CD21S and CD21L at the mRNA level

FDCs are reported to express the long isoform of CD21; detection of this isoform within these cells was confirmed using qPCR. Primers were designed to amplify "total" CD21 message and CD21L specific message (Figure 10.3.7C) and assays undertaken using primary FDCs, FRCs, T and B cells isolated from human tonsil tissue (n=3 donors).

Primers for total CD21 detected message in both FDCs and B cells relative to gene expression in the total tonsil (n=3 independent donors, Figure 10.3.7A). FRCs act as a negative control within the assay. These data agree with the protein expression data (Figure 9.3.16), however FDCs express greater than 30-fold higher CD21 protein than B cells on their cell surface, whereas a 2-fold difference in CD21 mRNA is observed between FDCs and B cells. This difference could be due to the stability of mRNA compared with protein; protein is more stable and therefore degradation and high turnover of mRNA could be a reason for this discrepancy. Another interpretation of this data could be, cleavage of CD21 protein on the surface of B cells to form soluble protein is thought to occur (M. Masilamani et al., 2003), therefore more mRNA relative to the levels of CD21 detected on the cell membrane could be made by these cells.

Primers were designed around the 10a exon boundary to specifically detect CD21L mRNA expression (Figure 10.3.7C). These primers used a SYBR green based probed for detection of amplification whereas total CD21 was detected with TaqMan probes (commercially available). TaqMan probes are naturally more specific for their targets than SYBR green primers; products were run on an agarose gel after amplification by qPCR and one band, of the correct size, was observed using the primers designed for CD21L detection (data not shown – done by undergraduate project student), but as the resultant band was not sequenced, there is no way to confirm this band was CD21L. However, as expected, FDCs express high levels of CD21L mRNA relative to total tonsil and B cells do not appear to

express this CD21 isoform at the mRNA level (Figure 10.3.7B). Therefore, it is assumed that primers were specific for the long isoform of CD21 as this data reflects that previously reported in the literature. Raw C_t values (delta-delta C_t plotted in Figure 10.3.7, data not shown) were approximately equal for FDCs in both total CD21 and CD21L assays, suggesting all CD21 expressed by FDCs is the long isoform.

This data shows that the CD21L isoform is expressed in FDCs but not B cells at the mRNA level, confirming what was previously described in the literature. CD21L protein was assessed in further detail in the following data.

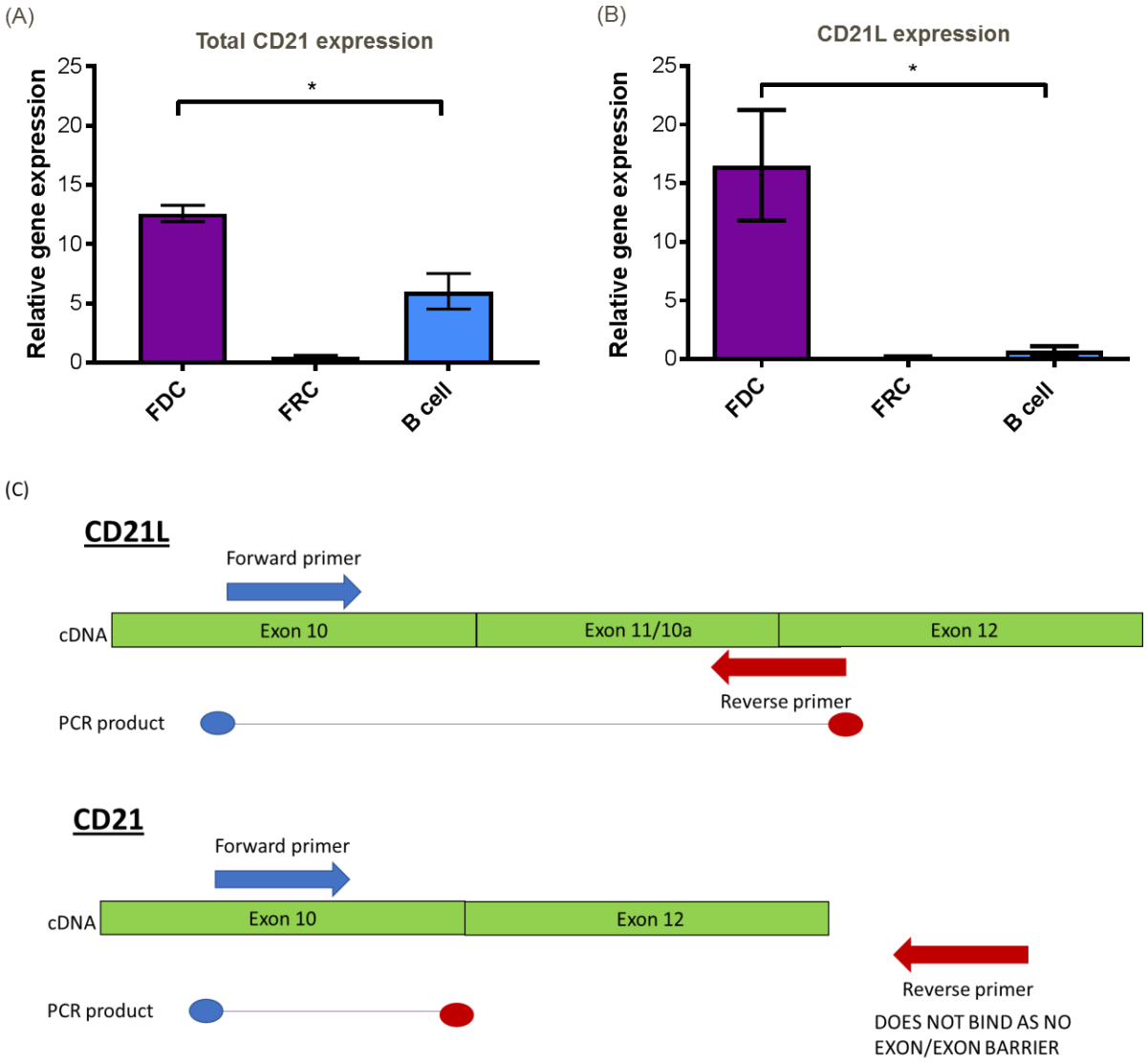

Figure 10.3. 7: FDCs express CD21L at the mRNA level, B cells express CD21S

(n=3, bars represent SD) SYBR green probes for CD21 and CD21L showed (A) FDCs and B cells express CD21 at the mRNA level relative to levels found in total tonsil. FRCs act as a negative control within this assay. CD21 probes will identify "total" CD21 mRNA, therefore both CD21S and CD21L isoforms will be detected. (B) FDCs express CD21L at the mRNA level relative to total tonsil. FRCs and B cells do not express CD21L at the mRNA level relative to total tonsil. CD21L SYBR green primers specifically identify CD21L isoform. (C) Primer design for CD21L SYBR green probes. Forward primer is located within exon 11/10a; the addition sequence added in the long isoform of the protein. The reverse primer spans the exon-exon boundary of exon 11/10a and exon 12. This design ensures products will only be produced is CD21L mRNA is present in the sample.

Immunohistochemistry staining of human tonsil tissue with CD21 antibody clone R4/23

In order to investigate CD21L at the protein level, isoform specific reagents are required. CD21L was first reported to be specifically expressed by FDCs using immunohistochemistry in a study utilising the CD21 antibody clone R4/23. This antibody was said to be specific for the long isoform of CD21 due to staining patterns of FDCs seen within human tonsil tissue whereas CD21 expression on B cells was absent (Naiem et al., 1983). This data was replicated in this study confirming that only the FDCs are identified when staining is carried out using R4/23 (Figure 10.3.8); however previous data revealed staining with the CD21 antibody clone Bu32 also reveals the same staining pattern, i.e. only CD21 expression on FDCs are detected (Figure 9.3.5). It was previously concluded that this result occurred due to the high numbers of CD21 receptors expressed by FDCs in comparison to B cells, therefore detection on CD21 expressed on B cells theoretically should be seen in zones devoid of FDCs; this observation was reported in the study using R4/23. Weak binding of B cells in zones outside of the germinal centre, in which there were no FDCs present, was visualised using this antibody (Naiem et al., 1983). This was the first indication that R4/23 may not be specific for the long form of CD21; therefore, further investigation was undertaken to confirm the isoform preference of the antibody.

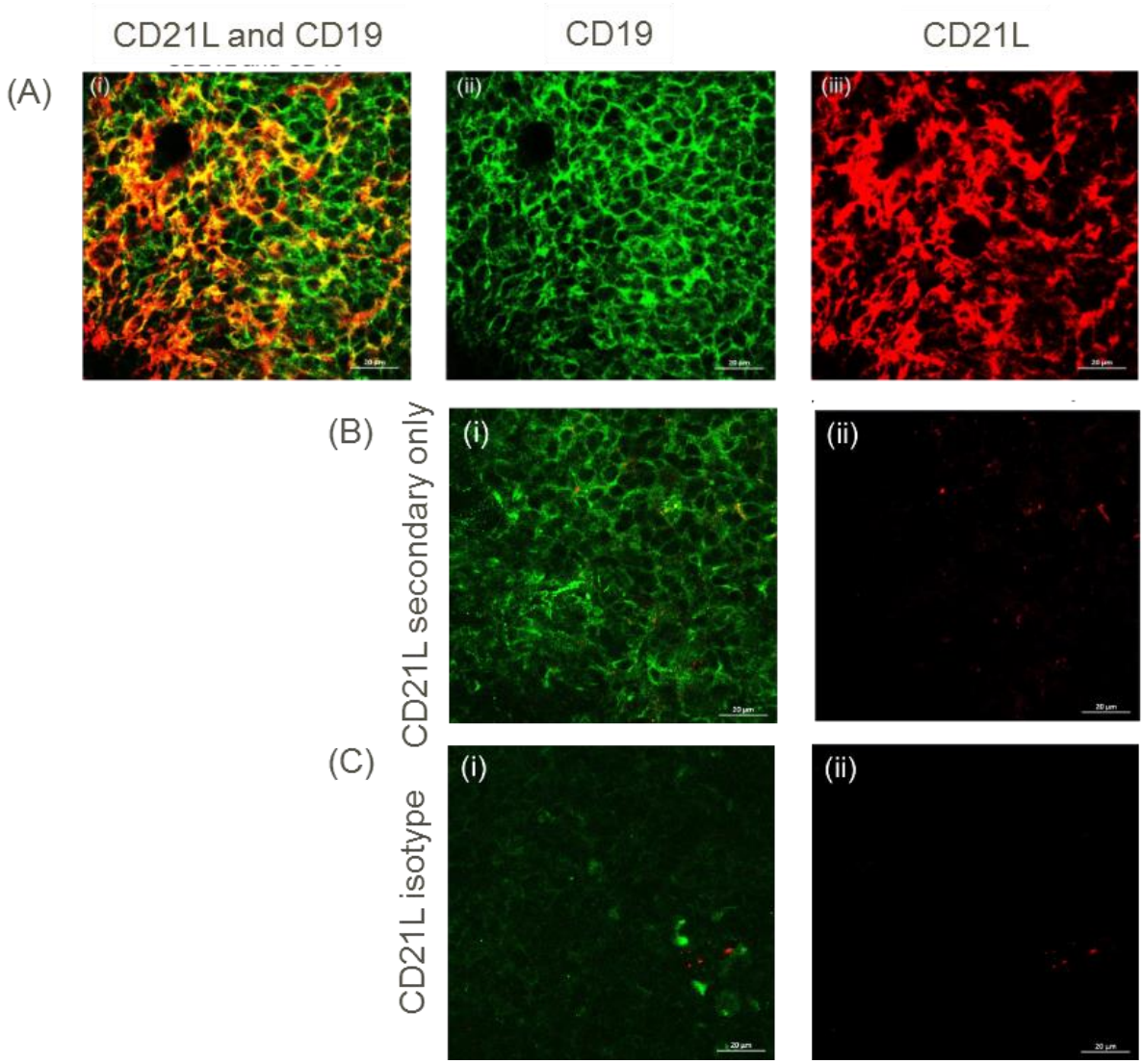

Figure 10.3. 8: Immunohistochemistry of secondary lymphoid organs with CD21 antibody clone R4/23 reveals the same staining pattern as Bu32

(A) Human tonsil tissue stained with R4/23 (A647-red) and CD19 (A488-green), magnification x63, scale bar 20 µm. (ii) green channel alone – CD19 (iii) red channel alone – R4/23. (B) R4/23 secondary alone control. No staining in (ii) confirms staining with this antibody is specific for R4/23. (C) R4/23 isotype control. No staining in (ii) confirms CD21 specific staining of the R4/23 antibody.

Using CD21S and CD21L transiently expressing HEK293T cells to assess R4/23 specificity

CD21 short and long isoforms were cloned into the vector pQCXIN (Materials and Methods section 8.12) with the final aim to create transiently transfected cell lines specifically expressing CD21S or CD21L in order to further understand the specificity of CD21L antibody reagents. HEK293T cells (HEK) were the cell line of choice in these experiments. HEK cells were transfected with plasmids using lipofectamine (methods section 8.14) and harvest 36 hours after transfection to assess CD21 expression. Supernatants were also collected and frozen at -80°C for future use.

CD21 expression was assessed using the Bu32 antibody clone. Flow cytometry analysis revealed transfections were successful; on average 69.5% of transfected cells were $CD21^{+}$ (n=4 independent transfections, Figure 38). Untransfected cells and cells stained with isotype antibody were all negative for CD21 (Figure 38).

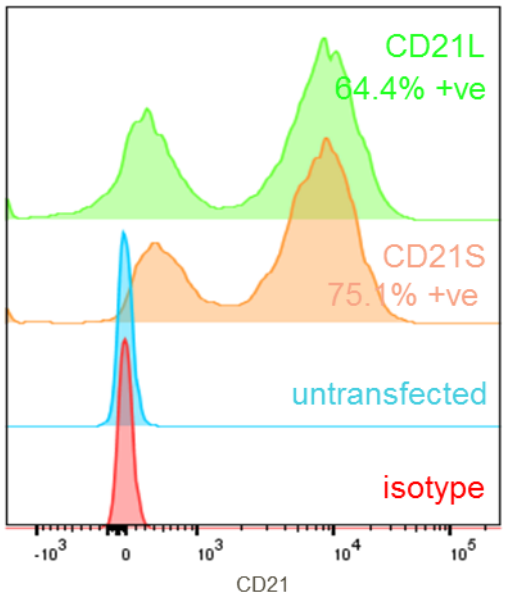

Figure 10.3. 9: Transfected HEK293T cells express CD21S and CD21L

Flow plot is representative of 4 individual transfections performed to obtaining the following data depicted in Figures 10.3.10, 10.3.12 and 10.3.13. 64.4% of cells transfected with pQXCIN-CD21L became CD21+ve. 75.1% of cells transfected with pQXCIN-CD21S became CD21+ve. Untransfected cells and cells stained with IgG1-PE isotype antibody are negative for CD21.

Expression of a single isoform within transfected cells was assessed using western blotting. There is a small size difference between CD21S and CD21L, 145 kDa versus 150 kDa respectively. This difference can be resolved on a western blot; assessment of protein lysate from untransfected HEKs and cells transfected with CD21S and CD21L using this method revealed no bands, a protein band at 145 kDa and a protein band at 150 kDa, respectively when blotted using the CD21 antibody clone Bu32 (Figure 10.3.10B). This observation confirmed HEK cells do not endogenously express CD21 and transfected cells are expressing CD21S or CD21L protein only. Additionally, PCR was performed using primers designed to result in a smaller band when CD21S is present and a larger band when CD21L is present (Figure 10.3.10C). Again, transfected HEK cells were shown to specifically express CD21L or CD21S only (Figure 10.3.10C). Raji cells and total tonsil acted as controls for this data, showing that Raji cells only express the short form of CD21, creating only the smaller of the two bands, and as total tonsil contains both CD21S and CD21L, presumably due to the presence of B cells and FDCs within the sample, both bands are present within this sample. It was previously reported that Raji cells express the long isoform of CD21, determined through binding of another CD21L antibody clone, 7D6, to surface expressed CD21 (Liu et al., 1997), however data presented here suggests, again this antibody may not be specific for the long isoform of CD21. Additionally, PCR for the CD21 gene within these cells, revealed only the short form is present at the mRNA level (Figure 10.3.10C) therefore cell surface protein will also be of the short isoform. This observation provides further evidence that this antibody clone also recognises the short isoform of CD21.

Transfected cells were used to investigate R4/23 specificity using flow cytometry. The antibody was seen to bind to cells expressing CD21S and CD21L (Figure 10.3.10A); therefore R4/23 is not specific for CD21L in a flow cytometry setting. Increased binding of the antibody to cells transfected with the long form of CD21 was observed, suggesting the antibody may preferentially bind to CD21L, but as this reagent has the capacity to also identify CD21S expressing HEK cells, it cannot be said that this reagent is specific for the

long isoform. The antibody clone, 7D6, also reported to bind to CD21L, was used to stain the transfected cells to test the isoform specificity of this clone. Using this antibody, no $CD21^+$ cells were identified; as cells were shown to be $CD21^+$ using Bu32 and R4/23 antibody staining, it can be concluded that 7D6 is not suitable for use in flow cytometry to identify CD21 expression (Figure 10.3.10A).

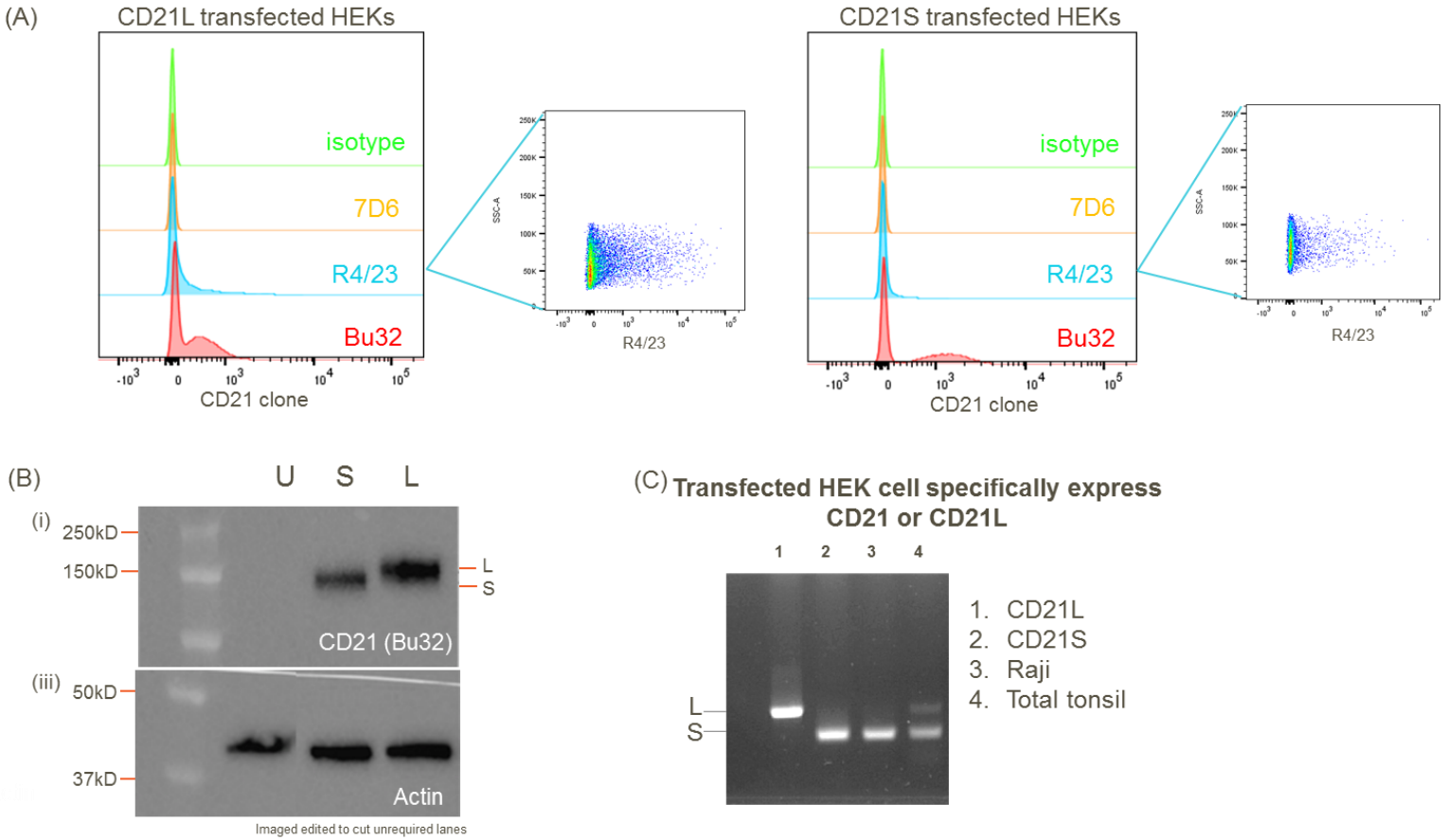

Figure 10.3. 10: R4/23 binds to HEK293T cells specifically expressing the short isoform of CD21

(A) R4/23 binds weakly binds to cells expressing CD21L and CD21S. 7D6, another reported CD21L specific antibody, does not identify CD21S or L in a flow cytometry setting. Bu32 confirms cells are CD21+ve, and identifies both isoforms. (B) Western blot confirms transfected HEK cells are expressing CD21S or CD21L only. (U=untransfected, S=CD21S transfected, L=CD21L transfected). CD21S expected size is 145kDa, CD21L expected size is 150kDa. (C) PCR reveals transfected cells express only CD21L or CD21S. Raji cells express CD21S and both isoforms are present within total tonsil.

To further assess isoform preference of the R4/23 antibody, an ELISA was developed using this CD21 clone as the capture antibody. Specificity for CD21S and CD21L was assessed using supernatants derived from transfected HEK293T cells, specifically expressing the long or the short form of CD21. Consequently, supernatants contained either soluble CD21S or CD21L, although protein concentrations were not high enough to visualise on western blot. Presence of CD21 within reagents was confirmed using a commercial human CD21 ELISA (abcam) that detects both the long and short form of CD21 ("total" CD21) (Figure 10.3.11A). Standards from the ELISA kit were also run during this assay to determine protein concentration within supernatant and confirm the assay was working as expected, detecting CD21 specifically. To form the R4/23 ELISA, components from the commercial CD21 ELISA were used, replacing the capture antibody with R4/23. HEK derived supernatants and kit standards were run using this assay to reveal detection of both CD21S and CD21L using R4/23 (Figure 10.3.11B). Interestingly, CD21 standards from the commercial ELISA were not detected in this assay, presumably as the protein was in a truncated form, and the epitope recognised by R4/23 had been removed. This data further suggested that R4/23 recognises both the long and the short form of CD21, but as CD21 within the supernatants could not be visualised, to confirm this observation, a standard curve using a recombinant form of CD21 (R&D systems) was run on the total CD21 and R4/23 ELISA (Figure 10.3.11C). Protein was detected in both assays, although signal was slightly reduced in the R4/23 assay, again suggesting the antibody may preferentially bind CD21L, but not specifically. As rc-CD21 is known to be the short form of CD21, it can be concluded that in an ELISA setting, R4/23 is not specific for CD21L and also has the ability to bind CD21S.

To summarise, the use of CD21S and CD21L HEK293T cells and supernatants derived from these cells, revealed that CD21 antibody clone R4/23, although may preferentially bind to the long CD21 isoform, is not specific for CD21L and also has binding capacity for CD21S. Therefore, there are no CD21L specific reagents readily available to assess protein expression in biology.

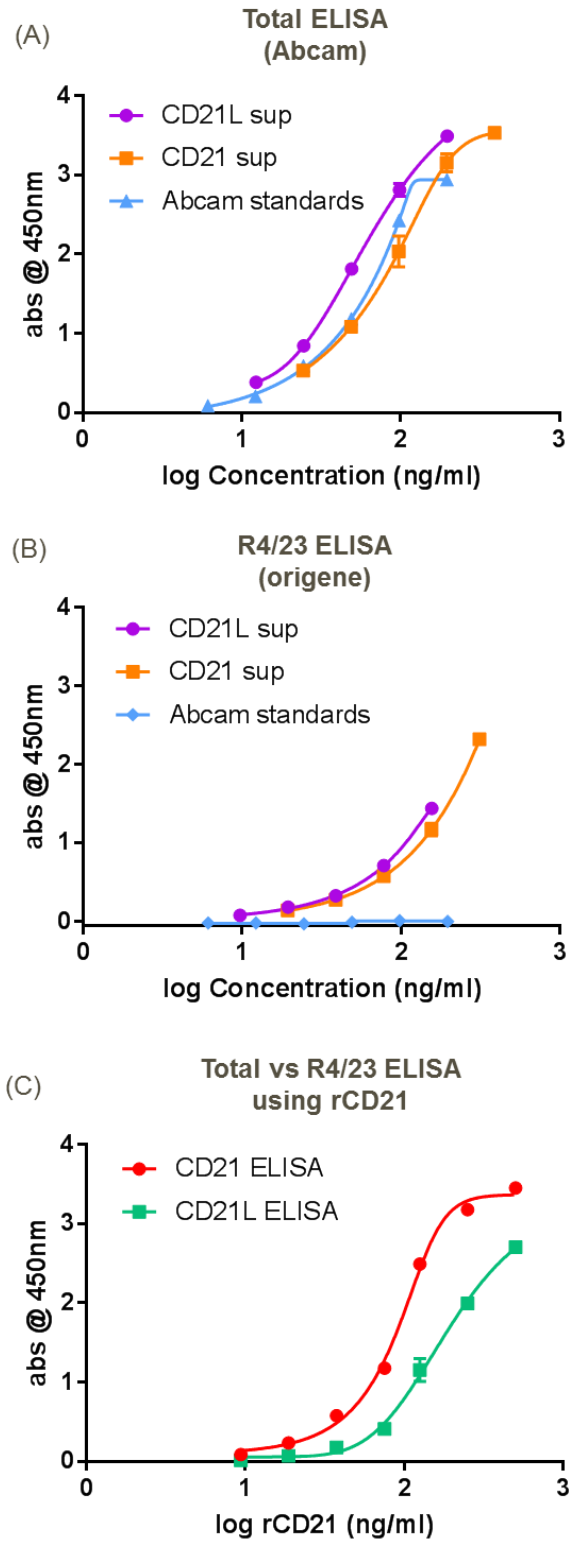

Figure 10.3. 11: R4/23 detects CD21L and CD21S in an ELISA setting

(A) Transfected HEK derived supernatants contain CD21S and CD21L protein, both isoforms of this protein are detected by the abcam CD21 ELISA. Standards from the abcam kit are also detected using this ELISA. (B) 5 µg/ml R4/23 was used to coat 96 well plates to act as a capture antibody in an ELISA. CD21L and CD21S HEK derived supernatants are detected. Abcam standards are not detected using R4/23 as a capture antibody. (C) Recombinant CD21, the short form of CD21, is detected on both ELISAs.

10.3.3 Assessing isoform differential binding functionality using transfected HEK293T cells expressing specific CD21 isoforms

As a specific CD21L antibody reagent was not available, to assess the differential C3dg binding capacity of CD21 isoforms, transfected HEK293T cells, transiently expressing CD21S or CD21L, were utilised (Figure 10.3.8). As with primary cells C3dg binding was assessed using C3dg-immune complexes (Figure 10.3.1). $CD21^{+}$ cells were gated on, determined as positive using CD21 isotype antibody stained samples and untransfected HEK cells stained with Bu32, the antibody clone of choice for identification of CD21 expressing cells (Figure 10.3.12).

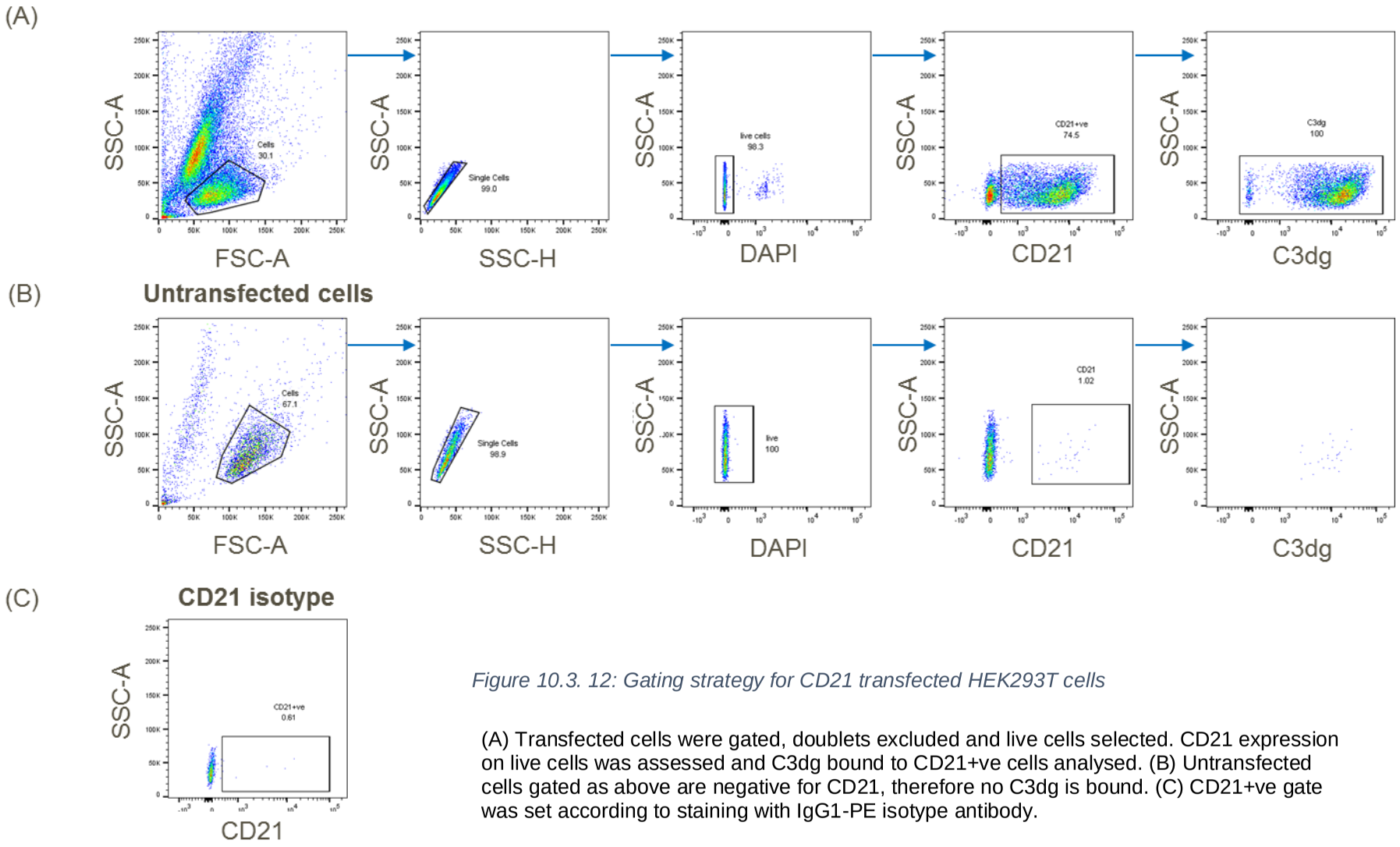

Figure 10.3. 12: Gating strategy for CD21 transfected HEK293T cells

(A) Transfected cells were gated, doublets excluded and live cells selected. CD21 expression on live cells was assessed and C3dg bound to CD21+ve cells analysed. (B) Untransfected cells gated as above are negative for CD21, therefore no C3dg is bound. (C) CD21+ve gate was set according to staining with IgG1-PE isotype antibody.

CD21 receptor expression was assessed using Quantibrite-PE beads as described in Material and Methods 2.9. Both CD21S and CD21L expressing HEKs were found to express ~ 15,000 CD21 receptors per cell (Figure 10.3.13A, n=4 independent transfections), as cells are expressing similar receptor numbers on their cell surface, any differences observed in C3dg binding can be said to be isoform specific, not due to receptor number expression.

Assays to assess C3dg binding capabilities of each isoform were performed by titrating C3dg-immune complexes from a starting concentration of 10 µg/ml C3dg and serially diluting 3-fold. C3dg was shown to bind to both isoforms in a concentration dependent manner (Figure 10.3.13B, n=4 independent transfections), however, as with primary cells (Figure 10.3.4), saturating concentrations of C3dg were not reached. Increased concentrations were not used due to limits to how much protein can be added in an assay. As the concentration of C3dg increases, CD21S binds to more of the available ligand. This suggests CD21S has a higher binding capacity for C3dg than CD21L.

Assays using FE8 to block C3dg binding to the two CD21 isoforms were performed by preincubating cells with unlabelled FE8 and adding a fixed concentration of C3dg-immune complex (1 µg/ml). A higher starting concentration of FE8 was needed to see complete blocking of C3dg binding to transfected cells than that used to block binding in primary cells, 40 nM compared with 13.3 nM respectively. FE8 was shown to block C3dg binding to CD21S and CD21L in a concentration dependent manner, the IC_{50} of each curve was 0.04 nM and 0.01 nM respectively. As IC_{50} values are similar for both isoforms, it can be concluded that FE8 binds equivalently to each CD21 form. This suggests the binding site of C3dg, FE8's epitope, is not changed between the two isoforms.

This data suggests that isoforms of CD21 do not differentially bind to C3dg. CD21S binds to more C3dg at higher concentrations; therefore it is thought that an increased affinity for C3dg is not the cause for antigen transfer between CD21S and CD21L.

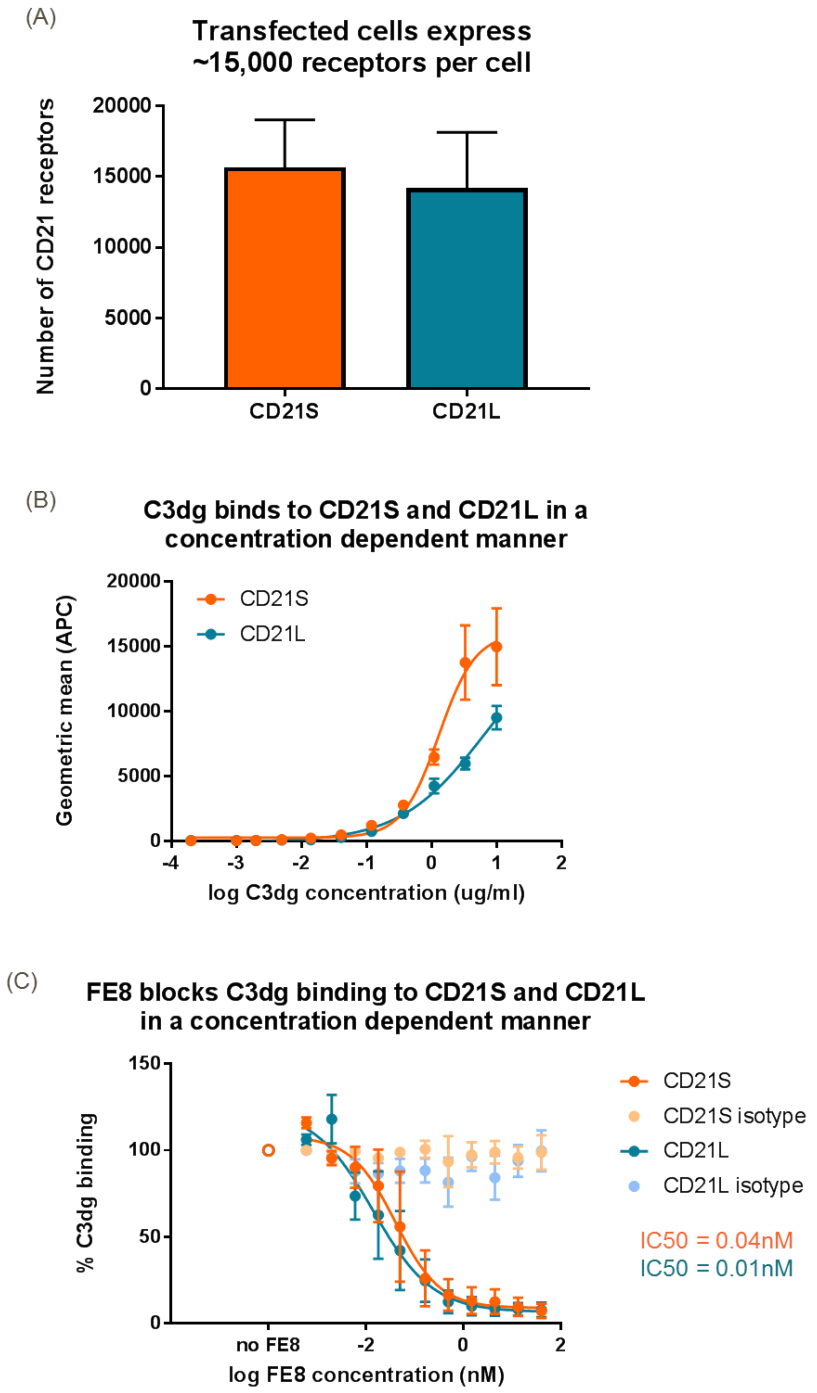

Figure 10.3. 13: Investigation of C3dg binding capacity of CD21S and CD21L expressing HEK293T cells

(A) The number of CD21 receptors on the surface of transfected cells was quantified using Quantibrite beads (Methods 8.9). Both cell types express an average of ~15,000 receptors per cell. n=4 individual transfections, bars represent SD. (B) C3dg titration starting at 10 µg/ml showed that C3dg binds to CD21S and CD21L in a concentration dependent manner. CD21S binds greater C3dg complexes at high concentrations of C3dg. Saturating concentrations were not reached for either isoform. n=4 individual transfections, bars represent SD. (C) Cells were preincubated with FE8 CD21 Ab clone at a starting concentration of 40 nM. 1 µg/ml C3dg was added to each sample. FE8 blocks C3dg binding to CD21S (IC50 = 0.04 nM) and CD21L (0.01 nM) in a concentration dependent manner. n=4 individual transfections, bars represent SD, NB: data points at 0.002 nM and 0.0006 nM FE8 are n=2.

10.3 Discussion:

The aim of this work was to investigate the C3dg binding functionality of the two CD21 isoforms, short and long. I hypothesised that unidirectional transfer of C3dg-antigen complexes between B cells and FDCs may be due to the differential expression of CD21 isoforms on each cell type. FDCs are reported to express CD21L, whereas B cells are reported to express CD21S (Liu et al., 1997).

Model immune complexes were formed using monobiotinylated-C3dg and fluorescently labelled streptavidin (Figure 10.3.1). These complexes of C3dg were assumed as tetramers, although this was not confirmed using size exclusion chromatography or other analytical methods, but empirically calculated. It has been previously reported that tetrameric C3dg-complexes are able to bind to B cells and cause improved specific-antibody responses and increased activation of cells (Youngkyun et al., 2005), whereas monomeric C3dg-complexes have been shown to inhibit these responses (Tsokos et al., 1990). This suggests that C3dg can act to both activate and inhibit the immune response depending on which form the molecule takes *in vivo*. Additionally, it has been shown that, binding of monomeric C3dg to recombinant CD21 does not occur under physiological conditions (Moore et al., 1989). Binding of a monomeric form of C3dg complexes can be visualised under the experimental conditions used here, but the signal detected is much lower than that of the tetrameric form (Figure 10.3.1B). As this work was assessing binding of C3dg by $CD21^{+}$ cells, it was important to use a tetrameric complex to ensure binding of the ligand to its receptor could be easily visualised; the increased valency of the complex subsequently increased the assay window for ligand binding assays. This artefact may be due to a low binding affinity of C3dg for CD21; suggested by studies using tetrameric complexes of T cell antigen to visualise populations of T cells expressing specific TCRs (Altman et al., 1996). These studies revealed that tetrameric complexes could be used to visualise weak binding interactions between ligand and receptor.

C3dg-immune complexes were shown to bind to primary FDCs, T and B cells in a concentration dependent manner (Figure 10.3.4). As no data was generated to confirm that C3dg was used in a tetrameric form, there is the potential for monomers to be present within the assay. As the concentrations used were chosen due to the likelihood of tetrameric complex formation, calculated by molar ratios, and the fact that brighter signal was observed using these complexes than the "monomeric" complexes (Figure 10.3.1B) suggests any monomers present did not dramatically affect the results collected. However, it is true that, an increased signal may have occurred if no monomers were present; this may be a reason that saturating concentrations of C3dg did not occur on any of the cell types investigated (Figure 10.3.4). Increased concentrations of complex were not used due to the occurrence of non-specific binding to $CD21^-$ cells at high concentrations. C3dg is known to bind to other membrane receptors and serum proteins, an action which has been interpolated as the molecule acting as a potential universal molecular adjuvant (Karen et al., 2004). These additional binding partners could explain the binding of high concentrations of C3dg to $CD21^-$ cells. As this binding is only observed at high concentrations, it is suggestive that C3dg has a higher ligand-receptor affinity with CD21 than with the other receptor interactions on $CD21^-$ cells. This non-specific signal was not seen at a C3dg-immune complex concentration of 1 µg/ml; therefore, this was the concentration of complex chosen for subsequent assays. As this investigation was focused on binding of C3dg via CD21, it was important to use a concentration of the ligand which would bind to CD21 expressing cells and where non-specific binding was not observed on $CD21^-$ cells, allowing all ligand to be bound by the cells of interest.

A monoclonal mouse CD21 antibody clone, FE8, was utilised to further investigate C3dg binding on primary human FDCs and B cells. FE8 has previously been shown to block the binding of C3dg to human tonsil B cells and infection of these cells with EBV (Wolfgang et al., 1998). This study concluded that the antibody blocked binding of CD21 ligands to their receptor by occupying an epitope sequence found in the recess formed between SCR1 and

SCR2; the ligand binding site. This study did not investigate the effect of this competitive antibody clone of C3dg binding on primary human FDCs or B cells derived from the blood. Data from the current investigation showed that FE8 was able to block C3dg binding to tonsil derived FDCs, B cells derived from tonsil and B cells derived from blood in a concentration dependent manner (Figure 10.3.6A). The CD21 antibody clone HB5 was used as a control for FE8 blocking ability in the early study, whereas an IgG1 isotype control was used here to show blocking was FE8 dependent (Figure 10.3.6B). In addition to blockage of C3dg binding, FE8 was also shown to remove C3dg ligands already bound to the CD21 receptor (Wolfgang et al., 1998); further supporting the idea that C3dg has a low affinity interaction with CD21. Interestingly, the IC_{50} of FE8 blocking binding of C3dg to FDCs is 6-fold greater than that on B cells, 0.4 nM and 0.07 nM, respectively. As FDCs express over 30-fold more CD21 receptors on their cell surface, the amount of FE8 needed to block binding of C3dg to CD21 on these cells was expected to be higher than 6-fold. Thus, it is possible that CD21L on FDCs has a lower affinity for C3dg than CD21S expressed by B cells; this was further investigated in subsequent experiments.

FDCs were confirmed to express the long isoform of CD21 at the mRNA level, whereas B cells were shown to express CD21S, detected with total CD21 TaqMan probes (Figure 10.3.7A). These probes will detect both CD21 and CD21L whereas the SYBR green based assay, specifically identifies CD21L mRNA expression (Figure 10.3.7B). Antibodies against CD21, Bu32 for example, bind to both the short and the long isoform of CD21 protein. However, this investigation revealed that no CD21L specific antibody reagents are currently available to detect this isoform at the protein level.

Antibody staining patterns in tonsil tissue using the antibody clone R4/23 revealed only the expression of CD21 on FDCs, an observation previously reported in the literature and the primary reason for the conclusion that R4/23 was specific for CD21L protein (Naiem et al., 1983). Immunohistochemical data presented in results chapter 1 also showed that staining secondary lymphoid organ tissue with antibodies against CD21, in this case the antibody

clone Bu32, also shows FDC expression of CD21 (Figure 9.3.6). It was concluded that this observation was due to the high number of CD21 receptors expressed on the cell surface of FDCs compared to B cells (Figure 9.3.16) and it is thought that CD21 expression would be observed on B cells in zones devoid of FDCs. Weak binding of R4/23 and 7D6, another CD21 Ab clone reported as specific for the long isoform (Liu et al., 1997), was reported against B cells outside of the FDC zones, indicating the antibodies do have some capacity to bind to CD21S, although their binding preference may be the long isoform. Data using antibodies in a flow cytometry setting to identify transfected HEK293T cells further highlight the non-specific nature of R4/23. Both CD21S and CD21L expressing cells were shown to be transfected to similar levels, around 70% of cells were $CD21^+$ when analysis was carried out using the Bu32 antibody clone by flow cytometry (Figure 38). In contrast, an increased staining for CD21L expressing cells was seen in comparison with CD21S cells when using R4/23 to identify $CD21^+$ cells (Figure 10.3.10). This observation further suggests that R4/23 preferred CD21L but is not specific for this isoform as both cell populations were detected. On the other hand, 7D6 did not identify CD21S or CD21L transfected cells, therefore cannot be used in a flow cytometry setting within this study (Figure 10.3.10). Transfected cells were shown to express only one form of the protein using both western blot analysis and PCR. PCR primers were designed outside of the SCR10a exon boundary which allowed a band of 273 bp to be formed if the exon was not present in CD21S transcripts, but a larger band of 413 bp to form when CD21L transcripts were present in the sample (Figure 10.3.10C). Both techniques confirmed expression of CD21S or CD21L in the transfected cells. The B cell lymphoma cell line, Raji, and total tonsil were used as controls in the PCR assay. Total tonsil contained both isoforms, as expected due to the presence of both FDCs and B cells within the sample, whereas Raji cells only formed the smaller PCR product, suggesting only CD21S is expressed by this cell line. This is interesting as these cells have previously been reported to express the long form of CD21 as they were shown to express the 7D6 epitope (Liu et al., 1997). Again, the data presented here contradicts these reports, and further shows these antibodies are not specific for detection of CD21L. Additional studies using

R4/23 as a capture antibody in an ELISA setting and HEK supernatants containing soluble CD21S or CD21L confirmed that this antibody could detect both forms of the protein (Figure 10.3.11B). The antibody could also detect recombinant CD21 (R&D systems) which is known to be the short form of the protein (Figure 10.3.11C). This data concludes that no specific CD21L antibody reagents are available, therefore to investigate the differential C3dg binding potential of CD21S and CD21L, HEK293T cells transfected to transiently express the long or short form of CD21 specifically were utilised.

Transfected HEK cells were shown to express ~15,000 CD21S or CD21L receptors per cell (Figure 10.3.13A), which is ~1.5-fold higher than that seen on the surface of B cells and ~10-fold lower than that expressed on FDCs (Figure 9.3.16). As both transfected cell lines averagely expressed similar numbers of receptors, any changes observed in C3dg-binding between the two lines is due to the isotype expression. C3dg-immune complexes were shown to bind to CD21S and CD21L in a concentration dependent manner (Figure 10.3.13B). At high concentrations of C3dg, CD21S binds more complex than CD21L. This is suggestive of CD21S having a higher affinity for C3dg than CD21L. FE8 blocked C3dg binding to CD21S and CD21L with the same affinity, IC_{50} was found to be 0.04 nM and 0.01 nM, CD21S and CD21L respectively (Figure 10.3.13C). This experiment only assesses FE8 affinity for the receptor, not the affinity of C3dg for the two isoforms. To investigate the affinity of C3dg for the CD21 receptor isoforms directly, an assay could be designed in which C3dg-immune complexes are allowed to pre-bind CD21 receptors before the addition of FE8 in varying concentrations. If the concentration of FE8 needed to displace the ligand from CD21 differed between isotypes, a conclusion of which isoform had the highest affinity to C3dg could be more accurately drawn. Previous studies have investigated C3dg displacement with FE8, but differential binding capacity of CD21S and CD21L was not assessed (Wolfgang et al., 1998). As FE8 binds to the ligand binding site and blocks C3dg, it is unlikely that the additional SCR found in CD21L changes the conformation of this site as

the antibody binds to each receptor with the same affinity. Thus, it is unlikely that the affinity of the receptor for C3dg is changed between isoforms.

To conclude, data collected in this investigation aimed to investigate the hypothesis that unidirectional antigen transfer occurs due to CD21L expression on FDCs having a higher affinity for C3dg than CD21S expressed on B cells. The binding capacity for C3dg of CD21S vs CD21L was investigated using transiently transfected HEK293T cells that on average expressed the same number of CD21 receptors on their cell surface; these experiments revealed no considerable differences in C3dg binding between CD21 isotypes. In contrast, differences in the ability of FE8 to block C3dg binding was seen in experiments using primary FDCs and B cells, which express CD21L and CD21S, respectively. When considering the observations discussed above, the differential ability of FE8 to block binding of C3dg to CD21 expressed on FDCs and B cells is thought to be due to receptor numbers on the cell surface and is not a consequence of the CD21L receptor having a greater affinity for C3dg; an increased number of CD21 receptors and size of FDCs results in increased FE8 needed to block C3dg binding. As the C3dg binding capacity of B cells and FDCs did not differ, saturating concentrations were not reached for either cell types (Figure 10.3.4), it is thought that the affinity for C3dg of the CD21 receptors expressed by these cell types also does not differ. This mechanism was also suggested after a study investigating antigen transport in mice (Phan et al., 2007). FDCs in mice also express higher levels of CD21/35 than follicular B cells, further supporting this mechanism as an explanation for antigen transfer. Heesters et al., (2014) suggested that unidirectional C3dg-antigen complex transfer occurs due to cell size. Antigen complexes are presumably opsonised with more than one C3dg molecule, therefore FDCs, with their increased size and number of CD21 receptors, are able to bind an increased number of the available C3dg molecules on the antigen complex than B cells. Contact between FDCs and a B cell during antigen transfer has been found to last up to 30 minutes (Suzuki et al., 2009). Within this time, C3dg is likely to naturally dissociate from its receptor due to the predicted low affinity of the ligand for CD21.

C3dg is thought to bind to CD21 with low affinity, primarily due to the fact tetrameric C3dg complexes allow greater visualisation of ligand-receptor binding compared with monomeric complexes in these and previously published studies. When the antigen dissociates from its receptor, the increased number of contacts the FDC has with the antigen complex allows transfer between the B cells and the FDCs. Alternatively, the increased contacts on the C3dg-antigen complexes and internalisation of CD21 receptors by FDCs into non-degradative endosomal compartments, actively pulls the complexes from the B cells and are sequestered by the FDCs. C3dg bound CD21 is retained and periodically cycled to the cell surface for presentation of antigen to specific B cells (Heesters et al., 2013).

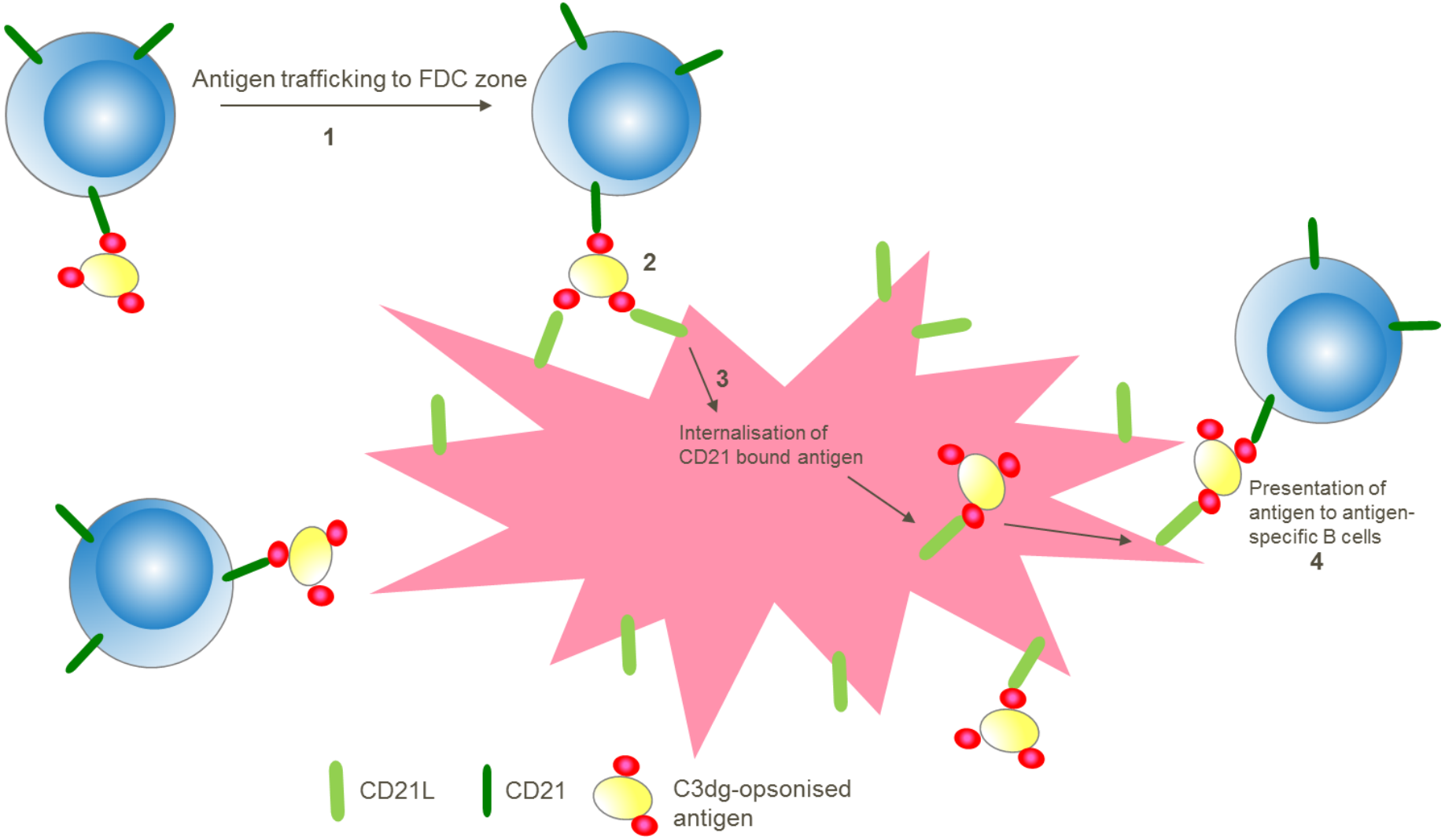

Figure 10.4. 1: Antigen transfer mechanism between B cells and FDCs

1. C3dg-opsonised antigen is trafficked to FDC zones bound to CD21 on the B cell surface. 2. Antigen is presented to FDCs and binds to an increased number of receptors on the surface of the cell due to high receptor numbers. 3. Antigen-bound CD21 is internalised, pulling the immune complex from CD21 receptors on the B cell, 4. and presented to antigen-specific B cells

The hypothesis of antigen transfer between CD21 receptors on B cell to FDCs was 2-fold. The studies detailed in results chapter 1 and 2 investigated whether this phenomenon was due to (1) receptor number on the cell surface or (2) CD21L expressed on FDCs having a higher affinity for C3dg binding allowing antigen transfer to occur. After reviewing the data discussed within these chapters, the following model is proposed (Figure 10.4.1). B cells collect C3dg-antigen complexes from SCS macrophages and consequently shuttle the antigen bound to CD21 receptors to FDC zones, attached through CXCL13 gradients (Figure 10.4.1-1). Contact between C3dg-antigen complexes on B cell CD21 and CD21 on FDCs occurs for up to 30 minutes (Figure 10.4.1-2). Within this time, C3dg could naturally dissociate from CD21 receptors on B cells and remains bound to those receptors on FDCs due to increased number of contacts and receptors on the cell surface. Alternatively, receptors are actively internalised, pulling antigen complexes off the B cell CD21 due to increased contacts between CD21 receptors on the FDC and the C3dg-opsonised antigen-complex (Figure 10.4.1-3). CD21 bound antigen is retained in non-degradative endosomal compartments and recycled to the cell surface for presentation to antigen-specific B cells leading to an increased specific antibody response (Figure 10.4.1-4).

11. Results chapter 3: Soluble CD21 in health and disease

11.1 Introduction

In addition to the membrane bound form, CD21 also exists in a soluble form found within the blood and synovial fluid. There are contradicting reports in the literature discussing the isoform of the soluble receptor. The earliest reports suggest that, although both isoforms are present, sCD21 is predominantly found as the long isoform (Ling et al., 1998). This study utilised the CD21 antibody clone R4/23, reported to be specific for CD21L, however this investigation reveals that this claim is incorrect, rendering the conclusions of this data questionable. An additional study using western blot analysis, identified two forms of sCD21 with molecular masses of 135 and 90 kDa, thought to be the long and short isoform respectively. The molecular mass of sCD21 is smaller than membrane bound CD21 due to the removal of the transmembrane and small cytoplasmic region to create the soluble form of the receptor (Figure 11.1.1). It was shown that CD21 can be released by a proteolytic cleavage through stimuli including the thiol antioxidants N-acetylcysteine and glutathione, and the oxidant pervanadate in murine splenic B cells (Hoefer et al., 2008) but it is currently unknown exactly how CD21 is shed from the membrane surface of cells in humans; though it is thought to be through the action of a yet unidentified protease. More recently, mass spectrometry was used to show that the short form of CD21 is predominantly shed to make to pool of sCD21 within the serum (Masilamani et al., 2003).

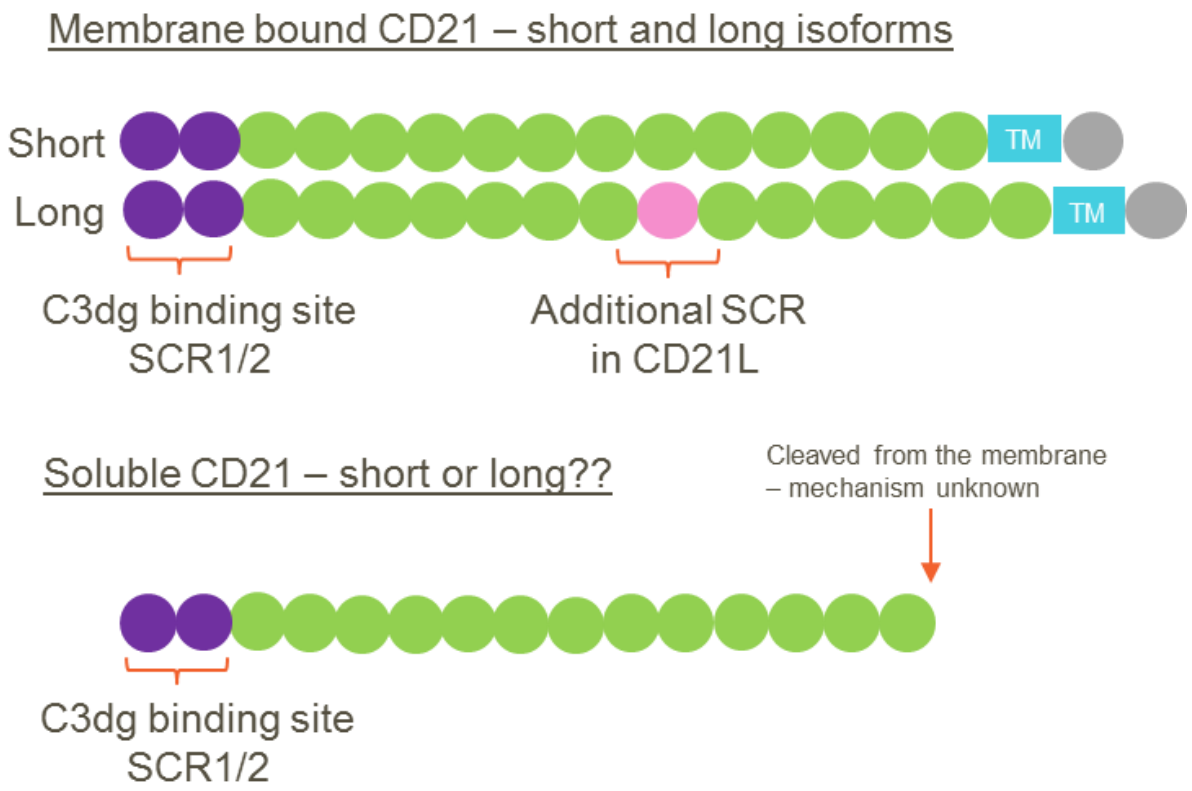

Figure 11.1. 1: Membrane and soluble CD21 receptors

Membrane bound CD21 is found as a long (16 SCRs) and a short (15 SCRs) isoform. The soluble form of CD21 is thought to be of the short isoform and is the extracellular portion of the receptor.

11.1.2 The origin of soluble CD21

The origin of sCD21 in humans has not been confirmed; however, a study investigating this question showed pre-B cells, peripheral T cells, myeloid, fibroblast and plasmacytoid lines to be non-producers of sCD21 (Ling et al., 1991). Additionally, there is published evidence towards B cells as major contributors to the sCD21 pool in humans. Soluble CD21 has been found in culture media from human T and B cells (Fremeaux-Bacchi et al., 1996) and crosslinking of the BCR and CD40 in B cells has been shown to induce shedding of CD21 paralleled by a decrease in membrane associated CD21 when cells were activated with PMA and Ca^{2+} (Masilamani et al., 2003). Additional observations that further support this hypothesis are increased sCD21 levels in patients with B cell chronic lymphocytic leukaemia (Lowe et al., 1989), in which B cell numbers in the blood are increased, and decreased sCD21 levels in patients with Common variable immune deficiency (CVID) (Ling et al., 1991), a condition in which patient B cells have been shown to have defects in CD21 expression.

11.1.3 Functions of soluble CD21

The function of sCD21 in humans has not been fully described. It has been shown to retain C3dg and EBV binding capacity (Ling et al., 1991) and to activate monocytes through binding of membrane CD23 (Masilamani et al., 2004). Recombinant sCD21 has also been shown to inhibit EBV infection of PBMC derived B cells in vitro (Nemerow et al., 1989). A $(CR2)_2$-IgG1 chimera was used to demonstrate the ability of sCD21 to bind C3dg within a murine model. The study showed that the $(CR2)_2$-IgG1 was able to compete for binding to C3dg with cellular CD21 and suppress antibody responses to a T cell-dependent antigen when administered to mice at the time of immunisation (Hebell et al., 1991). The same study used this model complex to demonstrate how sCD21 can inhibit the primary immune response to T-dependent antigen and subsequent isotype switching of murine B cells

(Hebell et al., 1991). Another study demonstrated a role for sCD21 in the inhibition of sCD23-induced IgE synthesis by IL-4 stimulated human peripheral B cells (Fremeaux-Bacchi et al., 1998). Western blot techniques were utilised to show sCD21 could bind to sCD23 in a trimeric form, this binding rendered sCD23 unable to induce antibody synthesis by B cells; another example of sCD21 dampening the immune response. These observations suggest a role for sCD21 in immune response regulation and activation.

11.1.4 Soluble CD21 in disease

It is widely reported that patients with autoimmune diseases have reduced levels of sCD21 compared with healthy individuals. Patients with Rheumatoid Arthritis (RA) (Masilamani et al., 2004), Multiple Sclerosis (Toepfner et al., 2012), Systemic Lupus Erythematosus (SLE) (Masilamani et al., 2004), Sjogren's Syndrome (Masilamani et al., 2004), Systemic Sclerosis (Tomita et al., 2012) and progressive Systemic Sclerosis (Masilamani et al., 2004) have all reported to have decreased levels of sCD21. Interestingly sCD21 levels have also been shown to decrease with pregnancy (Masilamani et al., 2008) and age (Masilamani et al., 2004) but conclusions as to why this occurs have not been reached.

In contrast to the decrease in autoimmune diseases, B cell malignancies such as B cell chronic lymphocytic leukaemia (Ling et al., 1991), EBV and EBV-associated malignancies (Larcher et al., 1995) have higher levels of sCD21 within the serum compared with healthy individuals. This is further evidence for B cells as a source of sCD21, as there are increased numbers of cells in the circulation and an increased sCD21 concentration.

As sCD21 levels are affected within disease phenotypes, a role for the soluble receptor in disease and regulation of the immune system is implied. Consequently, it has been suggested that measurement of sCD21 could serve as a marker for activation of the immune system and diseases involving the B cell lymphoid system (Huemer et al., 1993).

This investigation focuses on sCD21 levels within Rheumatoid Arthritis patient serum. Normal serum sCD21 levels have been reported to range between 100 and 477 ng/ml, decreasing with age (Maslamani et al., 2004). A further reduction is reported to levels between 50 and 300 ng/ml in patients with RA; this did not differ with age in RA patients in this particular study (Masilamani et al., 2004). In addition to the reduction on sCD21 reported in RA sera, a further decrease is seen within the synovial fluid of paired patient samples (Grottenthaler et al., 2006). The protein content of the synovial fluid is partially derived from the pannus tissue and inflammatory cells in the arthritic joint; it has been previously reported that expression of CD21 is reduced in synovial fluid compared with blood-derived B cells (Illges et al., 2000). This observation could explain the decreased levels of sCD21 within the synovial fluid of patients with RA. Blood-derived B cells from RA patients also have decreased levels of membrane bound CD21 compared to healthy volunteers, in addition to decreased FcγRIIB expression (Prokopec et al., 2010). This decrease of membrane CD21 is also observed in patients with SLE (Wilson et al., 1986). An additional study compared CD21 transcript levels between patients with RA and healthy volunteers and observed a decrease in transcript levels within the patient samples (Dash et al., 2016). Further analysis revealed a correlation between PBMC-CD21 transcript levels and DAS28 score. Those patients with increased DAS28 score (increased disease severity), expressed lower levels of CD21 transcript. After 6 months of treatment, the levels of CD21 transcript increased within these patients, accompanied with a decline in DAS28 scores.

DAS28 score is a measure of joint pain and is routinely used to classify RA disease severity. DAS28 scores above 5.1 are an indicator of more severe disease compared with those with scores under 5.1. Other factors on which RA diagnosis is based include; joint involvement, serology (rheumatoid factor, RhF, and anti-cyclic citrullinated peptide, anti-CPP), levels of acute phase reactants and the duration of the symptoms (Kourilovitch et al., 2014).

Disease	sCR2 (compared with normal levels)
Rheumatoid Arthritis	Lower levels
Common variable immune deficiency (CVID)	Lower levels
B cell chronic lymphocytic leukaemia	Higher levels
Pregnancy	Lower levels
Multiple Sclerosis (MS)	Lower levels
CSF	Higher levels
Systemic sclerosis	Lower levels
Progressive systemic sclerosis (pSS)	Lower levels
EBV	Higher levels
EBV-associated malignancies	Higher levels
Age	Lower levels

Figure 11.1. 2: Soluble CD21 levels in disease

11.1.5 Treatment of Rheumatoid Arthritis with Rituximab

Rituximab is a clinical formulation of the murine IgG1 monoclonal anti-CD20 antibody (Edwards et al., 2001). It was originally used as a therapeutic to treat B cell lymphoma however treatment of patients with rheumatoid arthritis in combination with corticosteroid and cyclophosphamide resulted in sustained improvement in disease (Edwards et al., 2001). This therapeutic antibody depletes all $CD20^{+}$ B cells, reducing the majority of auto-reactive B cells and therefore theoretically inducing the collapse of a pathogenic autoantibody-generating cycle, leading to remission. Patients treated with mono-therapy frequently relapse after finishing the treatment course, however in studies using a combination therapy, patient's B cells returned after treatment without relapse to a disease phenotype after the first or second course of treatment (Edwards et al., 2001). In addition, levels of Rheumatoid Factor (RhF) fell in all patients within the study. An additional study of 161 patients, revealed a greater clinical response in patients treated with Rituximab and a short course of corticosteroids in conjunction with methotrexate or cyclophosphamide than those patients treated with corticosteroids and methotrexate alone (Shaw et al., 2003). Patients that respond to Rituximab treatment have also shown a 75% decrease in anti-cyclic citrullinated peptide (CCP) and 60% decrease in RhF antibodies (Cambridge et al., 2003). However, follow-up analysis of Rituximab treated patients revealed that most undergo clinical relapse. In a study reported by Cambridge et al. (2003) 13 of the 15 patients treated relapsed within 17 months of B cell repletion, with the additional return of autoantibodies in all but one patient. This response is thought to occur through the generation of a new set of naïve B cells in the bone marrow.

Rheumatoid factors (RhF) are autoantibodies specific for the Fc portion of IgG, they can be detected in 30% of normal individuals but these RhFs are low affinity and low titre, therefore have no significant pathology (Kyburz et al., 1999). A study using mice transgenic for human IgM RhF showed that peripheral encounter with soluble human IgG leads to the deletion of high-affinity RhF B cells (Tighe et al., 1995). Another study demonstrated how blockade of

CD40L-CD40 interactions allowed IgG to delete the RhF precursor cells (Kyburz et al., 1999); therefore, it was concluded that human RhF production is dependent on CD40 signalling. This was confirmed by showing activating antibodies to CD40 could substitute for T cell help in promoting the survival of RhF precursors and in stimulating RhF synthesis in T cell deficient mice (Kyburz et al., 1999). RhF was shown to have no direct pathogenesis in RA using the skg mouse model of RA, in which transfer of RF-positive serum into these mice was not sufficient to confer disease (Sakaguchi et al., 2003). While RhF alone is not sufficient to induce disease, RhF-containing immune complexes may promote synoviocytes to induce local release of inflammatory factors and exacerbate the inflammatory cascade.

RhF has been shown to interfere with antibody-based immunoassays by non-specifically binding detection reagents (Todd et al., 2011); therefore, it is important when using RA samples to validate the assay in the presence of RhF, ensuring results are not affected by the presence of these antibodies. Measures can be taken to prevent interference should it occur; reagents such as Heteroblock have been shown to block the activity of heterophilic antibodies such as RhF (Olsson et al., 2016).

11.1.6 Pathogenic B cell and cytokine responses in autoimmune diseases

In healthy individuals, autoreactive B cells are removed by censoring performed by FDCs. A mouse model engineered to conditionally express a membrane-bound self-antigen on FDCs, demonstrated how presentation of this antigen by FDCs mediates effective elimination of self-reactive B cells at the transitional stage (Yau et al., 2012). It is possible that this effect is dependent on the expression level of self-antigen by the FDCs; if expression levels are too high, perhaps self-reactive B cells may persist, but this concept has not been investigated at present. When the elimination process does not occur, self-reactive B cells persist and become pathogenic, resulting in disease.

Pathogenic B cells are thought to contribute to RA in several ways. The B cells committed to producing IgG RhF can perpetuate their own existence and are known to “bypass” T cell help by providing their own antigen complexes with C3dg (Edwards et al., 1999). Subsets of these B cells are also thought to induce both articular and extra-articular features of RA by generating tumour necrosis factor α (TNFα) through interaction with the IgG Fc receptor FcγRIIIa (Abrahams et al., 2000). Additionally, stromal cells from synovial and bone marrow compartments may support the survival of these autoreactive B cells and plasma cells (Edwards et al., 1997).

B cell populations which down-regulate CD21 have been reported in SLE (Wehr et al., 2004), CVID (Warnatz et al., 2002) and RA (Isnardi et al., 2010). These $CD21^{-/low}$ B cells express germline autoreactive antibodies, which recognise nuclear and cytoplasmic structures and have abnormal BCR signalling, implicating them as pathogenic within these diseases. These cells fail to induce tyrosine phosphorylation cascades or increased concentration of intracellular calcium upon BCR aggregation, responses known to be enhanced by CD21/CD19 co-complex ligation to the BCR. It is thought that chronic BCR exposure to self-antigens desensitises BCR signalling abilities (Gauld et al., 2005). Transcriptome analysis of $CD21^{-/low}$ B cells from rheumatoid arthritis patients revealed up-regulation of many genes encoding molecules to increase B cell activation and proliferation such as SOX4, TBET and BCL11B (Isnardi et al., 2010). It is feasible to suggest, overexpression of these molecules replaces the need for stimulation through the BCR to allow proliferation of the $CD21^{-/low}$ B cell subset, and therefore the cells may be contributing towards their own survival. These studies also revealed that most Ig genes expressed by $CD21^{-/low}$ cells were devoid of somatic hypermutations, indicating that this subset are naïve B cells. In addition, the cells were shown to have a specific extracellular surface marker phenotype characterised by the down-regulation of receptors that normally favour B cell activation, such as BAFF-R. A study using a mouse model expressing mDEL showed that provision of excess BAFF does not rescue self-reactive B cells (Yau et al., 2012) further

indicating these autoreactive cells are sufficient to maintain their own survival and do not require extracellular signals.

More recently, a B cell subset expressing the IgA receptor FcRL4 has been shown to participate in the autoimmune response in patients with rheumatoid arthritis (Amara et al., 2017). Sequencing of this subset of cells revealed enrichment for the IgA isotype immunoglobulin genes; IgA and IgG antibodies heavily make up the autoantibody pool in autoimmune disease. $FcRL4^{+}$ B cells have the capacity to make autoantibodies against citrullinated proteins (Amara et al., 2017); this observation further supports their suggested role in RA as 60-80% of patients have B cell responses characterised by the production of autoantibodies recognising citrullinated proteins, mainly fibrogen, vimentin and α-enolase (Klareskog et al., 2014). T cells within lymphoid aggregates of inflamed synovial tissues in patients with RA have been shown to be a source of RANKL using immunohistochemistry and in situ hybridisation (Quinn et al., 1998); a cytokine that has roles in bone destruction and development of lymphoid structures. The FcRL4+ B cell subset was shown to express RANKL, further supporting an involvement for these cells in RA autoimmune responses. Interestingly, these cells also express low levels of CD21, which could be associated with the low level of sCD21 observed in RA patients and the pathogenic responses of $CD21^{-/low}$ B cells shown in the investigations discussed above. Taking these observations into account, it is possible that these cells are less dependent on CD21 downstream pathways and don't require the co-activation action of the CD19/CD21 complex due to the provision of sufficient signals by the cell to promote self-activation.

Cytokines expressed by B cells, such as IL-6, IL-10 and LTβ, have been implicated in the onset of early phase of pathogenesis of rheumatoid arthritis by promoting autoimmunity, maintaining chronic inflammatory synovitis and by driving the destruction of adjacent joint tissue (Mcinnes et al., 2007). Cytokines involved in B cell survival and activation are also found in high levels in ectopic germinal centres that form during RA, further solidifying their role in disease. Mature DCs in synovial membranes produce high levels of APRIL (Seyler et

al., 2005) and macrophages and synovial fibroblasts produce BAFF (Ohata et al., 2005), molecules with the ability to maintain the survival of autoreactive B cells within these structures. Two key proinflammatory cytokines involved in RA are IL-1 and TNFα. TNFα is released by synovial macrophages and induces lymphocyte and endothelial-cell activation. IL-1 stimulates articular cells to release prostaglandins and metalloproteinases, resulting in further inflammation (Henderson et al., 1984). The initial studies implicating these molecules within disease involved direct injection of recombinant cytokines directly into the knee joints of rabbit and rodents. Subsequent results suggested TNFα was an inflammatory mediator and IL-1 was the crucial cytokine responsible for both arthritis and cartilage destruction (Henderson et al., 1989). Later studies showed that the development of arthritis in TNF transgenic mice could be prevented with antibodies against TNFα but could also be blocked using antibodies against the IL-1 receptor (Williams et al., 1992). These investigations lead to the conclusion that IL-1 is the secondary mediator responsible for the arthritic changes and TNFα alone is neither arthritogenic nor destructive towards the joints but works synergistically with IL-1 in pathogenesis. Therapeutic blockade of TNF in RA patients results in decreased levels of IL-6, suppression of leukocyte migration, endothelial-cell deactivation and recovery of regulatory T-cell function and phenotype in 70% of patients (Nadkarni et al., 2007), together resulting in an improvement in disease severity.

11.1.7 The role of CD21 in B cell activation

CD21 on the B cell surface co-ligates with CD19 and CD81 to form a protein complex, coupling the innate immune recognition of microbial antigens by the complement system to the activation of B cells. Put simply, CD21 binds C3dg-opsonised antigen and co-stimulates signalling through the antigen receptor, membrane immunoglobulin. Not all CD19 expressed by on the B cell surface is in complex with CD21 as at all stages of B cell development CD19 is in molar excess of CD21 on the cell surface (Fearon et al., 2000). In contrast, CD21 is

always complexed with both CD19 and CD81 (Matsumoto et al., 1991) or CD35 on B cells (Carter et al., 1991). Upon ligation of CD21 to CD19, the complex is translocated to lipid rafts, a cholesterol dependent mechanism, to allow signalling to occur (Cherukuri et al., 2001). CD19/CD21 complex co-ligation was shown to extend the retention of the BCR within lipid rafts, allowing for prolonged signalling (Cherukuri et al., 2001). FDCs have also been shown to express CD19, but at levels lower than that seen on B cells (Barrington et al., 2009), suggesting this protein may not always be in complex with CD21 on the surface of this cell.

It has been shown that crosslinking either CD19 or CD21 to IgM receptors on the B cells surface enhances cellular responses 10- to 1000-fold (Carter et al., 1992). Responses include elevation of intracellular Ca^{2+}, proliferation and activation of mitogen-activated protein (MAP) kinases (Carter et al., 1991); signalling is mediated through the co-ligated CD19 molecule. Phenotypes for $Cd21^{-/-}$ and $Cd19^{-/-}$ mice are similar, however $Cd19^{-/-}$ mice are more severely immunodeficient than $Cd21^{-/-}$ mice (Engel et al., 1995). CD19 signalling couples extracellular ligation to intracellular signalling pathways by tyrosine phosphorylation, which may occur following ligation of either membrane IgM or the CD19/CD21 complex alone but is increased when they are co-ligated (O'Rourke et al., 1998). Lyn and Fyn, members of the src family of tyrosine kinases, have been reported to associate with CD19 (van Noesel et al., 1993). A phosphorylation cascade occurs (Figure 11.1.3) leading to activation of MAP kinases, ERK2, JNK1 and p38. In primary murine B cells, co-ligation of the CD19/CD21 complex to membrane IgM caused a 5- to 10-fold increase in activation of all three of the MAP kinases, relative to activation through IgM alone (Tooze et al., 1997). Enhanced activation of ERK2 has been shown in B cell lines due to the co-ligation of membrane IgM and the CD19/CD21 complex (Weng et al., 1997). A study investigating the costimulation of enzymes that lead to activation of ERK2 concluded; stimulation of membrane IgM alone targets Ras and leads to an intermediate level of ERK activity and the addition of signalling by co-ligation of the CD21/CD19 complex to IgM generates a second

signal activating MEK1 and inducing an enhanced ERK2 activation (Li et al., 1998). The downstream effects of this costimulation signalling pathway are poorly understood, however one study described the induction of the anti-apoptotic protein, bcl-2, by co-ligating CD19/CD21 with membrane IgM, but not by membrane IgM alone (Roberts et al., 1999). This finding suggests a role for CD19/CD21 complex in B cell responses to T-dependent antigens, for example in the development or maintenance of memory B cells that exit the germinal centre, as bcl-2 expressed by these cells (Bovia et al., 1998). As B cells found in the germinal centre express very low levels of this protein (Liu et al., 1991), the CD19/CD21 complex may not be used for this purpose at this site. Low level expression of bcl-2 in germinal centre B cells may be to permit negative selection of autoreactive B cells and subsequent apoptosis.

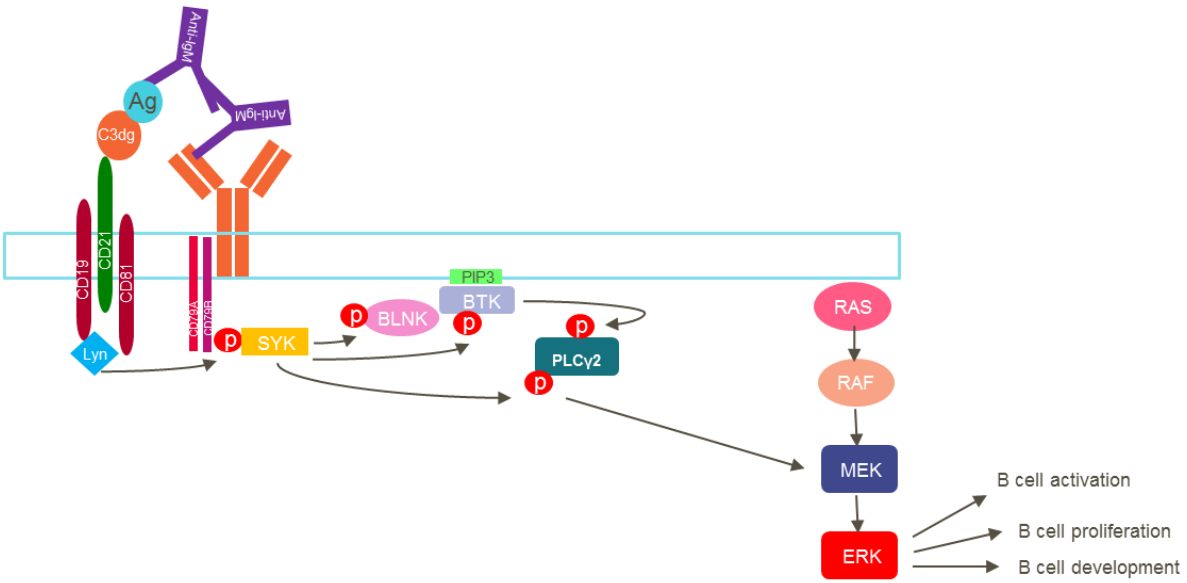

Figure 11.1. 3: CD21/CD19 signalling pathway

Adapted from Bojarczuk et al., 2015

11.1.8 B cell development within humanised mouse models

Humanised mice (hu-mice) are considered a valuable tool for studying the human immune system. Immunodeficient mouse lines have been used as recipients of $CD34^+$ human hematopoietic stem cells in efforts to create a model human immune system. The most common mouse lines used include;

1) Mice that are deficient for recombinant activating gene 2 (Rag2) and common gamma chain of the IL2 receptor (IL2Rγ) in the BALB/c background (BRG)
2) $IL2R\gamma^{null}$, non-obese diabetic (NOD) mice in the NOD/SCID background (NSG)
3) $IL2R\gamma^{null}$ mice in the NOD/Shi- SCID background (NOG).

Deletion of Rag2 prevents the generation of mature T and B cells and further disruption of IL2Rγ produces mice completely deficient for B, T, NK and NKT cells, due to the need for signalling through multiple cytokines through this receptor chain to induce cell development (Watanabe et al., 2009). Backcrossing an IL2Rγ knockout with mice with NOD background and SCID mutations results in mice with almost no functional endogenous immune system. Use of these models have allowed for more efficient and stable reconstitution of human hematopoietic cells, with varying results in the development of human B cells.

A study using NOG mice showed development of human B cells was partially blocked and a significant number of B cells progenitors were found accumulated in the spleen (Watanabe et al., 2009). Those cells that could mature ($CD19^+IgM^+IgD^+$ human B cells) produced antigen-specific IgG in vivo and in vitro, however there was a predominant IgM production suggesting only a partial reconstitution of the human adaptive immune system is achieved in these mice.

NSG mice irradiated and injected with human foetal thymus, bone and autologous foetal liver-derived $CD34^+$ cells resulted in a balanced and stable development of T and B cells and follicular lymphoid structures with functional germinal centres enriched with FDCs and activated GC B cells (Chung et al., 2015). Mice also had an increased presence of human

plasma cells within these structures, a strong indication of antibody production through class switch recombination. After immunisation, mice were shown to produce antigen-specific hIgG at comparable levels to those seen in adult humans, compared with previous reports.

A more recent study was able to restore lymph node (LN) development by inducing expression of thymic-stromal-cell-derived lymphopoietin (TSLP) in a Balb/c $Rag2^{-/-}Il2rg^{-/-}Sirpa^{NOD}$ (BRGS) HIS mouse model (Li et al., 2018). TSLP exhibits structural and functional homology to IL7 and signals through CD127, a receptor disrupted by removal of the Il2rg protein from the model. This molecule requires a ligand-binding TSLP receptor that is independent of Il2rg, therefore IL7 signalling can occur with expression of this ligand. This model resulted in organised human T and B cell structures within LNs, something that was not previously observed. These cells had enhanced antigen-specific responses after immunisation.

Work using a new strain of hu-mice is currently emerging. NSG mice were crossed with NOD/SCID-SGM3 mice; the resultant mouse strain has transgenic expression of human cytokines SCF, GMCSF and IL-3 (Wunderlich et al., 2009). This strain allows for sustained human B cell engraftment and has been shown to have improved B cell maturation and antigen-specific antibody responses to dengue virus infection (Jangalwe et al., 2016). This is the strain of mice chosen for the hu-mouse serum aspect of this project.

11.2 Summary and aims:

The observation that sCD21 decreases in disease suggests a role for this protein in health and disease. I hypothesise that soluble CD21 inhibits C3dg antigen complexes binding to B cells, consequently dampening C3dg-mediated immune responses. As sCD21 levels are decreased in Rheumatoid Arthritis, this break on the immune system does not occur, resulting in pathogenic B cell responses.

These studies further investigate sCD21 decrease within serum from rheumatoid arthritis patients by examination of receptor levels with respect to disease severity, clinical treatment and longitudinal clinical effects. Using these observations and a humanised mouse model, which were shown to develop human B cells but are devoid of human FDCs, work was carried out towards discovery of the origin of the soluble form of this receptor. Additionally, the function and role of sCD21 in the immune system was explored using peripheral B cells and B cell lines, Raji and Ramos, to determine the effect of sCD21 on C3dg binding and activation of these cells, respectively. Therefore, the aims of this chapter are:

1. Further understand sCD21 levels within healthy volunteer and rheumatoid arthritis patient serum, including investigation into age, disease severity, clinical treatment and longitudinal effects.
2. Investigate the origin of human sCD21 using clinical data and serum obtained from humanised mouse models.
3. Investigate the function of human sCD21 using C3dg- and C3dg/anti-IgM-immune complexes; specifically, the examination of ability to block C3dg binding to peripheral B cells and capacity to block C3dg-dependent activation of B cell lines.

11.3 Results

11.3.1 Measuring sCD21 in healthy volunteer and Rheumatoid Arthritis patient serum

Validating the human CD21 ELISA for use with human serum

A commercial human CD21 ELISA kit (abcam) was used to collect the following data, however before use, it was important to first validate the assay for use with human serum and clinical Rheumatoid Arthritis samples. Pooled human serum from healthy patients obtained from the NHS was used (sourced at GSK) for validation experiments.

Firstly, it was essential to determine whether detection of sCD21 concentration within human serum was affected by freeze/thaw cycles. As the RA clinical samples are part of a collaborative biobank, many of the samples would have undergone multiple thaws before analysis in this assay. Therefore, it was important to confirm this process did not change the amount of sCD21 measured within the sample, determining whether the protein was stable after the freeze/thaw process. Serum underwent freeze thaw cycles using the following process; serum was thawed on ice, allowed to stand for 5 minutes at room temperature before refreezing on dry ice. The process was repeated up to 3 times and sCD21 concentration calculated using the ELISA as described in Method Section 8.17. Results confirm sCD21 levels measured do not change within the sample over the course of three freeze thaw cycles (Figure 11.3.1A); therefore, the concentration measured within the RA serum would not be affected by prior thawing of the clinical samples.

It is recommended in the manufacturer's protocol (abcam) that samples be diluted 1in4 before loading onto the ELISA plate. To determine if sCD21 concentration within human serum could be measured at this dilution and the linearity of dilution of the samples within this assay, a dilution series of healthy pooled human serum was undertaken starting with neat serum and diluting 2-fold until the lowest concentration of 1in8 was reached. CD21 concentration was interpolated from the standard curve and multiplied by the dilution factor to calculate the neat concentration of sCD21 within the sample. The absorbance measured

for 1in8 diluted samples was too low to interpolate from the standard curve, therefore these samples were not analysed further, and it was concluded that this dilution was too low to accurately interpolate CD21 concentration from serum. Interpolation of sCD21 concentration within 1in2 and 1in4 diluted serum determined that serum can be diluted and concentration of sCD21 within the samples accurately interpolated in a linear manner (Figure 11.3.1B). The decision to use the recommended dilution of 1in4 for samples within the assay was due to the smaller volume of clinical sample that needed to be available to run samples in duplicate.

Next, whether human serum caused matrix interference in the assay was assessed. Standard curves were made using rc-CD21 (R&D Systems) within assay buffer and human serum diluted 1in4 and 1in8 in assay buffer. Standard curves made within diluted human serum have a greater absorbance than the curve made within assay buffer (Figure 11.3.1C); therefore, human serum causes matrix interference within the assay. In order to overcome this problem, all subsequent standard curves were made within 1in4 diluted serum and background absorbance (1in4 diluted serum only) subtracted from measured absorbances of all samples, ensuring remaining absorbance is from sCD21 only and there is no matrix contribution within the final result.

It has been reported that Rheumatoid factor (Rhf) also interferes with assays such as ELISAs (Todd et al., 2011). Because Rhf could be present within the RA serum samples, it was important to determine whether this protein interfered with the human CD21 ELISA (abcam). Standard curves were made using rc-CD21 (R&D Systems) within 1in4 diluted serum. Four standard curves were made from; serum only, serum plus 125 IU/ml Rhf, serum plus 150 µg/ml heteroblock and serum plus heteroblock and Rhf, 125 IU/ml and 150 µg/ml, respectively. Rhf concentrations were chosen according to the concentrations likely present in patient samples and concentrations of heteroblock chosen according to reports of use in the literature (Olsson et al., 2016). Heteroblock has been confirmed to block interference from Rhf (Olsson et al., 2016) and therefore could be used within the assay if interference

was measured. Addition of this reagent to the standard curve alone allows confirmation heteroblock itself does not cause matrix interference within the assay. Addition of both heteroblock and Rhf to the standard curve determines whether any effect Rhf has on the assay is neutralised by the presence of heteroblock. Standard curves were not affected by the addition of either reagent (Figure 11.3.1D). At the lower concentration of CD21 within the curve plus heteroblock, there is a slight shift in absorbance, however as the other curves are not affected this can be said to be due to human error or natural variation within the assay. Therefore, as Rhf was shown to have no effect on sCD21 measurement, heteroblock was not included in the final assay.

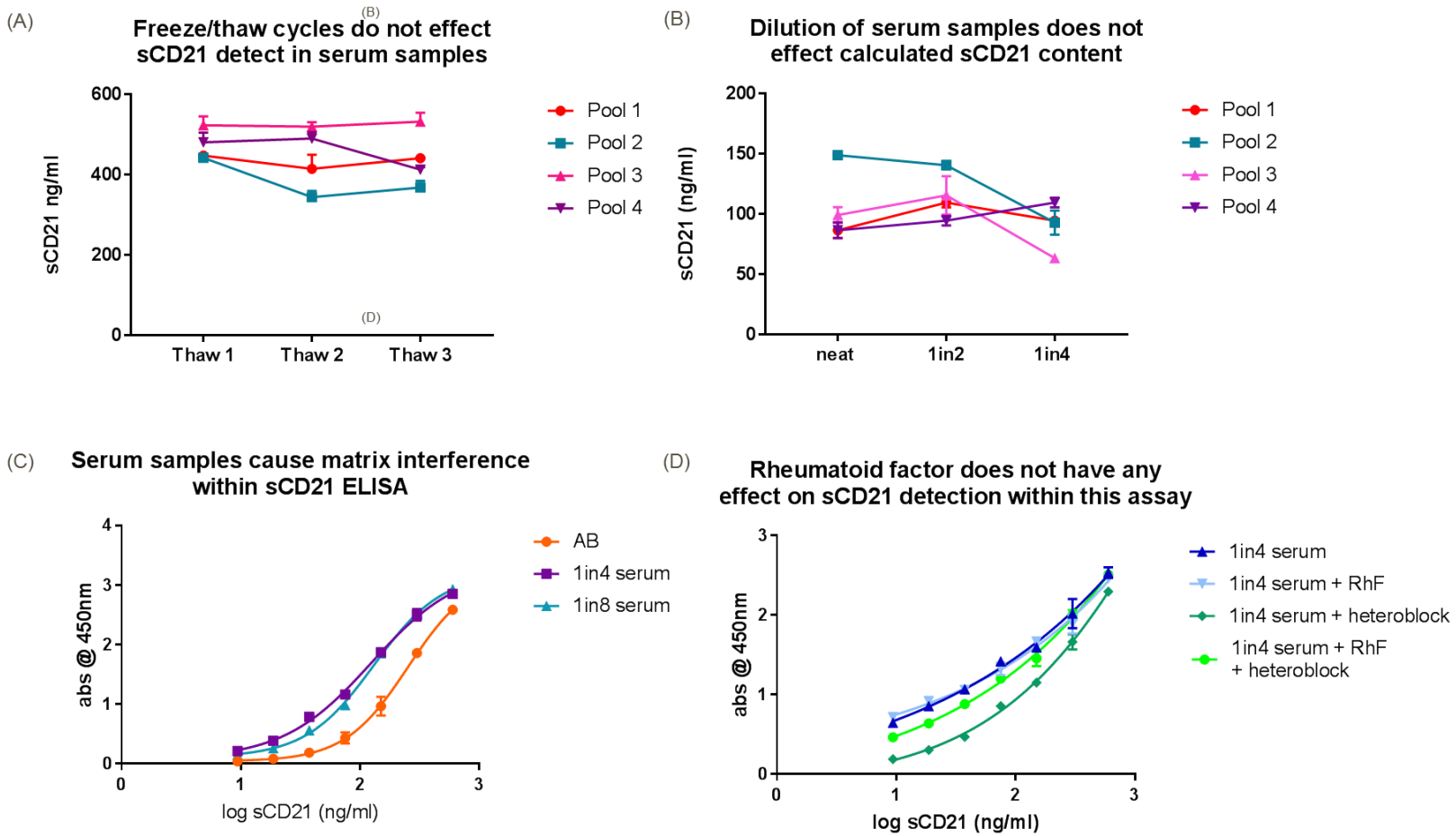

Figure 11.3. 1: Validation of CD21 ELISA (abcam)

AB = assay buffer. (A) Up to three freeze/thaw cycles of serum samples do not affect the concentration of sCD21 detected, samples were run in duplicate. (B) Serum samples can be linearly diluted and sCD21 concentration accurately interpolated with a dilution factor of up to 1in4. Samples were run in duplicate. (C) Human serum causes matrix interference using the CD21 ELISA, standard curves were made within 1in4 diluted human serum to remove background signal. Samples were run in duplicate. (D) Rheumatoid factor and heteroblock do not interfere with the CD21 ELISA. Samples were run in duplicate.

It is important while running clinical samples that the assay is reliable and reproducible. As multiple plates were run assessing sCD21 concentration with healthy volunteer and RA patient serum, it was essential to run quality control samples on each plate, assessing the performance of each individual assay. These samples were made by spiking rc-CD21 into neat human serum at 4x the final concentration to interpolate. Human serum was then diluted 1in4 in assay buffer and loaded in duplicate to each plate. Final concentrations of sCD21 measured were 20ng/ml, 50ng/ml and 100ng/ml; concentrations were chosen to ensure CD21 concentration could be accurately calculated close to the lower limit of quantitation of the assay (9.3 ng/ml, Figure 11.3.2) and at points within the standard curve where sCD21 concentrations within RA patient samples were predicted to fall. The concentration of rc-CD21 within the serum was interpolated from the standard curve from each respective plate (Figure 11.3.3). The controls confirm that sCD21 concentration was being accurately interpolated reproducibly on each plate run.

Together, these validation experiments confirm that the sCD21 ELISA (abcam) can be used to measure the concentration of protein within human serum, producing reliable, accurate and reproducible results.

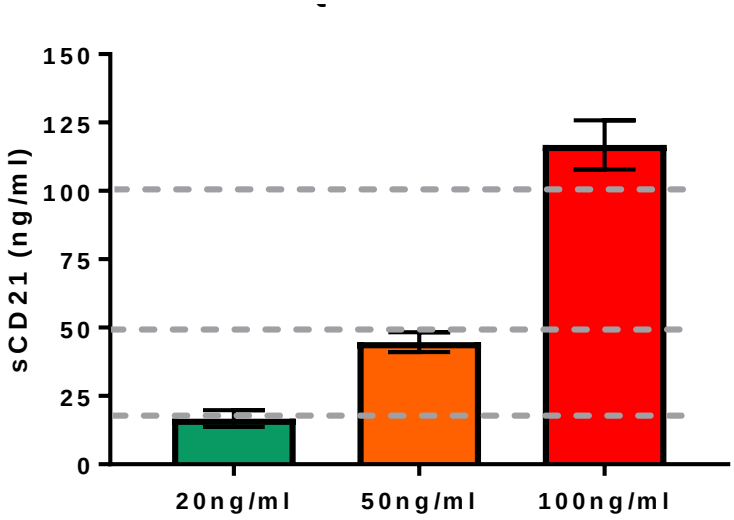

Figure 11.3. 2: Quality control samples confirm the assay is reproducible and CD21 can be detected above background absorbance

For each assay plate run with clinical samples, recombinant CD21 was spiked into neat serum 4x final concentration and diluted 1in4 in the final assay. Concentrations of original spike into neat serum were; 80, 200 and 400 ng/ml.. n=9, bars represent SD.

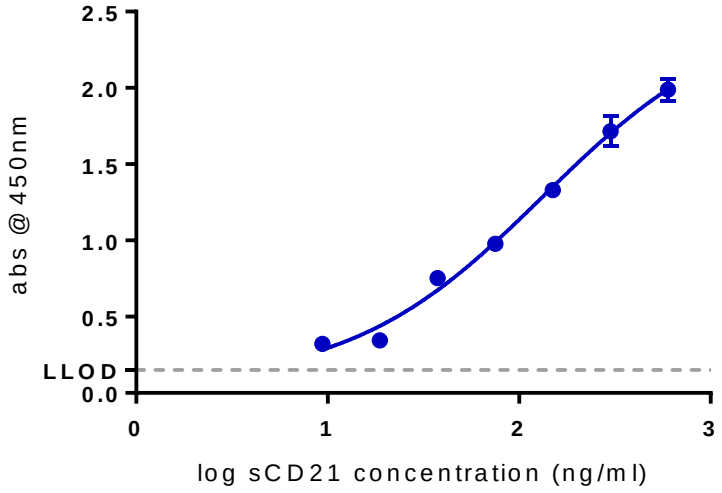

Figure 11.3. 3: Example standard curve for healthy volunteer and RA clinical sample CD21 ELISA data

Standard curve was made in 1in4 diluted human serum and background absorbance subtracted from measured absorbance values. Lower limit of detection = 0.15, lower limit of quantitation = 9.3 ng/ml, samples below this limit were considered 0. Each point on the standard curve is done in duplicate for each plate run.

Measuring sCD21 levels in healthy volunteer and Rheumatoid Arthritis serum samples

In addition to disease, sCD21 concentration has been reported to decrease with age (Masilamani et al., 2004*).* The average age group of the initial RA cohort (30 patients) was between 45 and 70 years old; therefore, healthy volunteer blood samples were obtained from the blood donation unit (20 samples, 10 male, 10 female) at GSK from individuals within this age range. Samples from volunteers under the age of 25 were also obtained (20 samples, 10 male, 10 female) and serum extracted from each cohort. sCD21 concentration was measured within these samples following the protocol detailed in Method Section 8.17. Concentration of sCD21 was interpolated from standard curves made in 1in4 diluted serum, with a lower limit of quantitation of 9.3ng/ml; any samples with sCD21 concentrations measured below this value were considered 0 (Figure 11.3.4). Results confirmed the observation that sCD21 decrease in the 45-70yrs age group, with an average sCD21 concentration of 257.1 ± 25.39 ng/ml, compared with the >25yrs group, which has an average sCD21 concentration of 474 ± 47.02 ng/ml (Figure 11.3.4). Due to this observation, it was essential that the healthy volunteer samples were age-matched to the average age of the rheumatoid arthritis cohort and conclusions of sCD21 levels between health and disease were drawn between these two cohorts.

Subsequently, sCD21 levels were measured within 80 baseline RA serum samples, obtained from the University of Birmingham as part of the Beacon Cohort. Samples were diluted 1in4 and protocol performed as detailed in Method Section 8.17. Analysis revealed sCD21 concentration decreased in RA samples compared to healthy volunteer samples aged between 45-70yrs (Figure 11.3.4). The average sCD21 concentration decreased from 257.1 ± 25.39 ng/ml in healthy volunteers to 85.33 ± 10.3 ng/ml in RA patients; this data confirms observations made in the current literature. Additional observations about the role of sCD21 in RA were made by exploring correlations between age, disease severity and sCD21 concentration within these patients.

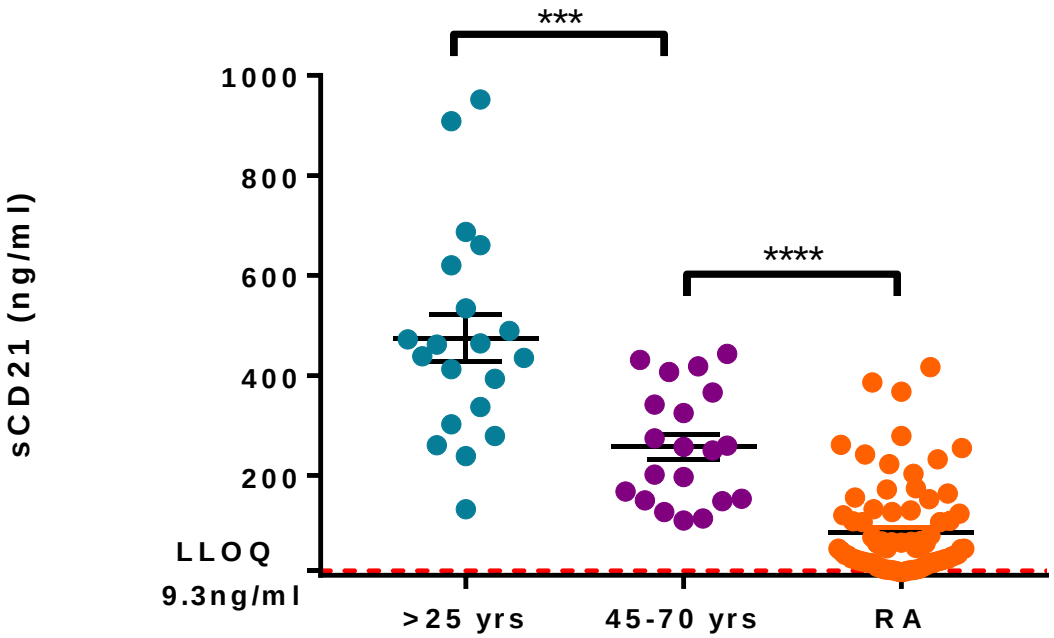

Figure 11.3. 4: sCD21 concentration in the serum decreases with age and Rheumatoid Arthritis

Healthy volunteer >25 yrs, n=20, 10 male, 10 female. Healthy volunteer 45-70 yrs, n=20, 10 male, 10 female. RA, n=80, 50 female, 30 male. Samples were run in duplicate and the average interpolated concentration represented on the graph. Bars represent SD. LLOQ = 9.3 ng/ml, concentrations detected lower than this were considered 0. Results are significant with an unpaired t-test. Test was done between >25 yrs and 45-70 yrs group and 45-70 yrs and RA group.

As sCD21 concentration decreases with age in healthy volunteers (Figure 11.3.4), it is interesting to also investigate whether this phenomenon occurs within RA patients. When sCD21 concentration in the serum and the age of the patient at the time of sample collection were compared, no correlation was observed (Figure 11.3.5); showing the age of the patient does not affect the sCD21 concentration, unlike in healthy volunteers. Therefore, the age of the patient does not dictate the sCD21 concentration in disease. Additionally, the age of the patient was shown to have no effect on the severity of the disease phenotype, determined through the lack of correlation of DAS28 score and age (Figure 11.3.6). However, when sCD21 concentration within patient serum was compared to DAS28 score, a correlation between disease severity and sCD21 measured within the serum was observed (Figure 11.3.7, r^2=0.077); patients with a higher DAS28 score, therefore presenting with more severe disease, have a lower concentration of sCD21 present within their serum. This suggests that the concentration of sCD21 within the serum may be a modulator of disease; patients with lower sCD21 concentrations have a greater disease phenotype, suggesting a role for sCD21 in protection from disease, a mechanism that is further supported by the observed reduction in sCD21 between healthy and disease samples (Figure 11.3.4).

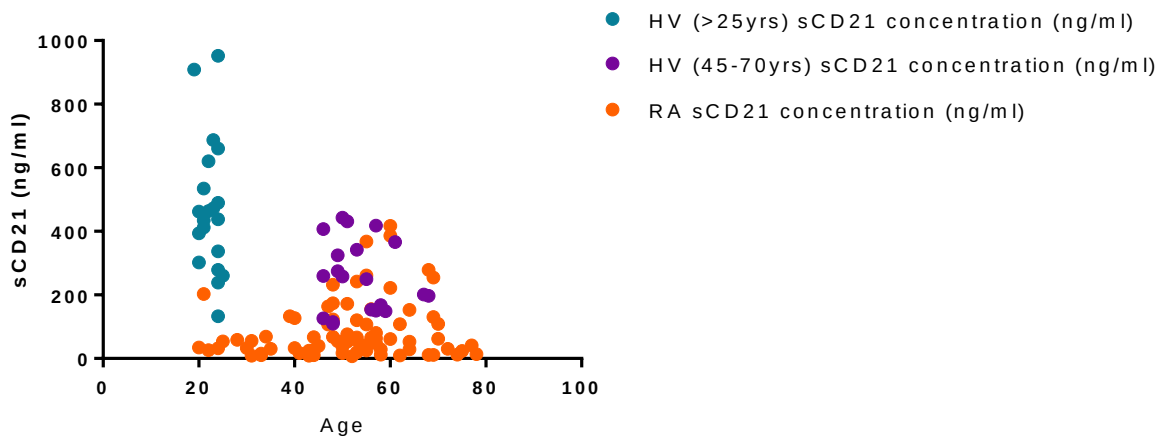

Figure 11.3. 5: Age does not affect sCD21 concentration in Rheumatoid Arthritis patients

Healthy volunteer >25 yrs, n=20, 10 male, 10 female. Healthy volunteer 45-70 yrs, n=20, 10 male, 10 female. RA, n=80, 50 female, 30 male. Samples were run in duplicate and the average interpolated concentration represented on the graph.

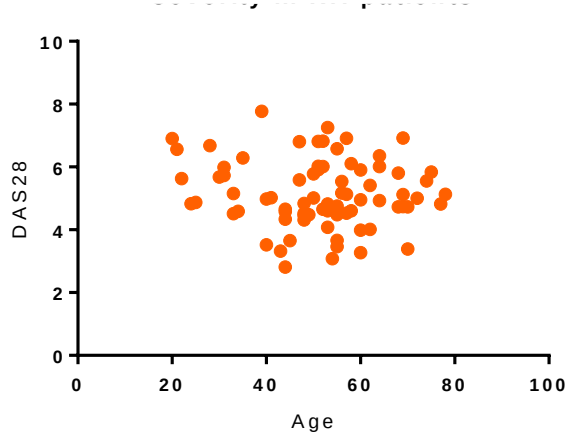

Figure 11.3. 6: Age does not affect disease severity in Rheumatoid Arthritis patients

n=80, samples were run in duplicate and average interpolated sCD21 concentration represented here. There is no correlation between the age of the patient and the severity of their disease.

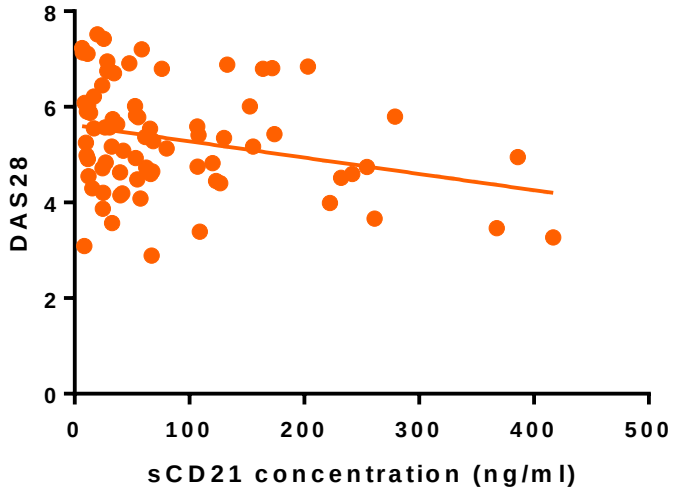

Figure 11.3. 7: Increased disease severity correlates with decreased sCD21 concentration in RA patient serum

n=80, samples were run in duplicate and average interpolated sCD21 concentration represented here. Patients with higher DAS28 scores have lower sCD21 concentrations within the serum. Rsquared = 0.077, p value = 0.013

Analysis of 10 patients over the course of 12 months after diagnosis was carried out, measuring sCD21 concentration within the serum of these patients at baseline (day 1 in the clinic), 6 months after diagnosis and 12 months after diagnosis. All patients were treated with methotrexate, a commonly used immune system suppressant, along with steroid treatment in many cases. After 6 months of treatment, the average sCD21 concentration of the cohort increased from 15.15 ng/ml ± 3.811 to 40.46 ng/ml ± 10.64 (Figure 11.3.8A, significant using unpaired t test). After 12 months of treatment, the average sCD21 concentration increased further still to 47.49 ng/ml ± 9.91 (Figure 11.3.9B, significant using unpaired t test). In addition to these observations, when patient's disease severity scores were tracked over time, generally disease phenotype decreased (Figure 11.3.9C). These data further suggest a role for sCD21 concentration in disease severity and disease modulation; as sCD21 concentration increases over time with treatment of disease, disease severity decreases (Figure 11.3.7), therefore the increase in sCD21 within the serum may be acting to modulate the immune response, dampening pathogenic immune responses leading to the resulting decrease in disease phenotype.

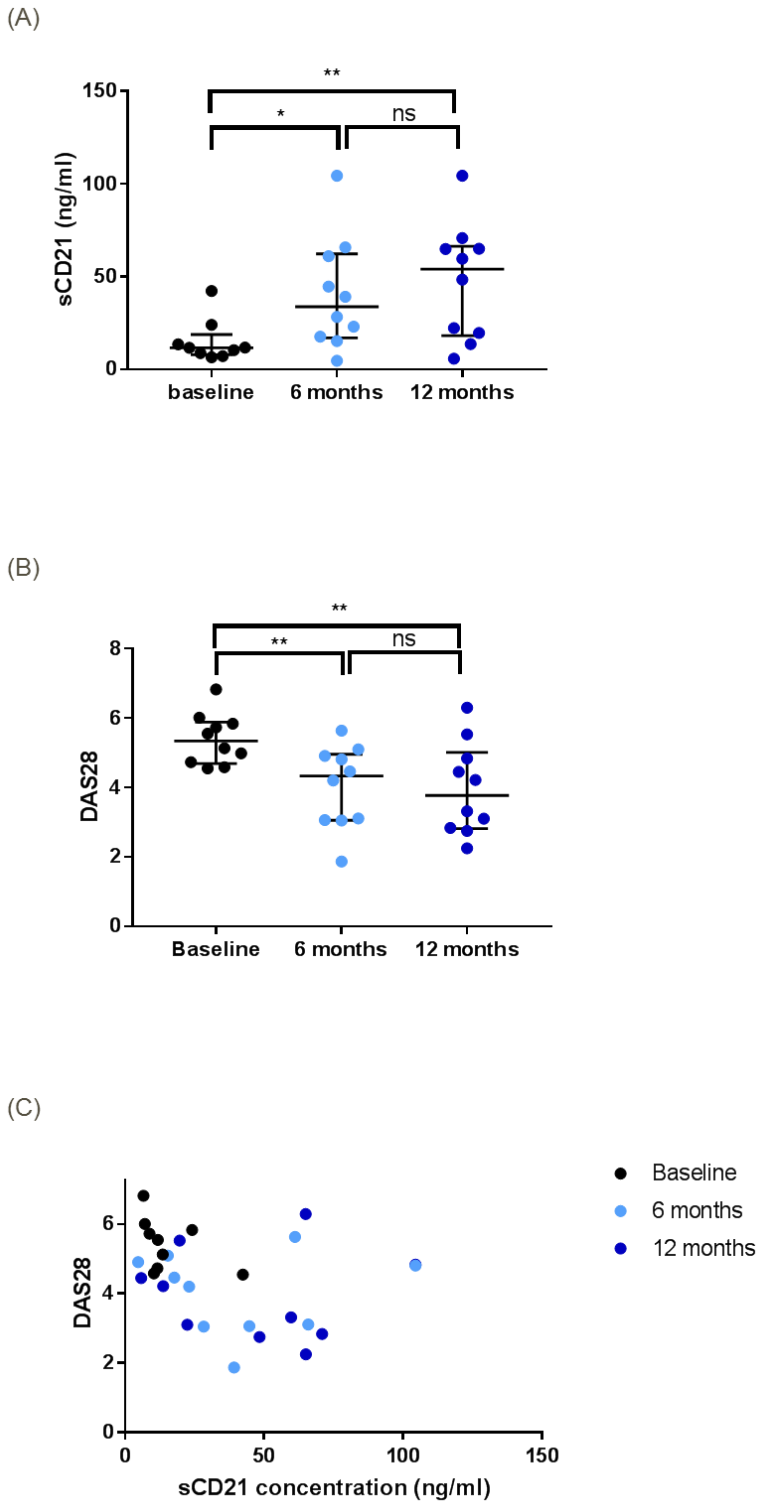

Figure 11.3. 8: Disease severity of patients with Rheumatoid Arthritis decrease upon diagnosis and treatment

n=10 patients in each group, patients had samples taken upon arrival at the clinic (baseline), 6 months and 12 months after arrival. All patients had been treated with methotrexate, among other drugs. sCD21 concentrations increase over time, with treatment of disease. Significance of data analysed using unpaired t tests. Bars represent SD. (A) sCD21 concentrations increase overtime after RA diagnosis. (B) Disease severity decreases overtime in RA patients. (C) Disease severity vs sCD21 concentration over time.

Although treatment of patients with topical steroids and immune suppressants was shown to increase sCD21 concentration within the serum (Figure 11.3.8), serum from patients treated with rituximab were shown to have a further decrease in sCD21 concentration post-treatment (Figure 11.3.9). Rituximab is a human CD20 monoclonal antibody which depletes B cells, thereby improving the condition of patients by removing a disease modulator. This data suggests that B cells could be implicated as a producer of sCD21, as removal of these cells lead to a further decrease in the concentration of this protein. Interestingly, DAS28 scores were observed to first raise after the initial treatment (Year 3) before falling below the initial score at first measurement (Year 1) (Figure 11.3.9 B). This data also suggests that removal of pathogenic B cells leads to a less severe disease phenotype.

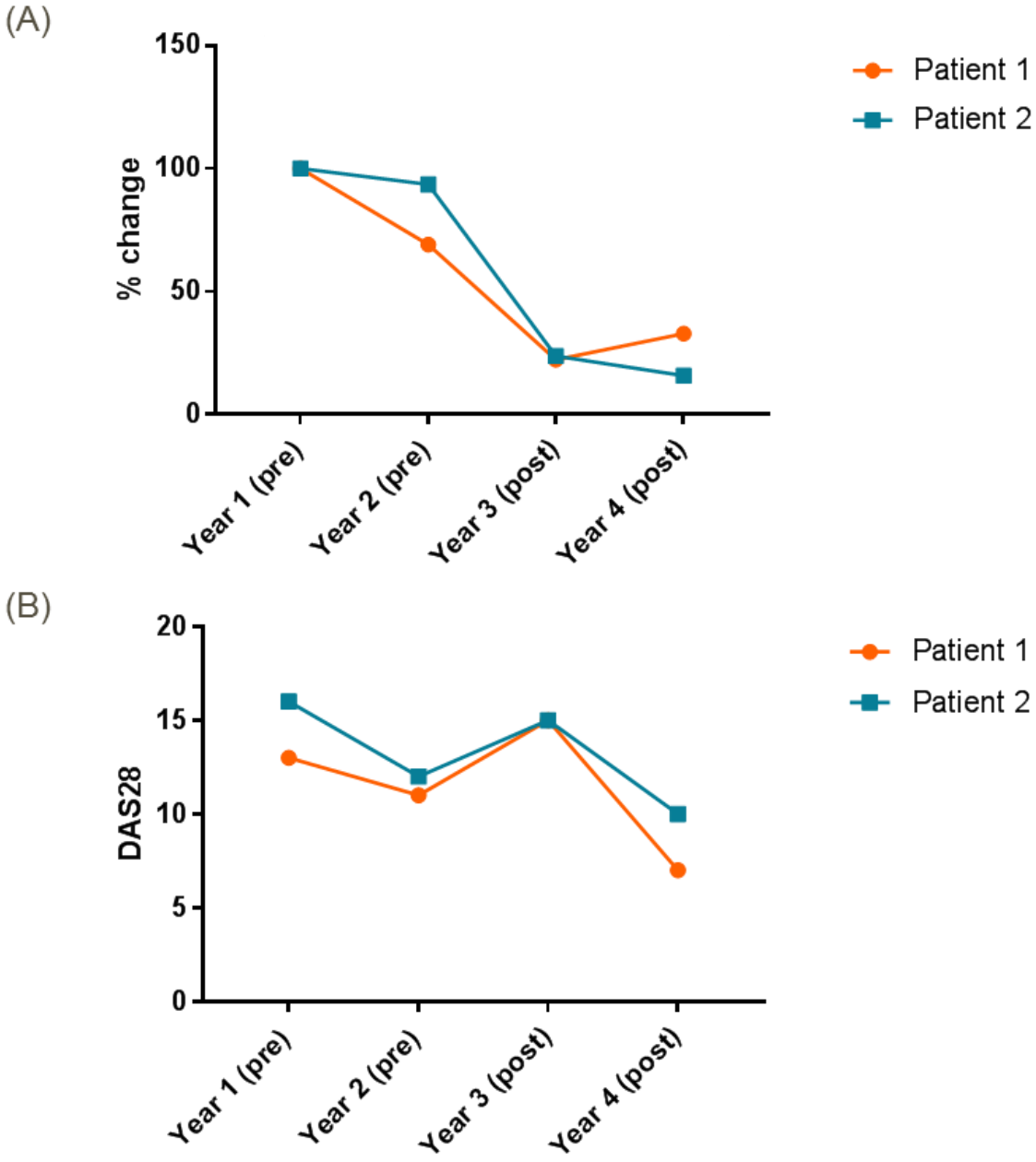

Figure 11.3. 9: Rituximab treatment further reduces sCD21 concentration in Rheumatoid Arthritis serum

Patient serum was taken at two time points before treatment with Rituximab (Year 1 and 2) and a further twice after the course of treatment (Year 3 and 4) had been undertaken. Samples were taken within a year of each other. (A) sCD21 levels were measured with CD21 ELISA revealing a decrease in sCD21 concentration in samples taken post treatment compared with those taken before administration of the drug. Pre1 was set at 100% and % change calculated from this value for the other time points from respective patients. (B) After treatment DAS28 score first increased before falling rapidly to below original diagnostic score. n=2

To further investigate B cells as an origin of sCD21, CD21 receptor number was determined, using Quantibrite-PE beads (Materials and methods section 8.9), on the surface of PBMC derived B cells from the healthy volunteers, whose sCD21 concentrations had been measured previously. As sCD21 levels were shown to decrease with age (Figure 11.3.4), the number of receptors on B cells within the two age groups, >25 and 45-70 yrs, was investigated. This analysis revealed no significant difference between the number of surface CD21 receptors on B cells from either age group (Figure 11.3.10A, n=20 in each group). However, when the number of surface CD21 molecules was compared with the sCD21 concentration measured in each of the volunteers, a correlation between higher sCD21 concentrations and higher cell surface receptors on B cells was observed (Figure 11.3.10B, n=20, r^2=0.059). This further supports B cells as an origin of the soluble protein, as subjects with a greater number of membrane bound receptors have more sCD21 present in their serum suggesting these B cells are able to produce more soluble protein.

In summary, measurement of sCD21 concentrations within serum from patients with RA confirmed observations within the literature that sCD21 decreases in age and further still in disease. Additional information was added to these observations by investigating sCD21 concentration relative to disease severity (DAS28), revealing a correlation between a lower sCD21 concentration and a greater DAS28 score, indicating a greater disease phenotype. Samples taken from patients over a 12-month time period revealed that upon treatment with conventional drugs administered to treat RA, sCD21 concentration increases, accompanied by a decrease in disease severity scores. Additionally, patients treated with Rituximab were shown to have a further decrease in sCD21 levels after administration of the drug, implicating B cells as a source of this protein.

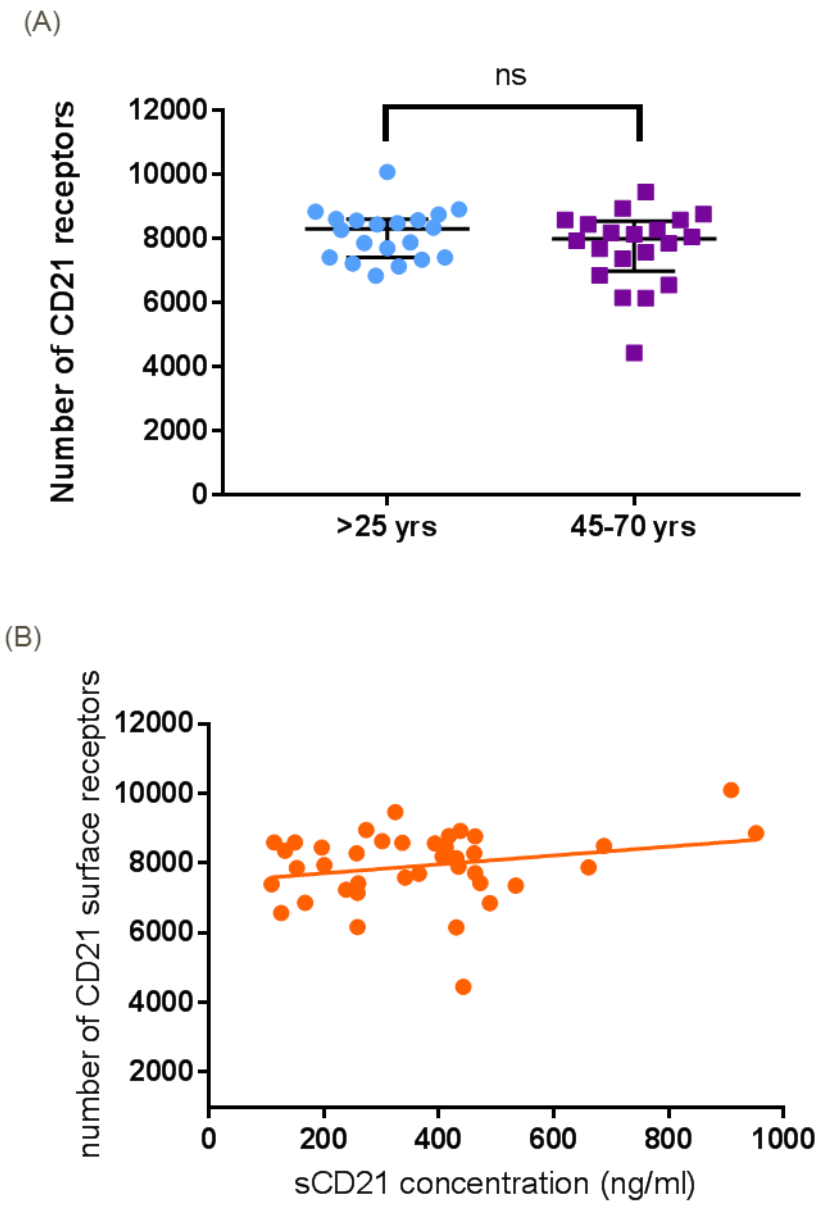

Figure 11.3. 10: Expression of CD21 surface receptor number does not change with age

n=40, samples were run in duplicate, bars represent SD. (A) Quantibrite beads were used to receptor numerate CD21 receptors on blood derived B cells. Receptor number did not change between age groups, was not significant using t-test. (B) There is a correlation between surface receptor number and concentration of soluble CD21. n=20, rsquared= 0.059, p value = 0.13

11.3.2 The origin of sCD21 – measuring human sCD21 within humanised mouse serum

With the aim to further investigate the origin of sCD21, serum from a humanised mouse model was utilised. 4-week old female NSG-SGM3 mice were irradiated and reconstituted with approximately 35,000 human $CD34^+$ cord blood cells for 98 days before +/- schistosome infection (70 cercariae). Infection was allowed to persist for 7 weeks and the mice harvested at d147 post-reconstitution (d49 post-infection). These mice were part of a study independent from the projects detailed in this thesis, therefore work was carried out by another lab and thus methods are not detailed here; serum and secondary lymphoid organs were kindly donated to this study from the Hitchcock and Hewitson lab (University of York).

Firstly, expression of human immune cells by these mice was confirmed using RNA derived from the hu-mouse thymus and qPCR for human cell markers. Wild-type mouse thymus and human tonsil mRNA were used as negative and positive controls respectively. Wild-type mice were negative for all genes investigated, as expected, confirming the primers were specific for human cell markers and expression of these genes in hu-mice was determined relative to expression levels measured in the human tonsil samples. Humanised mice expressed hCD19, hCD21 and hCD3 (Figure 11.3.11B, C and F respectively). This suggests mice had developed human T and B cells upon reconstitution with human derived haemopoietic cells. No expression of hCD35, hCXCL13 or hCCL21 was detected within these mice, suggesting an absence of human stromal cells, i.e. no human FDCs or FRCs (Figure 11.3.11A, D and F respectively).

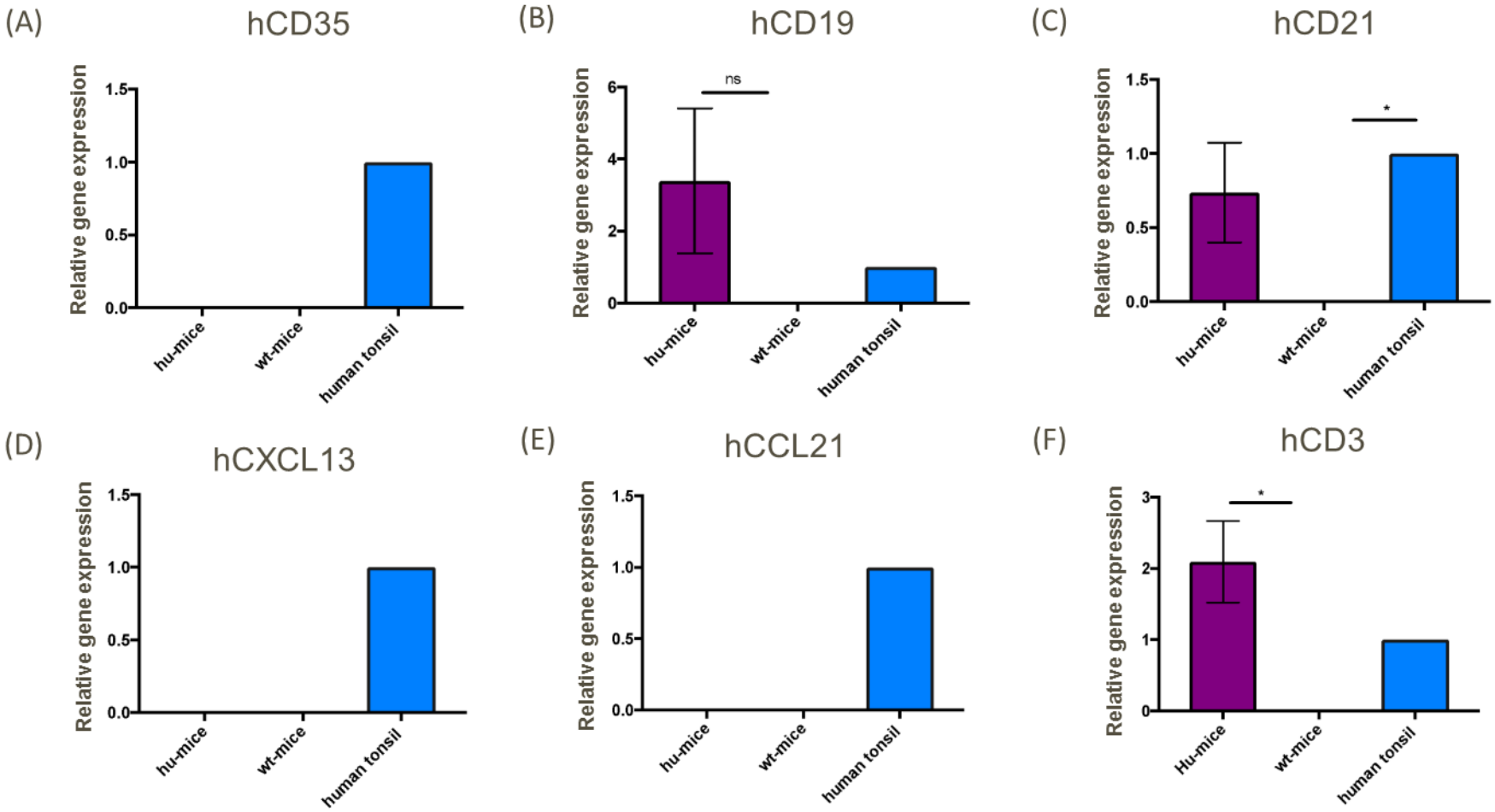

Figure 11.3. 11: Expression of human cell markers by humanised mice

n=3, bars represent SD, significance measured using an un-paired T test. Expression of human cell marker genes was assessed within hu-mice spleen. Gene expression is represented relative to expression levels within human tonsil. Wildtype mouse spleen is used as a negative control, no expression was detected for any gene investigated. (A) hu-mice do not express hCD35 at the mRNA level. (B) hu-mice express high levels of hCD19 at the mRNA level, suggesting human B cells are present in the spleen. (C) hu-mice express hCD21 at the mRNA level. (D) hCXCL13 was not detected within hu-mice. (E) hCCL21 was not detected within hu-mice. (F) hu-mice express hCD3 at the mRNA level, suggesting human T cells are present within the spleen.

Presence of human immune cells was further investigated using immunohistochemical analysis of hu-mouse spleen. Co-staining with hCD3 and hCD21 reveals the presence of human T cells within the hu-mice spleen but shows that these cells are not responsible for the expression of hCD21 as staining for these markers does not overlap (Figure 11.3.12). No hCD21 is seen within the T cell zone (determined with hCD3 presence) of the human tonsil tissue. This is due to proper organisation of the SLO microarchitecture, resulting in the absence of B cells within T cell zones and vice versa (Figure 11.3.12C). The observation of hCD21 staining in the presence of human T cells suggests disorganisation of the SLO's within this hu-mice model. Antibodies were determined to be specific for human CD21 and CD3 using wild-type mouse spleen. Staining is negative for both antibodies in these sections using the same microscope settings to acquire images (Figure 11.3.12B), therefore there is no cross reactivity for mouse CD3 or CD21 and confirming the origin of these cells within hu-mice to be human.

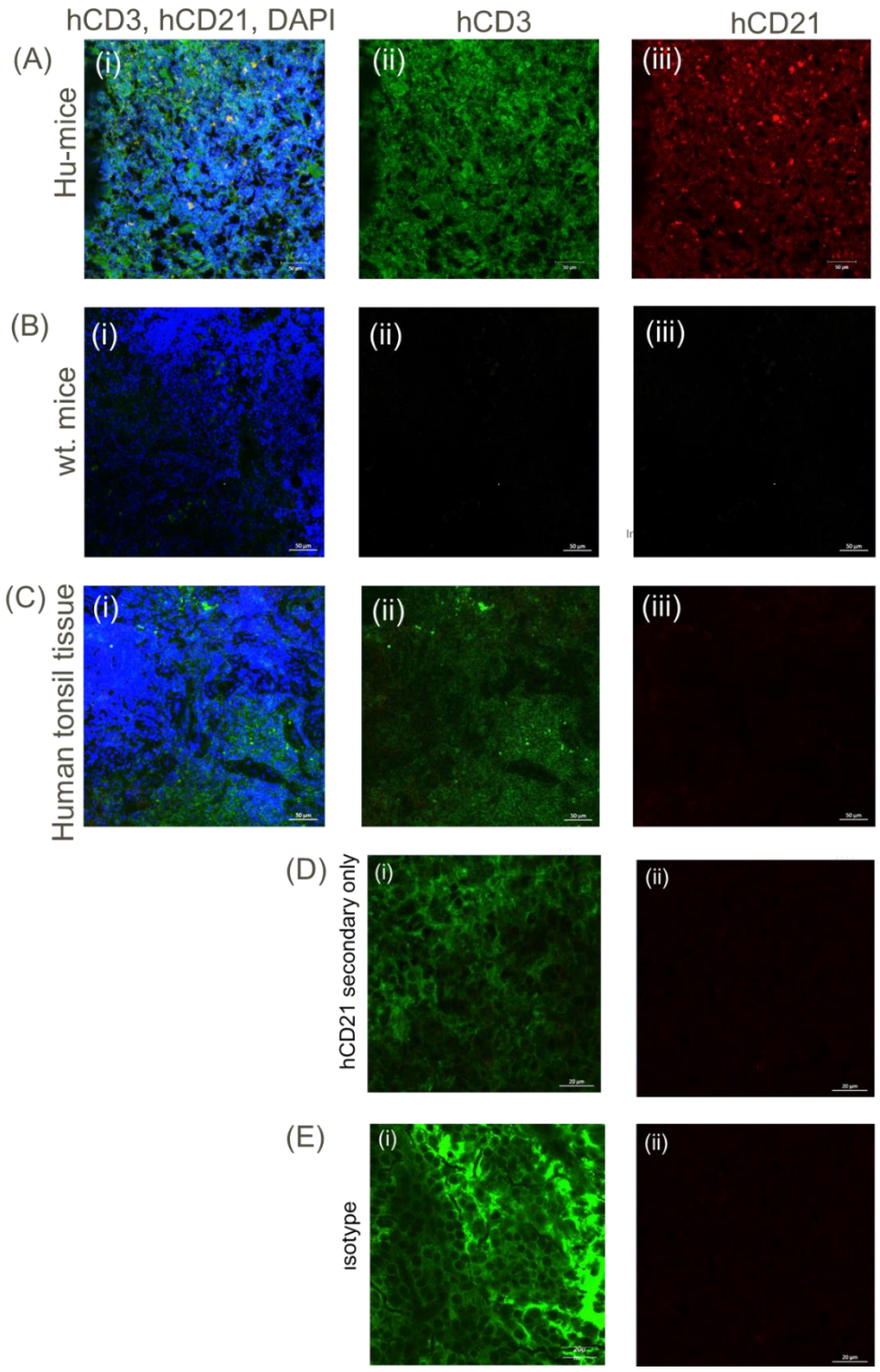

Figure 11.3. 12: hu-mice spleen contains human T cells

Images are reprehensive of 3 independent uninfected animals, multiple sections were stained from each animal. (A) (i) hu-mouse spleen stained for hCD3 (green-A488) and hCD21 (red-A647). Magnification x63, scale bar 50 µm (ii) hCD3 alone – green channel only (iii) hCD21 alone – red channel only. (B) wild-type mouse spleen stained for hCD3 (green-A488) and hCD21 (red-A647). Magnification x63, scale bar 50 µm. No staining seen, human antibodies do not cross react with mouse proteins (ii) hCD3 alone – green channel only (iii) hCD21 alone – red channel only. (C) human tonsil tissue stained for hCD3 (green-A488) and hCD21 (red-A647). Magnification x63, scale bar 50 µm. No CD21 staining is seen due to CD3 staining in a T cell zone (ii) hCD3 alone – green channel only (iii) hCD21 alone – red channel only. (D) (i) human tonsil tissue stained with hCD3 (A488-green) and hCD21 secondary antibody (A647-red). Magnification x63, scale bar 50 µm (ii) hCD21 secondary antibody only – red channel only. (E) human tonsil tissue stained with hCD3 (A488-green) and IgG1 isotype antibody (A647-red). Magnification x63, scale 50 µm (ii) isotype antibody only – red channel only.

Hu-mice spleen co-stained with hCD19 and hCD21 revealed the presence of human B cells within the spleen which express hCD21 (Figure 11.3.13A). Within the human tonsil, CD21 expression is only observed on FDCs (Figure 11.3.13C) due to the high receptor number expression by these cells, however as human FDCs appear absent from the hu-mice model system, suggested by qPCR data for FDC markers, hCD21 expression is detected on the B cells. Absence of human FDCs in hu-mice was confirmed using staining for hCD35 (Figure 11.3.14A). Sections costained with hCD19 and hCD35 would identify human B cells and FDCs respectively. Human B cells were present, but no hCD35 staining was observed in hu-mice or wt. mice (Figure 11.3.14A and C). Together with the qPCR data discussed above, it can be concluded that these humanised mice do not develop human FDCs. CD35 is detected within human tonsil, confirming the antibody can detect the presence of hFDCs (Figure 11.3.14C).

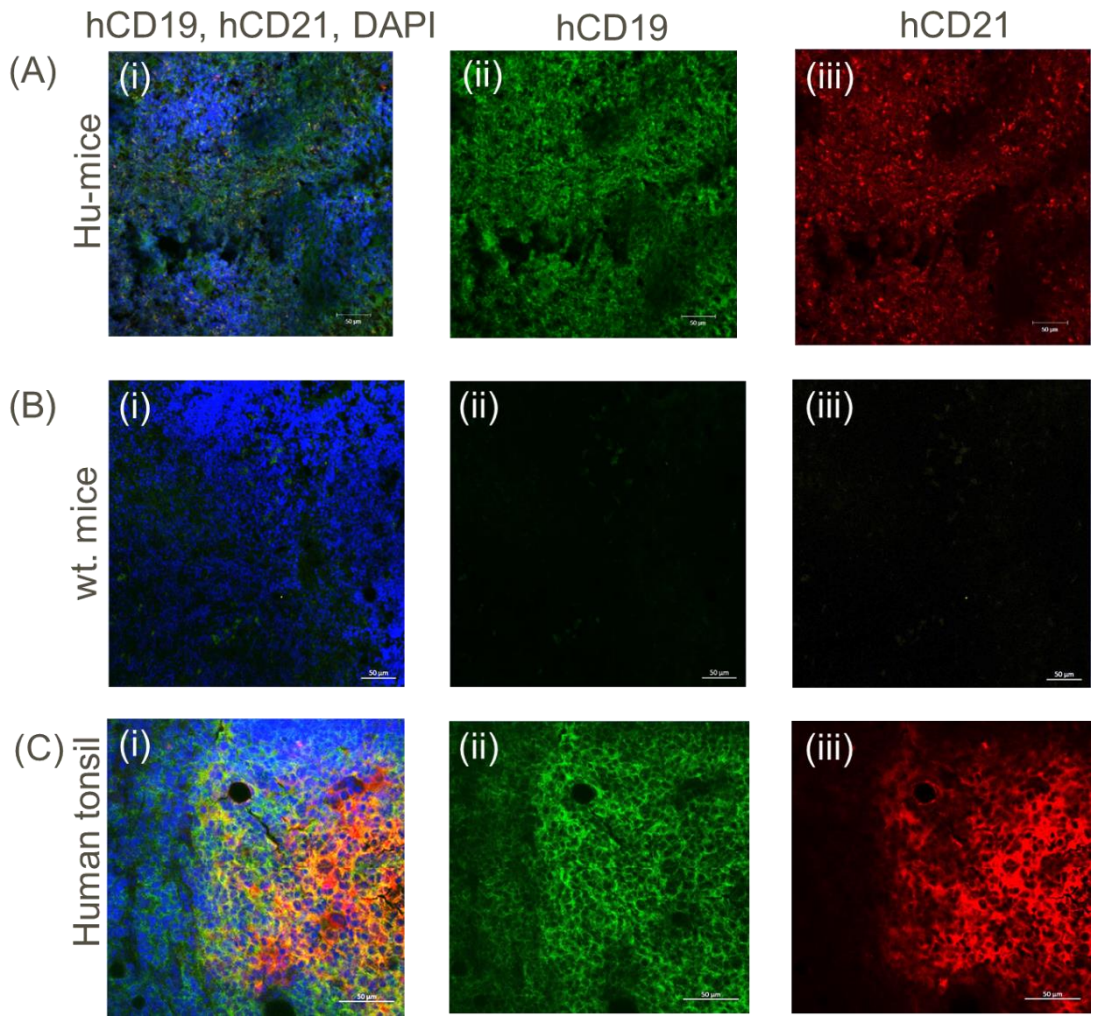

Figure 11.3. 13: hu-mice spleen contains human B cells

Images are representative of 3 independent uninfected animals, multiple sections were stained from each animal sample. (A) (i) hu-mice spleen stained for hCD19 (A488-green) and hCD21 (A647-red). Magnification x20, scale bar 200 µm (ii) hCD19 alone – green channel only (iii) hCD21 alone – red channel only. (B) wildtype mouse spleen stained with hCD19 (A488-green) and hCD21 (A647-red). Magnification x63, scale bar 50 µm. No staining is seen confirming human antibodies are species specific (ii) hCD19 alone – green channel only (iii) hCD21 alone – red channel only. (C) Human tonsil tissue stained with hCD19 (A488-green) and hCD21 (A647-red). Magnification x63, scale bar 50 µm. (ii) hCD19 alone – green channel only (iii) hCD21 alone – red channel only.

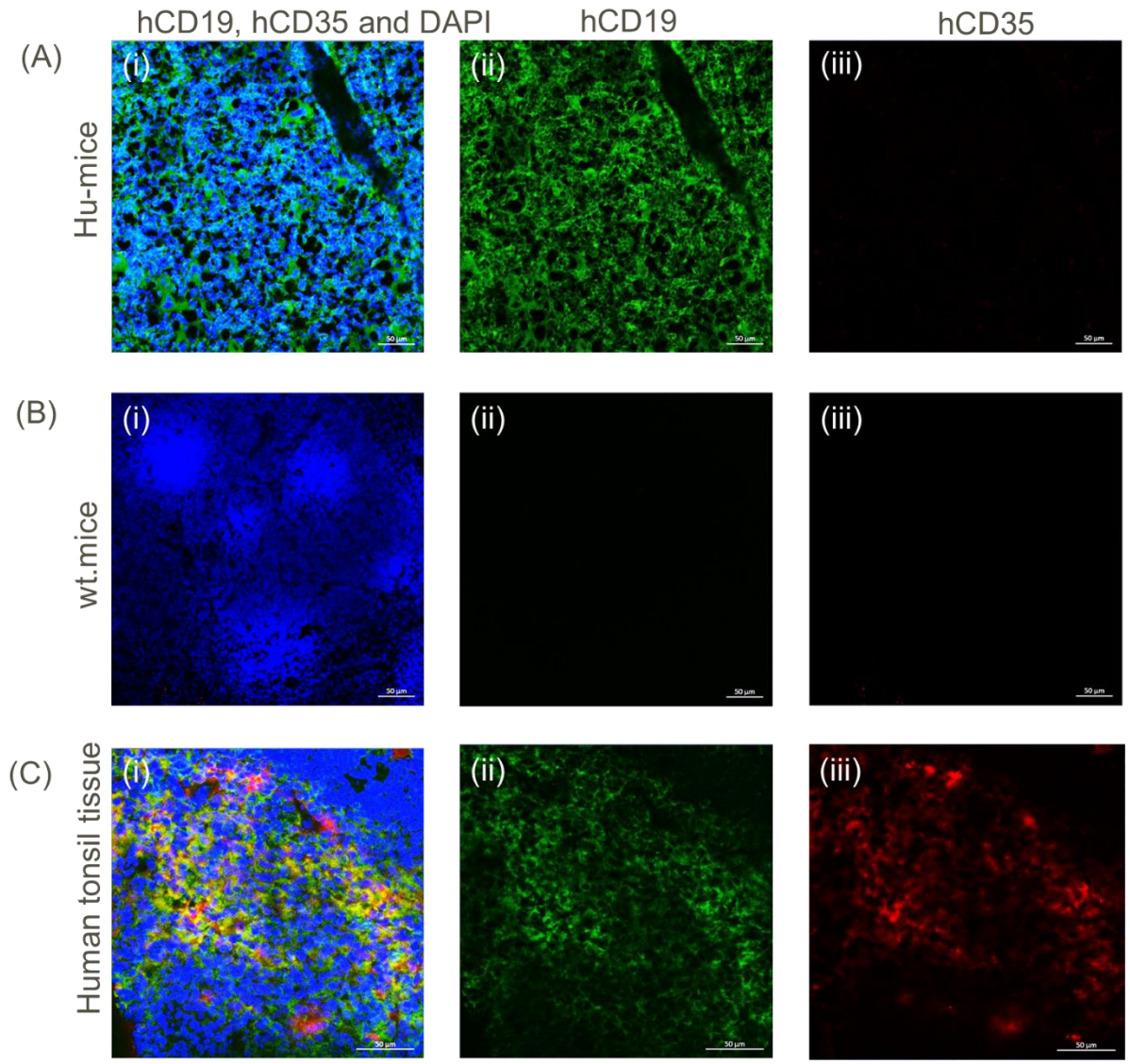

Figure 11.3. 14: hu-mice spleen do not develop human FDCs

Images are representative of 3 individual uninfected animals, multiple sections were stained and analysed from each animal. (A) hu-mice spleen stained for hCD19 (green-A488) and hCD35 (red-A647). Magnification x63, scale bar 50 µm. No staining for hCD35 is present (ii) hCD19 alone – green channel only (iii) hCD35 alone – red channel only (B) wildtype mouse spleen stained for hCD19 (green-A488) and hCD35 (red-A647). Magnification x63, scale bar 50 µm. No signal is seen, therefore antibodies are species specific (ii) hCD19 alone – green channel only (iii) hCD35 alone – red channel only. (C) human tonsil tissue stained with hCD19 (green-A488) and hCD35 (red-A647). Magnification x63, scale bar 50 µm. (ii) hCD19 alone – green channel only (iii) hCD35 alone – red channel only.

Costaining for hCD19 and hCD3 revealed human T and B cells in the hu-mice spleen within the same region of the organ (Figure 11.3.15A). Within human tonsil, these two cell subsets are organised into isolated T and B cell zones (Figure 11.3.15C and D), however within these mice it is evident that proper microarchitectural organisation of secondary lymphoid organs has not occurred and the human T and B cells present are interspersed within the spleen. Proper organisation of T and B cells into specified zones within murine SLO's was demonstrated using wild-type mouse spleen. This tissue was first co-stained with mCD19 and mCD21/35, coexpressed as one gene in mice, to identify B cells and FDCs. Staining revealed bright mCD21/CD35 signal on stromal cells, likely to be mouse FDCs (Figure 11.3.16A). Expression of CD21/CD35 on mouse FDCs is also known to be higher than that on mouse B cells and may be the cause of brighter staining of FDC expressed CD21 than that of B cells. It is presumed that if FDCs were not present then the lower level of CD21 expression on B cells would be detected, as seen in the humanised mouse spleen (Figure 11.3.13A). mCD19 staining is within the same zone as mCD21/CD35 staining, suggesting this structure is a germinal centre (Figure 11.3.16A). Antibody specificity was confirmed by staining of human tonsil tissue; no signal was detected using the same acquisition settings, therefore antibodies are specific to mouse proteins (Figure 11.3.16B). Costaining with mCD3 and mCD21/35 identified T cells and FDCs within wildtype mice. Staining revealed mCD21/CD35 was contained to the germinal centre/B cell zone, whereas mCD3 staining is specific to a distinct section within this tissue, the T cell zone (Figure 11.3.17A). Human tonsil tissue was also stained with these antibodies, confirming species specificity as no staining was observed (Figure 11.3.17B). These data allow comparison of the true organisation of mouse SLO's to that observed in the humanised mouse model; confirming within this hu-mouse model these organs are not organised in the proper manor. This is likely to be due to the absence of human FDCs and hCXCL13, both of which have been shown as essential for development of SLO and germinal centres. Insufficient development of these structures may have an impact on the functionality of the cells within this model system.

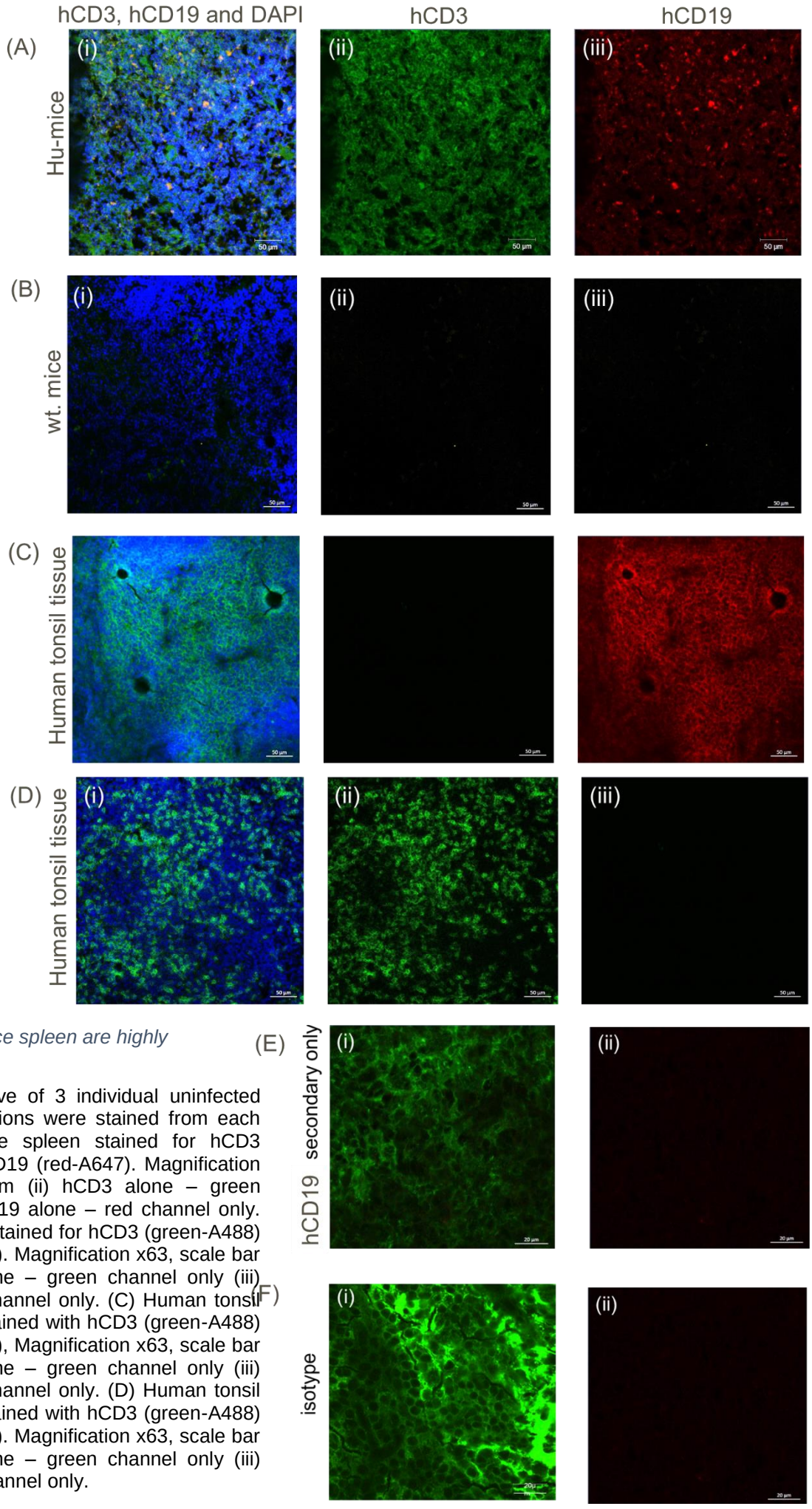

Figure 11.3. 15: hu-mice spleen are highly organised

Image is representative of 3 individual uninfected animals, multiple sections were stained from each animal. (A) hu-mouse spleen stained for hCD3 (green-A488) and hCD19 (red-A647). Magnification x63, scale bar 50 µm (ii) hCD3 alone – green channel only (iii) hCD19 alone – red channel only. (B) wt-mouse spleen stained for hCD3 (green-A488) and hCD19 (red-A647). Magnification x63, scale bar 50 µm (ii) hCD3 alone – green channel only (iii) hCD19 alone – red channel only. (C) Human tonsil tissue, B cell zone, stained with hCD3 (green-A488) and hCD19 (red-A647), Magnification x63, scale bar 50 µm (ii) hCD3 alone – green channel only (iii) hCD19 alone – red channel only. (D) Human tonsil tissue, T cell zone, stained with hCD3 (green-A488) and hCD19 (red-A647). Magnification x63, scale bar 50 µm (ii) hCD3 alone – green channel only (iii) hCD19 alone – red channel only.

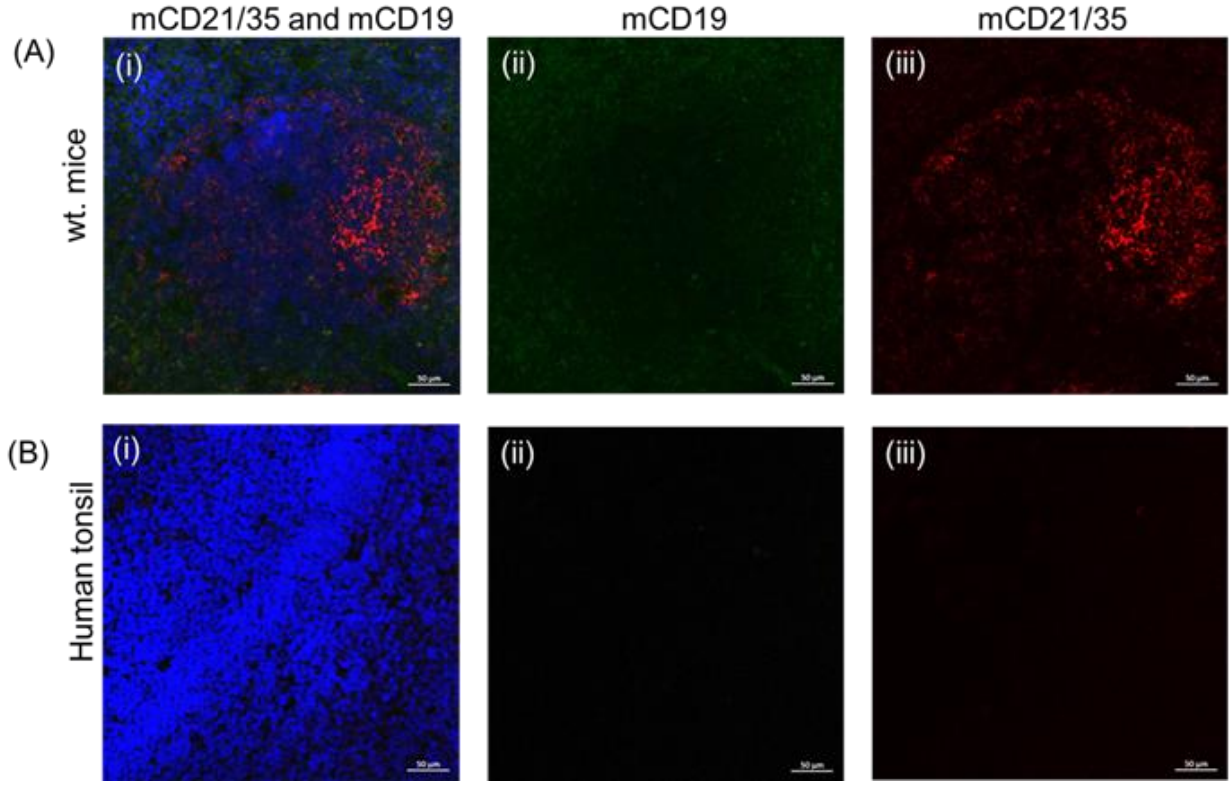

Figure 11.3. 16: wildtype mice have organised germinal centre structures within the spleen

Images are representative of 3 individual uninfected animals, muliple sections were stained and several images taken from each section and animal. (A) wildtype mouse spleen stained with mCD19 (A488-green) and mCD21/35 (A647-red). Magnification x63, scale bar 50 µm (ii) mCD19 alone – green channel only (iii) mCD21/35 alone – red channel only. (B) human tonsil tissue stained with mCD19 (A488-green) and mCD21/CD35 (A647-red). Magnification x63, scale bar 50 µm. No signal is obtained confirming antibodies are species specific. (ii) mCD19 alone – green channel only (iii) mCD21/35 alone – red channel only.

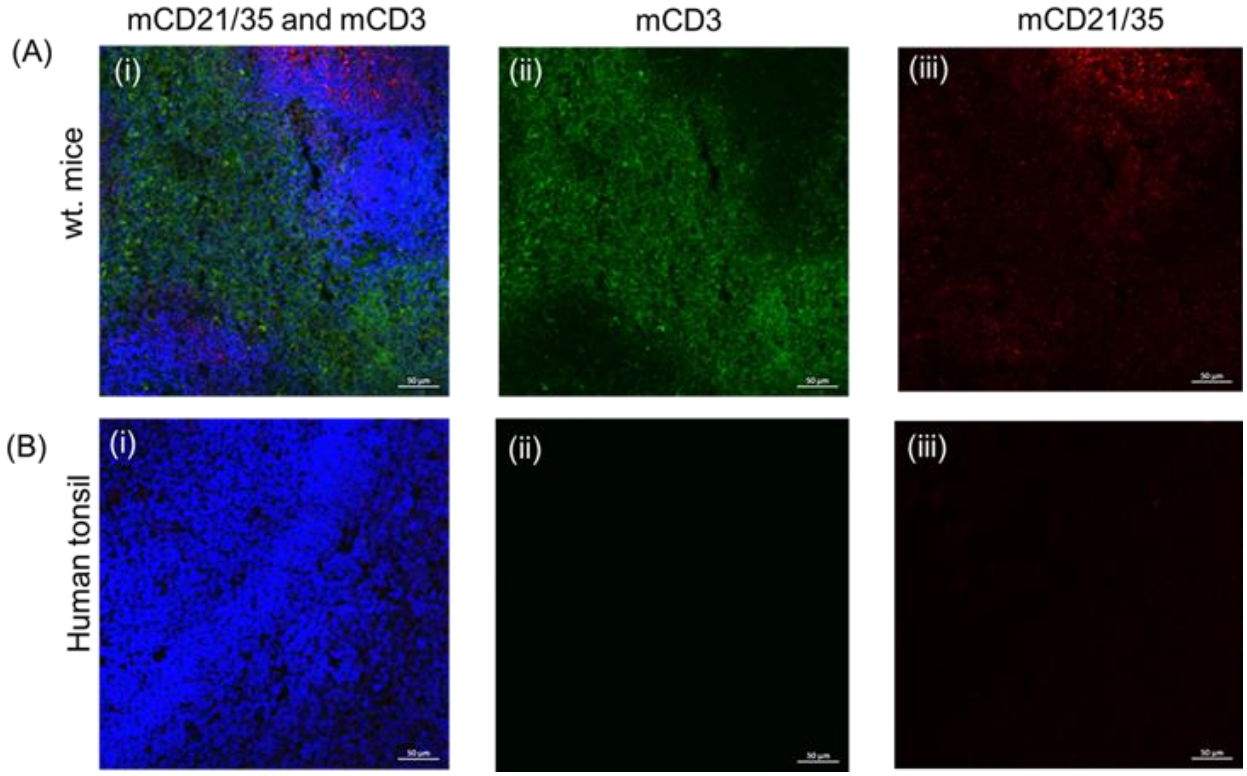

Figure 11.3. 17: wildtype mice have distinct T cell zones

Images are representative of 3 individual uninfected animals, multiple sections were analysed from each animal. (A) Wildtype mouse spleen stained with mCD3 (A488-green) and mCD21/35 (A647-red). Magnification x63, scale bar 50 µm (ii) mCD3 alone – green channel only (iii) mCD21/35 alone – red channel only. (B) human tonsil tissue stained with mCD3 (A488-green) and mCD21/35 (A647-red). Magnification x63, scale bar 50 µm. No signal is seen confirming antibodies are species specific. (ii) mCD3 alone – green channel only (iii) mCD35/21 alone – red channel only.

This analysis determined hu-mice have human B cells but are devoid of human FDCs. Therefore, when investigating the presence of human sCD21 within hu-mice serum, any protein detected can be assumed to be derived from the human B cells, the only cell present in the model expressing human CD21.

Before serum was analysed on the human CD21 ELISA (abcam), used previously in the RA study, it was important to determine there was no cross reactivity between mouse serum and the assay. Standard curves were made using human rc-CD21 within assay buffer, human serum and wildtype mouse serum. Serum was diluted 1in4, a concentration determined by previous validation of the assay (Section 11.3.1). Assays were run, and data processed according to the protocol detailed in Methods Section 8.17. Standard curves made within assay buffer and mouse serum showed no significant differences in the detection of rc-CD21 using this assay (Figure 11.3.18A). This confirms that mouse serum does not cause any matrix interference with the human CD21 ELISA. Human serum has previously been shown to cause matrix interference with the assay and therefore a shift in the standard curve is observed (Figure 11.3.18A), however this is not the case with mouse serum. Spike recovery of human sCD21 was also tested within mouse serum. Human rc-CD21 was spiked into neat mouse and human serum 4-fold higher than the final concentration to be detected. A low (final concentration 50 ng/ml), mid (final concentration 100 ng/ml) and high (final concentration 200 ng/ml) concentration of rc-CD21 was chosen to spread a range of concentrations that could be present when measuring levels within the hu-mice serum samples. Serum was then diluted 1in4 in assay buffer and the concentration of sCD21 interpolated using standard curves made in respective species serum. Human sCD21 concentration was accurately detected within both mouse and human serum, determining both that the assay can measure sCD21 reliably and that human sCD21 concentration can be accurately detected above mouse serum background absorbance (Figure 11.3.18B). These experiments conclude mouse serum does not cross-react with the human CD21 ELISA and human sCD21 can accurately be detected within mouse serum, therefore this

assay can be used to investigate the presence of human CD21 within humanised mouse serum.

(A)

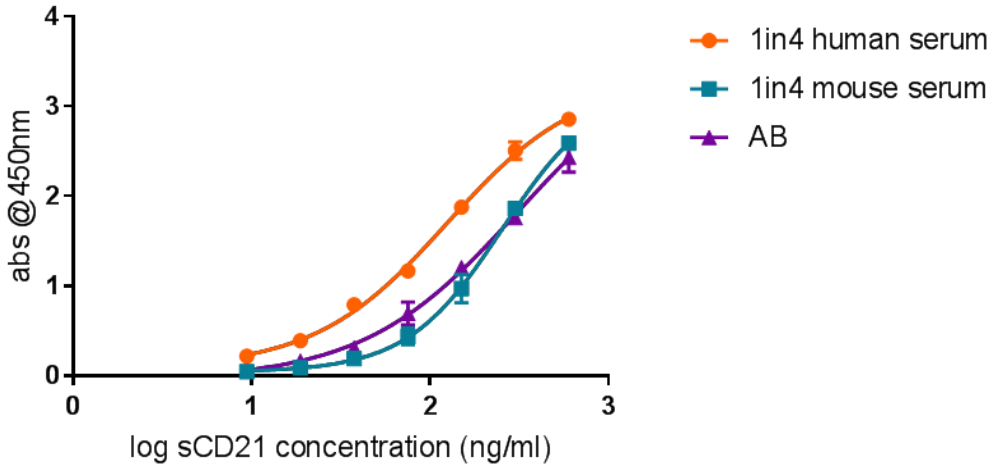

(B)

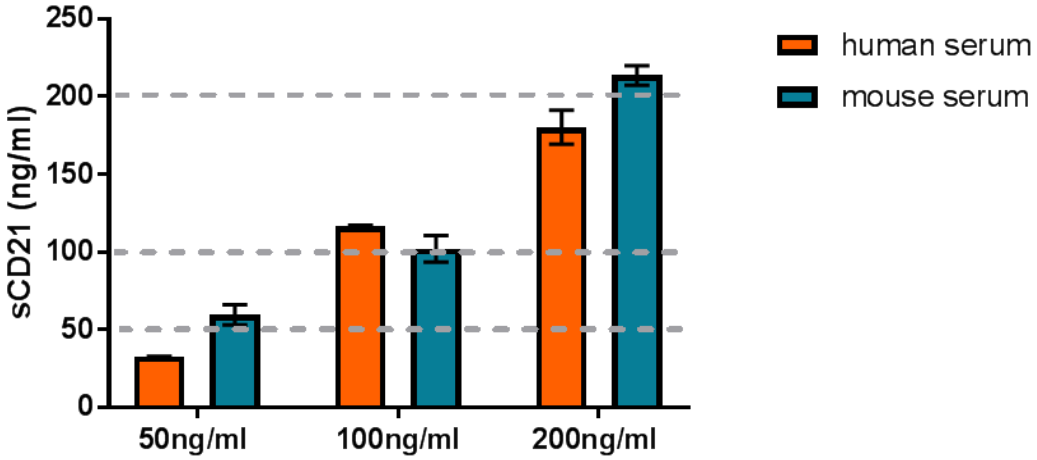

Figure 11.3. 18: Mouse serum does not cross-react with human CD21 ELISA (abcam)

(A) Standard curves made in assay buffer, human or mouse serum with recombinant CD21 revealed mouse serum does not cause matrix interference with the ELISA unlike human serum. Assay is specific for human protein. (B) recombinant CD21 was spiked into human and mouse serum and concentration interpolated using standard curve made in respective species serum. Human CD21 can be accurately detected above mouse serum background absorbance. Samples were run in duplicate.

Mouse serum was diluted 1in4 and samples were run in duplicate. This dilution was chosen due to the small volume of serum available and the final sample volume needing to be 100 µl. Additionally, this dilution was the chosen concentration in all previous assays using this ELISA kit (abcam). A standard curve of human rc-CD21 was performed as before and absorbances measured in the mouse serum interpolated to find the concentration of sCD21 within the samples. Samples from six mice were investigated, three naïve and three infected, in all cases the absorbance measured for each repeat was below the lower limit of detection for the assay (data not shown). This result suggests the humanised mouse model used here do not produce human soluble CD21, however as only a small volume of sample was available the dilution made in to run the assay may have reduced the concentration of protein within the sample to undetectable levels. Alternatively, B cells within this model may not be producing sCD21 due to other factors such as altered development and gene expression due to disorganised SLO structures, which were not investigated here.

In summary, this data show that within this humanised mouse model, human T and B cells develop in the SLOs but human stromal cells, FDCs and FRCs, are absent. CD21 is expressed within the cells in this model, predominately by the B cells, as shown by IHC (Figure 11.3.13). Although these SLOs contain human immune cells, proper organisation of the organs fails to develop (Figure 11.3.12), therefore suggesting that the cells may not be producing the relevant factors, potentially leading to the absence of sCD21 in this mouse model.

11.3.3 The function of sCD21 – blocking C3dg binding in peripheral B cells and activation in B cell lines

The current observations made in the literature suggest sCD21 may have a role in disease and control of the immune system, therefore it is important to further understand the role of human sCD21 in biology.

Investigating the ability of sCD21 to block C3dg model immune complex binding to B cells

A recombinant form of sCD21 has previously been shown to bind C3dg (G. Nemerow et al., 1989); in this investigation recombinant CD21, full length receptor, and SCR1/2, the ligand binding site of CD21, were used to demonstrate the ability of soluble CD21 to block binding of C3dg to peripheral B cells. B cells were identified using CD19 antibody staining and C3dg binding assessed on this population (Figure 11.3.19) in the presence of varying sCD21 concentrations, the highest concentration being 144 nM.

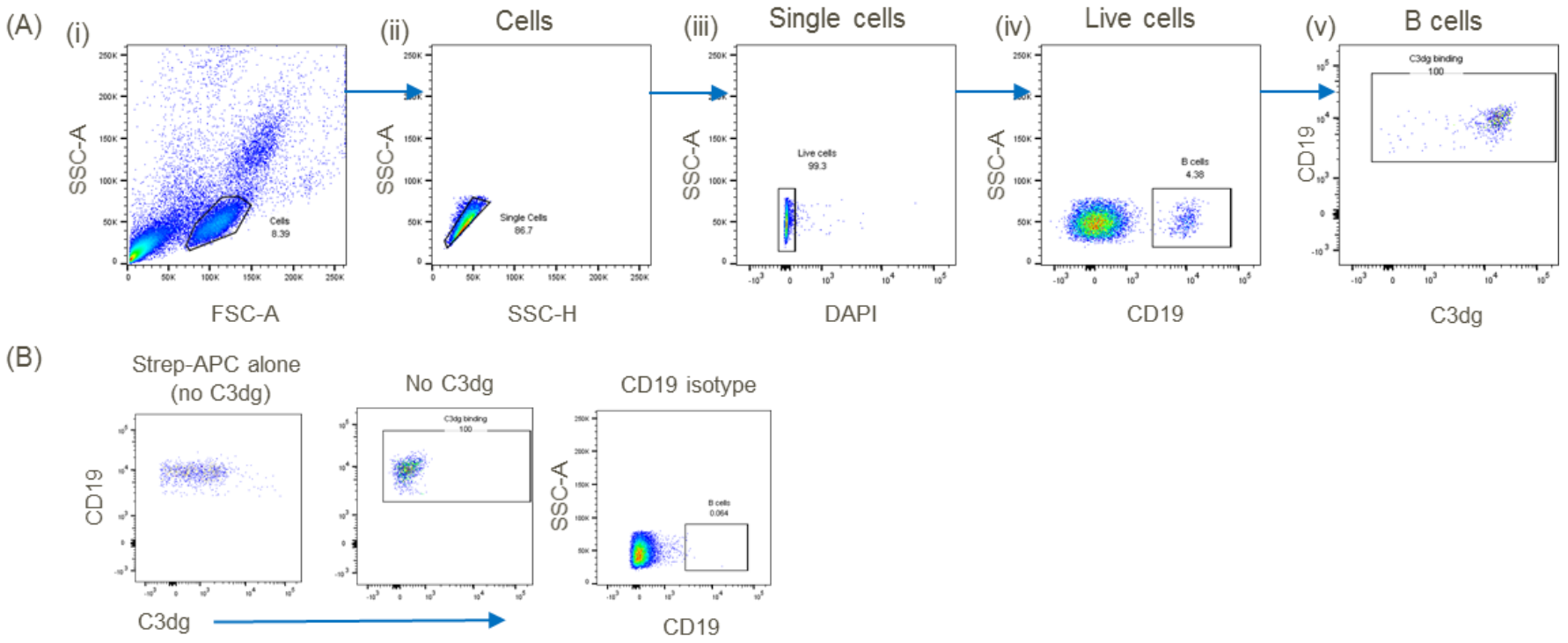

Figure 11.3. 19: Identification of C3dg bound B cells

(A) Cells are gated (i) then single cells (ii) and live cells selected (iii). B cells are identified by CD19 expression (iv) and C3dg binding assessed (v). (B) Strep-APC does not cause background staining. CD19 positive gate was set using isotype stained samples

Before assessing blockage of binding, the concentration of C3dg-immune complexes was first optimised to find an assay window in which this may be observed. As the concentration of sCD21 reagents that could be added to the assay was the limiting factor in this investigation, a low concentration of C3dg-immune complex must be used. Investigations into binding of monomeric and tetrameric complexes were undertaken; in previous experiments a tetrameric complex was used as a greater assay window is achieved when using these complexes, thought to be due to weak ligand-receptor interactions (Altman et al., 1996). Comparing monomeric and tetrameric complex binding confirmed that a greater signal is achieved by using tetrameric complexes (Figure 11.3.20) but binding could still be visualised with the monomeric form. Blocking C3dg binding with sCD21 (144 nM) revealed that it was easier to prevent binding of monomeric C3dg-complexes to peripheral B cells than tetrameric complexes; this may be due to the C3dg being more diffusely spread over Strep-APC molecules when in a monomeric form than in the tetramer (Figure 11.3.20Aii and 66Bii). For this reason, monomeric C3dg complexes were used. At concentrations lower than 0.02 µg/ml monomeric C3dg-complexes, binding could not be visualised, and the assay window lost, therefore this was the final concentration of C3dg-complexes used in the subsequent experiment.

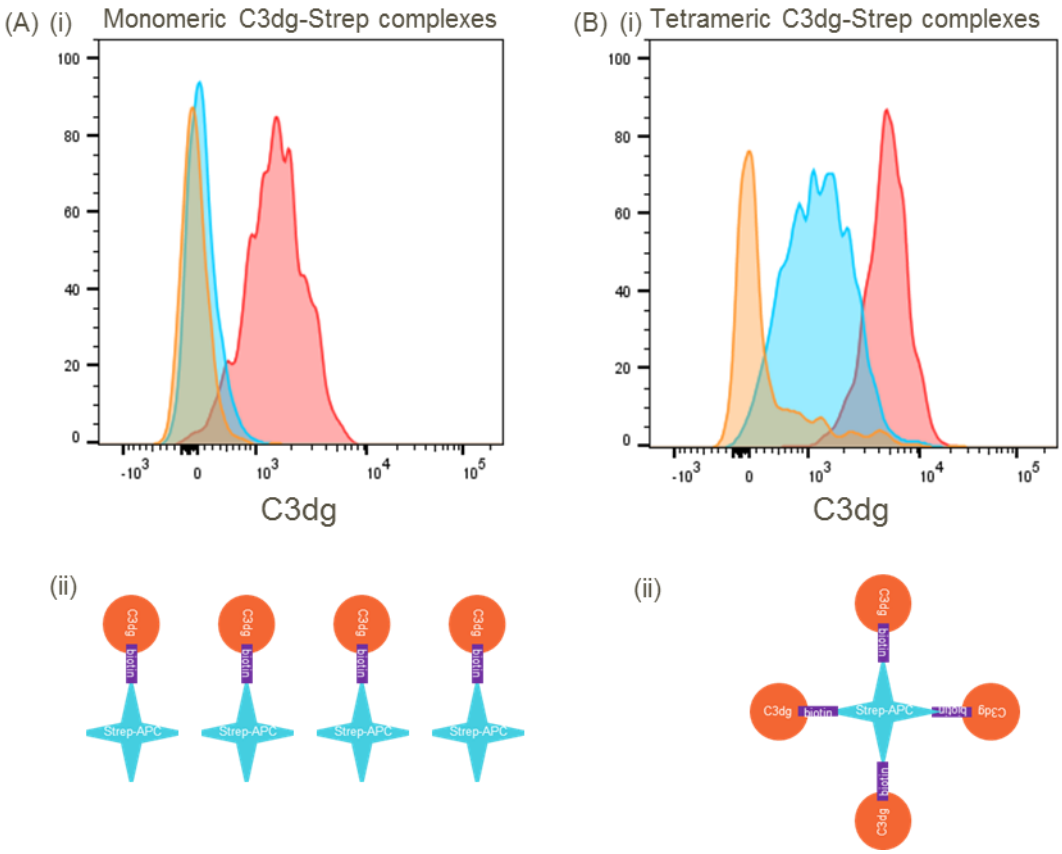

Figure 11.3. 20: Blocking monomeric vs tetrameric C3dg-streptavidin complex binding to peripheral B cells

Orange= plus FE8, Blue= plus sCD21, Red= complex alone. (A) (i) 0.02 µg/ml monomeric C3dg-StrepAPC complexes bind peripheral B cells; binding can be blocked using CD21 Ab clone FE8 (120nM) and sCD21 (144nM) (ii) C3dg molecules are spread over Streptavidin molecules to create monomers. (B) (i) 0.02 µg/ml tetrameric C3dg-StrepAPC complexes bind peripheral B cells; binding can be blocked using CD21 Ab clone FE8 (120nM) and sCD21 (144nM) (ii) C3dg molecules are bound to form a tetramer on Streptavidin molecules.

Experiments in which monomeric C3dg-complexes were preincubated with varying concentrations of rc-CD21 before addition to cells, revealed that sCD21 has the ability block C3dg binding to peripheral B cells in a concentration dependent manner. Interestingly, full length CD21 (recombinant CD21) is able to block C3dg binding to B cells at lower concentrations than the ligand binding site alone (SCR1/2). The IC_{50} for rc-CD21 was calculated at 3.94 nM, whereas the IC_{50} for SCR1/2 is 5-fold higher at 19.2 nM (Figure 11.3.21, n=3). This result was surprising as it was assumed addition of the C3dg binding site alone would have a higher binding affinity for the C3dg immune complexes, however these results suggests the whole protein provides the receptor with a greater affinity to C3dg, perhaps due to conformational differences in the ligand binding site in the full-length protein. Physiological levels of sCD21 within healthy volunteers were shown to be ~400 ng/ml, equivalent to 2.75 nM (Figure 11.3.4). At these concentrations, C3dg binding to B cells is blocked by rc-CD21 but not SCR1/2 (Figure 11.3.21). The physiological levels of C3dg are unknown, and as the distribution of the protein at any given time is difficult to determine, it is reasonable to conclude that sCD21 blocks C3dg binding to B cells at physiological conditions.

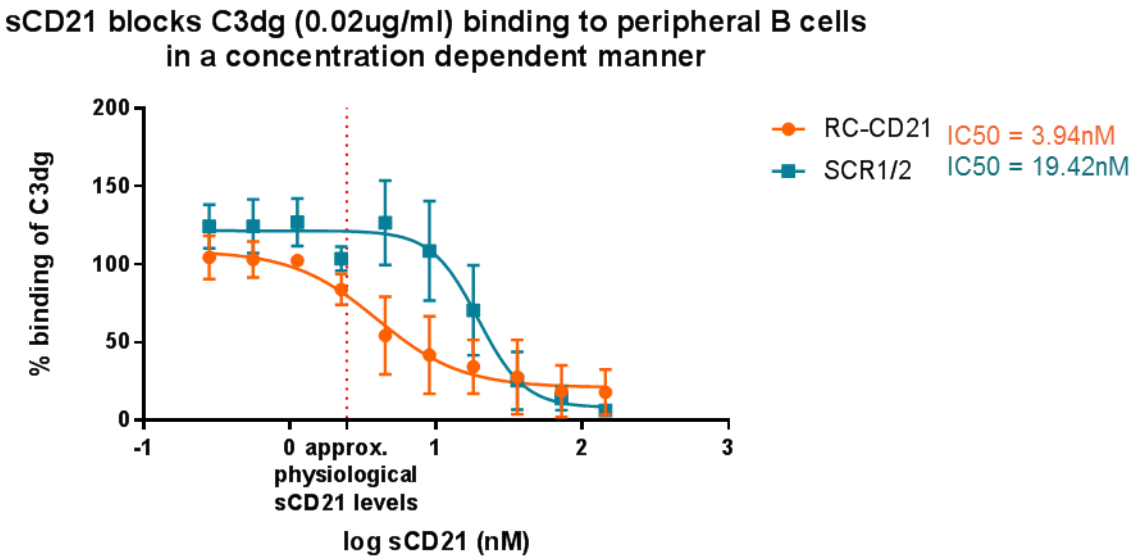

Figure 11.3. 21: Soluble CD21 can block C3dg-immune complex binding to peripheral B cells

n=3. sCD21 (recombinant CD21 or SCR1/2) was titrated at a starting concentration of 144 nM and shown to block the binding of 0.02 µg/ml C3dg in a concentration dependent manner. sCD21 and C3dg-APC immune complexes were preincubated prior to the addition to PBMCs. RC-CD21 has an IC50 of 3.94 nM and SCR1/2 has an IC50 of 19.42 nM. Physiological levels of sCD21 is approximately 2.75 nM.

Investigating B cell line activation using anti-IgM/C3dg model immune complexes

As C3dg binding to CD21/CD19 complexes allows for co-activation of B cells, sCD21's ability to block this response by preventing this interaction was investigated. Cells were stimulated using an immune complex composed of biotinylated Fab2 anti-IgM and biotinylated C3dg which are co-ligated together using neutravidin to form a tetramer, calculated empirically (Figure 11.3.22). Anti-IgM stimulates membrane bound IgM receptors on B cells and C3dg stimulates the cells through binding CD21 in the CD21/CD19 co-complex.

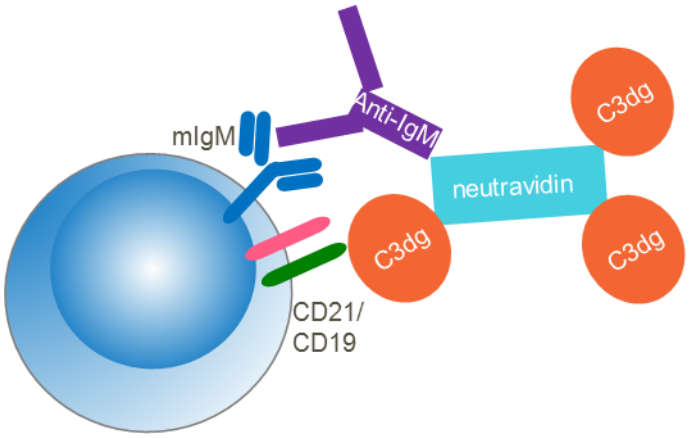

Figure 11.3. 22: Stimulation complex used for B cell line activation pERK assays

Stimulation complexes are composed of biotinylated Fab2 anti-IgM and biotinylated C3dg which are co-ligated together using neutravidin. The complex is a tetramer, the ideal complex ratio is 3 C3dg: 1 neutravidin: 1 anti-IgM, however this is dependent individual reagent concentration.

For these experiments B cell lines were utilised due to lack of success developing a robust and reliable signalling assay in primary B cells. To determine which cell lines were suitable for use in the activation assay, expression of IgM and CD21 was assessed on Raji, Daudi and Ramos B cell lines. Ramos cells were shown to be $CD21^-$ and IgM^+ (Figure 11.3.23), therefore can only be activated by anti-IgM stimulation and thus act as a negative control in the assay. Daudi cells express both CD21 and IgM (Figure 11.3.23) and Raji are also $CD21^+$ but express IgM at low levels (Figure 11.2.23). Raji cells were used in the assay due to their low IgM expression as this cell line was thought to be a model more similar to primary B cells, which were also shown to express lower IgM levels on their cell surface than that observed in the Daudi cell line (Figure 11.2.23). The number of CD21 receptors was quantified on the surface of the chosen cell lines using Quantibrite-PE beads, using the methods detailed in Methods Section 8.9. Cells were stained with 1 µg/ml CD21-PE (Bu32) and the number of receptors calculated. Raji cells were found to express an average of 21,000 CD21 receptors on the surface of each cell. This expression is 2.5-fold higher than primary B cells (Figure 11.2.23C, n=3), which were found to express an average of 8,000 CD21 receptors per cell. Increased CD21 receptor number on the Raji cells line may explain why an assay window for C3dg activation could be successfully developed in B cells lines but not in primary cells.

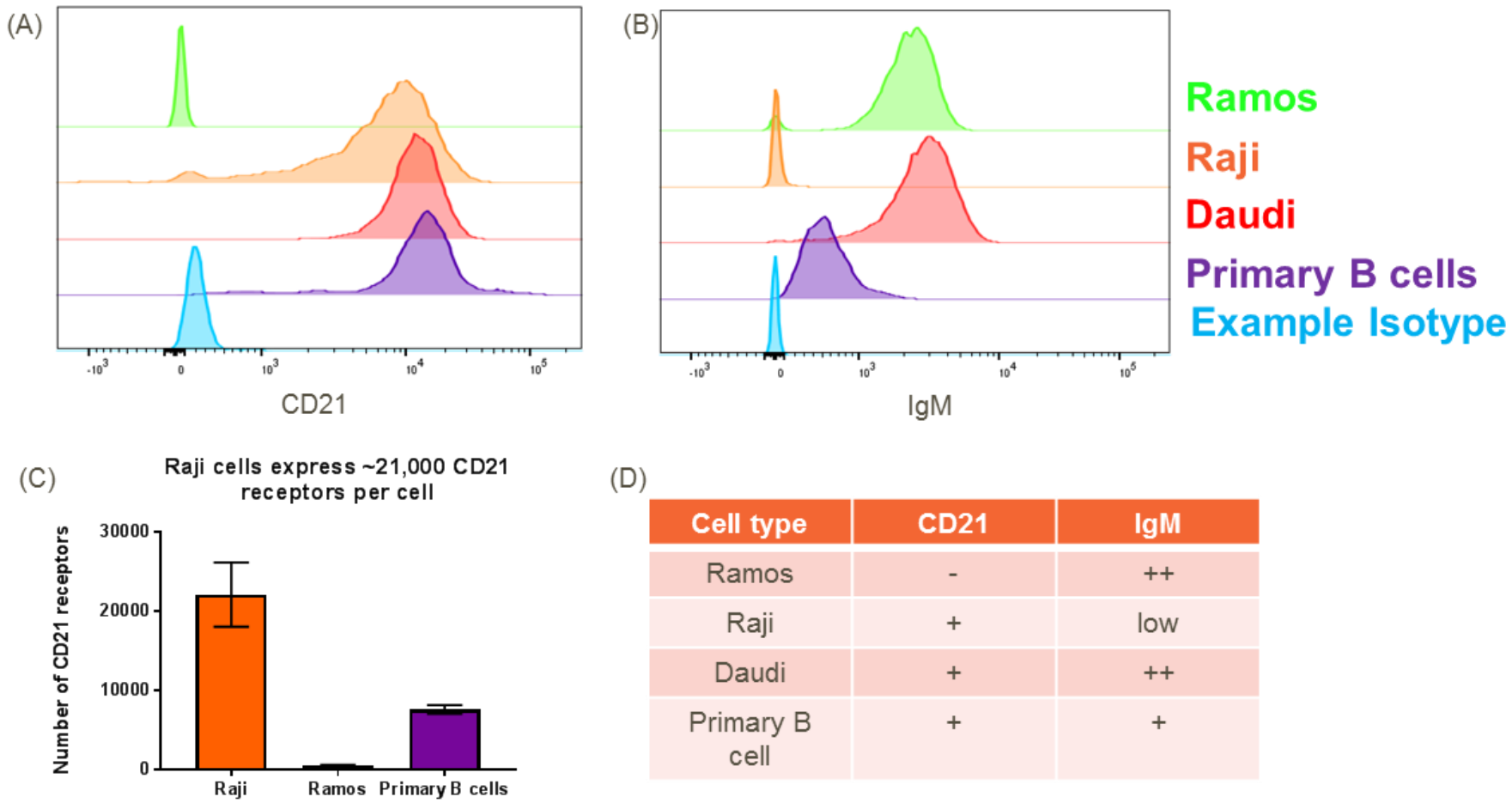

Cell type	CD21	IgM
Ramos	-	++
Raji	+	low
Daudi	+	++
Primary B cell	+	+

Figure 11.3. 23: Expression of anti-IgM and CD21 in B cell lines

(A) CD21 expression in B cell lines. Raji and Daudi cells express high levels of CD21, Ramos cells are negative for CD21. Isotype measured on Ramos cells, representative staining. (B) IgM expression in B cell lines. Ramos and Daudi cells express high levels of CD21. Raji cells express low levels of anti-IgM, levels are slightly higher than isotype staining levels. Isotype measured on Ramos cells, representative staining. (C) Quantibrite beads were used to numerate the absolute CD21 receptor number on the surface of cell lines. Raji cells express an average of 21,000 receptors per cell n=3. Ramos cells are negative for CD21. (D) Summary table of CD21 and anti-IgM expression in B cell lines.

Firstly, anti-IgM concentration was titrated, plus and minus C3dg (0.3 µg/ml and 1 µg/ml), starting at a concentration of 10 µg/ml, to show that anti-IgM activated B cell lines, Raji and Ramos, in a concentration dependent manner (Figure 11.3.25, n=3). The neutravidin concentration (1 µg/ml) was kept constant in all complexes in this particular experiment. Addition of C3dg to the stimulation complex, enhanced activation of $CD21^+$ Raji cells (Figure 11.3.25A, n=3). This effect was also concentration dependent; addition of 0.3 µg/ml C3dg decreased the EC_{50} of anti-IgM stimulation alone 12.5-fold from 0.51 µg/ml to 0.06 µg/ml. The addition of 1 µg/ml C3dg to the anti-IgM titration further decreased the EC_{50} to 0.04 µg/ml. At low concentrations (0.3 µg/ml), C3dg alone does not activate cells, however at higher concentrations (1 µg/ml), 13.8% of $CD21^+$ B cells are pERK+ve due to stimulation with C3dg alone. As these experiments were investigating the co-activation response of C3dg, for the rest of the investigation, C3dg was used at the concentration of 0.3 µg/ml. Ramos cells confirm the enhanced activation with C3dg was CD21 dependent as no co-activation response is seen in these $CD21^-$ cells with the addition of this reagent (Figure 11.3.25B, n=3). A small increase in EC_{50} was observed with the addition of C3dg, from 0.12 µg/ml to 0.23 µg/ml and 1.3 µg/ml with 1 µg/ml and 0.3 µg/ml C3dg respectively. This effect may be due to the inclusion of C3dg within the stimulation complex potentially causing steric hinderance and preventing anti-IgM from binding IgM receptors on the cell surface.

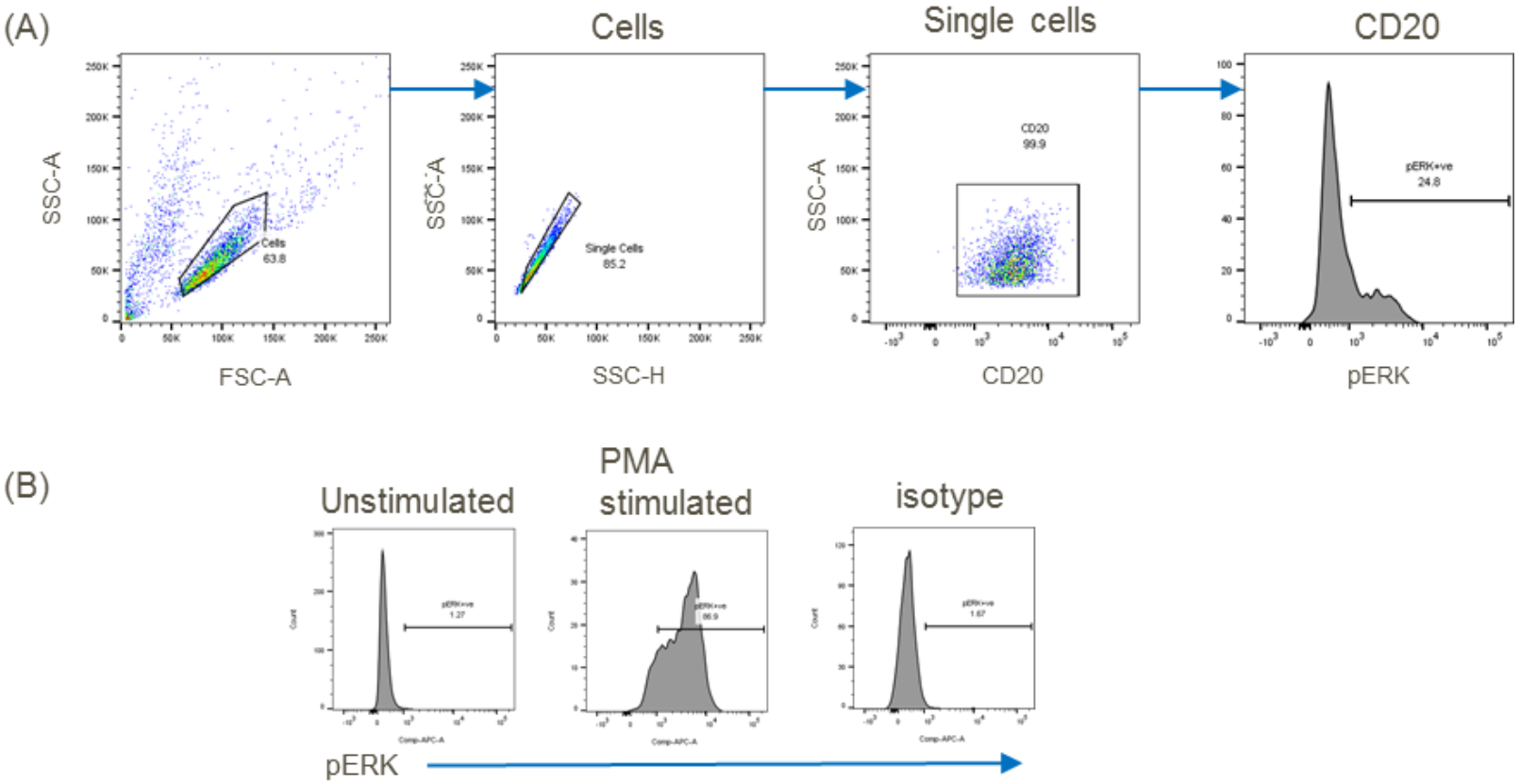

Figure 11.3. 24: Gating strategy for anti-IgM/C3dg activation assays in B cell lines Raji and Ramos

Raji cell example (A) Cells were gated on and single cells selected. Cells expressing intracellular CD20 were selected, confirming permeabilisation of cells had occurred. (B) pERK positive cells were selected using gates set by unstimulated, isotype and PMA stimulated samples.

(A)

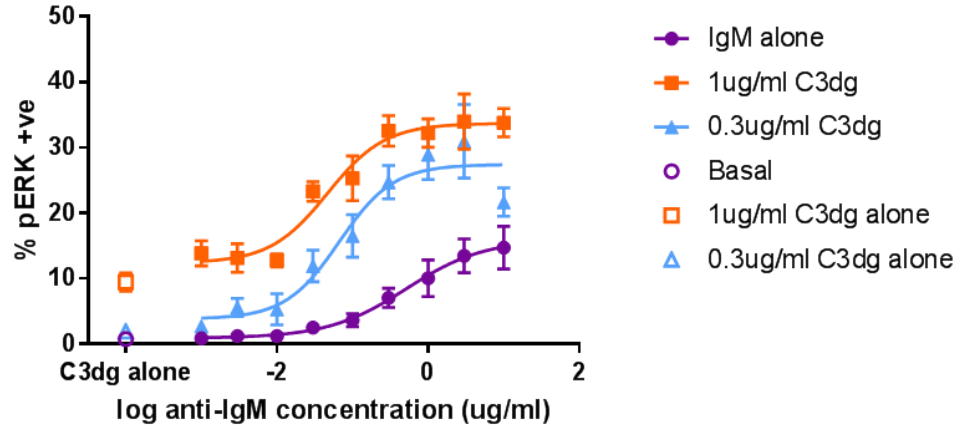

(B)

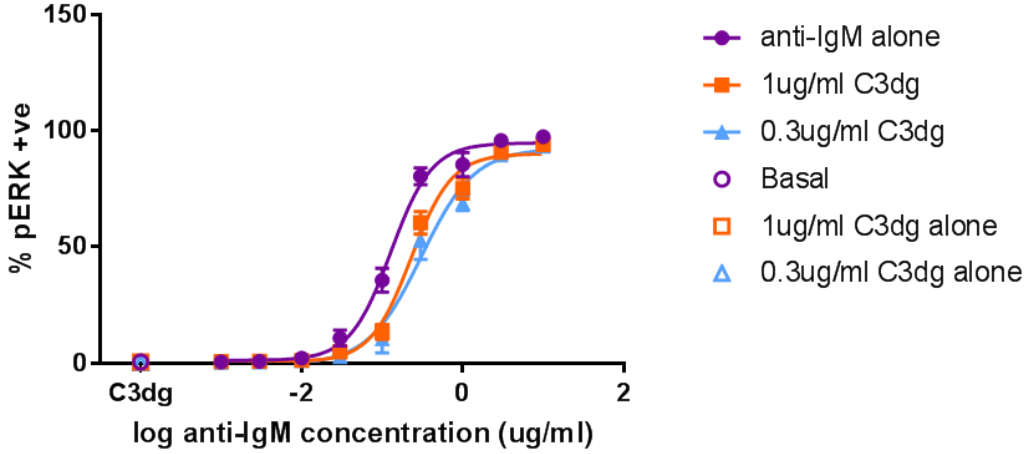

Figure 11.3. 25: C3dg lowers the threshold for activation of CD21+ve Raji B cell lines

n=3 individual assays. Anti-IgM concentrations start at 10 µg/ml and complexes are formed by the addition of 1 µg/ml neutravidin. C3dg is added at concentrations of 1 µg/ml and 0.3 µg/ml. (A) anti-IgM activates Raji cells (CD21+ve) in a concentration dependent manner. Addition of C3dg increases activation (%pERK positive cells), this increase is concentration dependent, 1 µg/ml C3dg increases activation further than 0.3 µg/ml C3dg. (B) anti-IgM activation Ramos cells (CD21-ve) in a concentration dependent manner. Addition of C3dg has no effect on activation status of these cells.

In addition to C3dg lowering the threshold for activation of $CD21^+$ B cell lines, it was shown that C3dg acts synergistically with low anti-IgM concentrations to activate cells to levels equivalent to high anti-IgM stimulation (Figure 11.3.26A, n=3). Cells stimulated with C3dg alone (0.3 µg/ml) or low anti-IgM concentrations (0.03 µg/ml) do not become activated, however when the two reagents are added together complexed with neutravidin, co-stimulation occurs and 12% of cells become pERK+ve. Stimulation of Raji cells with high concentrations of anti-IgM (1 µg/ml) also caused 11% of cells to become pERK+ve, therefore C3dg lowers the concentration of anti-IgM required to activate cells. Again, Ramos cells demonstrate this effect is CD21 dependent as co-stimulation with C3dg (0.3 µg/ml) and low anti-IgM concentrations (0.03 µg/ml) result in the same response as stimulation with low anti-IgM concentrations alone (Figure 11.3.26B, n=3). When these cells are stimulated with a high anti-IgM concentration (1 µg/ml), activation increases from 2.1% pERK+ve (low anti-IgM stimulation) to 35.7% pERK+ve.

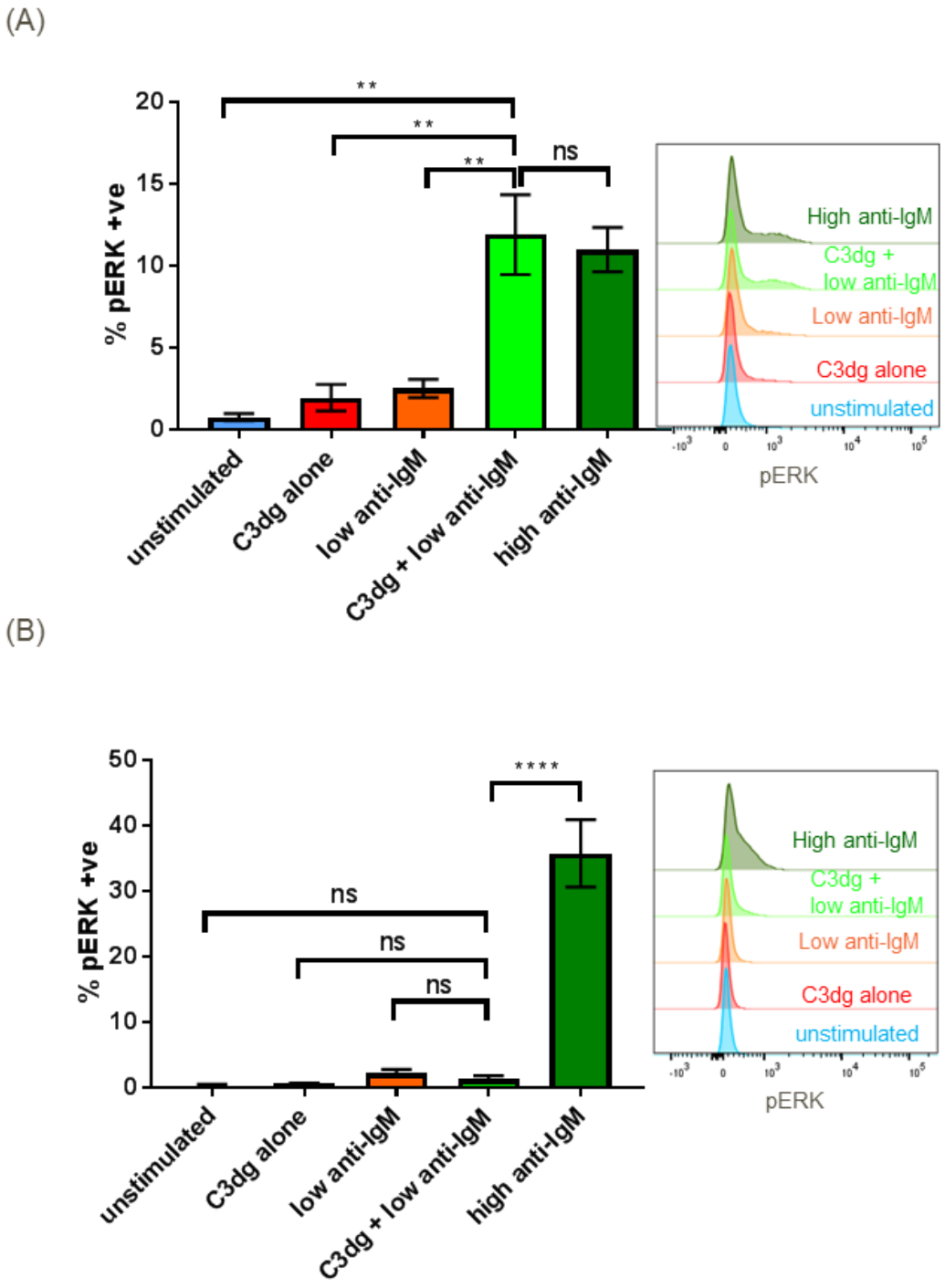

Figure 11.3. 26: C3dg acts synergistically with low anti-IgM concentrations to activate CD21+ve Raji B cell lines to levels of high anti-IgM stimulation

n=3 individual assays, significance measured using ANOVA test, bars represent SD. Concentrations of reagents in data shown: 0.3 µg/ml C3dg, 0.03 µg/ml anti-IgM, 1 µg/ml neutravidin. (A) C3dg and low anti-IgM concentrations (0.03 µg/ml) do not activate Raji cells alone; when added together synergy between the two reagents is seen to cause activation to levels of high anti-IgM stimulation (1 µg/ml). (B) Low anti-IgM concentration (0.03 µg/ml) and C3dg alone do not activation Ramos cells, together synergy does not occur but high anti-IgM concentrations (1 µg/ml) alone activate the CD21-ve cells.

Stimulation complexes were made with and omitting neutravidin (1 µg/ml). These experiments demonstrated the need for co-ligation of anti-IgM and C3dg to induce the co-activation response seen in $CD21^+$ cells (Figure 11.3.27). The concentration dependent activation of cells with anti-IgM is not affected by the presence or absence of neutravidin (Figure 11.3.27, n=3); however, for the co-stimulation with C3dg to occur, neutravidin must be present. Removal of this reagent from the stimulation results in a response equivalent to anti-IgM stimulation alone (Figure 11.3.27, n=3). Therefore, to get a C3dg-dependent activation response from $CD21^+$ cells, all three components of the stimulation complex, C3dg, anti-IgM and neutravidin, are needed (Figure 11.3.27A). This observation suggests that in biology opsonisation of antigen with both anti-IgM and C3dg is needed to cause the co-activation response in B cells. The presence of neutravidin has no effect on the activation of Ramos cells (Figure 11.3.27B, n=3), as they do not respond to C3dg stimulation.

During assay optimisation, neutravidin concentration was decreased from 1 µg/ml, used previously, to 0.2 µg/ml in order to further understand how the molar ratios of reagents within the complex affects activation of the cells with hope this would lead to insight into which complex should be used in the final blocking assay. Cells were activated with complexes containing 0.3 µg/ml C3dg, 0.2 µg/ml neutravidin and varying anti-IgM concentrations (starting at 10 µg/ml and diluted 3-fold to create a titration). Lowering the concentration of neutravidin does not affect activation responses of Ramos cells at high anti-IgM concentrations as C3dg inclusion within the stimulation complexes does not affect activation status of this cell line (Figure 11.3.28B, n=3). However, when concentrations of anti-IgM reached above 0.1 µg/ml in this assay, co-activation with C3dg was lost within Raji cells (Figure 11.3.28A, n=3). This can be explained by considering the molar ratios of the reagents within the complex. For example, within the complex containing 0.3 µg/ml C3dg (7.5 nM), 3 µg/ml anti-IgM (20 nM) and 0.2 µg/ml neutravidin (3 nM), the theoretical complex would contain a molar ratio of approximately 1:2.5:7M neutravidin:C3dg:anti-IgM respectively. Therefore, at these concentrations, complex formation would be inefficient and

preferentially contain only anti-IgM molecules. This explains the observed loss of C3dg-dependent co-activation at high concentrations of anti-IgM (Figure 11.3.28A, n=3). A reduction in activation is also seen when using neutravidin at concentrations of 1 µg/ml (14.7 nM) when complexes are formed using 10 µg/ml anti-IgM (66 nM) and 0.3 µg/ml C3dg (7.5 nM) (Figure 11.3.28A, n=3). Using these molar concentrations, complexes would form with a molar ratio of 1:0.5:5 neutravidin:C3dg:anti-IgM respectively. Again, there is now an excess of anti-IgM within this complex, causing the majority of complexes to form containing only anti-IgM molecules. Consequently, loss of co-activation is seen when reagents are added at these concentration. These investigations conclude that molar ratios of reagents within the complex are an important factor in the activation of $CD21^+$ Raji cells.

To summarise, these experiments show that $CD21^+$ Raji cells can be activated in a concentration dependent manner with the stimulation complex, and that C3dg lowers the threshold for activation in these cells, but not in $CD21^-$ Ramos cells. Investigations continued to explore the roles of sCD21 in blocking this co-activation through its ability to bind to C3dg.

(A)

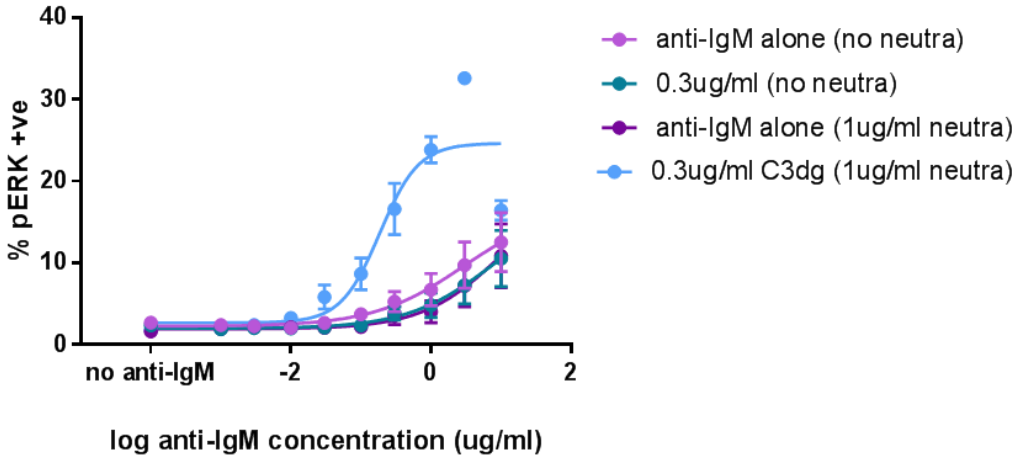

(B)

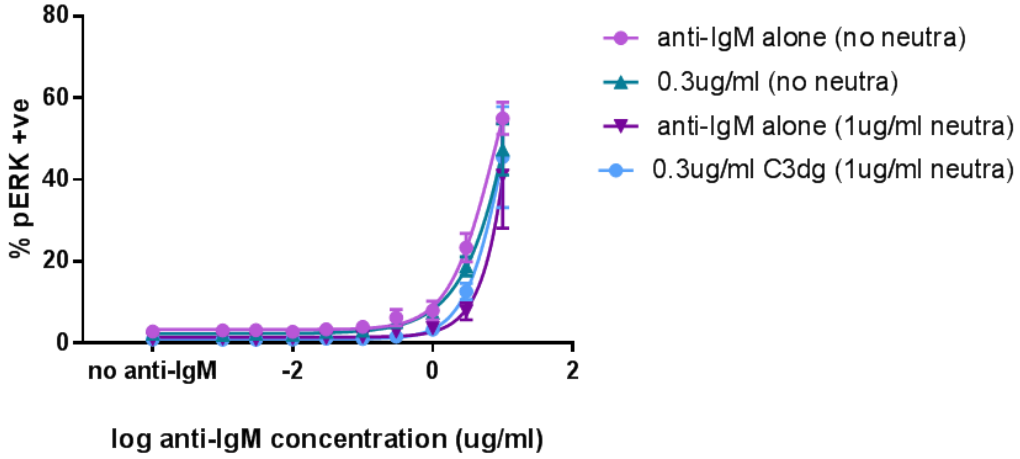

Figure 11.3. 27: Co-ligation of C3dg and anti-IgM is needed for C3dg-dependent activation of CD21+ve Raji cells

n=3 independent experiments, bars represent SD. (A) Removal of neutravidin from stimulation complexes results in loss of C3dg-dependent activation in CD21+ve Raji cells. (B) Removal of neutravidin from stimulation complexes has no effect on activation of CD21-ve Ramos cells

(A)

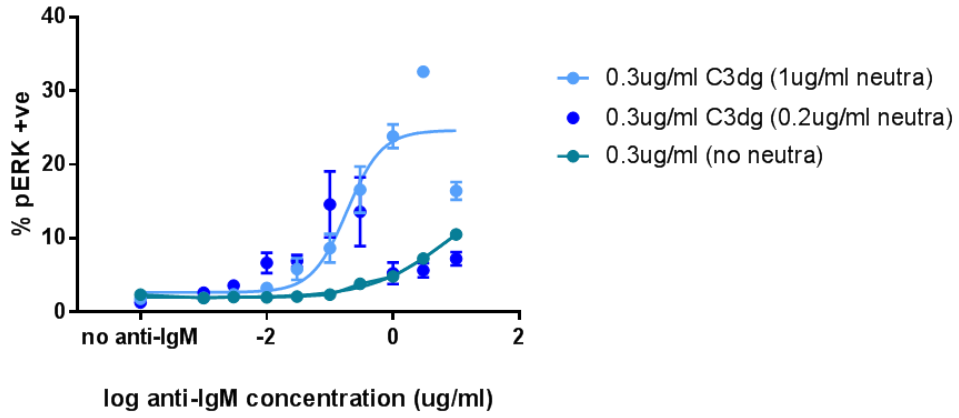

(B)

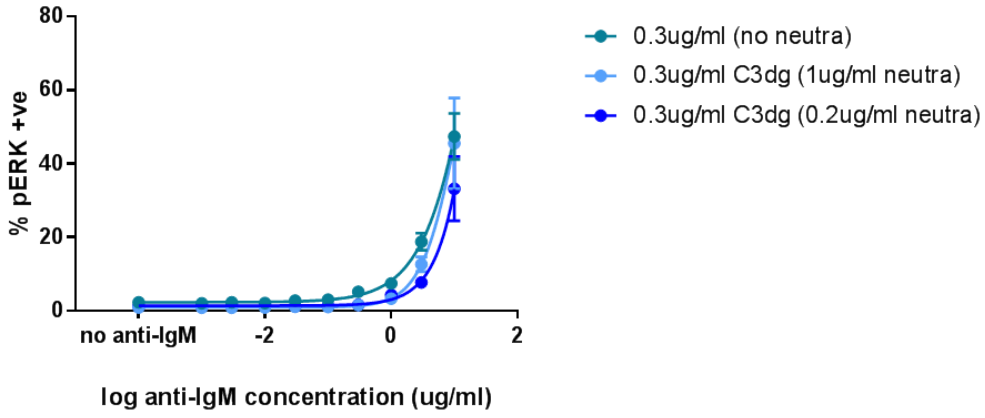

Figure 11.3. 28: Low neutravidin and high anti-IgM concentrations leads to insufficient complex formation to cause C3dg-dependent activation of CD21+ve Raji cells

n=3 independent experiments, bars represent SD. (A) Lowering the concentration of neutravidin to 0.2 µg/ml is insufficient to make complexes at high anti-IgM concentrations, resulting in loss of C3dg-dependent co-activation of Raji cells. (B) Decreasing neutravidin concentration has no effect on activation of CD21-ve Ramos cells.

Investigating a role for sCD21 in blocking C3dg-dependent activation in CD21$^+$ B cell lines

As the molar ratios of reagents within the stimulation complex is important for the activation response in CD21$^+$ cells (Figure 11.3.28), the percentage of pERK+ve cells after stimulation with different complexes was assessed to determine which complex should be used in the final blocking assay (See Figure 11.3.29 for respective reagent concentrations). In all cases, 0.3 µg/ml anti-IgM was used in the complex as this concentration was shown to be the lowest anti-IgM concentration to cause an activation response (Figure 11.3.25); therefore, creating the largest assay window for additional activation seen due the coactivation response with C3dg. For all complexes, all 3 reagents in the stimulation complex were required to achieve C3dg-dependent co-activation (Fgure 76). Complexes formed to the molar ratio of 1:3:1 neutravidin:C3dg:anti-IgM respectively, could be described as the "ideal" complex shown in Figure 11.3.22. Under these conditions, 3 C3dg molecules and 1 anti-IgM molecule would be bound to each neutravidin. Although this is the "ideal" complex for activation, it may prove challenging to block with sCD21 as there are 3-C3dg molecules per complex. In contrast, when the neutravidin concentration is increased from 0.2 µg/ml to 1 µg/ml within in this complex, the molar ratio of the complex is changed to 5:2.5:1 neutravidin:C3dg:anti-IgM respectively, and the C3dg becomes more diffuse over the increased amounts of neutravidin available. Although complexes may not be fully formed, stimulation with this complex results in 16.5% of cells becoming pERK+ve, the greatest activation window compared with other complexes considered. Additionally, activation using this complex may be easier to block using sCD21 as C3dg will more widely distributed. Complexes containing a lower concentration of C3dg were also considered for use in the blocking assay; complexes contained a molar ratio of 5:1:1 and 1:1:1 neutravidin:C3dg:anti-IgM respectively. Activation with these complexes resulted in a response of 6.93% and 10.62% pERK+ve respectively (Figure 11.3.31, n=3). Although a lower concentration of C3dg would be easier to block with sCD21, stimulation with lower concentrations of this

reagent result in a smaller assay window of activation compared with low anti-IgM alone (0.3 µg/ml), which results in 5.24% of cells becoming pERK+ve (Figure 11.3.31, n=3). For these reasons, the complex containing 0.3 µg/ml C3dg, 0.3 µg/ml anti-IgM and 1 µg/ml neutravidin was chosen to use in subsequent blocking experiments.

Complex molar ratio (neutravidin:C3dg: anti-IgM)	Neutravidin		C3dg		Anti-IgM	
	Concentration (µg/ml)	Molarity (nM)	Concentration (µg/ml)	Molarity (nM)	Concentration (µg/ml)	Molarity (nM)
5:2.5:1	1	14.7	0.3	7.5	0.3	3
5:1:1	1	14.7	0.1	2.5	0.3	3
1:3:1	0.2	3	0.36	9	0.3	3
1:1:1	0.2	3	0.1	2.5	0.3	3

Figure 11.3. 29: Concentrations and molar ratios of stimulation complexes

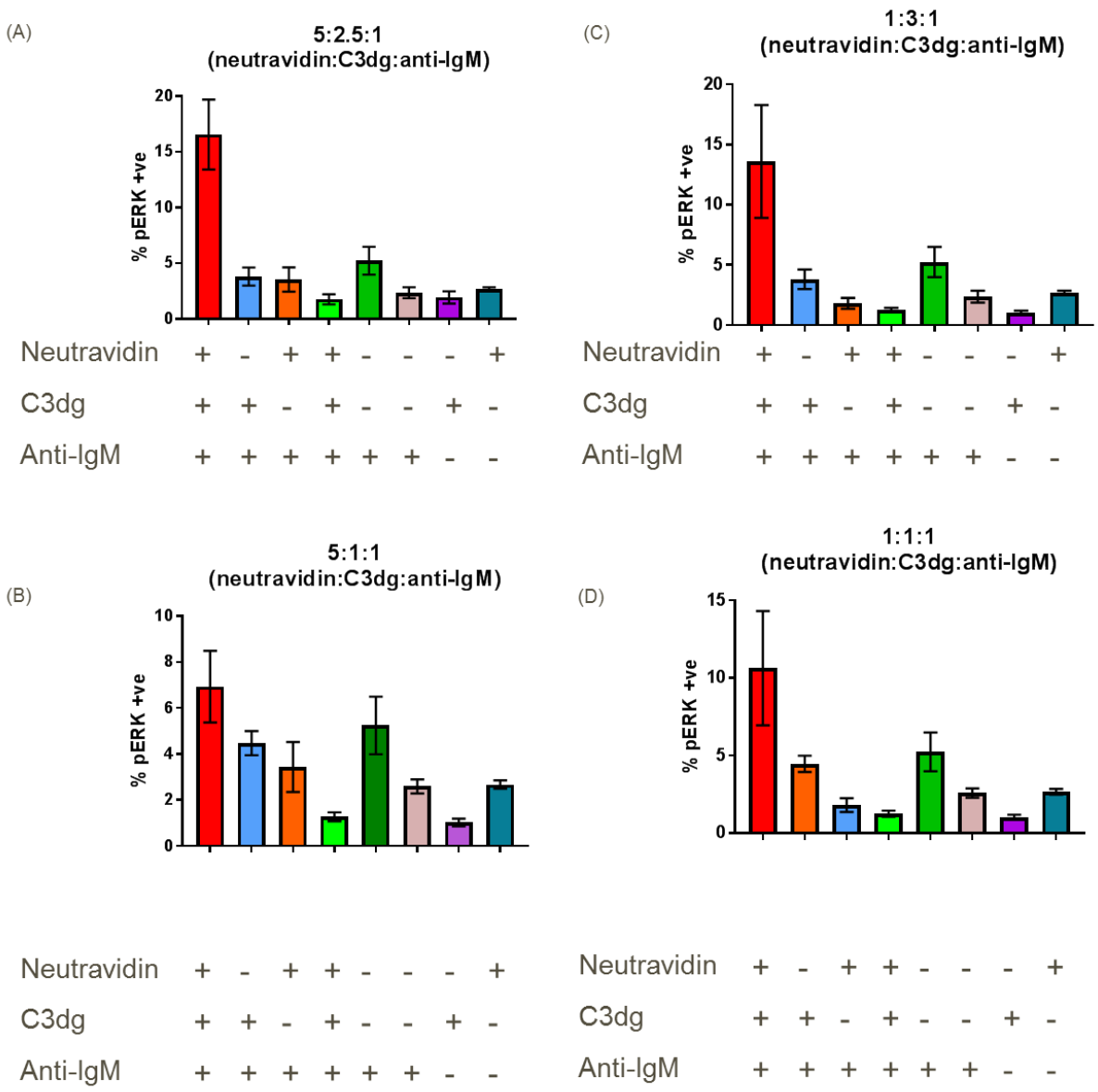

Figure 11.3. 30: C3dg, neutravidin and anti-IgM are required for synergistic activation of CD21+ Raji cells

n=3, bars represent SD (A) Complex has a calculated molar ratio of 5:2.5:1 neutravidin:C3dg:anti-IgM respectively. Concentrations of reagents within the complex are 1µg/ml neutravidin, 0.3µg/ml C3dg and 0.3µg/ml anti-IgM. (B) Complex has a calculated molar ratio of 5:1:1 neutravidin:C3dg:anti-IgM respectively. Concentration of reagents within the complex are 1µg/ml neutravidin, 0.1µg/ml C3dg, 0.3µg/ml anti-IgM. (C) Complex has a calculated molar ratio of 1:3:1 neutravidin:C3dg:anti-IgM respectively. Concentration of reagents within the complex are 0.1µg/ml neutravidin, 0.36µg/ml C3dg and 0.3µg/ml anti-IgM. (D) Complex has a calculated molar ratio of 1:1:1 neutravidin:C3dg:anti-IgM respectively. Concentration of reagents within the complex are 0.2µg/ml neutravidin, 0.1µg/ml C3dg and 0.3µg/ml anti-IgM.

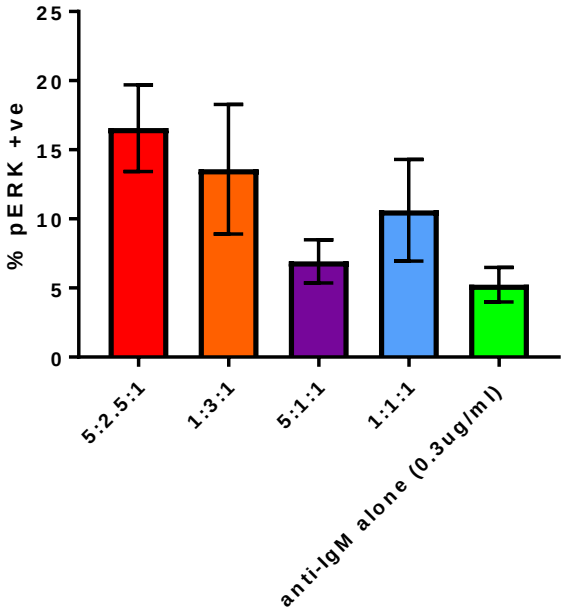

Figure 11.3. 31: Complex with ratio 5:2.5:1 (neutravidin:C3dg:anti-IgM) has the greatest assay window over anti-IgM stimulation alone

n=3, bars represent SD. Complex with 5:2.5:1 molar ratio was chosen for stimulation in activation blocking assays.

In the final assay, the capacity of CD21 blocking antibody clone, FE8 (starting concentration 120 nM), and a recombinant form of sCD21 (starting concentration 1250 nM) to block CD21/C3dg-dependent activation was investigated. The two assays differ in their method of blocking the receptor-ligand interaction; FE8 will block by binding to the ligand binding site of membrane bound CD21; blocking ligand binding to the receptor, whereas sCD21 will bind the ligand C3dg and prevent it binding to membrane bound CD21. These reagents were added to cells stimulated with the chosen anti-IgM/C3dg complex (0.3 µg/ml C3dg, 0.3 µg/ml anti-IgM and 1 µg/ml neutravidin) and the effect on activation observed.

Both reagents were shown to block activation of $CD21^{+}$ Raji cells in a concentration dependent manner (Figure 11.3.32, n=3), these data further confirm the C3dg-dependence of the co-activation response. FE8 has an IC_{50} of 0.12 nM (Figure 11.3.32A, n=3), whereas the isotype antibody control does not cause a blocking response at any concentration, confirming results are due to FE8 specific actions. Ramos cell activation status is not affected by FE8 or isotype antibody. sCD21 blocks activation of Raji cells at a concentration of 132.9 nM (IC_{50}) (Figure 11.3.32B, n=3). sIL7R acts as a control for the addition of high concentrations of protein to the assay; no effect on activation is seen with the addition of this protein, confirming blocking effect of sCD21 is specific to the action of this protein. Again, no effect is seen with either protein on the activation status of Ramos cells. Physiological levels of sCD21 were shown to be ~2.75 nM; in this experiment this concentration of sCD21 is not sufficient to block activation of the Raji B cell line. However, sCD21 may still have the capacity to block activation of B cells in vivo. B cells are predominantly activated within the Germinal Centre and it is not known how much C3dg is present within these microstructures, if C3dg levels are lower than that used in this assay, lower concentrations of sCD21 would be needed to block B cell activation. This assay used the lowest concentration of C3dg (0.3 µg/ml) sufficient to observe an assay window for activation, therefore the assay is working at the limits of detection and lower concentrations of this reagent could not be used.

Additionally, the germinal centre is a closed system which could result in local concentrations of sCD21 having a greater impact on activation status of B cells than within the current assay.

It was shown that within this system, C3dg and low anti-IgM concentrations synergistically stimulated Raji cells to levels equivalent of stimulation with high anti-IgM concentrations (Figure 11.3.26). In this experiment cells were also stimulated with high anti-IgM (1 µg/ml) and, to further demonstrate that sCD21 and FE8 block through the C3dg-dependent co-activation mechanism, FE8 (120 nM) and sCD21 (1250 nM) were added to this stimulation. Activation of Raji cells with high anti-IgM concentrations was not blocked by either reagent (Figure 11.3.33A), cells remain around 13% pERK+ve, similar to stimulation with the activation complex (0.3 µg/ml C3dg, 0.3 µg/ml anti-IgM and 1 µg/ml neutravidin). The same is true of activation of Ramos cells with high anti-IgM concentrations alone, however a difference is noted in the levels of activation seen between high anti-IgM stimulation and stimulation with the activation complex (0.3 µg/ml C3dg, 0.3 µg/ml anti-IgM and 1 µg/ml neutravidin). As Ramos cells do not respond to co-activation with C3dg, cells activated with the complex are ~20% pERK+ve, whereas cells activated with high anti-IgM are ~80% pERK+ve (Figure 11.3.33B); this is due to cells responding only to anti-IgM stimulation.

These data sets reveal a role for sCD21 in binding C3dg and blocking B cell activation which could act as a mechanism to control the immune response to C3dg-dependent stimulation.

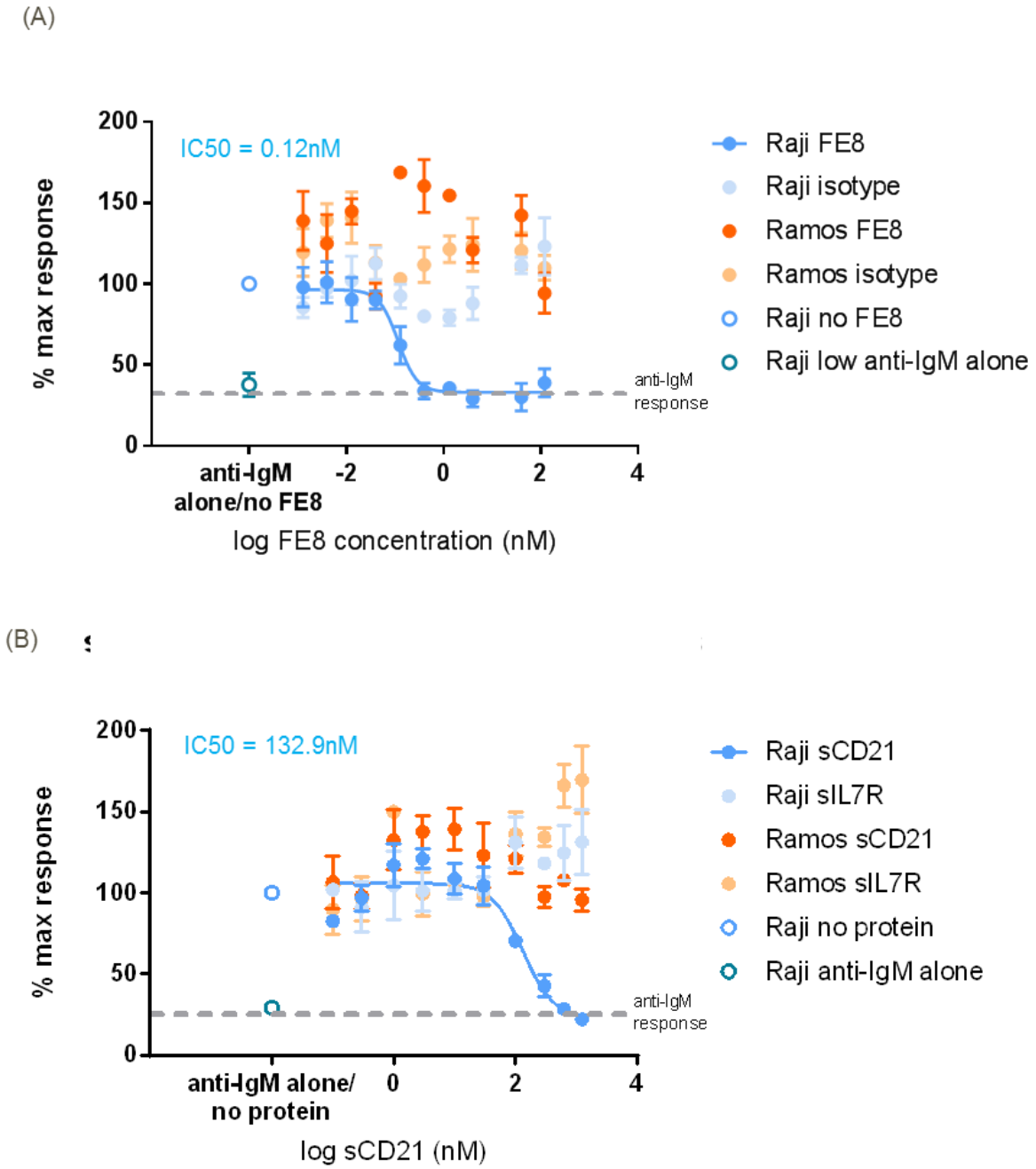

Figure 11.3. 32: sCD21 and FE8 block CD21+ Raji B cell line activation in a concentration dependent manner

n=3 individual experiments, bars represent SD. (A) FE8 blocks CD21 positive cell activation in a concentration dependent manner. IC50= 0.12nM. FE8 has no effect on CD21 negative Ramos cells. No response to isotype antibody concentrations is seen with either cell type. (B) sCD21 blocks activation of CD21 positive cells in a concentration dependent manner. IC50= 132.9nM. sCD21 has no effect on activation of CD21 negative Ramos cells. sIL7R protein has no effect on activation in either cell type.

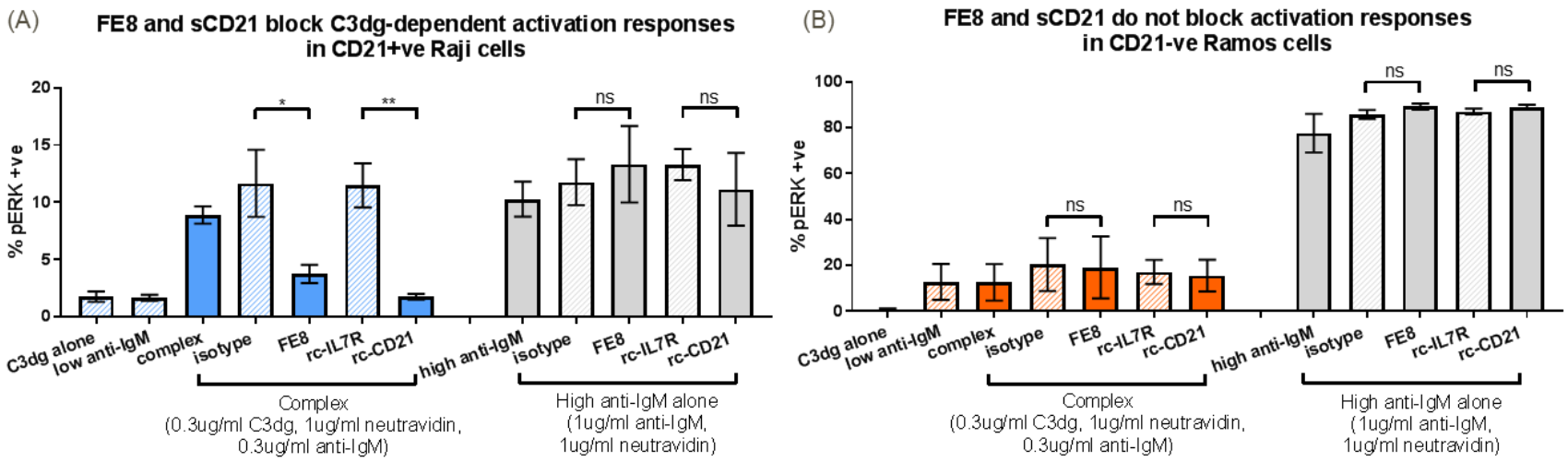

Figure 11.3. 33: sCD21 and FE8 block C3dg-dependent activation of CD21+ Raji B cell lines

n=3 individual experiments, bars represent SD, significance tested using ANOVA. (A) FE8 and rc-CD21 block activation of B cells with stimulation complex made with neutravidin, C3dg and low concentrations of anti-IgM. Reagents do not block activation of Raji cells stimulated with high anti-IgM concentration. Addition of isotype antibody and the random protein IL7R have no effect on activation. (B) FE8 and rc-CD21 do not block the low level of activation seen with stimulation complex on Ramos cells. Stimulation with high anti-IgM causes an increased activation response. Addition of isotype antibody and the random protein IL7R have no effect on activation.

11.4 Discussion:

This chapter focuses on the role of the soluble form of the CD21 receptor in health and disease. It is well documented in the literature that sCD21 is decreased in many autoimmune diseases such as Rheumatoid Arthritis (Masilamani et al., 2004). These reports lead to the hypothesis that sCD21 inhibits C3dg antigen complexes from binding to B cells, consequently preventing activation of these cells and thus dampening C3dg-mediated immune responses. Therefore, it is possible that a decrease in sCD21 concentration results in pathogenic B cell responses and disease as this break on the immune system is depleted in these systems.

The first aim of this work was to further investigate this decrease in sCD21 in disease using serum samples from RA patients and age-matched healthy volunteers. Age-matching the healthy samples to that of the RA serum samples was important as sCD21 levels have been shown to decrease with age (Masilamani et al., 2004); an observation that was mirrored in this data (Figure 11.3.4). As the majority of RA patients are between the ages of 45-70yrs, and in healthy volunteers sCD21 is decreased compared to subjects of ages >25yrs, this natural decrease may be a reason why age is a risk factor of development of RA, however when sCD21 concentration in RA patients was compared with their age, no correlation to suggest older patients have less sCD21 than younger patients were observed (Figure 11.3.5). Analysis of sCD21 concentration within the serum from RA patients revealed a further decrease compared to levels found in healthy volunteers (Figure 11.3.4).

To further investigate these findings, sCD21 concentration in RA patients was considered in relation to disease severity (DAS28 score). Results revealed that an increase in disease severity correlated with a decrease in sCD21 concentrations (Figure 11.3.7). This observation implicates sCD21 as a marker of disease severity and a contributor to manifestation of RA.

Additional evidence to add to the observation that lower sCD21 concentration lead to an increased disease phenotype comes from analysis of longitudinal patient data. sCD21 concentration was shown to increase in patients after treatment with methotrexate and various topical steroids 6 months after entering the clinic (baseline) and increase further still after 12 months of treatment (Figure 11.3.8A). Disease severity (DAS28 score) was also shown to decrease over the time points measured in these patients (Figure 11.3.8B). These data suggest there is a correlation between the increase in sCD21 concentrations and the decrease in disease severity.

Serum samples taken from patients pre- and post-rituximab treatment revealed a further decrease in sCD21 levels after treatment (Figure 11.3.9). As rituximab is a depleting monoclonal antibody against CD20, it can be assumed that these patients are deficient or have decreased number of B cells, excluding plasma cells which do not express CD20. Thus, these results give indication of the origin of sCD21; as sCD21 concentrations decrease upon B cell depletion it is reasonable to suggest these cells as a source of sCD21. Data from this study has suggested that lower sCD21 concentrations further increases the severity of disease, however as B cell subsets are known to be pathogenic within RA (Abrahams et al., 2000), depletion of these cells removes a major mediator of disease, allowing resolution and improvement of symptoms independent of sCD21 concentrations.

The source of sCD21 was further investigated using a hu-mouse model. NSG-SGM3 mice reconstituted with human $CD34^+$ cells were shown to express human cell surface markers for T and B cells (CD3 and CD19 respectively) (Figure 11.3.11), but did not express human CD35, CXCL13 or CCL21, suggesting that human stromal cells, FDCs and FRCs, were not present within these mice (Figure 11.3.11). Human CD21 however was detected in splenic mRNA, presumably from expression by human B cells as FDCs were thought to be absent. Immunohistochemical analysis further confirmed these observations, revealing positive staining for hCD3 (Figure 11.3.12), hCD19 (Figure 11.3.13) and hCD21 (Figure 11.3.13) and an absence of hCD35 staining (Figure 11.3.14). Thus, this humanised mouse model

develops human T and B cells but not FDCs. As FDCs do not develop from the haematopoietic lineage, this was expected after reconstitution by the chosen method. This analysis also revealed that the secondary lymphoid organs were disorganised, potentially an indication that development of human cells was not complete and cells may not respond in the same ways as in human SLOs.

When investigating the presence of sCD21 within the serum of the humanised mouse model, levels of this protein were not detected, suggesting these mice do not produce the soluble version of this protein. However, this result may be due to the low concentration of serum used; only a small volume of serum was available which was required to be diluted 1in4 in order to run the assay in duplicate, therefore this may have diluted the sample too far to detect the presence of sCD21 within the samples. Alternatively, B cells within this model do not secrete sCD21. This could be due to a number of reasons; the development of the cells may not be correct within the mouse model, expression of other factors such as IgG levels were not measured within these mice therefore it is hard to say if the B cells were responding in the correct manner. If development was not correct, perhaps expression of the signalling pathways or cleavage factors to produce sCD21 is not expressed within these cells. Additionally, as the SLO's in this model were shown to be disorganised (Figure 11.3.12); this could affect sCD21 production as the correct signals to produce the soluble protein may not be received within this environment. Therefore, this result does not rule out B cells as a source of sCD21 within humans.

B cell populations which down-regulate CD21 have been reported in RA (Isnardi et al., 2010). Data from the current study suggests B cells as a source of sCD21 production; therefore, if B cells in disease down-regulate CD21 on their surface, it is also plausible that less sCD21 is produced by these cells. Thus, $CD21^{-/low}$ may have another pathogenic response not yet explored. As sCD21 has been shown to have the ability to bind to C3dg and prevent binding to B cells in this and previous studies (Ling et al., 1991), this decrease would subsequently cause an increase in the number of C3dg-immune complexes available

to bind to and activate these and other autoreactive B cells. This is an alternative mechanism in which these $CD21^{-/low}$ cells could be contributing to the development and manifestation of autoimmune disease. Data presented in this investigation also showed that, in healthy volunteers, the number of CD21 receptors expressed on the cell surface of peripheral B cells, correlates with increased sCD21 concentration measured within the serum, again suggesting that sCD21 may be produced by these cells.

Additional evidence supporting B cells as an origin for sCD21 is the increased concentration of this protein within patients with B cell malignancies such as B cell chronic lymphocytic leukaemia (Ling et al., 1991) and EBV/EBV-associated malignancies (Larcher et al., 1995) compared with healthy individuals. As these diseases are characterised by an increase in the number of circulating B cells, it is probable that the increase in sCD21 correlates to this phenotype.

Next, the function of sCD21 was further investigated using C3dg-immune complexes. In the first experiment assessing function, the C3dg-strepavidinAPC complex was utilised to understand whether sCD21 can block the binding of C3dg to peripheral B cells. When binding was previously assessed in results chapter 2, a tetrameric C3dg complex was used to enable greater visualisation of binding on the cells of interest. In these experiments the concentration of sCD21 it was possible to add to the assay to block binding was a limiting factor, therefore exploration of the use of monomeric C3dg-strep complexes was further investigated. Theoretically, using a monomeric complex would result in a lower concentration of sCD21 required to block all C3dg molecules binding to membrane bound CD21 than that needed to block C3dg in a tetrameric form. Using monomers decreased the signal observed upon binding to cells compared with tetrameric complexes (Figure 11.3.20), but signal was still sufficient to allow visualisation of the ligand-receptor interaction. The decrease in signal when using monomeric complexes has been well studied (Altman et al., 1996); data showed that when weak ligand-receptor interactions occur, visualisation of these interactions can be observed by using tetrameric complexes. Complexes were blocked with high sCD21

concentrations (144 nM), resulting in complete blockage of binding of monomeric C3dg-complexes to B cells, similar to that of FE8 blocking (Figure 11.3.20). Partial blockage of tetrameric complex binding occurred when using the same sCD21 concentration (Figure 11.3.20). This confirmed that monomeric complexes were easier to block using sCD21 than tetrameric complexes, and since sCD21 concentration was the limiting factor in this assay, monomeric complexes were chosen for these experiments. Previous studies had reported that monomeric C3dg was unable to bind to rc-CD21 (Moore et al., 1989), however observations made in this investigation contradict this result. Experimental differences may be the cause of this discrepancy as the published study used sedimentation analyses to assess binding, which could not be observed under physiological conditions, but low levels of binding were seen at low ionic strength, whereas this study assessed binding in an *in vitro* flow cytometry assay. Other publications have shown tetrameric C3dg to augment B cell activation, whereas monomeric C3dg inhibits these responses (Bohnsack et al., 1988). It is possible that within this study, binding of monomeric C3dg-complexes to peripheral B cells caused inhibition of activation, but as this particular experiment was investigating sCD21's ability to block C3dg binding to CD21 on the surface of B cells, the resultant activation response was not of interest.

sCD21 was shown the block C3dg binding to peripheral B cells in a concentration dependent manner. Interestingly, full-length rc-CD21 was able to block binding more effectively than the ligand binding site only, SCR1/2, shown by the reagents having IC_{50} values of 3.94 nM and 19.42 nM, respectively (Figure 11.3.21). Surface plasmon resonance studies investigating interactions between CD21 and C3dg reported Kd values for binding of C3dg to SCR1/2 and SCR1-15 (full length protein) as 22.4 nM and 27.1 nM, respectively (Ling et al., 1991). These binding kinetics suggest that the full-length protein has an increased affinity for C3dg than the binding site alone, as C3dg both associated and dissociated 10-fold slower from SCR1-15 and SCR1-2. These results correspond to the observation of increased binding of C3dg by full length sCD21 compared with SCR1/2 alone in this study. Together these results imply

that the full-length protein affects the kinetics of C3dg binding and hence improves the affinity for its ligand.

Physiological levels of sCD21 in healthy volunteers were found to be around 400 ng/ml; this is equivalent to 2.75 nM. At these concentrations, full length rc-CD21 can block binding of 0.02 µg/ml C3dg to peripheral B cells. It is unknown at what concentrations C3dg is found within physiology as C3dg specific reagents are limited. However, this data suggests that physiological levels of sCD21 can bind C3dg and therefore prevent the binding of immune complexes to B cells, preventing downstream C3dg-dependent pathways. It is possible that sCD21-C3dg complexes are then cleared using an unknown mechanism, and hence sCD21 acts as a break on the immune system. It is known that C3d levels are increased in RA and SLE (Morrow et al., 1983). As C3d is a precursor to C3dg, it is reasonable to suggest that this molecule is also increased in these diseases, although this has not been studied in the published literature. Interestingly this study showed that increased C3d levels were proportional with worsening disease activity in RA (Morrow et al., 1983). Together these data sets propose a mechanism in which a decreased sCD21 concentration in RA disease allows for increased availability of C3dg-immune complexes, as they are no longer bound by sCD21. These complexes are then able to bind to B cells causing activation of potentially pathogenic cells resulting in an increase in disease prevalence. This mechanism would explain an increase in disease severity with a further decrease in sCD21, as the lower concentration of sCD21 present in the serum allows more C3dg to activate B cells.

To further develop this model, experiments investigating the ability of sCD21 to block B cell activation were undertaken. For these studies B cell lines were utilised due to the inconsistent and unreliable results generated using primary B cells. Raji cells were chosen as the $CD21^+$ B cell line as they expressed IgM receptors at a similar level to that of primary B cells in comparison to the other $CD21^+$ cell line considered for these experiments, Daudi (Figure 11.2.23). $CD21^-$ Ramos cells were used as a negative control, to ensure that responses seen were CD21-dependent.

For these experiments' cells were activated using a stimulation complex composed of C3dg, anti-IgM and neutravidin. This complex will activate cells through membrane bound IgM receptors and the CD21/CD19 complex. This co-activation has previously been reported to lower the threshold for activation of B cells (Carter et al., 1992), data which is reproduced in the $CD21^+$ Raji cell line (Figure 11.3.25A). Activation with the stimulation complexes was shown to be synergistic in that, although C3dg (0.3 µg/ml) and low anti-IgM (0.3 µg/ml) do not activate cells individually, together they activate $CD21^+$ cells to levels similar to stimulation with high anti-IgM (1 µg/ml) (Figure 11.3.26A). Interestingly, high concentrations of C3dg alone (1 µg/ml) cause activation of $CD21^+$ cells, but again co-activation occurs with anti-IgM. This was also reported by Tsokos et al., (1990), whom first suggested that crosslinking CD21 and IgM ligand would further increase B cell responses compared to multivalent C3dg only. These observations are CD21/C3dg-dependent as these effects were not seen in $CD21^-$ Ramos cells, which were only activated with anti-IgM in a concentration dependent manner (Figure 11.3.26B).

It was shown that co-ligation of C3dg and anti-IgM using neutravidin was essential for this co-activation effect to occur (Figure 11.3.27). In the absence of neutravidin, activation only occurs through anti-IgM stimulation. In the absence of neutravidin, C3dg is most likely to be in a monomeric form. It is reported in this study that monomeric C3dg is able to bind to CD21, whereas other studies have published conflicting data using monomeric C3dg (Moore et al., 1989), reporting an inability of monomeric C3dg to bind to rc-CD21. As the same batch of biotinylated-C3dg was used in these experiments as in C3dg binding experiments, it is assumed that monomeric C3dg is able to bind CD21 in these experiments, but B cell activation is not enhanced when this occurs. The absence of an activation response using monomeric C3dg is supported by previously published data reporting inhibition of B cell activation when using monomeric C3dg-complexes (Ling et al., 1991). Within the same study, stimulation with tetrameric complexes augmented activation responses. The stimulation complex used in these experiments mimics an C3dg-antigen complex found in

physiology; neutravidin acting as the antigen which would be bound with antibody, anti-IgM, and C3dg. Therefore in vivo C3dg-antigen complexes are able to bind to membrane bound IgM and CD21 simultaneously, causing increased Lyn recruitment and subsequent activation of cell signalling pathways leading to increased MEK activation which phosphorylates ERK leading to B cell activation, proliferation and development (Bojarczuk et al., 2015). Taken together, these results suggest that if monomeric C3dg (i.e. not within complex with antigen and antibody) binds CD21, B cells do not respond. This could be a potential mechanism to prevent over-activation of B cells in the presence of free-C3dg; in addition to sCD21 preventing C3dg binding membrane bound CD21.

A stimulation complex containing the final molar ratios of 5:2.5:1 neutravidin:C3dg:anti-IgM revealed the greatest assay window for stimulation compared with activation with low anti-IgM (Figure 11.3.31) so was determined as the most suitable for blocking experiments with sCD21 and CD21 blocking antibody clone, FE8. Both sCD21 and FE8 were shown to block activation of $CD21^+$ B cell lines in a concentration dependent manner (Figure 11.3.32A and Figure 11.3.32B, respectively). FE8 binds to the receptor on the cell surface to block binding of C3dg, and hence co-activation of B cells. The IC_{50} for this blocking effect is 0.12 nM, previous experiments using this antibody to block the binding of C3dg to primary B cells revealed 0.06 nM FE8 is needed to block the binding of C3dg tetrameric complexes to these cells. Receptor numeration revealed Raji cells express 2.5-fold more CD21 receptors on their cell membrane than primary B cells, ~20,000 and ~8,000 receptors, respectively (Figure 11.3.23C). This increase in receptor number is responsible for the increased FE8 needed to block binding and subsequent C3dg-dependent activation. sCD21 blocks activation by binding to the ligand, C3dg. The IC_{50} of sCD21 is 132.9 nM, which is much higher than that found in physiology, 2.75 nM. Therefore, under these conditions, physiological concentrations of sCD21 do not block activation of $CD21^+$ B cell lines. As this B cell line expresses 2.5-fold more CD21 receptors than primary B cells, it is assumed less sCD21 would be needed to block activation of B cells in vitro. As the concentration of C3dg

within the germinal centre, where most of B cell activation occurs, has not been measured, it is hard to determine what concentration of sCD21 is needed to block C3dg-dependent activation responses. Additionally, within these systems, blockage of all C3dg-responses would cause defects in the immune response; therefore it is likely that in physiology C3dg is in excess to sCD21. The sCD21 that is present is acting to ensure over activation of B cells does not occur, binding some but not all C3dg-immune complexes, again acting as a brake on the immune system.

Blockage of activation using FE8 and sCD21 was shown to be C3dg/CD21-dependent as no effect was observed on activation of Ramos cells (Figure 11.3.24B). Additionally, activation with high anti-IgM concentrations could not be blocked with these reagents on either cell type (Figure 11.3.24).

To summarise, data presented in this chapter shows that sCD21 concentrations decrease with age and further in autoimmune disease, in this case RA (Figure 11.3.4). sCD21 concentration directly correlates to disease severity (Figure 11.3.7) and increasing sCD21 concentration upon treatment of disease also correlate with a decrease in disease phenotype, suggesting a role for sCD21 in pathology. Rituximab treatment further decreases sCD21 concentration in RA patients (Figure 11.3.9), suggesting B cells are a source of sCD21. The function of sCD21 was further investigated and was shown to have the ability to block C3dg binding to peripheral B cells and block the activation of $CD21^{+}$ B cell lines.

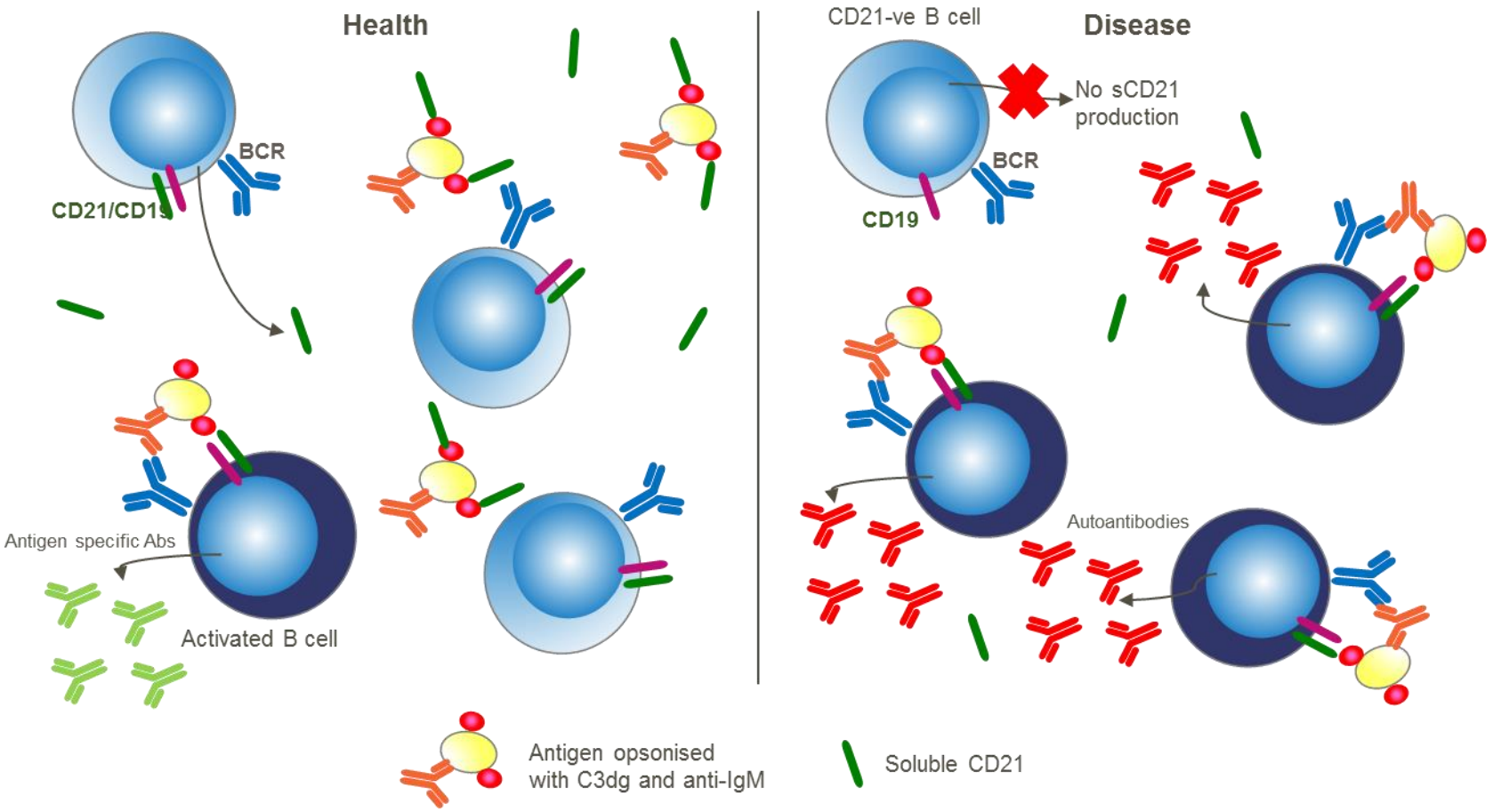

Figure 11.4. 1: A role for sCD21 in health and disease

Within health sCD21 is produced by B cells and prevents binding of opsonised immune complexes to B cells, hence modulating the activation of the immune response. In disease, CD21 negative B cells do not produce sCD21, therefore the decrease in soluble protein concentration leads to opsonised antigen complex binding to B cells and overactivation of the immune response.

Taking these observations into account, the following model for sCD21's role in health and disease is proposed. In health, sCD21 is produced by B cells at concentrations sufficient to allow C3dg-complexes to bind antigen-specific B cells and produce specific antibody responses, but still block excessive C3dg-mediated activation, therefore acting as a break on the immune system. In autoimmune disease phenotypes, such as Rheumatoid Arthritis, autoreactive B cell downregulate CD21 expression and can self-regulate through multiple different pathways; the decrease in CD21 expression by these cells leads to a decreased production of sCD21. A decrease in sCD21 allows all C3dg-immune complexes to activate autoreactive B cells, resulting in autoantibody production and pathogenic B cell responses, manifesting itself as disease. Therefore, the lower the concentration of sCD21, the more severe the disease, as a greater immune response can be elicited with the removal of sCD21 acting as a break on B cell activation responses (Figure 11.4.1).

This mechanism and the data presented here supports the hypothesis of this work, suggesting that sCD21 can inhibit C3dg-mediated immune responses and decreased sCD21 levels remove this break on the immune system, resulting in pathogenic B cell responses and disease.

12. General Discussion

12.1 Thesis hypothesis and aims

This thesis focused on exploring the roles of CD21 in the germinal centre as a membrane bound receptor and within the periphery as a soluble protein.

As the essential function of CD21 in the GC response relies on the transfer of C3dg-opsonised antigen transfer from CD21 on B cells to FDCs, it was important to further investigate how this unidirectional transfer may occur between the two cell types. A clear mechanism for this transfer is not currently described within the literature, and most studies are carried out within murine models. These studies lead to suggestions that unidirectional transfer of antigen could occur due to cell size (Heesters et al., 2014) or increased receptor numbers on FDCs compared to that on B cells (Phan et al., 2007). These observations, together with the differential expression of CD21 isoforms by these two cell types, lead to the following hypothesis; *C3dg-opsonised antigen transfer between human FDCs and B cells is due to (1) CD21 receptor number on the cell surface and/or (2) the CD21L isoform expressed by FDCs having a higher affinity for C3dg than CD21S, expressed by B cells.*

This work further investigated the functions of the soluble form of the CD21 receptor by analysing the potential mechanisms of the decrease in sCD21 levels observed in serum from patients with autoimmune disease. Due to the observation of decrease sCD21 in disease, I hypothesised: *a key function of sCD21 is to act as a break on the immune system preventing C3dg-mediated immune responses. The decrease in sCD21 levels in disease, removes this break on the immune system and therefore, overactivation of pathogenic B cells and the immune response can occur, subsequently resulting in disease phenotypes.*

These hypothesise lead to the following thesis aims:

1) Isolate and characterise human FDCs from human tonsil. Assess CD21 absolute receptor number on FDCs (tonsil derived), T and B cells (tonsil and blood derived).

2) Assess C3dg binding capacity of CD21 on FDCs (tonsil derived) and B cells (tonsil and blood derived), investigating potential functionality differences between CD21S and CD21L isoforms.
3) Further understand the function and role of sCD21 in healthy volunteers and disease patients.

12.2 Summary of results and significance

12.2.1 Unidirectional transfer of C3dg-opsonised antigen complexes between B cells and FDCs

12.2.1.1 CD21 receptor number expression on FDCs and B cells

Histological studies on human tonsil and lymph node tissue, confirmed cell specific expression of known markers as well as cellular interactions within the germinal centre microarchitecture. These data allowed identification of FDCs as $CD35^{+}CD21^{+}CXCL13^{+}$ cells (Figure 9.3.1, 15 and 12 respectively) and B cells as $CD19^{+}$ cells (Figure 9.3.1). It is known that B cells also express CD21 on their cell surface, confirmed using qPCR (Figure 9.3.11) and flow cytometry analysis (Figure 9.3.13). However, in alignment with other published studies (Naiem et al., 1983), these cells were not found to be $CD21^{+}$ within FDC zones using immunohistochemistry techniques. This was the first indication within this study that CD21 receptor number expression may differ between FDCs and B cells; resulting in a masking of the CD21 staining on the B cells by the high expression of membrane bound CD21 receptors on FDCs. CD21 antibody clones, R4/23 (Naiem et al., 1983) and 7D6 (Lui et al., 1997), have been reported as FDC specific antibodies and, therefore, CD21L specific, with weak reactivity to B cells outside of FDC zones. Results from these studies were interpreted as FDC specificity rather than considering possible differences in receptor number expression or relative affinities of the antibody clones. Results within this study confirmed that R4/23 was able to recognise CD21S expressing cells (Figure 10.3.10), therefore was not specific for the long form of CD21. Additional experiments staining human tonsil B cells in areas devoid of FDCs using the antibody clones Bu32 and R4/23, utilised within this study, to confirm identification of CD21 expression on these cells in the absence of FDCs, would further support this concept.

These studies also showed that CD19 expression could be visualised on B cells using IHC, however, FDCs appear negative for this marker (Figure 9.3.1). In contrast with these observations, a low level of CD19 expression has been reported at the mRNA level within

FDCs within these studies (Figure 9.3.11) and previously published data (Barrington et al., 2009). As with the lack CD21 staining visualised on B cells, the reason for these discrepancies is thought to be due to the high number of CD19 receptors expressed by B cells and this consequently masks CD19 staining of the receptor on the FDC surface. The role of CD19 on FDCs remains unclear. On the B cell surface, CD19 is expressed in molar excess to CD21 and therefore it is thought that all CD21 receptors are contained within the CD19/CD21 complex (Fearon et al., 2000) acting to lower the threshold for activation of the B cell (Carter et al., 1992). As CD21 is expressed in excess of CD19 in FDCs, the majority of the CD21 receptors will not be contained within the CD19/CD21 complex; these observations suggest that the role of CD19 on FDCs is unlikely to be cell activation. Interestingly, CD81, the tetraspanin molecule involved in anchoring the CD19/CD21 complex in B cells, is highly expressed by murine FDCs (Rodda et al., 2018), therefore it is possible that the CD21 receptor and this protein are still in close association on the FDC, but this has not been investigated at present. As CD81 has been shown to traffic CD19 along the secretory pathway, it is possible that together these proteins have a role in the internalisation and recycling of CD21 receptors to the FDC cell surface, although there is no evidence at present to suggest this be the case.

There are limited protocols available within the literature for the isolation of human FDCs. Replication of available methods proved unreliable and results were not reproducible using human tonsil tissue. Therefore, a robust isolation method of human FDCs from human tonsil tissue was developed to enable further assessment of CD21 functionality on this cell population. The method detailed in Materials and Methods Section 8.2 produces replicable results for the isolation of human FDCs from tonsil tissue and this protocol was successfully utilised to allow the following investigations on human FDCs and CD21 receptor biology.

To address the hypothesis that transfer of C3dg-immune complexes from B cells to FDCs occurs due to receptor number, absolute CD21 receptor number on the cell surface was determined on isolated human FDCs (tonsil derived), T and B cells (tonsil and blood

derived), something that has not previously been reported in the current literature. Results revealed that FDCs express over 30-fold more CD21 receptors on their cell surface than B cells, ~150,000 versus ~8000 receptors (Figure 9.3.16). As FDCs are ~10-fold larger than B cells, the density of CD21 receptors on these cells is around 3-fold greater than that on B cells. Therefore, it is possible that the increased size of these cells, along with the high receptor number on the cell surface, allows for unidirectional transfer to occur as a result of increased binding of CD21 receptors to available C3dg ligands on the immune complexes. Spacing of antigen complexes, and hence CD21 receptors, on the FDC membrane has been studied using electron microscopy (Shikh et al., 2010). Antigen complexes were spaced periodically 200 to 500 Angstroms apart on the FDC cell membrane; this spacing was thought to be optimal for FDC-immune complexes to engage multiple BCRs simultaneously. In terms of antigen transfer, this spacing suggests that FDCs can bind to multiple C3dg molecules on opsonised immune complexes, creating greater contracts with the complex than that by the B cell. Increased interactions between the cell and the complex could lead to transfer of the complex through dissociation of the ligand off the B cell surface and/or internalisation of CD21 receptors, leading to the removal of complexes from CD21 on B cells.

Investigations using murine B cells and FDCs, lead to suggestions that unidirectional transfer of C3dg-antigen complexes could occur due to cell size (Heesters et al., 2014) and/or, CD21/35 receptor number (Phan et al., 2007). This study showed that murine FDCs expressed higher numbers of CD21/35 receptors than B cells; although absolute receptor number quantification was not reported. Together with the data presented here, these observations suggest antigen transfer likely occurs due to the increased density of CD21 receptors on the surface of FDCs, leading to increased interactions between the cell and C3dg-opsonised immune complexes. Therefore, these interactions may be important in the successful competition with migrating B cells for the capture and retention of noncognate immune complexes.

12.2.1.2 C3dg binding functionality of CD21 on FDCs and B cells

The second part of the transfer hypothesis regards the differential expression of CD21 isoforms on FDCs and B cells. FDCs are known to express the long form of CD21 and B cells express the short form (Figure 10.3.7). The short form of the receptor is made of 15 SCR protein units, whereas the long isoform has an additional SCR in the middle of the protein (Figure 10.1.2), bringing the whole protein to a total of 16 SCRs. It is possible that these two isoforms have differential binding affinities for their ligand, C3dg, consequently leading to unidirectional transfer between the short isoform on the B cells to the long isoform on FDCs.

To investigate ligand binding by CD21 receptors, a C3dg immune-complex was used, consisting of mono-biotinylated C3dg complexed to a Streptavidin-APC molecule to form a tetramer (Figure 11.3.20). The use of tetrameric complexes in these experiments suggests that the interactions between receptor and ligand are of low affinity; an artefact that was demonstrated using tetrameric complexes of T cell antigen to visualise weak ligand-receptor interactions on a population of T cells expressing specific TCRs (Altman et al., 1996). Interestingly, previous studies have shown that monomeric C3dg does not bind to recombinant CD21 under physiological conditions (Moore et al., 1989), although this was not the case in this investigation (Figure 11.3.20). Monomeric C3dg was shown to have the ability to bind to CD21 in flow cytometry experiments, however it was still important to use a tetrameric complex for binding assays due to the increased assay window created by the increased valency of the complex and thus increased binding of membrane bound receptors (Figure 10.3.1B).

This C3dg immune complex was shown to bind the FDCs, T and B cells in a concentration dependent manner (Figure 10.3.4). As only ~20% of T cells express very low levels of CD21, ~200 receptors per $CD21^{+}$ cell (Figure 9.3.16), these cells were no longer investigated as part of this work as the expression of this receptor is unlikely to be physiologically relevant.

The hypothesis of differential ligand binding affinity by receptor isoforms was assessed by investigating C3dg binding to CD21 in the presence of a blocking CD21 antibody clone, FE8, which was shown to prevent binding of C3dg to CD21 receptors (Figure 10.3.5) and is known to bind to an epitope spanning SCR1/2 (Wolfgang et al., 1998), the ligand binding site of this receptor. This antibody was shown to block binding of C3dg immune-complexes to FDCs (tonsil derived) and B cells (tonsil and blood derived) in a concentration dependent manner (Figure 10.3.6). Blockage of C3dg binding to CD21 on human tonsil derived B cells using FE8 has been previously reported (Wolfgang et al., 1998), but experiments using human FDCs and B cells derived from the periphery had not been undertaken. The IC_{50} of FE8 blocking C3dg binding to FDCs was shown to be 6-fold higher than that of B cells, which was the same in cells derived from tonsil and blood, 0.4 nM, 0.06 nM and 0.07 nM, respectively. This increase in IC_{50} was predicted due to the increased receptor number on the surface of FDCs, therefore more antibody is needed to block the binding sites of C3dg. However, receptor numeration experiments revealed FDCs express over 30-fold CD21 receptors on their surface than B cells (Figure 9.3.16), therefore a 6-fold increase in IC_{50} is surprisingly low in relation to the increased number of receptors FE8 needs to bind to prevent C3dg immune complex binding to all receptors on the FDC surface. This data may imply that CD21L expressed on FDCs has a lower affinity for its ligand, C3dg.

To further investigate these results, a specific CD21L antibody was needed to ensure the results were due to isoform expression. Clones, such as Bu32, recognise total CD21; therefore bind to an epitope present in both the long and the short isoform of CD21. The CD21 antibody clone, R4/23, was reported to bind specifically to FDCs and therefore said to recognise the long isoform of this receptor (Naiem et al., 1983). Antibody staining patterns in tonsil tissue using this CD21 antibody clone revealed only the expression of CD21 on FDCs, like the published report (Figure 10.3.8). However, staining with the CD21 antibody Bu32 also reveals the same staining pattern, in that CD21 expression on B cells are not detected (Figure 9.3.6) due to an increased number of CD21 molecules expressed on the surface of

FDCs compared to B cells, not differential isoform expression. Therefore, high CD21 receptor numbers on FDCs leads to a bright staining pattern that masks signal from CD21 stained B cells. Further investigations using the R4/23 antibody revealed that, although the antibody may preferentially bind CD21L, it is not specific for this isoform. Using the antibody clone R4/23, CD21S or CD21L isoforms derived from transfected HEK293T cells both in a membrane bound form using flow cytometry (Figure 10.3.10) and as a soluble protein by ELISA (Figure 10.3.11). Therefore, reports that these CD21 antibody clones are specific for FDCs and the CD21L isoform are not correct.

Due to the lack of available isoform specific CD21 reagents and therefore the ability to determine specific protein isoform expression on the cell surface of FDCs and B cells by flow cytometry, the transiently transfected HEK293T cells expressing CD21 were utilised to further investigate C3dg immune complex binding by the two CD21 isoforms. On average, the transfected cell lines expressed similar numbers of CD21 receptors (~15,000 receptors per cells, Figure 9.3.16), any changes observed in C3dg-binding between these cell lines can be said to be due to the isotype expression. C3dg was shown to bind in a concentration dependent manner to both receptor isoforms; however, cells expressing the CD21S protein bound an increased amount of C3dg at higher complex concentrations (Figure 10.3.13B). This could suggest that the short isoform has a higher affinity for its ligand than the long, but further experiments to confirm this were beyond the scope of this work. Previously published experiments using surface plasmon resonance have been undertaken comparing the affinity of the ligand binding site, SCR1/2, and the full-length receptor, SCR1-15, for C3dg (Ling et al., 1991), revealing the full-length protein has an increased affinity for its ligand. To date, comparisons between the affinity of the short and the long isoforms for C3dg have not explored in this manner. Although the data presented here suggests little difference between the binding affinities of the two CD21 isoforms, it would be important to consider the off rates of C3dg to each of the receptors, and hence the stability of ligand-receptor interactions, before eliminating this mechanism as a possible method of antigen transfer altogether.

The CD21 antibody clone, FE8, was used to block the binding of C3dg immune complexes to these isoform specific cells (Figure 10.3.13C). Data showed that there was no change in IC_{50} for the blockage of ligand binding by FE8 to either isoform; this confirms that the additional SCR added in the long isoform of CD21 does not change the binding site, SCR1/2, as FE8 is able to bind to both receptors with equal affinity. Thus, it is unlikely that the affinity for the receptor for C3dg is changed between isoforms, potentially disproving the hypothesis that differential isoform expression is responsible for unidirectional transfer of antigen between B cells and FDCs.

12.2.2 The function of sCD21 in health and disease

12.2.2.1 sCD21 levels decrease in autoimmune disease

It is known that sCD21 levels change in disease; in autoimmune diseases, for example Rheumatoid Arthritis, sCD21 levels decrease. Data presented here confirmed this observation, firstly demonstrating that age matched healthy donors must be used due to a decrease in sCD21 levels with age and secondly, repeating observations from the literature, confirming that sCD21 levels decrease in RA (Figure 11.3.4). A correlation between sCD21 levels and disease severity, assessed by DAS28 score revealed that lower sCD21 concentrations are found in patients with more severe disease (Figure 11.3.7), therefore suggesting a role for sCD21 in disease modulation. This relates to the hypothesis that sCD21 acts as a break on the immune system, preventing C3dg-antigen complex binding to B cells, consequently dampening C3dg-mediated immune responses. As sCD21 levels are decreased in RA, this break on the immune system does not occur, allowing pathogenic B cell responses to occur.

Interestingly, further supporting this hypothesis, when following the treatment of RA patients over time, sCD21 concentrations increase followed by a decrease in disease severity upon treatment with steroids and other conventional drugs.

Further investigation of RA patients treated with Rituximab, a human CD20 depleting monoclonal antibody resulting in the removal of B cells upon administration, revealed a further decrease in sCD21 concentration in the serum after treatment (Figure 11.3.9). This data suggests B cells may be the source of sCD21, as removal of these cells decreases the concentration of protein detected. Further investigations were carried out using a humanised mouse model which was shown to express CD21 at the mRNA level and develop human B cells but not FDCs (Figure 11.3.11). The presence of sCD21 within the serum of these mice was investigated as if this protein was detected this would further suggest that the B cells are an origin of the soluble form of CD21. Unfortunately, sCD21 was not detected within the serum of these mice, however this does not rule out B cells as the source of the protein as SLO's within these mice were highly disorganised (Figure 11.3.12), suggesting the human T and B cells within these animals were not properly developed, a factor that could also be affecting the production of sCD21 by these cells.

Within the published literature, there is evidence for B cells as the source of sCD21, but this is not currently confirmed. Analysis of culture media from human T and B cells revealed the presence of sCD21 (Fremeaux-Bacchi et al., 1996) showing these cells have the ability to release this protein from their cell surface *in vitro*. B cells have also been induced to shed membrane bound CD21 by crosslinking the BCR and CD40 (Masilamani et al., 2003). As CD21 expression is lost during differentiation of B cells into B-blastoid cells, a role for CD21 shedding and sCD21 in the initial steps of B cell activation during the immune response is suggested. This observation further adds to the work demonstrated here. As cells become activated during the immune response, sCD21 is shed from the B cell surface, thereby potentially preventing the overactivation of the immune response by modulation of C3dg-mediated responses by this addition sCD21.

Clinical observations of increased sCD21 levels in diseases with increased B cell numbers (Lowe et al., 1989) and decreased levels of sCD21 in patients with defective CD21

expression on B cells (Ling et al., 1991), also provide strong evidence that these cells are the source of sCD21.

Of course, as it is known that B cells depletion in mice leads to loss of FDCs in mice (Anolik et al., 2008), FDCs cannot be disregarded as a potential source of sCD21. In this model, the removal of B cells by treatment with rituximab would lead to a subsequent loss in FDCs and a resultant decrease in sCD21 concentration. FDCs have not been confirmed as a source of sCD21 in current published literature as culture of human FDCs for long periods of time is very difficult and without standardised protocols. Additionally, as T cells were shown to produce sCD21 (Ling et al., 1991), and the soluble protein can be detected with the culture media of these cells *in vitro* (Fremeaux-Bacchi et al., 1996), these cells may be responsible for the shedding of sCD21. Although this is a possible mechanism, it is not very probable due to the low CD21 receptor number expressed on T cells. Data presented in the current study revealed only ~20% of T cells (tonsil and blood derived) express CD21 and these cells were seen to have only ~200 receptors per cell; much lower than that of B cells and FDCs (Figure 9.3.16) and therefore these cells are unlikely to be the sole source of sCD21.

Publications have also reported a B cell population which down-regulate CD21 expression within patients with RA (Isnardi et al., 2010). As data from this study suggests B cells are a source of sCD21 production, downregulation of CD21 expression on the surface of these B cells may lead to a decreased concentration of sCD21 within the serum of these patients as sCD21 is thought to be cleaved from the cell surface by an unknown protease (M. Masilamani et al., 2003).

12.2.2.2 sCD21 blocks binding of C3dg to peripheral B cells

To further understand the role of sCD21 in health and disease, functional assays were undertaken, firstly using the C3dg immune-complex used in FE8 blocking assays. For these experiments a monomeric form of the complex was used; as the aim of the assay was to block C3dg binding to peripheral B cells, blockage of a monomeric form of C3dg would

theoretically need less sCD21 to prevent binding of ligand to CD21 receptors on the surface of B cells, and therefore it was more likely that a larger assay window would be observed for blockage of binding using the complex in this form. It has previously been reported that monomeric C3dg is unable to bind to rc-CD21 (Moore et al.,1989), however binding using the monomeric form of C3dg was observed to CD21 receptors on the surface of B cells in the current study. As the previous study used sedimentation analyses under physiological conditions to assess binding, whereas this data was generated using *in vitro* flow cytometry assays, differences in assay design may be the cause of this discrepancy and therefore perhaps binding of monomeric C3dg does not occur in physiology.

sCD21 was shown to block C3dg binding to peripheral B cells in a concentration dependent manner (Figure 11.3.21). It is published in the literature that C3d levels are increased in RA and SLE (Morrow et al., 1983), suggesting, as C3d is a precursor to C3dg, this molecule may also be increased within these diseases, although this is not published within the current literature. Exploration into the C3dg levels with the RA serum samples used in this report would have shed light onto this unanswered question, but due to the lack of C3dg-specific ELISA reagents commercially available, this was not investigated in the present study. The published study showed that increased C3d levels were proportional with increased disease activity in RA (Morrow et al., 1983), suggesting a mechanism in which the decrease in sCD21 within these patients leads an increased number of C3dg-immune complexes available to bind and activate cells as less C3dg is cleared by sCD21, resulting in worsened disease. This mechanism would explain the observation that decreased sCD21 levels correlate with an increased disease severity observed within the patients investigated within this study (Figure 11.3.7). Interestingly, C3dg is reported to have a plasma half-life of 4 hours (Teisner et al., 1983) and the estimated half-life of sCD21 is approximately 20 hours (Ciechanover et al., 1989). As sCD21 has the ability to bind to this protein, it is feasible to suggest that this action affects the half-life of C3dg by binding and clearing it from the system. If this were to be true, the half-life of C3dg within patients with lower sCD21 levels

would increase, leading to the increased levels found in the plasma and an increase C3dg-mediated immune response; another mechanism in which decreased levels of sCD21 could lead to increased pathology symptoms.

A recent publication reported that a fibroblast subset, characterised by the expression of podoplanin, THY1 membrane glycoprotein and cadherin-11, but lacking CD34, is expanded in patients with RA compared with those with osteoarthritis (Mizoguchi et al., 2018). These cells were shown to be proliferative and to secrete proinflammatory cytokines, therefore are thought to have a pathogenic role in the development of the RA disease phenotype, subsequently shown to be inflammatory sublining layer fibroblasts (Croft et al., 2019). It is known that an increase in synovial lining fibroblasts correlates with disease severity (DAS28 score) and disease duration (Izquierdo et al., 2011). Single cell analysis of synovial fibroblasts in both human and mice show that C3 is produced by the sublining inflammatory fibroblasts in the joint of both RA patient biopsies and in mice (Croft et al., 2019). The precursors C2 and C4 producing the C3 convertase are also expressed by fibroblasts. These results further suggest that there could be an increased concentration of C3dg produced within the joint of RA patients leading to a microenvironment for activation of pathogenic joint B cells. As sCD21 concentration is decreased within these patients and has been shown to have the ability to prevent the binding of C3dg to B cells, the “brake” is removed from the system and therefore this increase in C3dg is not removed and overactivation of the immune system can occur. These data further support the hypothesis that sCD21 could have an important role in the modulation of the immune response.

Two forms of sCD21 were used in experiments investigating the proteins ability to block C3dg binding to B cells; full length rc-CD21 and the ligand binding site only, SCR1/2. Interestingly, the full-length receptor blocks binding of C3dg more efficiently than SCR1/2, IC_{50} 3.94 nM and 19.42 nM, respectively (Figure 11.3.21). These results reflect published surface plasmon resonance studies investigating interactions between CD21 and C3dg (Ling et al., 1991). These studies showed that the Kd value for C3dg binding to SCR1/2 was lower

than that of the full-length protein, SCR1-15, 22.4 nM and 27.1 nM, respectively. This data also suggests that the full-length protein has a higher affinity for C3dg than the binding site alone, mirroring the data within this report. This is important as blockage of binding can still occur at physiological concentrations, ~2.75 nM sCD21, using full length receptor but does not occur at this concentration using the binding site alone.

12.2.2.3 sCD21 blocks activation of $CD21^+$ B cell lines

As it was shown that physiological concentrations of sCD21 can block binding of C3dg to its receptor, the next step in this investigation was to understand if the soluble receptor could block activation of B cells by disrupting C3dg-receptor interactions. It has been shown in the literature that C3dg lowers the threshold for activation of B cells (Carter et al., 1992), data which was replicated in this study (Figure 11.3.25). Experiments used a stimulation complex consisting of anti-IgM and C3dg, co-ligated with a neutravidin molecule (Figure 11.3.22). This co-ligation was shown to be essential to the co-activation action of C3dg (Figure 11.3.27). These studies, using B cell lines Raji and Ramos, $CD21^+$ and $CD21^-$ respectively (Figure 11.3.23A), showed that activation with anti-IgM occurs in a concentration dependent manner and that stimulation with anti-IgM/C3dg complexes causes increased activation of $CD21^+$ Raji cells (Figure 11.3.25A). This response was confirmed as CD21-dependent, as the addition of C3dg to the stimulation complex had no effect on $CD21^-$ Ramos cells, which are only activated by anti-IgM (Figure 11.3.25B). C3dg (0.3 µg/ml) was shown to synergistically activate $CD21^+$ Raji cells with low anti-IgM concentrations (0.03 µg/ml) (Figure 11.3.26A). Stimulation with these reagents alone had no effect on activation status of the cell, however together activation was observed at levels similar to stimulation with high concentrations of anti-IgM (1 µg/ml), therefore confirming that C3dg lowers the threshold for activation of $CD21^+$ B cells. This synergistic response was not seen in $CD21^-$ Ramos cells (Figure 11.3.26B).

Soluble CD21 and the CD21 blocking antibody, FE8, were then used to investigate whether blockage of B cell activation could be a role of sCD21, something that has not been

previously reported in human studies. Both reagents were shown to block activation of $CD21^+$ Raji cells in a concentration dependent manner using the chosen stimulation complex (1 µg/ml neutravidin, 0.3 µg/ml C3dg and 0.3 µg/ml anti-IgM) (Figure 11.3.31). Activation was not blocked in $CD21^-$ Ramos cells or cells stimulated with high anti-IgM concentrations alone (1 µg/ml) using these reagents, confirming the response was CD21- and C3dg-dependent.

Together these experiments support the hypothesis that sCD21 can block activation of B cells by binding to C3dg-opsonised immune complexes and preventing them from binding to membrane bound CD21 expressed by these cells. As these data have shown that sCD21 has the ability to bind C3dg, thereby preventing binding to CD21 (Figure 11.3.21) and co-activation of B cells (Figure 11.3.33), a decrease in sCD21 levels, seen in RA patient serum (Figure 11.3.4), would subsequently cause an increase in the number of C3dg-immune complexes available to bind to and activate these cells and other autoreactive B cells. Therefore, the lower the concentration of sCD21 within the system, an increased number of potentially harmful B cells can be activated; supported by the correlation between lower sCD21 concentrations in patients with more severe symptoms in RA (Figure 11.3.7). As this decrease in sCD21 could be due to a reduced expression of CD21 on B cells, the $CD21^{-/low}$ B cell population may have another pathogenic response that has not yet been explored. Together with observations that $CD21^{-/low}$ B cell populations fail to induce tyrosine phosphorylation cascades or increased concentrations of intracellular calcium upon BCR aggregation, both responses known to be enhanced by CD21/CD19 co-complex ligation to the BCR, the loss of CD21 and therefore the CD21/CD19 complex could lead to defects in B cell activation. Coligation of the CD21/CD19 complex to membrane IgM has been shown to lower the threshold for activation of B cells in this and previous studies (Carter et al., 1992), however, it has been reported that $CD21^{-/low}$ B cells up-regulate genes encoding molecules to increase B cell activation and proliferation (Isnardi et al., 2010) and are known to “bypass” T cell help in activation pathways by providing their own antigen complexes with C3dg

(Edwards et al., 1999). Due to these observations, it is feasible to suggest that, the CD21$^{-/low}$ B cell subset replaces the need for co-activation with CD21 and even stimulation through the BCR to allow proliferation, therefore the cells may be contributing towards their own survival.

12.3 Remaining questions and future work

12.3.1 Unidirectional transfer of C3dg-opsonised antigen between CD21 expressed on B cells and FDCs

The data presented in this study suggests that it is higher CD21 receptor number expression on FDCs compared to B cells that allows for unidirectional antigen transfer to occur rather than the differential expression of the long isoform of CD21 by FDCs.

Although FDCs were shown to express over 30-fold more CD21 receptors on their cell surface than B cells and the receptor density was predicted to be ~3-fold greater on these cells; experiments to confirm receptor density were not undertaken. Therefore, this remains a question to answer to further validate this mechanism of antigen transfer.

Results from experiments using FE8 to block binding of C3dg immune complexes to CD21 receptors on FDCs and B cells, as well as transiently transfected HEK293T cells expressing CD21S or CD21L, suggest that the CD21L isoform does not have higher affinity ligand interactions than that of CD21S, therefore this may not be the reason for unidirectional transfer of antigen complexes. To further expand on these observations, competition assays between C3dg and FE8 in which C3dg is pre-bound to CD21 receptors on the surface of the cell and FE8 is used to compete for binding of the ligand binding site could be undertaken. Previous studies have demonstrated that FE8 can remove prebound ligands from the CD21 receptor in B cells derived from human tonsil (Wolfgang et al., 1998), however the comparison between CD21 receptors on FDCs and B cells, and hence the two isoforms, has not been undertaken at present. These experiments would shed further light towards a

conclusion about potential differential affinity of the CD21 receptor for its ligands on FDCs and B cells.

Additionally, experiments to further investigate the differential affinity of C3dg binding between the long and the short isoform directly would include using immobilised long and short specific CD21 protein, SCR1-16 and SCR1-15 respectively, and surface plasmon resonance techniques. This has been done previously using the receptor binding site alone, SCR1-2, and the full-length receptor, SCR1-15, revealing the full-length receptor has a higher affinity for its ligand than the binding site alone (Ling et al., 1991). These experiments would further confirm binding affinity however it is also important to consider the K_{off} rate of C3dg from the different isoforms of CD21. It is possible that the long form of CD21 is able to bind to its ligand for a longer time period than CD21S and therefore the interactions between CD21L and its ligand may be more stable than that of CD21S. This could be another potential mechanism responsible for unidirectional transfer of C3dg between B cells and FDCs.

If this work was to be undertaken, the hypothesis that receptor number is responsible for unidirectional transfer, presented here, would be further solidified.

12.3.1 The function of sCD21 in health and disease

The remainder of the work in this thesis focused on the function of the soluble form of CD21. Data presented here suggests a role for sCD21 in the modulation of the immune response through binding C3dg-opsonised immune complexes to prevent activation of B cells.

pERK activation experiments were undertaken using B cell lines Raji and Ramos, due to the lack of replicable data obtained using primary B cells within these assays. To add further relevance to this data, and if additional time had been available, modifications could be made to the current protocol to allow assays to be undertaken in primary B cells that result in the production of more reliable data.

This report reproduced data from the literature, showing how sCD21 concentration decreases in the serum of RA patients compared to age-matched healthy volunteers (Figure 11.3.4). Additional observations were added to what is already know by assessing disease severity, which revealed a correlation between lower concentrations of sCD21 and a more prevalent disease phenotype (Figure 11.3.7). In contrast to the decrease in sCD21, it is known that C3d levels are increased in RA (Morrow et al., 1983), suggesting that C3dg may also be increased in these diseases. The increase in C3d and decrease in sCD21 suggests a lack of clearance of complement components may occur. It would be interesting to explore the concentration of C3dg within the RA patient samples used within this study and compare C3dg and sCD21 levels. This would confirm whether a decrease in sCD21 leads to the increase in complement found in RA. As no specific C3dg reagents are available at present, a C3dg-specific ELISA would need to be developed to investigate this question and measure protein levels within the serum.

Data from patients treated with Rituximab suggest B cells as a source of sCD21. In disease, populations of $CD21^{-/low}$ B cells are found, which could be a mechanism leading to the decrease in sCD21 in these pathologies. Further experiments would be needed to confirm this response; these could include measuring the amount of sCD21 produced *in vitro* by $CD21^{-/low}$ B cells and $CD21^{+}$ B cells. Additionally, culture and measurement of sCD21 produced by B cells derived from patients with RA compared to healthy controls would also provide additional evidence that these cells produce less soluble protein in disease phenotypes.

At present the mechanism for production of sCD21 is only speculative. It is thought to be cleaved from the cell surface but no direct evidence for this has been published to date. To address this further, as well as further investigating B cells as a source of sCD21, the effect of proteases and protease inhibitors could be assessed by measuring the sCD21 concentration of cell cultures. Increases in sCD21 concentration within culture media, assessed by ELISA, and decreased in membrane CD21 receptors on the surface of the

cells, assessed by flow cytometry, would indicate a role for that protease in cleavage of the protein to form sCD21. In contrast, a decrease in sCD21 production and an increase in CD21 receptors on the surface upon addition of a protease inhibitor would imply a function for that protease in the release of the protein. Of course, it is possible that sCD21 is not released from the cell surface by proteatic cleavage at all, but as the protein is identical to its membrane bound form minus the transmembrane and intracellular domain, cleavage by a membrane protease is a very likely mechanism for protein release.

12.4 Thesis synopsis

The first hypothesis of this work addressed the unidirectional transfer of C3dg-opsonised antigen complexes between CD21 receptors on B cells and CD21 receptors on FDCs. The hypothesis was two-fold, first investigating whether this transfer was due to receptor number on the cell surface of the different cell types and the secondly investigating differential ligand binding abilities by CD21S and CD21L expressed on B cells and FDCs, respectively. As data collected here suggests that CD21L does not have a higher affinity for C3dg than CD21S, the following mechanism for unidirectional transfer of antigen is proposed (Figure 12.4.1).

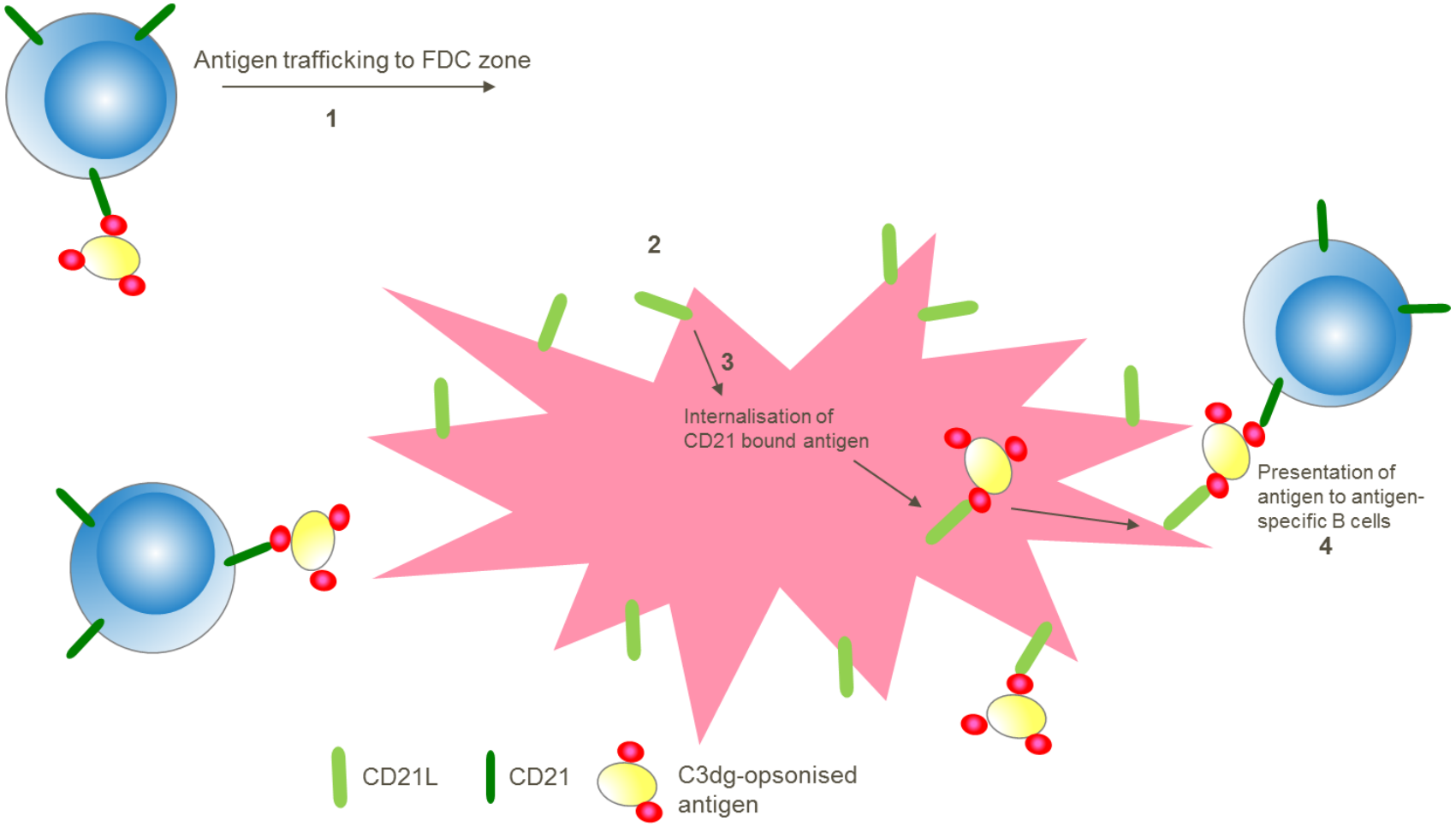

Figure 12.4. 1: Antigen transfer mechanism between B cells and FDCs

1. C3dg-opsonised antigen is trafficked to FDC zones bound to CD21 on the B cell surface. 2. Antigen is presented to FDCs and binds to an increased number of receptors on the surface of the cell due to high receptor numbers. 3. Antigen-bound CD21 is internalised, pulling the immune complex from CD21 receptors on the B cell, 4. and presented to antigen-specific B cells

B cells collect C3dg-antigen complexes from SCS macrophages and shuttle the antigen bound to their CD21 cell surface receptors to FDCs zones. Interaction between these cells occurs through the binding of CD21 on the FDC to C3dg on the immune complex. As FDCs express an increased number of CD21 receptors on their cell surface compared to B cells, a greater number of interactions between the FDC and the opsonised immune complex occurs. C3dg may naturally dissociate from CD21 receptors on the B cell surface due to weak ligand-receptor interactions, and due to the increased interactions on FDCs remains bound to this cell and is subsequently internalised by the cell. Alternatively, as antigen bound CD21 receptors are actively internalised by FDCs, antigen complexes are pulled off the B cells due to the high number of interactions between membrane bound CD21 receptors on FDCs compared with that of B cells, if dissociation has not already occurred. CD21 bound antigen is retained in non-degradative endosomal compartments and recycled to the cell surface for presentation to antigen-specific B cells leading to an increased specific antibody response.

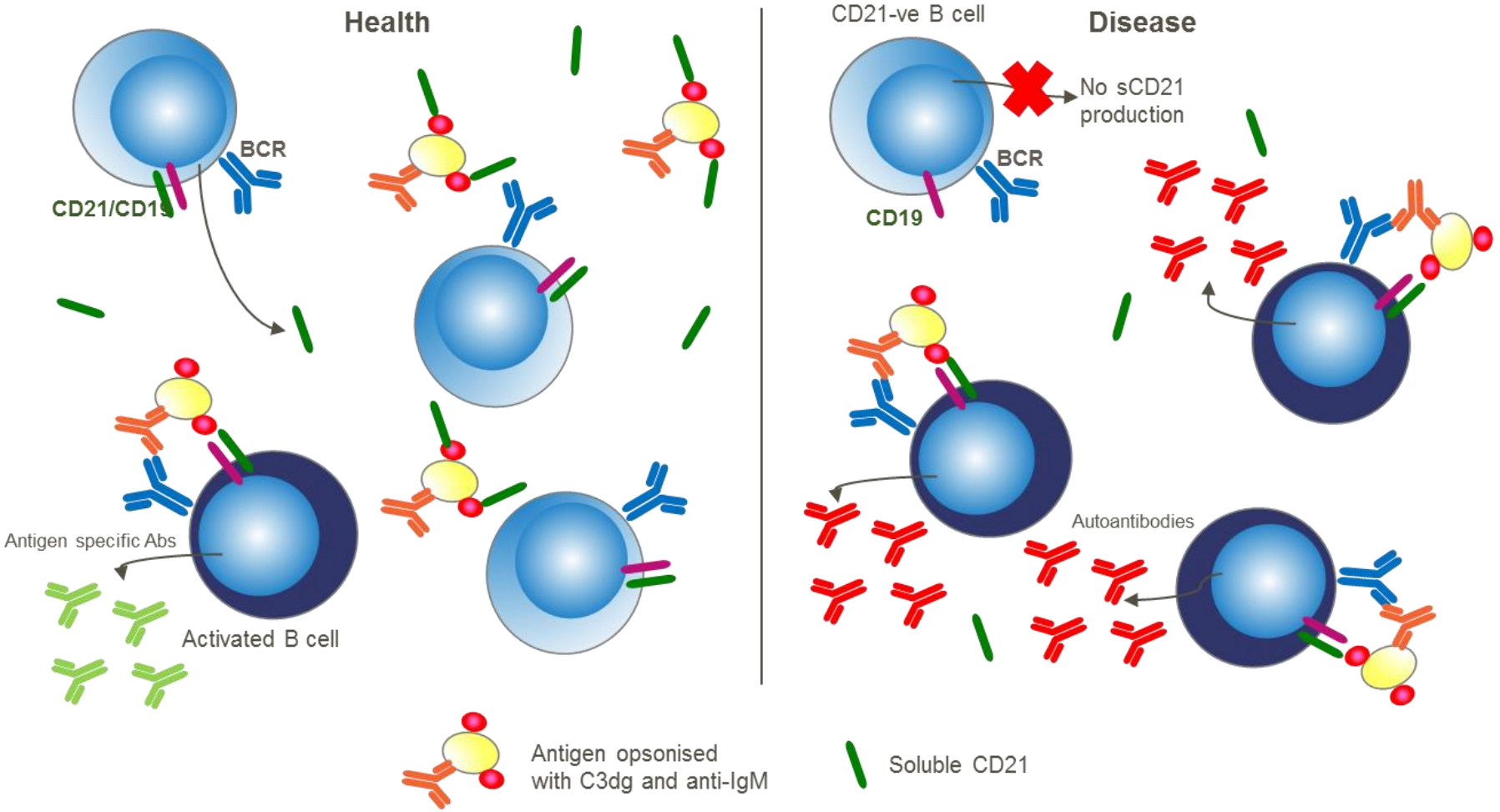

Figure 12.4. 2: A role for sCD21 in health and disease

Within health sCD21 is produced by B cells and prevents binding of opsonised immune complexes to B cells, hence modulating the activation of the immune response. In disease, CD21 negative B cells do not produce sCD21, therefore the decrease in soluble protein concentration leads to opsonised antigen complex binding to B cells and overactivation of the immune response.

The second hypothesis investigated as part of this work concerned the soluble form of CD21 and its role in health and disease. The hypothesis was derived from the observation that sCD21 concentrations decrease in autoimmune diseases, therefore this protein may be acting as a break on the immune system to dampen C3dg-mediated immune responses, a mechanism that is removed in diseases with decreased sCD21 concentrations, consequently leading to pathogenic immune responses that result in disease phenotypes. Results presented in this investigation show that sCD21 levels in RA patients treated with Rituximab have further decreased sCD21 levels, suggesting B cells as an origin of this protein. Additionally, sCD21 was shown to have the ability to prevent C3dg binding to B cells and prevent co-activation of B cells with anti-IgM/C3dg stimulation complexes. Taken together these results point to the following mechanism for the role of sCD21 in health and disease.

In health, sCD21 is produced by $CD21^{+}$ B cells at a concentration allowing the balance of activation of B cells by C3dg immune complexes and blockage of the binding of these complexes to CD21 receptors on B cells to prevent over activation of the immune response. In disease, a population of pathogenic B cells which are $CD21^{low/-}$ are described. As these cells express lower levels of CD21, and B cells are thought to be the origin of sCD21, this could be a reason for decreased sCD21 production within patients with autoimmune disease (Figure 12.4.2). Pathogenic fibroblast subsets, expanded in RA, produce increased C3 levels (Mizoguchi et al., 2018), potentially leading to increased C3dg within the serum. The low sCD21 concentration is unable to prevent binding of this C3dg and opsonised immune complexes to B cells, therefore resulting in the overactivation of the immune response and pathogenic B cell responses.

Together this data has provided additional insight into the mechanism of antigen transfer in germinal centres and suggested a potential mechanism for autoimmune disease development through investigating the functions of CD21 in the germinal centre as a membrane bound receptor and periphery as a soluble protein.

13. References

Adams, D. J., Van Der Weyden, L., Mayeda, A., Stamm, S., Morris, B. J., & Rasko, J. E. J. (2001). ZNF265 - A novel spliceosomal protein able to induce alternative splicing. Journal of Cell Biology, 154(1), 25–32.

Agbay, R. L. M. C., Medeiros, L. J., Khoury, J. D., Salem, A., Bueso-Ramos, C. E., & Loghavi, S. (2017). Characteristics and Clinical Implications of Reactive Germinal Centers in the Bone Marrow. Human Pathology. Human Pathology, 68, 7-21

Aguzzi, A., Kranich, J., & Krautler, N. J. (2014). Follicular dendritic cells: origin, phenotype, and function in health and disease. Trends in Immunology, 35(3), 105–113.

Aguzzi, A., & Krautler, N. J. (2010). Characterizing follicular dendritic cells: A progress report. European Journal of Immunology, 40, 2134–2138.

Ahearn, J. M., Fischer, M. B., Croix, D., Goerg, S., Ma, M., Xia, J., Carroll, M. C. (1996). Disruption of the Cr2 Locus Results in a Reduction in B-1a Cells and in an Impaired B Cell Response to T-Dependent Antigen, Immunity, 251–262.

Allen, C. D. C., & Cyster, J. G. (2008). Follicular dendritic cell networks of primary follicles and germinal centers : Phenotype and function, Seminars in Immunology, 20(1), 14–25.

Allen, C. D. C., & Okada, T. (2007). Imaging of Germinal Center Selection events during affinity maturation, Science, 315(5811), 528–532.

Aloisi, F., & Pujol-borrell, R. (2006). Lymphoid neogenesis in chronic inflammatory diseases, Nature Review Immunology, 6(3), 14–17.

Amara, K., Clay, E., Yeo, L., Ramsköld, D., Spengler, J., Sippl, N., Scheel-toellner, D. (2017). Immunoglobulin characteristics and RNAseq data of FcRL4 + B cells sorted from synovial fluid and tissue of patients with rheumatoid arthritis. Journal of Autoimmunity, 81, 34-43.

Ansel, K. M., Ngo, V. N., Hyman, P. L., Luther, S. a, Förster, R., Sedgwick, J. D., … Cyster, J. G. (2000). A chemokine-driven positive feedback loop organizes lymphoid follicles. Nature, 406(6793), 309–314.

Arai, S., Maehara, N., Iwamura, Y., Honda, S., Nakashima, K., Kai, T.… Miyazaki, T. (2013). Article Obesity-Associated Autoantibody Production Requires AIM to Retain the Immunoglobulin M Immune Complex on Follicular Dendritic Cells. CellReports, 3(4), 1187–1198.

Arredouani, M. S., Bhasin, M. K., Sage, D. R., Dunn, L. K., Gill, M. B., Agnani, D., & Libermann, T. A. (2014). Analysis of Host Gene Expression Changes Reveals Distinct Roles for the Cytoplasmic Domain of the Epstein-Barr Virus Receptor / CD21 in B-Cell Maturation, Activation, and Initiation of Virus Infection, Journal of Virology, 88(10), 5559–5577.

Ars, E., Serra, E., García, J., Kruyer, H., Gaona, a, Lázaro, C., & Estivill, X. (2000). Mutations affecting mRNA splicing are the most common molecular defects in patients with neurofibromatosis type 1. Human Molecular Genetics, 9(2), 237–247.

Asokan, R., Hua, J., Young, K. A., Gould, H. J., Hannan, J. P., Kraus, D. M., … Holers, V. M. (2006). Characterization of Human Complement Receptor Type 2 (CR2/CD21) as a Receptor for IFN- : A Potential Role in Systemic Lupus Erythematosus. The Journal of Immunology, 177(1), 383–394.

Autoreactive, P., Responses, B. C., Das, A., Heesters, B. A., Bialas, A., Carlesso, G., Carroll, M. C. (2017). Follicular Dendritic Cell Activation by TLR Ligands Article Follicular Dendritic Cell Activation by TLR Ligands Promotes Autoreactive B Cell Responses. Immunity, 46(1), 106–119.

Baje, M., & Germain, R. N. (2009). B-cell follicle development remodels the conduit system and allows soluble antigen delivery to follicular dendritic cells. Blood 114(24), 4989–4998.

Balbo, M., Barel, M., Lottin-Divoux, S., Jean, D., & Frade, R. (2005). Infection of human B lymphoma cells by Mycoplasma fermentans induces interaction of its elongation factor with the intracytoplasmic domain of Epstein-Barr virus receptor (gp140, EBV/C3dR, CR2, CD21). FEMS Microbiology Letters, 249(2), 359–366.

Ballanti, E., Perricone, C., Greco, E., Ballanti, M., Di Muzio, G., Chimenti, M. S., & Perricone, R. (2013). Complement and autoimmunity. Immunologic Research, 56(2–3), 477–491.

Balogh, P., Aydar, Y., Tew, J. G., & Szakal, A. K. (2002). Appearance and phenotype of murine follicular dendritic cells expressing VCAM-1. Anatomical Record, 268(2), 160–168.

Barinov, A., Luo, L., Gasse, P., Meas-Yedid, V., Donnadieu, E., Arenzana-Seisdedos, F., & Vieira, P. (2017). Essential role of immobilized chemokine CXCL12 in the regulation of the humoral immune response. Proceedings of the National Academy of Sciences, 114(9), 2319-2324

Barrington, R. a, Pozdnyakova, O., Zafari, M. R., Benjamin, C. D., & Carroll, M. C. (2002). B lymphocyte memory: role of stromal cell complement and FcgammaRIIB receptors. The Journal of Experimental Medicine, 196(9), 1189–1199.

Bekeredjian-Ding, I., & Jego, G. (2009). Toll-like receptors - Sentries in the B-cell response. Immunology, 128(3), 311–323.

Beltman, J. B., Allen, C. D. C., Cyster, J. G., & de Boer, R. J. (2011). B cells within germinal centers migrate preferentially from dark to light zone. Proceedings of the National Academy of Sciences of the United States of America, 108(21), 8755–8760.

Bergtold, A., Desai, D. D., Gavhane, A., & Clynes, R. (2005). Cell Surface Recycling of Internalized Antigen Permits Dendritic Cell Priming of B Cells, Immunity, 23, 503–514.

Berney, C., Herren, S., Power, C. a, Gordon, S., Martinez-Pomares, L., & Kosco-Vilbois, M. H. (1999). A member of the dendritic cell family that enters B cell follicles and stimulates primary antibody responses identified by a mannose receptor fusion protein. The Journal of Experimental Medicine, 190(6), 851–860.

Bevington, S. L., Cauchy, P., Piper, J., Bertrand, E., Lalli, N., Jarvis, R. C., Cockerill, P. N. (2016). Inducible chromatin priming is associated with the establishment of immunological memory in T cells. The EMBO Journal, 35(5), 515–535.

Björck, P., Elenström-Magnusson, C., Rosén, A., Severinson, E., & Paulie, S. (1993). CD23 and CD21 function as adhesion molecules in homotypic aggregation of human B lymphocytes. European Journal of Immunology, 23(8), 1771–1775.

Boackle, S. a. (2003). Complement and autoimmunity. Biomedicine and Pharmacotherapy, 57(7), 269–273.

Boackle, S. A., Holers, V. M., Chen, X., Szakonyi, G., Karp, D. R., Wakeland, E. K., & Morel, L. (2001). Cr2 , a Candidate Gene in the Murine Sle1c Lupus Susceptibility Locus , Encodes a Dysfunctional Protein, Immunity, 15, 775–785.

Boniface, J. J., Rabinowitz, J. D., Wu, C., Hampl, J., Reich, Z., Altman, J. D., … Davis, M. M. (1998). Initiation of Signal Transduction through the T Cell Receptor Requires the Multivalent Engagement of Peptide / MHC Ligands, Immunity, 9, 459–466.

Boross, P., Arandhara, V. L., Martin-ramirez, J., Carlucci, F., Kaa, J. Van Der, Breukel, C., … Kaa, J. Van Der. (2011). The inhibiting Fc receptor for IgG, FcgRIIB, is a modifier of Autoimmune Susceptibility. Journal of Immunology; 187, 3909

Bossolasco, S., Nilsson, A., Milito, A. De, Lazzarin, A., Linde, A., Cinque, P., & Chiodi, F. (2001). Soluble CD23 in cerebrospinal Fl uid : a marker of AIDS- related non-Hodgkin ' s lymphoma in the brain. AIDS, 15(9): 1109-13

Boucheix, C., & Rubinstein, E. (2014). Tetraspanins at a glance. Journal of Cell Science, 127, 3641–3648.

Bouillie, S., Barel, M., & Frade, R. (1999). Signaling through the EBV/C3d receptor (CR2, CD21) in human B lymphocytes: activation of phosphatidylinositol 3-kinase via a CD19-independent pathway. Journal of Immunology, 162(1), 136–143.

Bourke, E., Bosisio, D., Golay, J., Polentarutti, N., & Mantovani, A. (2003). The toll-like receptor repertoire of human B lymphocytes : inducible and selective expression of TLR9 and TLR10 in normal and transformed cells. Blood, 102(3), 956–963.

Braun, M., Melchers, I., Peter, H. H., & Illges, H. (1998). Human B and T lymphocytes have similar amounts of CD21 mRNA , but differ in surface expression of the CD21 glycoprotein, International immunology, 10(8), 1197–1202.

Briggs, F. B. S., Evsyukova, I., Barcellos, L. F., Gregory, S. G., Garcia-blanco, M. A., Briggs, F. B. S., … Kennedy, E. M. (2017). Human Epistatic Interaction Controls IL7R Splicing and Increases Multiple Sclerosis Risk Article Human Epistatic Interaction Controls IL7R Splicing and Increases Multiple Sclerosis Risk, Cell, 169(1), 72–84.

Browning, J. L., Ngam-ek, a., Lawton, P., DeMarinis, J., Tizard, R., Chow, E. P., … Ware, C. F. (1993). Lymphotoxin beta, a novel member of the TNF family that forms a heteromeric complex with lymphotoxin on the cell surface. Cell, 72, 847–856.

Browning, J. L. (2006). B cells move to centre stage: novel opportunities for autoimmune disease treatment. Nature Reviews. Drug Discovery, 5(7), 564–576.

Buettner, M., Pabst, R., & Bode, U. (2010). Stromal cell heterogeneity in lymphoid organs. Trends in Immunology, 31(2), 80–86.

Burrell, B. E., Ding, Y., Nakayama, Y., Park, K., Xu, J., & Yin, N. (2011). Tolerance and lymphoid organ structure and function, Frontiers in Immunology, 1–16.

Butch, a W., Chung, G. H., Hoffmann, J. W., & Nahm, M. H. (1993). Cytokine expression by germinal center cells. Journal of Immunology, 150(1), 39–47.

Cañete, J. D., Celis, R., Yeremenko, N., Sanmartí, R., van Duivenvoorde, L., Ramírez, J., … Baeten, D. L. (2015). Ectopic lymphoid neogenesis is strongly associated with activation of the IL-23 pathway in rheumatoid synovitis. Arthritis Research and Therapy, 17(1), 1–12.

Caron, G., Le Gallou, S., Lamy, T., Tarte, K., & Fest, T. (2009). CXCR4 expression functionally discriminates centroblasts versus centrocytes within human germinal center B cells. Journal of Immunology, 182(12), 7595–7602.

Carpenter, E. L., Mick, R., Rüter, J., & Vonderheide, R. H. (2009). Activation of human B cells by the agonist CD40 antibody CP-870,893 and augmentation with simultaneous toll-like receptor 9 stimulation. Journal of Translational Medicine, 7, 93.

Carrasco, Y. R., Fleire, S. J., Cameron, T., Dustin, M. L., Batista, F. D., & Fields, I. (2004). LFA-1 / ICAM-1 Interaction Lowers the Threshold of B Cell Activation by Facilitating B Cell Adhesion and Synapse Formation, Immunity, 20, 589–599.

Carroll, M. C. (1998). CD21/CD35 in B cell activation. Seminars in Immunology, 10(4), 279–286.

Carroll, M. C. (2004). The complement system in B cell regulation. Molecular Immunology, 41(2–3), 141–146.

Carroll, M. C., & Isenman, D. E. (2012). Regulation of Humoral Immunity by Complement. Immunity, 37(2), 199–207.

Carter, R. H., Fearon, D. T., & Alerts, E. (1992). Pillars Article : CD19 : Lowering the Threshold for Antigen Receptor Stimulation, Science, 256(5053) 105–108.

Castagnaro, L., Lenti, E., Maruzzelli, S., Spinardi, L., Migliori, E., Farinello, D., … Brendolan, A. (2013). Nkx2-5+islet1+ mesenchymal precursors generate distinct spleen stromal cell subsets and participate in restoring stromal network integrity. Immunity, 38(4), 782–791.

Chan, M. A., Gigliotti, N. M., Matangkasombut, P., Gauld, S. B., Cambier, J. C., & Rosenwasser, L. J. (2010). CD23-mediated cell signaling in human B cells differs from signaling in cells of the monocytic lineage. Clinical Immunology, 137(3), 330–336.

Chang, J. E., & Turley, S. J. (2015). Stromal infrastructure of the lymph node and coordination of immunity. Trends in Immunology, 36(1), 30–39.

Chaplin, D. D., & Fu, Y.-X. (1999). Development and maturation of secondary lymphoid tissues. Annual Review of Immunology, 17, 399–433.

Chen, J., Cai, Z., Zhang, L., Yin, Y., Chen, X., Chen, C., … Wang, X. (2017). Lis1 Regulates Germinal Center B Cell Antigen Acquisition and Affinity Maturation. The Journal of Immunology, 198(11), 4304-4311.

Chen, K., Dai, X., & Wu, J. (2015). Alternative splicing: An important mechanism in stem cell biology. World Journal of Stem Cells, 7(1), 1–10.

Chen, M., Daha, M. R., & Kallenberg, C. G. M. (2010). The complement system in systemic autoimmune disease. Journal of Autoimmunity, 34(3), J276–J286.

Chen, Y., & Morel, L. (2005). Genetics of T Cell Defects in Lupus, Cellular and Molecular Immunology, 2(6), 403–409.

Cherukuri, A., Cheng, P. C., & Pierce, S. K. (2001). The Role of the CD19/CD21 Complex in B Cell Processing and Presentation of Complement-Tagged Antigens. Journal of Immunology, 167(1), 163-72.

Cherukuri, A., Cheng, P. C., Sohn, H. W., & Pierce, S. K. (2001). The CD19 / CD21 Complex Functions to Prolong B Cell Antigen Receptor Signaling from Lipid Rafts. Immunity, 14, 169–179.

Cho, K.-A., Kim, J.-Y., Kim, H. S., Ryu, K.-H., & Woo, S.-Y. (2012). Tonsil-derived mesenchymal progenitor cells acquire a follicular dendritic cell phenotype under cytokine stimulation. Cytokine, 59(2), 211–214.

Choe Jongseon, Kim Han-Soo, Zhang Xinhong, Armitage Richard J., A., & Choi Yong Sung. (1996). Cellular and molecular factors that regulate the differentiation and apoptosis of germinal center B cells. Anti-Ig down-regulates Fas expression of CD40 ligand-stimulated germinal center B cells and inhibits Fas-mediated apoptosis. The Journal of Immunology, 157(3), 1006–1016.

Choe, J., & Choi, Y. S. (1998). IL-10 interrupts memory B cell expansion in the germinal center by inducing differentiation into plasma cells. European Journal of Immunology, 28(2), 508–515.

Choi, B., Chun, E., & Kim, M. (2011). Human B Cell Development and Antibody Production in Humanized NOD / SCID / IL-2R γ null (NSG) Mice Conditioned by Busulfan. Journal of Clinical Immunology, 31(2), 253–264.

Chung, Y. S., Son, J. K., Choi, B., Joo, S. Y., Lee, Y. S., Park, J. B., … Kim, S. J. (2015). Co-transplantation of human fetal thymus, bone and CD34+ cells into young adult immunodeficient NOD/SCID IL2Rγnull mice optimizes humanized mice that mount adaptive antibody responses. Clinical Immunology, 157(2), 156–165.

Cinamon, G., Zachariah, M. A., Lam, O. M., Jr, F. W. F., & Jason, G. (2008). Follicular shuttling of marginal zone B cells facilitates antigen transport. Nature Immunology, 9(1), 54–62.

Claes, N., Fraussen, J., Vanheusden, M., Stinissen, P., & Wijmeersch, B. Van. (2016). Age-Associated B Cells with Proinflammatory Characteristics Are Expanded in a Proportion of Multiple Sclerosis Patients. Journal of Immunology. 197(12), 4576-4583.

Clark, E. a, Grabstein, K. H., Gown, A. M., Skelly, M., Kaisho, T., Hirano, T., & Shu, G. L. (1995). Activation of B lymphocyte maturation by a human follicular dendritic cell line, FDC-1. Journal of Immunology, 155(2), 545–555.

Clark, E. a, Grabstein, K. H., & Shu, G. L. (1992). Cultured human follicular dendritic cells. Growth characteristics and interactions with B lymphocytes. Journal of Immunology, 148(11), 3327–3335.

Mizoguchi, F., Slowikowski, K., Wei, K., Marshall, J. L., (2018) Functionally distinct disease-associated fi broblast subsets in rheumatoid arthritis. Nature Communications. 9(789), 1–11.

Cornall, R. J., Goodnow, C. C., & Cyster, J. G. (1995). The regulation of self-reactive B cells. Current Opinion in Immunology, 7(6), 804–811.

Cuff, C. A., Schwartz, J., Bergman, C. M., Russell, K. S., Bender, J. R., & Ruddle, N. H. (1998). Lymphotoxin alpha3 induces chemokines and adhesion molecules: insight into the role of LT alpha in inflammation and lymphoid organ development. J Immunol, 161(12), 6853–6860.

Cukierman, E., Pankov, R., & Yamada, K. M. (2002). Cell interactions with three-dimensional matrices. Current Opinion in Cell Biology, 14(5), 633–639.

Cupedo, T., Lund, F. E., Ngo, V. N., Randall, T. D., Jansen, W., Greuter, M. J., … Mebius, R. E. (2004). Initiation of cellular organization in lymph nodes is regulated by non-B cell-derived signals and is not dependent on CXC chemokine ligand 13. Journal of Immunology, 173(8), 4889–4896.

Cupedo, T., & Mebius, R. E. (2005). Cellular interactions in lymph node development. Journal of Immunology, 174(1), 21–25.

Cyster, J. G., Ansel, K. M., Reif, K., Ekland, E. H., Hyman, P. L., Tang, H. L., … Ngo, V. N. (2000). Follicular stromal cells and lymphocyte homing to follicles. Immunological Reviews, 176, 181–193.

Cyster, J. G. (2014). Blown Away: The Unexpected Role of Lymphotoxin in Lymphoid Organ Development. The Journal of Immunology, 192(5), 2007–2009.

Cyster, J. G. (2010). B cell follicles and antigen encounters of the third kind. Nature Immunology, 11(11), 989–996.

Daridon, C., Jousse, S., Saraux, A., Jamin, C., & Youinou, P. (2005). BAFF Overexpression Is Associated with Autoantibody Production in Autoimmune diseases. Annual New York academy of sciences. 39(33), 34–39.

Dash, R., Kumar, U., Kanjilal, M., & Das, N. (2016). Expression and modulation of complement receptor 2 (CR2 / CD21) in the pathophysiology of rheumatoid arthritis. International Journal of Research in Medical Sciences. 4(8), 3394–3401.

De Togni, P. (1994). Abnormal development of peripheral lymphoid organs in mice deficient in lymphotoxin. Science, 264(5159), 703-707.

Del Nagro, C. J., Kolla, R. V, & Rickert, R. C. (2005). A critical role for complement C3d and the B cell coreceptor (CD19/CD21) complex in the initiation of inflammatory arthritis. Journal of Immunology, 175(8), 5379–5389.

Delsol, G., Meggetto, F., Brousset, P., Cohen-knafo, E., Saati, T. Al, Rochaix, P., … Chittal, S. (1993). Relation of Follicular Dendritic Reticulum Cells to Reed-Sternberg Cells of Hodgkin ' s Disease with Emphasis on the Expression of CD21 Antigen. American Journal of Pathology, 146(6), 1729–1738.

Dendritic, F., Lines, C. C., Lindhout, B. E., Lakeman, A., & Mevissen, M. L. C. M. (1994). Functionally Active Epstein-Barr Virus-transformed Follicular Dendritic Cell-like Cell Lines. Journal of Experimental Medicine. 179, 1173-1184.

Deng, C., Goluszko, E., Yang, H., Christadoss, P., & Alerts, E. (2002). Resistance to Experimental Autoimmune Myasthenia Gravis in IL-6-Deficient Mice Is Associated with Reduced Germinal Center Formation and C3 Production. Journal of Immunology. 169(2), 1077-1083.

Denton, A. E., & Linterman, M. A. (2017). Stromal networking: cellular connections in the germinal centre. Current Opinion in Immunology, 45, 103–111.

Denzer, K., Eijk, M. Van, Kleijmeer, M. J., Groot, C. De, & Geuze, H. J. (2000). Follicular Dendritic Cells Carry MHC Class II-Expressing Microvesicles at Their Surface. Journal of Immunology. 165(3), 1259-1265.

Di Niro, R., Lee, S. J., Vander Heiden, J. A., Elsner, R. A., Trivedi, N., Bannock, J. M., … Shlomchik, M. J. (2015). SalmOnella Infection Drives Promiscuous B Cell Activation Followed By Extrafollicular Affinity Maturation. Immunity, 43(1), 120–131.

Di Trapani, M., Bassi, G., Ricciardi, M., Fontana, E., Bifari, F., Pacelli, L., … Krampera, M. (2013). Comparative study of immune regulatory properties of stem cells derived from different tissues. Stem Cells and Development, 22(22), 2990–3002.

Division, G. D. R., Thornton, B. P., & Ve, V. (1996). Function of C3 in a humoral response : iC3b / C3dg bound to an immune complex generated with natural antibody and a primary antigen promotes antigen uptake and the expression of co-stimulatory molecules by all B cells , but only stimulates immunoglobulin synthesis by antigen-specific B cells. Clinical Experimental immunology. 104(3), 531–537.

Douglas, K. B., Windels, D. C., Zhao, J., Gadeliya, A. V, Wu, H., Kaufman, K. M., … Petri, M. (2009). Complement receptor 2 polymorphisms associated with systemic lupus erythematosus modulate alternative splicing. Genes Immunology. 10(5), 457–469.

Dufaud, C. R., McHeyzer-Williams, L. J., & McHeyzer-Williams, M. G. (2017). Deconstructing the germinal center, one cell at a time. Current Opinion in Immunology, 45, 112–118.

Dumont, N., Aubin, E., Proulx, D. P., Lemieux, R., & Bazin, R. (2009). Increased secretion of hyperimmune antibodies following lipopolysaccharide stimulation of CD40-activated human B cells in vitro. Immunology, 126(4), 588–595.

Dunkelberger, J. R., & Song, W. (2010). Complement and its role in innate and adaptive immune responses. Cell Research, 20(1), 34–50.

Edwards, J. C., Leigh, R. D., & Cambridge, G. (1997). Expression of molecules involved in B lymphocyte survival and differentiation by synovial fibroblasts. Clinical and Experimental Immunology, 108(3), 407–414.

Eha, R. A. I. F. S. G. (1997). Impaired CD19 expression and signaling , enhanced antibody response to type II T independent antigen and reduction of B-1 cells in CD81-deficient mice. National academy of science USA, 94(20) 10844–10849.

Ehrnthaller, C., Ignatius, A., Gebhard, F., & Huber-Lang, M. (2011). New insights of an old defense system: structure, function, and clinical relevance of the complement system. Molecular Medicine (Cambridge, Mass.), 17(3–4), 317–329

Eizirik, D. L., Sammeth, M., Bouckenooghe, T., Bottu, G., Sisino, G., Igoillo-Esteve, M., … Cnop, M. (2012). The human pancreatic islet transcriptome: Expression of candidate genes for type 1 diabetes and the impact of pro-inflammatory cytokines. PLoS Genetics, 8(3).

Ekland, E. H., Forster, R., Lipp, M., & Cyster, J. G. (2004). Requirements for follicular exclusion and competitive elimination of autoantigen-binding B cells. Journal of Immunology (Baltimore, Md.: 1950), 172(8), 4700–4708.

El Shikh, M. E. M., El Sayed, R. M., Wu, Y., Szakal, A. K., & Tew, J. G. (2007). TLR4 on follicular dendritic cells: an activation pathway that promotes accessory activity. Journal of Immunology, 179(7), 4444–4450.

El Shikh, M. E., El Sayed, R., Szakal, A. K., & Tew, J. G. (2006). Follicular dendritic cell (FDC)-FcgammaRIIB engagement via immune complexes induces the activated FDC phenotype associated with secondary follicle development. European Journal of Immunology, 36(10), 2715–2724.

Endres, R., Alimzhanov, M. B., Plitz, T., Fütterer, A., Kosco-Vilbois, M. H., Nedospasov, S. A., … Pfeffer, K. (1999). Mature follicular dendritic cell networks depend on expression of lymphotoxin

beta receptor by radioresistant stromal cells and of lymphotoxin beta and tumor necrosis factor by B cells. The Journal of Experimental Medicine, 189(1), 159–168.

Epron, G., Ame-Thomas, P., Le Priol, J., Pangault, C., Dulong, J., Lamy, T., … Tarte, K. (2012). Monocytes and T cells cooperate to favor normal and follicular lymphoma B-cell growth: role of IL-15 and CD40L signaling. Leukemia, 26(1), 139–148.

Estes, J. D., Thacker, T. C., Hampton, D. L., Kell, S. A., Keele, B. F., Palenske, E. A., … Burton, G. F. (2004). Follicular dendritic cell regulation of CXCR4-mediated germinal center CD4 T cell migration. The Journal of Immunology, 173(11), 6169–6178.

Ettinger, R., Sims, G. P., Fairhurst, A.-M., Robbins, R., da Silva, Y. S., Spolski, R., … Lipsky, P. E. (2005). IL-21 Induces Differentiation of Human Naive and Memory B Cells into Antibody-Secreting Plasma Cells. The Journal of Immunology, 175(12), 7867–7879.

Etzioni, A. (2003). Immune deficiency and autoimmunity, Autoimmunity Reviews. 2(6), 364–369.

Faber, K., Glatting, K.-H., Mueller, P. J., Risch, A., & Hotz-Wagenblatt, A. (2011). Genome-wide prediction of splice-modifying SNPs in human genes using a new analysis pipeline called AASsites. BMC Bioinformatics, 12(Suppl 4), S2.

Fang, Y., Xu, C., Fu, Y. X., Holers, V. M., & Molina, H. (1998). Expression of complement receptors 1 and 2 on follicular dendritic cells is necessary for the generation of a strong antigen-specific IgG response. Journal of Immunology (Baltimore, Md. : 1950), 160(11), 5273–5279.

Femino, A. M., Fay, F. S., Fogarty, K., & Singer, R. H. (1998). Dependence of germinal center {B} cells on expression of {CD}21/{CD}35 for survival. Science, 280(5363), 585–589.

Ferguson, A. R., Youd, M. E., & Corley, R. B. (2004). Marginal zone B cells transport and deposit IgM-containing immune complexes onto follicular dendritic cells, International Immunology. 16(10), 1411–1422.

Fischer, E., Lecoanet-henchoz, S., Mani, J., Bonnefoy, J., & Kazatchkine, M. D. (1998). Soluble CD21 (sCD21) forms biologically active complexes with CD23 : sCD21 is present in normal plasma as a complex with trimeric CD23 and inhibits soluble CD23-induced IgE synthesis by B cells. International Immunology. 10(10), 1459–1466.

Fischer, M. B., Goerg, S., Shen, L., Prodeus, A. P., Goodnow, C. C., Kelsoe, G., & Carroll, M. C. (1998). Dependence of Germinal Center B Cells on Expression of CD21 / CD35 for Survival. Science 280(5363l), 582-5.

Forster, B. R., Emrich, T., Kremmer, E., & Lipp, M. (1994). Expression of the G-Protein-Coupled Receptor BLRl Defines Mature, Recirculating B Cells and a Subset of T-Helper Memory Cells. Blood. 84(3), 830–840.

Fournier, S., Rubio, M., Delespesse, G., & Sarfati, M. (1994). Role for low-affinity receptor for IgE (CD23) in normal and leukemic B-cell proliferation. Blood, 84(6), 1881–1886.

Frank, M. M. (2012). CD21 deficiency, complement, and the development of common variable immunodeficiency. Journal of Allergy and Clinical Immunology, 129(3), 811–813.

Frcmeaux-bacchil, V., Bernard, I., Man, J., Fontaine, M., & Bonnefoy, J. (1996). Human lymphocytes shed a soluble form of CD21 (the C3dg / Epstein = Barr virus receptor , CR2) that binds iC3b and CD23. European Journal of Immunology. 26(7), 1497–1503.

Fujisaku, A., Harley, J. B., Frank, M. B., Gruner, B. A., Frazier, B., & Holers, V. M. (1989). Genomic organization and polymorphisms of the human C3d/Epstein-Barr virus receptor. Journal of Biological Chemistry, 264(4), 2118–2125.

Fukunaga, R., Ishizaka-Ikeda, E., & Nagata, S. (1993). Growth and differentiation signals mediated by different regions in the cytoplasmic domain of granulocyte colony-stimulating factor receptor. Cell, 74(6), 1079–1087.

Garin, A., Meyer-Hermann, M., Contie, M., Figge, M. T., Buatois, V., Gunzer, M., … Kosco-Vilbois, M. H. (2010). Toll-like Receptor 4 Signaling by Follicular Dendritic Cells Is Pivotal for Germinal Center Onset and Affinity Maturation. Immunity, 33(1), 84–95.

Garin, A., Meyer-hermann, M., Contie, M., Figge, M. T., Buatois, V., Gunzer, M… Kosco-vilbois, M. H. (2010). Article by Follicular Dendritic Cells Is Pivotal for Germinal Center Onset and Affinity Maturation. Immunity, 33(1), 84–95.

Gatto, D., & Brink, R. (2010). The germinal center reaction. Journal of Allergy and Clinical Immunology, 126(5), 898–907.

Gil, M., Park, S. J., Chung, Y. S., & Park, C. S. (2010). Interleukin-15 enhances proliferation and chemokine secretion of human follicular dendritic cells. Immunology, 130(4), 536–544.

Gilbert, H. E., Asokan, R., Holers, V. M., & Perkins, S. J. (2006). The 15 SCR Flexible Extracellular Domains of Human Complement Receptor Type 2 can Mediate Multiple Ligand and Antigen Interactions. Journal of Molecular Biology, 362(5), 1132–1147.

Gilbert, H. E., Eaton, J. T., Hannan, J. P., Holers, V. M., & Perkins, S. J. (2005). Solution structure of the complex between CR2 SCR 1-2 and C3d of human complement: An X-ray scattering and sedimentation modelling study. Journal of Molecular Biology, 346(3), 859–873.

Gonzalez, S. F., Lukacs-kornek, V., Michael, P., Pitcher, L. A., Degn, S. E., Shannon, J., & Carroll, M. C. (2010). Complement-Dependent Transport of Antigen into B Cell Follicles. Journal of Immunology. 185(5), 2659-2664.

Good, K. L., Bryant, V. L., & Tangye, S. G. (2006). Kinetics of Human B Cell Behavior and Amplification of Proliferative Responses following Stimulation with IL-21. The Journal of Immunology, 177(8), 5236–5247.

Gorelik, L., Cutler, A. H., Thill, G., Miklasz, S. D., Shea, D. E., Ambrose, C., … Kalled, S. L. (2004). Cutting Edge: BAFF Regulates CD21/35 and CD23 Expression Independent of Its B Cell Survival Function. The Journal of Immunology, 172(2), 762–766.

Gretz, B. J. E., Norbury, C. C., Anderson, A. O., Proudfoot, A. E. I., & Shaw, S. (2000). Lymph-borne Chemokines and Other Low Molecular Weight Molecules Reach High Endothelial Venules via Specialized Conduits While a Functional Barrier Limits Access to the Lymphocyte Microenvironments in Lymph Node Cortex. Journal of Experimental Medicine. 192(10), 1425-1440.

Grottenthaler, T., Von Kempis, J., Goldacker, S., & Illges, H. (2006). Soluble CD21 in sera and synovial fluid of arthritic patients. Rheumatology International, 26(3), 240–243.

Guthridge, J. M., Rakstang, J. K., Young, K. A., Hinshelwood, J., Aslam, M., Robertson, A., … Holers, V. M. (2001). Structural studies in solution of the recombinant N-terminal pair of short consensus/complement repeat domains of complement receptor type 2 (CR2/CD21) and interactions with its ligand C3dg. Biochemistry, 40(20), 5931–5941.

Haas, K. M., Toapanta, F. R., Oliver, J. A., Poe, J. C., Weis, J. H., Karp, D. R., … Tedder, T. F. (2004). Cutting Edge: C3d Functions as a Molecular Adjuvant in the Absence of CD21/35 Expression. Journal of Immunology. 172, 5833-5837.

Halickman, I., Bastien, Y., Zhuang, Q., Mazer, M. B., Toledano, B., & Mazer, B. D. (2005). Platelet-activating factor antagonists decrease follicular dendritic-cell stimulation of human B lymphocytes. Allergy, Asthma, and Clinical Immunology : Official Journal of the Canadian Society of Allergy and Clinical Immunology, 1(2), 49–57.

Hanten, J. a, Vasilakos, J. P., Riter, C. L., Neys, L., Lipson, K. E., Alkan, S. S., & Birmachu, W. (2008). Comparison of human B cell activation by TLR7 and TLR9 agonists. BMC Immunology, 9, 39.

Harnett, M. M., Katz, E., & Ford, C. A. (2005). Differential signalling during B-cell maturation. Immunology letters. 98, 33–44.

He, D. N., Chen, W. L., Long, K. X., Zhang, X., & Dong, G. F. (2016). Association of Serum CXCL13 with Intrarenal Ectopic Lymphoid Tissue Formation in Lupus Nephritis. Journal of Immunology Research. 2016.

Hebell, T., Ahearn, J., & Fearon, D. (1991). Suppression of the immune response by a soluble complement receptor of B lymphocytes. Science, 254(5028), 102–105.

Heesters, B. a, Chatterjee, P., Kim, Y.-A., Gonzalez, S. F., Kuligowski, M. P., Kirchhausen, T., & Carroll, M. C. (2013). Endocytosis and recycling of immune complexes by follicular dendritic cells enhances B cell antigen binding and activation. Immunity, 38(6), 1164–1175.

Heesters, B. A., Lindqvist, M., Vagefi, P. A., Scully, E. P., Schildberg, F. A., Altfeld, M., … Carroll, M. C. (2015). Follicular Dendritic Cells Retain Infectious HIV in Cycling Endosomes. PLoS Pathogens, 11(12),

Heesters, B. a, Myers, R. C., & Carroll, M. C. (2014). Follicular dendritic cells: dynamic antigen libraries. Nature Reviews. Immunology, 14(7), 495–504.

Hein, W. R., Dudler, L., Marston, W. L., Landsverk, T., Young, a J., & Avila, D. (1998). Ubiquitination and dimerization of complement receptor type 2 on sheep B cells. Journal of Immunology (Baltimore, Md. : 1950), 161(1), 458–466.

Heinemann, D. E. H., & Peters, J. H. (2005). Follicular dendritic-like cells derived from human monocytes. BMC Immunology, 6, 23.

Henderson, B., & Court, L. (1989). Arthritogenic actions of recombinant IL-1 and tumour necrosis factor a in the rabbit : evidence for synergistic interactions between cytokines in vivo. Clinical experimental immunology. 75(2), 306–310.

Herndler-brandstetter, D., Shan, L., Yao, Y., Stecher, C., Plajer, V., & Lietzenmayer, M. (2017). Humanized mouse model supports development , function , and tissue residency of human natural killer cells, National Academy of Science USA. 114(45), 9626-9634.

Heterogeneity, C. R. N., Rodda, L. B., Lu, E., Bennett, M. L., Luster, A. D., Ye, C. J., … Cyster, J. G. (2018). Single-Cell RNA Sequencing of Lymph Node Stromal Resource Single-Cell RNA Sequencing of Lymph Node Stromal Cells Reveals Niche-Associated Heterogeneity. Immunity, 48(5), 1014–1028.e6.

Heuts, F., Rottenberg, M. E., Salamon, D., Rasul, E., Adori, M., Klein, G., … Nagy, N. (2014). T Cells Modulate Epstein-Barr Virus Latency Phenotypes during Infection of Humanized Mice. Journal of Virology. 88(6), 3235–3245.

Hietala, M. A., Jonsson, I., Tarkowski, A., Kleinau, S., & Pekna, M. (2002). Complement Deficiency Ameliorates Collagen-Induced Arthritis in Mice. Journal of Immunology. 169(1), 454-9.

Hoefer, M. M., Aichem, A., Knight, A. M., & Illges, H. (2008). Modulation of murine complement receptor type 2 (CR2 / CD21) ectodomain shedding by its cytoplasmic domain. Molecular Immunology, 45, 2127–2137.

Holers, V. M. (2014). Complement and its receptors: new insights into human disease. Annual Review of Immunology, 32, 433–459.

Holers, V. M., & Banda, N. K. (2018). Complement in the initiation and evolution of Rheumatoid Arthritis. Frontiers of Immunology. 28(9), 1057.

Hu, H., Martin, B. K., Weis, J. J., & Weis, J. H. (1997). Expression of the murine CD21 gene is regulated by promoter and intronic sequences. The Journal of Immunology, 158(10), 4758–4768.

Huang, Y.-S., Zhou, X., Yang, Z.-F., & Lv, Z.-T. (2018). Elevated soluble CD23 level indicates increased risk of B cell non-Hodgkin's lymphomas: evidence from a meta-analysis. Annals of Hematology. 97(8), 1317-1325.

Huber, C., Thielen, C., Seeger, H., Schwarz, P., Montrasio, F., Wilson, M. R., … Aguzzi, A. (2005). Lymphotoxin- Receptor-Dependent Genes in Lymph Node and Follicular Dendritic Cell Transcriptomes. The Journal of Immunology, 174(9), 5526–5536.

Huebner, K., Linnenbach, a, Weidner, S., Glenn, G., & Croce, C. M. (1981). Deoxyribonuclease I sensitivity of plasmid genomes in teratocarcinoma-derived stem and differentiated cells. Proceedings of the National Academy of Sciences of the United States of America, 78(8), 5071–5075.

Humphrey, J. H., & Grennan, D. (1984). The origin of follicular dendritic cells in the mouse and the mechanism of trapping of immune complexes on them. European journal of immunology. 14(9), 859–864.

Illges, H., Braun, M., Peter, H. H., & Melchers, I. (2000). Reduced expression of the complement receptor type 2 (CR2, CD21) by synovial fluid B and T lymphocytes. Clinical and Experimental Immunology, 122(2), 270–276.

Importance, C., & Potential, T. (2005). Protective Autoantibodies Role in Homeostasis , Clinical Importance , and Therapeutic Potential. Arthritis Rheumatology 52(9), 2599–2606

Inoue, T., Shinnakasu, R., Ise, W., Kawai, C., Egawa, T., & Kurosaki, T. (2017). The transcription factor Foxo1 controls germinal center B cell proliferation in response to T cell help. Journal of Experimental medicine. 214(4), 1181-1198.

Ioannidis, J. P. A., Vassiliou, V. A., & Moutsopoulos, H. M. (2002). Long-Term Risk of Mortality and Lymphoproliferative Disease and Predictive Classification of Primary Sjogren ' s Syndrome. Arthritis Rheumatology. 46(3), 741-477.

Ishikawa, Y., Usui, T., Shiomi, A., & Shimizu, M. (2014). Functional engraftment of human peripheral T and B cells and sustained production of autoantibodies in NOD / LtSzscid / IL-2R γ − / − mice. European Journal of Immunology. 44, 3453–3463.

Isnardi, I., Ng, Y., Menard, L., Meyers, G., Saadoun, D., Srdanovic, I., … Meffre, E. (2010). Complement receptor 2 / CD21 ⁻ human naive B cells contain mostly autoreactive unresponsive clones. Blood. 115(24), 5026–5037.

Izquierdo, E., Can, J. D., Celis, R., Rey, M. J. Del, Usategui, A., Marsal, S., … Criado, G. (2011). Synovial Fibroblast Hyperplasia in Rheumatoid Arthritis Clinicopathologic Correlations and Partial Reversal by Anti – Tumor Necrosis Factor Therapy. Arthritis Rheumotology. 63(9), 2575–2583.

Jacobson, A. C., & Weis, J. H. (2008). Comparative Functional Evolution of Human and Mouse CR1 and CR2. Journal of Immunology (Baltimore, Md. : 1950), 181(5), 2953–2959.

Jacobson, D. L., Gange, S. J., Rose, N. R., & Graham, N. M. H. (1997). Epidemiology and Estimated Population Burden of Selected Autoimmune Diseases in the United States. Clinical Immunology and Immunopathology. 84(3), 223–243.

Jain, S., Chodisetti, S. B., & Agrewala, J. N. (2011). CD40 signaling synergizes with TLR-2 in the BCR independent activation of resting B cells. PLoS ONE, 6(6), 1–11.

James, S., Fox, J., Afsari, F., Lee, J., Clough, S., Knight, C., … Genever, P. (2015). Multiparameter Analysis of Human Bone Marrow Stromal Cells Identifies Distinct Immunomodulatory and Differentiation-Competent Subtypes. Stem Cell Reports, 4(6), 1004–1015.

Jarjour, M., Jorquera, A., Mondor, I., Wienert, S., Narang, P., Coles, M. C., … Bajénoff, M. (2014). Fate mapping reveals origin and dynamics of lymph node follicular dendritic cells. The Journal of Experimental Medicine, 211(6), 1109–1122.

Jiang, W., Lederman, M. M., Harding, C. V., Rodriguez, B., Mohner, R. J., & Sieg, S. F. (2007). TLR9 stimulation drives negative B cells to proliferate and to attain enhanced antigen presenting function. European Journal of Immunology, 37(8), 2205–2213.

Jung, J., Choe, J., Li, L., & Choi, Y. S. (2000). Regulation of CD27 expression in the course of germinal center B cell differentiation: the pivotal role of IL-10. European Journal of Immunology, 30(8), 2437–2443.

Justice, B. a., Badr, N. a., & Felder, R. a. (2009). 3D cell culture opens new dimensions in cell-based assays. Drug Discovery Today, 14(1–2), 102–107.

Kálmán, S., Garbett, K., Vereczkei, A., Shelton, R. C., Korade, Z., & Mirnics, K. (2014). Metabolic stress-induced microRNA and mRNA expression profiles of human fibroblasts. Exp Cell Res., 320(2), 343–353.

Kapasi, Z. F., Qin, D., Kerr, W. G., Kosco-Vilbois, M. H., Shultz, L. D., Tew, J. G., & Szakal, a K. (1998). Follicular dendritic cell (FDC) precursors in primary lymphoid tissues. Journal of Immunology (Baltimore, Md. : 1950), 160(3), 1078–1084.

Karampoor, S., Zahednasab, H., Etemadifar, M., & Keyvani, H. (2018). The levels of soluble forms of CD21 and CD83 in multiple sclerosis. Journal of Neuroimmunology, 320, 11–14.

Katakai, T. (2004). Lymph Node Fibroblastic Reticular Cells Construct the Stromal Reticulum via Contact with Lymphocytes. Journal of Experimental Medicine, 200(6), 783–795.

Katakai, T., Suto, H., Sugai, M., Gonda, H., Togawa, A., Suematsu, S., … Shimizu, A. (2008). Organizer-Like Reticular Stromal Cell Layer Common to Adult Secondary Lymphoid Organs. The Journal of Immunology, 181(9), 6189–6200.

Katakai, T., Suto, H., Sugai, M., Togawa, A., Suematsu, S., Katagiri, K., … Alerts, E. (2008). Organizer-Like Reticular Stromal Cell Layer Common to Adult Secondary Lymphoid Organs. Journal of Immunology. 181(9), 6189-6200.

Keller, B., Stumpf, I., Strohmeier, V., Usadel, S., Verhoeyen, E., Eibel, H., & Warnatz, K. (2017). High SYK Expression Drives Constitutive Activation of CD21 low B Cells. The Journal of Immunology, 198(11), 4285–4292.

Kim, H. S., Zhang, X., Klyushnenkova, E., & Choi, Y. S. (1995). Stimulation of germinal center B lymphocyte proliferation by an FDC-like cell line, HK. Journal of Immunology, 155(3), 1101–1109.

Kim, J., Kim, D. W., Chang, W., Choe, J., Kim, J., Park, C., … Lee, I. (2012). Wnt5a Is Secreted by Follicular Dendritic Cells To Protect Germinal Center B Cells via Wnt/Ca 2+ /NFAT/NF- κ B − B Cell Lymphoma 6 Signaling. Journal of Immunology. 188(1), 182-189.

Konforte, D., Simard, N., & Paige, C. J. (2009). IL-21: an executor of B cell fate. Journal of Immunology (Baltimore, Md. : 1950), 182(4), 1781–1787.

Koni, P. a, Sacca, R., Lawton, P., Browning, J. L., Ruddle, N. H., & Flavell, R. a. (1997). Distinct roles in lymphoid organogenesis for lymphotoxins alpha and beta revealed in lymphotoxin beta-deficient mice. Immunity, 6(4), 491–500.

Koning, J. J., & Mebius, R. E. (2012). Interdependence of stromal and immune cells for lymph node function. Trends in Immunology, 33(6), 264–270.

Kourilovitch, M., Galarza-Maldonado, C., & Ortiz-Prado, E. (2014). Diagnosis and classification of rheumatoid arthritis. Journal of Autoimmunity, 48–49, 26–30.

Kranich, J., & Krautler, N. J. (2016). How follicular dendritic cells shape the B-cell antigenome. Frontiers in Immunology, 7, 225-257.

Kranich, J., Krautler, N. J., Heinen, E., Polymenidou, M., Bridel, C., Schildknecht, A., … Aguzzi, A. (2008). Follicular dendritic cells control engulfment of apoptotic bodies by secreting Mfge8. The journal of Experimental Medicine. 205(6), 1293–1302.

Kräutler, N. J., Suan, D., Butt, D., Bourne, K., Hermes, J. R., Chan, T. D., … Brink, R. (2017). Differentiation of germinal center B cells into plasma cells is initiated by high-affinity antigen and completed by Tfh cells. The Journal of Experimental Medicine. 214(5), 1259-1267.

Krautler, N. J., Kana, V., Kranich, J., Tian, Y., Perera, D., Lemm, D., … Aguzzi, A. (2012). Follicular dendritic cells emerge from ubiquitous perivascular precursors. Cell, 150(1), 194–206.

Kröncke, R., Loppnow, H., Flad, H. D., & Gerdes, J. (1996). Human follicular dendritic cells and vascular cells produce interleukin-7: a potential role for interleukin-7 in the germinal center reaction. European Journal of Immunology, 26(10), 2541–2544.

Kubota, Y., Angelotti, T., Niederfellner, G., Herbst, R., & Ullrich, a. (1998). Activation of phosphatidylinositol 3-kinase is necessary for differentiation of FDC-P1 cells following stimulation of type III receptor tyrosine kinases. Cell Growth & Differentiation : The Molecular Biology Journal of the American Association for Cancer Research, 9, 247–256.

Kuppers, R., Zhao, M., Hansmann, M., & Rajewsky, K. (1993). Tracing B cell development in human germinal centres by molecular analysis of single cells picked from histological sections. EMBO. 12(13), 4955–4967.

Kurosaki, T., Kometani, K., & Ise, W. (2015). Memory B cells. Nature Reviews Immunology, 15(3), 149–159.

Kurtz, C. B., O'Toole, E., Christensen, S. M., & Weis, J. H. (1990). The murine complement receptor gene family. IV. Alternative splicing of Cr2 gene transcripts predicts two distinct gene products that share homologous domains with both human CR2 and CR1. Journal of Immunology (Baltimore, Md. : 1950), 144(9), 3581–3591.

Lalonde, E., Ha, K. C. H., Wang, Z., Bemmo, A., Kleinman, C. L., Kwan, T., … Majewski, J. (2011). RNA sequencing reveals the role of splicing polymorphisms in regulating human gene expression. Genome Res. 21(4), 545–554.

Lämmermann, T., Bader, B. L., Monkley, S. J., Worbs, T., Wedlich-Söldner, R., Hirsch, K., … Sixt, M. (2008). Rapid leukocyte migration by integrin-independent flowing and squeezing. Nature, 453(7191), 51–55.

Larcher, R. C., & Petzer, L. (1993). Determination of soluble CD21 as a parameter of B cell activation. Clinical Experimental Immunology. 93(2), 195-199.

Lebien, T. W., & Tedder, T. F. (2008). ASH 50th anniversary review B lymphocytes : how they develop and function. Blood. 112(5), 1570–1581.

Lee, Y., Haas, K. M., Gor, D. O., Karp, D. R., Greenspan, N. S., Poe, J. C., … Tedder, T. F. (2010). Augment or Inhibit B Lymphocyte Activation and Humoral Complex Engagement 1. Journal of Immunology. 184, 2231-2232.

Lesley, R., Kelly, L. M., Xu, Y., & Cyster, J. G. (2006). Naive CD4 T cells constitutively express CD40L and augment autoreactive B cell survival. Proceedings of the National Academy of Sciences of the United States of America, 103(28), 10717–10722.

Lesley, R., Xu, Y., Kalled, S. L., Hess, D. M., Schwab, S. R., Shu, H. B., & Cyster, J. G. (2004). Reduced competitiveness of autoantigen-engaged B cells due to increased dependence on BAFF. Immunity, 20(4), 441–453.

Li, B. L., Zhang, X., Kovacic, S., Long, A. J., Bourque, K., Wood, C. R., & Choi, Y. S. (2000). Identification of a Human Follicular D endritic Cell Molecule That Stimulates Germinal Center B Cell Growth. Journal of Experimental Medicine. 191(6), 1077–1083.

Li, J., Chen, X. H., Xiao, P. J., Li, L., Lin, W. M., Huang, J., & Xu, P. (2008). Expression pattern and splicing function of mouse ZNF265. Neurochemical Research, 33(3), 483–489.

Li, L., Zhang, X., Kovacic, S., Long, a J., Bourque, K., Wood, C. R., & Choi, Y. S. (2000). Identification of a human follicular dendritic cell molecule that stimulates germinal center B cell growth. J Exp Med, 191(6), 1077–1084.

Li, Y., Masse-Ranson, G., Garcia, Z., Bruel, T., Kök, A., Strick-Marchand, H., … Di Santo, J. P. (2018). A human immune system mouse model with robust lymph node development. Nature Methods, 15(8), 623–630.

Lindblom, R. P. F., Aeinehband, S., Ström, M., Al, F., Sandholm, K., Khademi, M., … Ekdahl, K. N. (2016). Complement Receptor 2 is increased in cerebrospinal fl uid of multiple sclerosis patients and regulates C3 function. Clinical Immunology, 166–167, 89–95.

Ling, N. R., Hardie, D. L., Johnson, G. D., & Maclennan, I. C. M. (1998). Origin and properties of soluble CD21 (CR2) in human blood. Clinical and Experimental Immunology, 113(3), 360–366.

Liu, C., Richard, K., Wiggins, M., Zhu, X., Conrad, D. H., & Song, W. (2016). CD23 can negatively regulate B-cell receptor signaling. Scientific Reports, 16(6), 1–8.

Liu, Y. J., Xu, J., de Bouteiller, O., Parham, C. L., Grouard, G., Djossou, O., … Moore, K. W. (1997). Follicular dendritic cells specifically express the long CR2/CD21 isoform. The Journal of Experimental Medicine, 185(1), 165–170.

Lo, C. G., Lu, T. T., & Cyster, J. G. (2003). Integrin-dependence of lymphocyte entry into the splenic white pulp. The Journal of Experimental Medicine, 197(3), 353–361.

Lopez-Matas, M., Rodriguez-Justo, M., Morilla, R., Catovsky, D., & Matutes, E. (2000). Quantitative expression of CD23 and its ligand CD21 in chronic lymphocytic leukemia. Haematologica, 85(11), 1140–1145.

Lu, T. T., & Browning, J. L. (2014). Role of the lymphotoxin/LIGHT system in the development and maintenance of reticular networks and vasculature in lymphoid tissues. Frontiers in Immunology, 11,, 5:47.

Luther, S. A., Bidgol, A., Hargreaves, D. C., Schmidt, A., Xu, Y., Paniyadi, J., … Cyster, J. G. (2002). Differing Activities of Homeostatic Chemokines CCL19, CCL21, and CXCL12 in Lymphocyte and Dendritic Cell Recruitment and Lymphoid Neogenesis. Journal of Immunology.169(1), 424-33.

Lynch, K. W., & Weiss, a. (2000). A model system for activation-induced alternative splicing of CD45 pre-mRNA in T cells implicates protein kinase C and Ras. Molecular and Cellular Biology, 20(1), 70–80.

Lynch, K. W. (2004). Consequences of regulated pre-mRNA splicing in the immune system. Nature Reviews. Immunology, 4(12), 931–940.

Ma, T., Grayson, W. L., Fröhlich, M., & Vunjak-Novakovic, G. (2009). Hypoxia and stem cell-based engineering of mesenchymal tissues. Biotechnology Progress, 25(1), 32–42.

Mabbott, N. A., Kenneth Baillie, J., Kobayashi, A., Donaldson, D. S., Ohmori, H., Yoon, S. O., … Summers, K. M. (2011). Expression of mesenchyme-specific gene signatures by follicular dendritic cells: insights from the meta-analysis of microarray data from multiple mouse cell populations. Immunology, 133(4), 482–498.

Mackay, F., Majeau, G. R., Lawton, P., Hochman, P. S., & Browning, J. L. (1997). Lymphotoxin but not tumor necrosis factor functions to maintain splenic architecture and humoral responsiveness in adult mice. European Journal of Immunology. 27(8), 2033–2042.

Makar, K. W., Pham, C. T. N., Dehoff, M. H., O'Connor, S. M., Jacobi, S. M., & Holers, V. M. (1998). An intronic silencer regulates B lymphocyte cell- and stage-specific expression of the human Complement Receptor Type 2 (CR2, CD21) gene. The Journal of Immunology, 160(3), 1268–1278.

Malkiel, S., Jeganathan, V., Wolfson, S., Manjarrez Orduï¿½o, N., Marasco, E., Aranow, C., … Diamond, B. (2016). Checkpoints for Autoreactive B Cells in the Peripheral Blood of Lupus Patients Assessed by Flow Cytometry. Arthritis and Rheumatology, 68(9), 2210–2220.

Mallinjoud, P., Villemin, J. P., Mortada, H., Espinoza, M. P., Desmet, F. O., Samaan, S., … Auboeuf, D. (2014). Endothelial, epithelial, and fibroblast cells exhibit specific splicing programs independently of their tissue of origin. Genome Research, 24(3), 511–521.

Manca, B. F., Fenoglio, D., Pira, G. L., & Celada, F. (1991). Effect of Antigen/Antibody Ratio on Macrophage Uptake, Processing, and Presentation to T Cells of Antigen Complexed with Polyclonal Antibodies. Journal of Experimental Medicine. 173(1), 37-48.

Manzo, A., Paoletti, S., Carulli, M., Blades, M. C., Barone, F., Yanni, G., … Matteo, I. S. (2005). Cellular immune response Systematic microanatomical analysis of CXCL13 and CCL21 in situ production and progressive lymphoid organization in rheumatoid synovitis. European Journal of Immunology. 35(5), 1347–1359.

Marchbank, K. J., Watson, C. C., Ritsema, D. F., & Holers, V. M. (2000). Expression of Human Complement Receptor 2 (CR2, CD21) in Cr2-/- Mice Restores Humoral Immune Function. The Journal of Immunology, 165(5), 2354–2361.

Marquart, H. V, Olesen, E. H., Johnson, A. A., Damgaard, G., & Leslie, R. G. (1997). A comparative study of normal B cells and the EBV-positive Burkitt's lymphoma cell line, Raji, as activators of the complement system. Scandinavian Journal of Immunology, 46(3), 246–253.

Martin, D. R., Marlowe, R. L., & Ahearn, J. M. (1994). Determination of the role for CD21 during Epstein-Barr virus infection of B-lymphoblastoid cells. Journal of Virology, 68(8), 4716–4726.

Martin, F., Chan, A. C., & Way, O. D. N. A. (2004). Pathogenic Roles of B Cells in Human Autoimmunity : Insights from the Clinic The pathogenic roles of B cells in human autoimmune. Immunity. 20(5), 517–527.

Masilamani, M., von Kempis, J., & Illges, H. (2004). Decreased levels of serum soluble complement receptor-II (CR2/CD21) in patients with rheumatoid arthritis. Rheumatology, 43(2), 186–190.

Masilamani, M., Nowack, R., Witte, T., Schlesier, M., Warnatz, K., Glocker, M. O., … Illges, H. (2004). Reduction of Soluble Complement Receptor 2 / CD21 in Systemic Lupus Erythomatosus and Sjo ¨ gren ' s Syndrome but not Juvenile Arthritis. Scandinavian Journal of Immunology. 60(6), 625–630.

Masilamani, M., Apell, H.-J., & Illges, H. (2002). Purification and characterization of soluble CD21 from human plasma by affinity chromatography and density gradient centrifugation. Journal of Immunological Methods, 270(1), 11–18.

Masilamani, M., Kassahn, D., Mikkat, S., Glocker, M. O., & Illges, H. (2003). B cell activation leads to shedding of complement receptor type II (CR2 / CD21). European Journal of Immunology. 33(9), 2391–2397.

Masilamani, M., Rajasekaran, N., Singh, A., Low, H. Z., Albus, K., Anders, S., … Illges, H. (2008). Systemic reduction of soluble complement receptor II/CD21 during pregnancy to levels reminiscent of autoimmune disease. Rheumatology International, 28(11), 1137–1141.

Masilamani, M., Von Seydlitz, E., Bastmeyer, M., & Illges, H. (2002). T cell activation induced by cross-linking CD3 and CD28 leads to silencing of Epstein-Barr virus/C3d receptor (CR2/CD21) gene and protein expression. Immunobiology, 206(5), 528–536.

Matsumoto, B. A. K., Kopicky-burd, J., Carter, R. H., Tuveson, D. A., Tedder, T. F., & Fearon, D. T. (1991). Intersection of the Complement and Immune Systems: A Signal Transduction Complex of the B Lymphocyte-containing Complement Receptor Type 2 and CD19. Journal of Experimental Medicine. 173(1), 55-64.

Mebius, R. E., Rennert, P., & Weissman, I. L. (1997). Developing lymph nodes collect CD4+CD3- LTbeta+ cells that can differentiate to APC, NK cells, and follicular cells but not T or B cells. Immunity, 7, 493–504.

Melkus, M. W., Estes, J. D., Padgett-thomas, A., Gatlin, J., Denton, P. W., Othieno, F. A., … Garcia, J. V. (2006). Humanized mice mount specific adaptive and innate immune responses to EBV and TSST-1. Nature Medicine. 12(11), 1316–1322.

Melzi, E., Caporale, M., Rocchi, M., Martín, V., Gamino, V., di Provvido, A., … Palmarini, M. (2016). Follicular dendritic cell disruption as a novel mechanism of virus-induced immunosuppression. Proceedings of the National Academy of Sciences, 113(41), E6238–E6247.

Mihai, S., & Nimmerjahn, F. (2013). The role of Fc receptors and complement in autoimmunity. Autoimmunity Reviews, 12(6), 657–660.

Milićević, N. M., Milićević, Z., & Westermann, J. J. (2011). Lipopolysaccharide-Induced In Vivo Activation of Follicular Dendritic Cells is Tumor Necrosis Factor Receptor-1 Independent. Anatomical Record. 295(1), 125-134.

Mizoguchi, A., Mizoguchi, E., Takedatsu, H., Blumberg, R. S., & Bhan, A. K. (2002). Generates IL-10-Producing Regulatory B Cell Subset Characterized by CD1d Upregulation. Immunity. 16(2), 219–230.

Mobarrez, F., Vikerfors, A., Gustafsson, J. T., Gunnarsson, I., Zickert, A., Larsson, A., … Svenungsson, E. (2016). Microparticles in the blood of patients with systemic lupus erythematosus (SLE): Phenotypic characterization and clinical associations. Scientific Reports, 25(6), 1–10.

Molina, H., Kinoshita, T., Inoue, K., Carel, J. C., & Holers, V. M. (1990). A molecular and immunochemical characterization of mouse CR2. Evidence for a single gene model of mouse complement receptors 1 and 2. Journal of Immunology (Baltimore, Md. : 1950), 145(9), 2974–2983.

Monlong, J., Calvo, M., Ferreira, P. G., & Guigó, R. (2014). Identification of genetic variants associated with alternative splicing using sQTLseekeR. Nature Communications, 5, 4698.

Moore, M. D., DiScipio, R. G., Cooper, N. R., & Nemerow, G. R. (1989). Hydrodynamic, electron microscopic, and ligand-binding analysis of the Epstein-Barr virus/C3dg receptor (CR2). Journal of Biological Chemistry, 264(34), 20576–20582.

Morgan, B. P., & Harris, C. L. (2015). Complement, a target for therapy in inflammatory and degenerative diseases. Nature Reviews Drug Discovery. 14(12), 857-77

Moriyama, M., Fukuhara, T., Britschgi, M., He, Y., Narasimhan, R., Villeda, S., … Wyss-Coray, T. (2011). Complement Receptor 2 Is Expressed in Neural Progenitor Cells and Regulates Adult Hippocampal Neurogenesis. Journal of Neuroscience, 31(11), 3981–3989.

Morrow, W. J. W., Williams, D. J. P., Ferec, C., Isenberg, D. A., Paice, E., Snaith, M. L., … Goff, P. L. E. (1983). The use of C3d as a means of monitoring clinical activity in systemic lupus erythematosus and rheumatoid arthritis. Annuals of the Rheumatic Diseases. 42, 668–671.

Moshkani, S., Kuzin, I. I., Adewale, F., Jansson, J., Sanz, I., & Schwarz, E. M. (2012). CD23 + CD21 high CD1d high B Cells in Inflamed Lymph Nodes Are a Locally Differentiated Population with Increased Antigen Capture and Activation Potential. Journal of Immunology. 188(12), 5944-53.

Mossalayi, M. D., & Blanc, C. (1990). Proliferation of Early Human Myeloid Precursors Induced by Interleukin-1 and Recombinant Soluble CD23. Blood. 7(10), 1924–1927.

Motta-Mena, L. B., Smith, S. A., Mallory, M. J., Jackson, J., Wang, J., & Lynch, K. W. (2011). A disease-associated polymorphism alters splicing of the human CD45 phosphatase gene by disrupting combinatorial repression by heterogeneous nuclear ribonucleoproteins (hnRNPs). Journal of Biological Chemistry, 286(22), 20043–20053.

Mueller, S. N., & Germain, R. N. (2009). Stromal cell contributions to the homeostasis and functionality of the immune system. Nature Reviews. Immunology, 9(9), 618–629.

Munoz-Fernandez, R., Blanco, F. J., Frecha, C., Martin, F., Kimatrai, M., Abadia-Molina, A. C., … Olivares, E. G. (2006). Follicular Dendritic Cells Are Related to Bone Marrow Stromal Cell Progenitors and to Myofibroblasts. The Journal of Immunology, 177(1), 280–289.

Munoz-Fernandez, R., Blanco, F. J., Frecha, C., Martin, F., Kimatrai, M., Abadia-Molina, A. C., … Olivares, E. G. (2006). Follicular dendritic cells are related to bone marrow stromal cell progenitors and to myofibroblasts. J Immunol, 177(1), 280–289.

Murphy, M., Walter, B. N., Pike-Nobile, L., Fanger, N. a, Guyre, P. M., Browning, J. L., … Epstein, L. B. (1998). Expression of the lymphotoxin beta receptor on follicular stromal cells in human lymphoid tissues. Cell Death and Differentiation, 5, 497–505.

Myers, R. C., King, R. G., Carter, R. H., & Justement, L. B. (2013). Lymphotoxin α1β2 expression on B cells is required for follicular dendritic cell activation during the germinal center response. European Journal of Immunology, 43(2), 348–359.

Myonesll, B. L., Holers, V. M., Carel, J.-C., & Frazier, B. (1990). Structural Requirements for C3d, g/Epstein-Barr Virus Receptor (CR2/CD21) Ligand Binding, Internalization, and Viral Infection. The Journal of Biological Chemistry, 265(21), 12293–12299.

Nagar, B., Jones, R. G., Diefenbach, R. J., Isenman, D. E., & Rini, J. M. (1998). X-ray crystal structure of C3d: a C3 fragment and ligand for complement receptor 2. Science (New York, N.Y.), 280(5367), 1277–1281.

Naiem, M., Gerdes, J., Abdulaziz, Z., Stein, H., & Mason, D. Y. (1983). Production of a monoclonal antibody reactive with human dendritic reticulum cells and its use in the immunohistological analysis of lymphoid tissue. Journal of Clinical Pathology, 36(2), 167–175.

Nandakumar, K. S., Andr, M., Martinsson, P., Bajtner, E., Holmdahl, R., & Kleinau, S. (2003). Induction of arthritis by single monoclonal IgG anti- collagen type II antibodies and enhancement of arthritis in mice lacking inhibitory Fc q RIIB. Arthritis Research and Therapy. 6(6), 2269–2277.

Ngo, B. V. N., Korner, H., Gunn, M. D., Schmidt, K. N., Riminton, D. S., Cooper, M. D., … Cyster, J. G. (1999). Required for Stromal Cell Expression of Homing Chemokines in B and T Cell Areas of the Spleen. Journal Experimental Medicine. 189(2), 403-12.

Ngo, V. N., Korner, H., Gunn, M. D., Schmidt, K. N., Riminton, D. S., Cooper, M. D., … Cyster, J. G. (1999). Lymphotoxin alpha/beta and tumor necrosis factor are required for stromal cell expression of homing chemokines in B and T cell areas of the spleen. The Journal of Experimental Medicine, 189(2), 403–412.

Nielsen, C. H., Leslie, R. G. Q., Jepsen, B. S., Kazatchkine, M. D., Kaveri, S. V, & Fischer, E. (2001). Natural autoantibodies and complement promote the uptake of a self antigen , human thyroglobulin , by B cells and the proliferation of thyroglobulin- reactive CD4 + T cells in healthy individuals. European Journal of Immunology, 31(9), 2660–2668.

Ogata, T., Yamakawa, M., Imai, Y., & Takahashi, T. (1996). Follicular dendritic cells adhere to fibronectin and laminin fibers via their respective receptors. Blood, 88(8), 2995–3003.

Okamoto, N., Chihara, R., Shimizu, C., Nishimoto, S., & Watanabe, T. (2007). Artificial lymph nodes induce potent secondary immune responses in naive and immunodeficient mice. Journal of Clinical Investigation, 117(4), 997–1007.

Otsuka, M., & Yakushijin, Y. (2004). Role of CD21 antigen in diffuse large B-cell lymphoma and its clinical significance. British Journal of Heamatology. 127(4), 416–424.

Pape, K. A., Catron, D. M., Itano, A. A., & Jenkins, M. K. (2007). The Humoral Immune Response Is Initiated in Lymph Nodes by B Cells that Acquire Soluble Antigen Directly in the Follicles. Immunity, 26(4), 491–502.

Park, C.-S., Yoon, S.-O., Armitage, R. J., & Choi, Y. S. (2004). Follicular dendritic cells produce IL-15 that enhances germinal center B cell proliferation in membrane-bound form. Journal of Immunology (Baltimore, Md. : 1950), 173(11), 6676–6683.

Park, S.-M., Park, H.-Y., & Lee, T. H. (2003). Functional effects of TNF-alpha on a human follicular dendritic cell line: persistent NF-kappa B activation and sensitization for Fas-mediated apoptosis. Journal of Immunology (Baltimore, Md. : 1950), 171(8), 3955–3962.

Pekalski, M. L., García, A. R., Ferreira, R. C., Rainbow, D. B., Smyth, D. J., Mashar, M., … Wicker, L. S. (2017). Neonatal and adult recent thymic emigrants produce IL-8 and express complement receptors CR1 and CR2. JCI Insight, 2(16).

Pettigrew, H. D., Teuber, S. S., & Gershwin, M. E. (2009). Clinical Significance of Complement Deficiencies, New York Academy of Science. 123, 108–123.

Phan, T. G., Grigorova, I., Okada, T., & Cyster, J. G. (2007). Subcapsular encounter and complement-dependent transport of immune complexes by lymph node B cells. Nature Immunology, 8(9), 992–1000.

Pike, K. a, & Ratcliffe, M. J. H. (2002). Cell surface immunoglobulin receptors in B cell development. Seminars in Immunology, 14(5), 351–358.

Pillai, S., & Taylor, K. N. (2011). B-Cell Tolerance and Autoimmunity. Systemic Lupus Erythematosus. F1000 Research. 6, 107–113.

Prodeus, A. P., Goerg, S., Shen, L., Pozdnyakova, O. O., Chu, L., Alicot, E. M., … Carroll, M. C. (1998). A Critical Role for Complement in Maintenance of Self-Tolerance. Immunity. 9, 721–731.

Prodinger, W. M., Schwendinger, M. G., Köchle, M., Larcher, C., Dierich, M. P., Cr, T., & Ko, M. (1998). Characterization of C3dg Binding to a Recess Formed Between Short Consensus Repeats 1 and 2 of Complement Receptor Type 2 (CR2; CD21). Journal of Immunology. 161(9), 4604-10.

Prodinger, W. M., Schwendinger, M. G., Schoch, J., Köchle, M., Larcher, C., & Dierich, M. P. (1998). Characterization of C3dg binding to a recess formed between short consensus repeats 1 and 2 of complement receptor type 2 (CR2; CD21). Journal of Immunology (Baltimore, Md. : 1950), 161(9), 4604–4610.

Prokopec, K. E., Rhodiner, M., Matt, P., Lindqvist, U., & Kleinau, S. (2010). Down regulation of Fc and complement receptors on B cells in rheumatoid arthritis. Clinical Immunology, 137(3), 322–329.

Prota, A. E., Sage, D. R., Stehle, T., & Fingeroth, J. D. (2002). The crystal structure of human CD21: Implications for Epstein-Barr virus and C3d binding. Proceedings of the National Academy of Sciences of the United States of America, 99(16), 10641–10646.

Purwada, A., Jaiswal, M. K., Ahn, H., Nojima, T., Kitamura, D., Gaharwar, A. K., … Singh, A. (2015). Ex vivo engineered immune organoids for controlled germinal center reactions. Biomaterials, 63, 24–34.

Qin, D., Wu, J., Carroll, M. C., Gregory, F., Szakal, A. K., & Tew, J. G. (1998). Cells in the Initiation of IgG Responses. Journal of Immunology, 161, 4549–4554.

Rennert, P. D., James, D., Mackay, F., Browning, J. L., & Hochman, P. S. (1998). Lymph node genesis is induced by signaling through the lymphotoxin receptor. Immunity, 9(1), 71–79.

Ribbens, C., Bonnet, V., Kaiser, M. J., Andre, B., Kaye, O., Franchimont, N., … Malaise, M. G. (2000). Increased synovial fluid levels of soluble CD23 are associated with an erosive status in rheumatoid arthritis (RA). Clinical and Experimental Immunology, 120(1), 194–199.

Rickert, R. C. (2005). Regulation of B lymphocyte activation by complement C3 and the B cell coreceptor complex. Current Opinion in Immunology, 17(3), 237–243.

Rochas, C., Hillion, S., Saraux, A., Mageed, R. A., Youinou, P., & Jamin, C. (2009). Transmembrane BAFF From Rheumatoid Synoviocytes Requires Interleukin-6 to Induce the Expression of Recombination-Activating Gene in B Lymphocytes, Arthritis Rheumatology. 60(5), 1261–1271.

Rodda, L. B., Bannard, O., Ludewig, B., Nagasawa, T., & Cyster, J. G. (2015). Phenotypic and Morphological Properties of Germinal Center Dark Zone Cxcl12-Expressing Reticular Cells. Journal of Immunology (Baltimore, Md. : 1950), 195(10), 4781–4791.

Roman, V., Dugas, N., Abadie, A., Amirand, C., Zhao, H., Dugas, B., & Kolb, J. P. (1997). Characterization of a constitutive type III nitric oxide synthase in human U937 monocytic cells: Stimulation by soluble CD23. Immunology, 91(4), 643–648.

Ron, Y., Baetselier, P. De, Gordon, J., Ron, Y., & Baetselier, P. De. (1981). Defective induction of antigen-reactive proliferating T cells in B cell-deprived mice. European Journal of Immunology. 11(12), 964–968.

Roozendaal, R., & Carroll, M. C. (2007). Complement receptors CD21 and CD35 in humoral immunity. Immunological Reviews, 219(1), 157–166.

Roozendaal, R., & Mebius, R. E. (2011). Stromal cell-immune cell interactions. Annual Review of Immunology, 29, 23–43.

Ruprecht, C. R., & Lanzavecchia, A. (2006). Toll-like receptor stimulation as a third signal required for activation of human naive B cells. European Journal of Immunology, 36(4), 810–816.

Savage, P. A., Boniface, J. J., & Davis, M. M. (1999). A Kinetic Basis For T Cell Receptor Repertoire Selection during an Immune Response. Immunity. 10, 485–492.

Scheid, J. F., Mouquet, H., Kofer, J., Yurasov, S., & Nussenzweig, M. C. (2011). Differential regulation of self-reactivity discriminates between IgG + human circulating memory B cells and bone marrow plasma cells. National Academy of Science USA. 108(44), 18044–18048.

Schriever, F., Freedman, a S., Freeman, G., Messner, E., Lee, G., Daley, J., & Nadler, L. M. (1989). Isolated human follicular dendritic cells display a unique antigenic phenotype. The Journal of Experimental Medicine, 169(6), 2043–2058.

Schwarzmeier, J. D., Shehata, M., Hilgarth, M., Marschitz, I., Louda, N., Hubmann, R., & Greil, R. (2002). The role of soluble CD23 in distinguishing stable and progressive forms of B-chronic lymphocytic leukemia. Leukemia and Lymphoma, 43(3), 549–554.

Shields, J., Pochon, S., Aubry, J. P., Flores-Romo, L., Jansen, K., Graber, P., & Bonnefoy, J. Y. (1992). The role of CD23 and its receptor in T-cell/B-cell interaction: implications for regulation of IgE synthesis. Research in Immunology, 143(4), 425–427.

Singh, A., Vastert, S. J., Prakken, B. J., & Illges, H. (2011). Decreased levels of sCD21 and sCD23 in blood of patients with systemic-juvenile arthritis, polyarticular-juvenile arthritis, and pauciarticular-juvenile arthritis. Rheumatology International, 32(6), 1581–1587.

Spengler, J., Amara, K., Clay, E., Yeo, L., Ramsk, D., Sippl, N., … Malmstr, V. (2017). B cells expressing the IgA receptor FcRL4 participate in the autoimmune response in patients with rheumatoid arthritis. Journal of Autoimmunity. 81, 34–43.

Spittler, a, Schiller, C., Willheim, M., Tempfer, C., Winkler, S., & Boltz-Nitulescu, G. (1995). IL-10 augments CD23 expression on U937 cells and down-regulates IL-4-driven CD23 expression on cultured human blood monocytes: effects of IL-10 and other cytokines on cell phenotype and phagocytosis. Immunology, 85(2), 311–317.

Suan, D., Sundling, C., & Brink, R. (2017). Plasma cell and memory B cell differentiation from the germinal center. Current Opinion in Immunology, 45, 97–102.

Sukumar, S., Szakal, A. K., & Tew, J. G. (2006). Isolation of functionally active murine follicular dendritic cells. Journal of Immunological Methods, 313(1–2), 81–95.

Suto, H., Katakai, T., Sugai, M., Kinashi, T., & Shimizu, A. (2009). CXCL13 production by an established lymph node stromal cell line via lymphotoxin-beta receptor engagement involves the cooperation of multiple signaling pathways. International Immunology, 21(4), 467–476.

Suto, H., Katakai, T., Sugai, M., Kinashi, T., & Shimizu, A. (2009). CXCL13 production by an established lymph node stromal cell line via lymphotoxin-beta receptor engagement involves the cooperation of multiple signaling pathways. International Immunology, 21(4), 467–476.

Suzuki, K., Grigorova, I., Phan, T. G., Kelly, L. M., & Cyster, J. G. (2009). Visualizing B cell capture of cognate antigen from follicular dendritic cells. Journal of Experimental Medicine. 206(7), 1485–1493.

Suzuki, K., Maruya, M., Kawamoto, S., Sitnik, K., Kitamura, H., & Agace, W. W. (2010). Article The Sensing of Environmental Stimuli by Follicular Dendritic Cells Promotes Immunoglobulin A Generation in the Gut. Immunity, 33(1), 71–83.

Suzuki, K., Maruya, M., Kawamoto, S., Sitnik, K., Kitamura, H., Agace, W. W., & Fagarasan, S. (2010). The sensing of environmental stimuli by follicular dendritic cells promotes immunoglobulin A generation in the gut. Immunity, 33(1), 71–83.

Szakonyi, G., Guthridge, J. M., Li, D., Young, K., Holers, V. M., & Chen, X. S. (2001). Structure of complement receptor 2 in complex with its C3d ligand. Science (New York, N.Y.), 292(5522), 1725–1728.

Taylor, R. T., Patel, S. R., Lin, E., Butler, B. R., Lake, J. G., Newberry, R. D., & Williams, I. R. (2007). Lymphotoxin-independent expression of TNF-related activation-induced cytokine by stromal cells in cryptopatches, isolated lymphoid follicles, and Peyer's patches. Journal of Immunology (Baltimore, Md. : 1950), 178(9), 5659–5667.

Tedder, T. F., Inaoki, M., & Sato, S. (1997). The CD19-CD21 complex regulates signal transduction thresholds governing humoral immunity and autoimmunity. Immunity, 6(2), 107–118.

Ten Dam, G. B., Zilch, C. F., Wallace, D., Wieringa, B., Beverley, P. C., Poels, L. G., & Screaton, G. R. (2000). Regulation of alternative splicing of CD45 by antagonistic effects of SR protein splicing factors. Journal of Immunology (Baltimore, Md. : 1950), 164(10), 5287–5295.

Ten, R. M., Mckinstry, M. J., Bren, G. D., & Paya, C. V. (1999). Signal transduction pathways triggered by the FcεRIIb receptor (CD23) in human monocytes lead to nuclear factor-κB activation. Journal of Allergy and Clinical Immunology, 376–387.

Teplova, M., Malinina, L., Darnell, J. C., Song, J., Lu, M., Abagyan, R., … Patel, D. J. (2011). Article Protein-RNA and Protein-Protein Recognition by Dual KH1 / 2 Domains of the Neuronal Splicing Factor Nova-1. Structure/Folding and Design. Structure. 19(7), 930–944.

Tessier, J., Cuvillier, A., Glaudet, F., & Khamlichi, A. A. (2007). Internalization and molecular interactions of human CD21 receptor. Molecular Immunology, 44(9), 2415–2425.

Thiel, J., Kimmig, L., Salzer, U., Grudzien, M., Lebrecht, D., Hagena, T., … Schlesier, M. (2012). Genetic CD21 deficiency is associated with hypogammaglobulinemia. Journal of Allergy and Clinical Immunology, 129(3).

Thorarinsdottir, K., Camponeschi, A., Cavallini, N., Grimsholm, O., Jacobsson, L., Gjertsson, I., & Mårtensson, I. L. (2016). CD21–/low B cells in human blood are memory cells. Clinical and Experimental Immunology, 185(2), 252–262.

Thorarinsdottir, K., Camponeschi, A., Gjertsson, I., & M??rtensson, I. L. (2015). CD21-/low B cells: A Snapshot of a Unique B Cell Subset in Health and Disease. Scandinavian Journal of Immunology, 82(3), 254–261.

Toapanta, F. R., & Ross, T. M. (2006). Complement-mediated activation of the adaptive immune responses: role of C3d in linking the innate and adaptive immunity. Immunologic Research, 36(1–3), 197–210.

Toepfner, N., Cepok, S., Grummel, V., & Hemmer, B. (2012). The role of the Epstein – Barr Virus receptor CD21 in Multiple Sclerosis. Journal of Neuroimmunology, 242(1–2), 47–51.

Tomita, M., Kadono, T., Yazawa, N., Kawashima, T., Tamaki, Z., Ashida, R., … Sato, S. (2012). Serum levels of soluble CD21 in patients with systemic sclerosis. Rheumatology International, 32(2), 317–321.

Troldborg, A. (2018). The c3dg Fragment of complement is superior to conventional c3 as a Diagnostic Biomarker in systemic lupus erythematosus. Frontiers in Immunology. 9, 1–10.

Trück, J., Ramasamy, M. N., Galson, J. D., Rance, R., Parkhill, J., Lunter, G., … Kelly, D. F. (2015). Identification of Antigen-Specific B Cell Receptor Sequences Using Public Repertoire Analysis. The Journal of Immunology, 194(1), 252–261.

Tsunoda, R., Bosseloir, a, Onozaki, K., Heinen, E., Miyake, K., Okamura, H., … Sugai, N. (1997). Human follicular dendritic cells in vitro and follicular dendritic-cell-like cells. Cell and Tissue Research, 288(2), 381–389.

Tuveson, D. A., Ahearn, J. M., Matsumoto, A. K., & Fearon, D. T. (1991). Molecular interactions of complement receptors on B lymphocytes: a CR1/CR2 complex distinct from the CR2/CD19 complex. The Journal of Experimental Medicine, 173(5), 1083–1089.

Uccelli, A., Moretta, L., & Pistoia, V. (2006). Immunoregulatory function of mesenchymal stem cells. European Journal of Immunology, 36(10), 2566–2573.

van de Pavert, S. A., & Mebius, R. E. (2010). New insights into the development of lymphoid tissues. Nature Reviews Immunology, 10(9), 664–674.

Victora, G. D., Schwickert, T. A., Fooksman, D. R., Kamphorst, A. O., Meyer-hermann, M., Dustin, M. L., & Nussenzweig, M. C. (2010). Germinal Center Dynamics Revealed by Multiphoton Microscopy with a Photoactivatable Fluorescent Reporter. Cell, 143(4), 592‑605.

Vinuesa, C. G., Sanz, I., & Cook, M. C. (2009). Dysregulation of germinal centres in autoimmune disease. Nature Reviews. Immunology, 9(12), 845–857.

Voigt, I., Camacho, S. A., Boer, B. A. De, Lipp, M., & Berek, C. (2000). CXCR5-deficient mice develop functional germinal centers in the splenic T cell zone, 560–567.

Wang, X., Cho, B., Suzuki, K., Xu, Y., Green, J. a., An, J., & Cyster, J. G. (2011). Follicular dendritic cells help establish follicle identity and promote B cell retention in germinal centers. Journal of Experimental Medicine, 208(12), 2497–2510.

Wang, X., Rodda, L. B., Bannard, O., & Cyster, J. G. (2014). Integrin-Mediated Interactions between B Cells and Follicular Dendritic Cells Influence Germinal Center B Cell Fitness. The Journal of Immunology, 192(10), 4601–4609.

Watanabe, Y., Takahashi, T., Okajima, A., Shiokawa, M., Ishii, N., Katano, I., … Sugamura, K. (2009). The analysis of the functions of human B and T cells in humanized NOD / shi-scid / g c null (NOG) mice (hu-HSC NOG mice). International immunology. 21(7), 843–858.

Weih, F., & Caamano, J. (2003). Regulation of secondary lymphoid organ development by the nuclear factor-kappa B signal transduction pathway. Blackwell Munksgaard, 195, 91–105.

Wentink, M. W. J., Lambeck, A. J. A., Zelm, M. C. Van, Simons, E., Dongen, J. J. M. Van, Ijspeert, H., … Burg, M. Van Der. (2015). CD21 and CD19 de fi ciency : Two defects in the same complex leading to different disease modalities. Clinical Immunology, 161(2), 120–127.

Wilke, G., Steinhauser, G., Gru, J., & Berek, C. (2010). In silico subtraction approach reveals a close lineage relationship between follicular dendritic cells and BP3 hi stromal cells isolated from SCID mice. European Journal of Immunology. 40(8), 2165–2173.

Wilson, J. G., Ratnoff, W. D., Schur, P. H., & Fearon, D. T. (1986). Decreased expression of the C3b/C4b receptor (CR1) and the C3d receptor (CR2) on B lymphocytes and of CR1 on neutrophils of patients with systemic lupus erythematosus. Arthritis & Rheumatism, 29(6), 739–747.

Winberg, L. K., Nielsen, C. H., & Jacobsen, S. (2017). Surface complement C3 fragments and cellular binding of microparticles in patients with SLE. Lupus Science and Medicine, 4(1), 1–9.

Wu, Y., El Shikh, M. E. M., El Sayed, R. M., Best, A. M., Szakal, A. K., & Tew, J. G. (2009). IL-6 produced by immune complex-activated follicular dendritic cells promotes germinal center reactions, IgG responses and somatic hypermutation. International Immunology, 21(6), 745–756.

Yu, H., Borsotti, C., Schickel, J., Zhu, S., Strowig, T., Eynon, E., … Flavell, R. A. (2017). A novel humanized mouse model with significant improvement of class- switched, antigen-specific antibody production. Blood. 129(8), 959-969.

Zabel, M. D., & Weis, J. H. (2001). Cell-specific regulation of the CD21 gene. International Immunopharmacology, 1(3), 483–493.

Zhang, T., Gonzalez, D. G., Cote, C. M., Kerfoot, S. M., Deng, S., Cheng, Y., … Haberman, A. M. (2017). Germinal center B cell development has distinctly regulated stages completed by disengagement from T cell help. ELife, 6, 1–20.

Zhang, X., Li, L., Jung, J., Xiang, S., Hollmann, C., & Choi, Y. S. (2001). The distinct roles of T cell-derived cytokines and a novel follicular dendritic cell-signaling molecule 8D6 in germinal center-B cell differentiation. Journal of Immunology (Baltimore, Md. : 1950), 167(1), 49–56.

Zhang, Y., Garcia-Ibanez, L., & Toellner, K. M. (2016). Regulation of germinal center B-cell differentiation. Immunological Reviews, 270(1), 8–19.

Zhi, H., & Dorothee, L. (2012). Enhanced CD21 expression and shedding in chronic lymphatic leukemia : a possible pathomechanism in disease progression. International Journal of Hematology. 96(3), 350–356.

Zhou, L., Smith, H. M., Waldschmidt, T. J., Schwarting, R., Daley, J., & Tedder, T. F. (1994). Tissue-Specific Expression of the Human CD19 Gene in Transgenic Mice Inhibits Antigen-Independent B-Lymphocyte Development. Molecular Cell Biology. 14(6), 3884–3894.